Sound Bullets from Nonlinear Granular Chains

By

Omololu Akanji

Submitted for the degree of

Ph.D. in Engineering

to the

University of Warwick

describing research conducted in the

School of Engineering

Submitted September 2015

Table of Contents

List of Figures

List of Tables

List of Symbols

c	Sound velocity	λ	Wavelength
f	Frequency	T	Period
c_1	Sound velocity in medium 1	c_2	Sound velocity in medium 2
C_L	Longitudinal velocity	C_S	Shear velocity
c_g	Group velocity	c_p	Phase velocity
σ	Poisson's ratio	ρ	Density
Y	Young's modulus	Z	Acoustic impedance
Z_1	Acoustic impedance of medium 1	Z_2	Acoustic impedance of medium 2
Tc	Transmission coefficient	Rc	Reflection coefficient
α	Angle of incidence	β	Angle of refraction
I_x	Intensity as a result of attenuation	I_0	Intensity of input signal
μ	coefficient of global attenuation	x	Distance
μ_a	molecular friction	μ_s	scattering
v_i	Particle velocity at the input plane	v_o	Particle velocity at the output
d_i	Diameter of the taper at the input plane	d_o	Diameter of the taper at the output plane
I_i	Intensity at the input plane	I_o	Intensity at the output plane
Rl	Focal length	wl	Focal width
D	Aperture diameter	K_1 , K_2	constants that depend on the aperture angle
Fd	Focal distance	f_0	Applied static force
f_m	Dynamic signal	γ	Surface energy

k	Spring constant
F	Hertzian force
R_i	Radius of particle i
r	Deformation
$a_{i,i+1}$	Constants of elasticity (Y and σ) of the respective spheres and their radii
a	Radius of a sphere
θ	effective Young's modulus associated with contact interactions
$\ddot{u}_i$	Second derivative of u_i
J_0	Arbitrary parameter
τ	Non-dimensionalised time
f_c	Cut-off frequency
u_0	Displacement generated by the transducer
θ_l, θ_m	Effective elastic constants
H	Heaviside function used to denote contact lost between spheres
PE	Potential energy
δ	Particle displacement/ overlap parameter
x_1, x_2	Centre coordinates of spheres 1 and 2
P	Pressure
$\bar{r}$	Contact area
$V(\delta)$	Hertz potential of the spheres
m	Mass
u_i	Displacement of particle i
δ_0	Displacement of the spheres centre
t	Normalised time
X	Non-dimensionalised distance
g	Acceleration due to gravity
δ_{0l}	Initial static displacement caused by the pre-compression
Q	Linear viscous damping
KE	Kinetic energy

Acknowledgements

I would like to express my sincere thanks and deep sense of gratitude to my thesis advisor Professor David Hutchins for his excellent guidance and encouragement during the course of my research. I would also like to thank Dr Lee Davis for the many hours spent in the labs demonstrating the equipment, for his advice and recommendations on the prototype designs and experimental procedure.

My gratitude to Dr Simon Leigh, Dr Chris Purcell, Mr Charles Joyce, Mr Frank Courtney, Mr David Robinson and the technicians in the engineering workshop for the technical advice, and for processing my purchase and work orders quickly and effectively.

I would like to take this chance to thank my colleagues: Dr Jia Yang, Ikhsan Mohamed, Stefano Laureti and Yazan Marmash for their continued assistance throughout my time at Warwick.

Special thanks to my parents and sibling. Without their generosity, love and support, I would not have accomplished this research.

Declaration

This thesis is submitted to the University of Warwick in support of my application for the degree of Doctor of Philosophy. It has been composed by myself and has not been submitted in any previous application for any degree [apart from the background material in sections 1.5.4, 2.2, 2.3, 2.4, 2.5 and 2.6 which were previously submitted for a Master's degree at University of Warwick in 2011].

The experimental work was performed by the present author, and contributed experimentally to a collaboration between the University of Warwick, the University of Leeds and University College London, funded by the Engineering and Physical Sciences Research Council (EPSRC). The theoretical modelling described in chapter 4 was developed as part of this research programme by a postdoctoral researcher; Dr Jia Yang. The model was based on the experimental work performed by the author.

All publications to date arising from this research are listed on the following pages.

Publications

1. O. Akanji, D. A. Hutchins, L. A. Davis, and S. Leigh, (2013). Micromachined structures for nonlinear ultrasonic transduction. In Ultrasonics Symposium (IUS), 2013 IEEE International, 1117-1120.
2. J. Yang, O. Akanji, D.A. Hutchins, P. J. Thomas, L. A. J. Davis, S. Freear, S. Harput, N. Saffari and P. Gelat, (2014). Time-delay estimation and correlation analysis of acoustic signals in granular media using wavelet decomposition. In Ultrasonics Symposium (IUS), 2014 IEEE International, 2529-2532.
3. D. A. Hutchins, J. Yang, O. Akanji, L. A. J. Davis, P. J. Thomas, Freear, S. Freear, S. Harput, N. Saffari and P. Gelat, (2014). The study of chain-like materials for use in biomedical ultrasound. In Ultrasonics Symposium (IUS), 2014 IEEE International, 2607-2610.
4. D .A. Hutchins, J. Yang, O. Akanji, P. J. Thomas, L. A. J. Davis, S. Freear, S. Harput, N. Saffari and P. Gelat, (2015). "Evolution of ultrasonic impulses in chains of spheres using resonant excitation), EPL,109, 54002.
5. D. A. Hutchins, J. Yang, O. Akanji, L. A. J. Davis, P.J. Thomas, Freear, S. Freear, S. Harput, N. Saffari and P. Gelat, (2015). Evolution of ultrasonic impulses in chains of spheres using resonant excitation. EPL (Europhysics Letters), 109(5), 54002.
6. J. Yang, D. A. Hutchins, O. Akanji, P. J. Thomas, L. A. J. Davis, S. Harput, P. Gelat, S. Freear, and N. Saffari, (2015). An analysis of solitary wave impulses in granular chains using ultrasonic excitation. [Accepted August 2015 for publication in Physics Procedia].
7. D. A. Hutchins, J. Yang, O. Akanji, P. J. Thomas, L. A. J. Davis, S. Freear, S. Harput, N. Saffari and P. Gelat, (Submitted August 2016) Ultrasonic propagation in finite-length granular chains, Ultrasonic Journal.
8. D. A. Hutchins, J. Yang, O. Akanji, P. J. Thomas, L. A. J. Davis, S. Freear, S. Harput, N. Saffari and P. Gelat, (2015). Generation of Impulses from Single Frequency Inputs Using Non-linear Propagation in Spherical Chains. Physics Procedia, 70, 131-134.
9. P. Gelat, N. Saffari, D. A. Hutchins, J. Yang, O. Akanji, P. J. Thomas, S. Harput and S. Freear, (2015, October). The dynamic excitation of a chain of pre-stressed spheres for biomedical ultrasound applications: contact mechanics finite element analysis and validation. In Ultrasonics Symposium (IUS), 2015 IEEE International. IEEE.

10. J. Yang, D. A. Hutchins, O. Akanji, P. J. Thomas, L. A. J. Davis, S. Harput, P. Gelat, S. Freear, and N. Saffari, (2015, October). Molecular dynamics simulation of nonlinear waves in granular media. In Ultrasonics Symposium (IUS), 2015 IEEE International. IEEE.
11. S. Harput, S. Freear, J. Yang, D. A. Hutchins, O. Akanji, P. J. Thomas, L. A. J. Davis, P. Gelat and N. Saffari, (2015, October). Non-linear generation of harmonic content within high intensity ultrasound signals using granular chains. In Ultrasonics Symposium (IUS), 2015 IEEE International.
12. D. A. Hutchins, J. Yang, O. Akanji, P. J. Thomas, L. A. J. Davis, S. Freear, S. Harput, N. Saffari and P. Gelat, (2015, October). The generation of impulses from narrow bandwidth signals using resonant spherical chains. In Ultrasonics Symposium (IUS), 2015 IEEE International.
13. S. Laureti, O. Akanji, L. Davis, M. Ricci, S. Leigh, D. Hutchins, (2015, October). Design and characterization of 3D printed phononic crystals for sub-MHz ultrasound manipulation. In Ultrasonics Symposium (IUS), 2015 IEEE International.

Abstract

The propagation of ultrasound along chains of granular particles has some interesting characteristics. These have the potential to dramatically improve the performance of HIFU (High Intensity Focussed Ultrasound) for the use in therapeutic ultrasound treatments and medical imaging. This thesis has investigated a novel approach for the creation of ultrasonic focussed energy in chains composed of spheres. Within these highly sensitive chains, non-linear propagation is possible which leads to the formation of highly robust localised pulses known as sound bullets. Subject to the right conditions, the chain of spheres become a dynamically tunable system where slight changes to the nature of the Herzian contact between the spheres produce drastic changes in the propagation velocity of the solitary wave. The nature and resulting characteristics of the system to variations such as input excitation frequency, effect of loading, changes in length and diameter of the chain were studied. It was observed that the system was highly dependent of each of these factors, with each situation altering the behaviour of the chain of spheres.

CHAPTER 1: Fundamentals of Acoustics and Ultrasound

1.1 Acoustics and Ultrasound

Acoustics, the science of sound, dates as far back as 580 BC, with the mathematical properties of stringed instruments written by Pythagoras [1]. In 1893, Sir Francis Galton fabricated the first instrument to produce ultrasound in the form of a whistle [2], and in 1917, Paul Langevin introduced the first technological application of ultrasound to detect submarines [3]. Sound is the coordinated vibration of molecules propagating via a medium, which can be in the solid, liquid or gaseous state. An acoustic signal is said to be ultrasonic if its frequency is above 20 kHz. Hence, ultrasound is a wave that propagates via a medium due to oscillation of the particles about their equilibrium points at frequencies above the human audible range (approximately 20 Hz – 20 kHz). Fig. 1.1 shows the acoustic field range and corresponding applications for different frequency ranges of ultrasound.

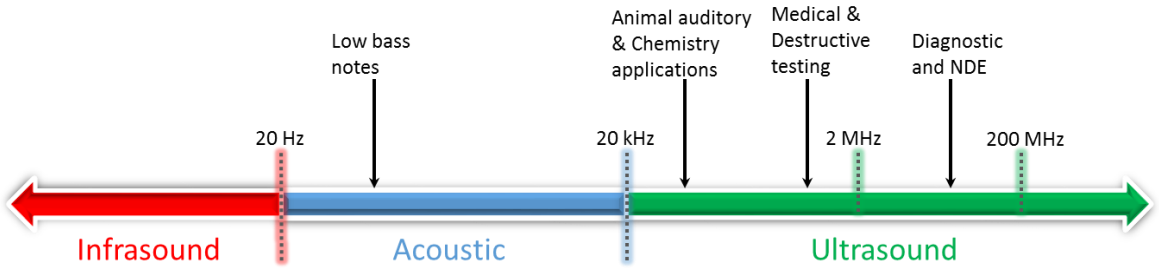

Fig. 1.1 Acoustic wave field with applications

Ultrasound is used in many fields such as non-destructive evaluation to detect faults in products and structures, for cleaning, mixing and for accelerating chemical reactions, and in devices to detect objects and measure distances. In medicine ultrasound is commonly used in imaging (sonography) and for applying therapeutic treatments. These medical applications are performed at a frequency range of 100 kHz to tens of MHz depending on the regime.

In this chapter, useful background information for the research described in later chapters will be presented. The research in this thesis will investigate ultrasonic waves within chains of

spheres using excitation from an ultrasonic transducer and horn. It is thus useful to discuss the various common wave propagation modes, properties, and how a transducer and horn operate. A brief discussion of biomedical ultrasound is also provided, as this is the primary field of interest for the application of the system of granular particles investigated in this research. The chapter concludes with a thesis outline providing a brief introduction to the remainder of the thesis.

1.2 Properties of Ultrasound

Ultrasound is a wave phenomenon that occurs at any frequency above 20 kHz. At such frequencies, the particle in the medium vibrates about its equilibrium position passing its energy to neighbouring particles. In biological tissues, gases and most liquid media, these movements and transference of energy between the particles tend to occur along the same direction. In other words, the direction of particle displacement is parallel to the direction of wave propagation; the result being known as longitudinal waves [4]. In solids, a transverse or shear wave mode [5] of propagation can also exist. In this mode, the motion of the particles is perpendicular to the direction of travel. Figs 1.2 (a) and (b) illustrates the mechanism of the longitudinal and transverse modes. Note that shear waves can also exist in some liquids and biological tissue, but tend to be highly attenuated.

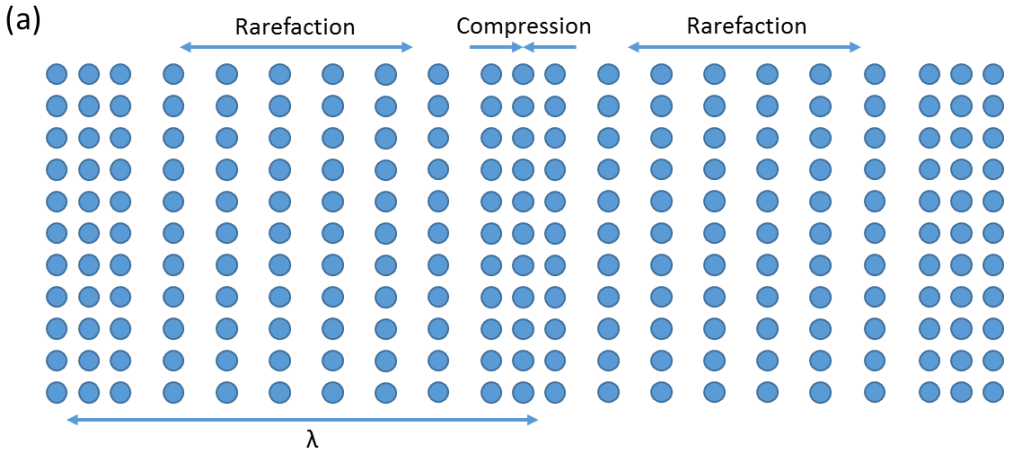

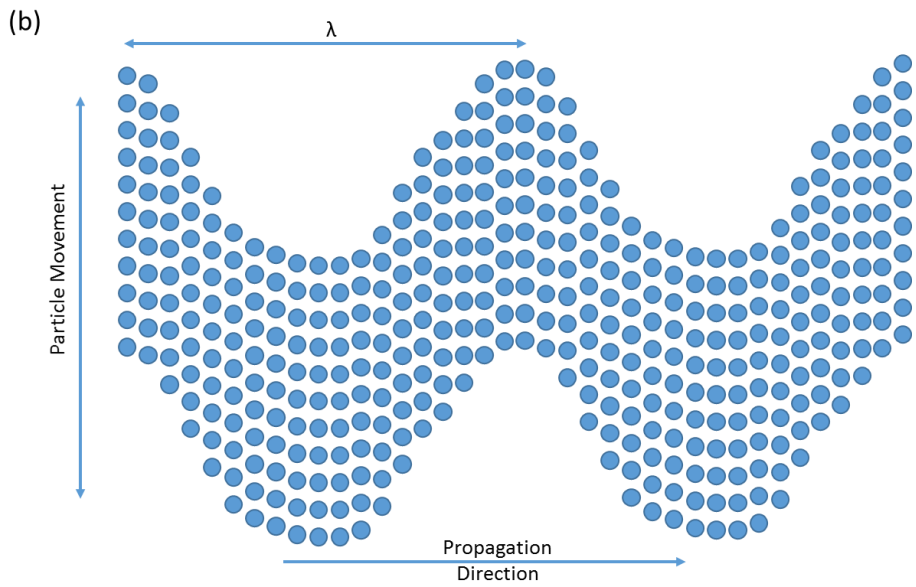

Fig. 1.2. Illustrating the particle movement in, (a) a longitudinal wave and (b) a shear wave.

The velocity of propagation of a wave in a medium is defined as the distance travelled by a wave front as a unit of time. Velocity, wavelength and frequency are the most important parameters to describe a wave. A simplified expression of propagation velocity as derived from the wave equation is given in equation (1.1).

$$c = \lambda f \qquad \text{and} \qquad T = \frac{1}{f} \tag{1.1}$$

Here, c is the velocity of propagation, λ is wavelength, f is frequency, and T is period (the time taken to complete one cycle).

The velocity of propagation of longitudinal waves in solids, C_L, is dependent on the physical properties of the material. Therefore it is possible to generate waves of differing velocity depending on the deformation mode. The longitudinal velocity in a solid medium is expressed as:

$$c_L = \sqrt{\frac{Y(1-\sigma)}{\rho(1+\sigma)(1-2\sigma)}} \tag{1.2}$$

For shear waves, the velocity of propagation can be expressed as:

$$c_S = \sqrt{\frac{Y}{2\rho(1+\sigma)}} \tag{1.3}$$

where σ is the Poisson's ration, ρ: is the density, and Y is the Young's modulus of the material.

1.2.1. **Acoustic Impedance**

Materials have a range of different physical properties, therefore, different propagation velocities of waves occur. Reflection occurs at the interface between two differing materials as a result of the two materials possessing different densities. As the wave travels through the interface of the materials, it encounters an impedance which alters the velocity of travel. The acoustic impedance of the materials determine the amount of reflection of the wave. The characteristic impedance of a material is calculated as shown in equation 1.4 measured in Rayls (kg/m^2s):

$$Z = \rho \cdot c \tag{1.4}$$

where $Z\ is$ acoustic impedance of the material, ρ is the density of the material and c is the velocity of the wave front.

1.2.2. **Reflection**

Reflection occurs at the interface between two media with different acoustic impedance [6]. At this boundary; when the incident planar wave is normal to the interface, some of the wave will have its energy reflected while some will be transmitted in accordance with the law of reflection [7] as illustrated in Fig. 1.3.

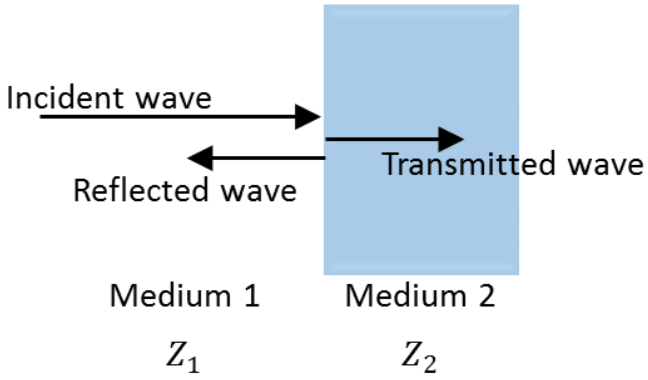

Fig. 1.3: Transmission and reflection of *a wave with incidence normal to a boundary between two media.*

The two resulting waves can be expressed in terms of the acoustic impedance of each medium:

$$Tc = \frac{4Z_1Z_2}{(Z_1 + Z_2)^2} \tag{1.5}$$

$$Rc = \left(\frac{Z_1 - Z_2}{Z_1 + Z_2}\right)^2 \tag{1.6}$$

where Z_1 is the acoustic impedance of medium 1, Z_2 is the acoustic impedance of medium 2, Tc is the transmission coefficient, and Rc is the reflected coefficient.

When two media have the same characteristic acoustic impedance *i.e.* the materials have an impedance match, we observe Tc = 1 and Rc = 0; therefore, perfect transmission occurs with the wave propagating via the interface with no reflections.

The transmitted waves obey Snell's law of refraction [8], which is used to describe the relationship between the angles of incidence and refraction. The law states that "*the ratio of the sine of the angles of incidence and refraction is equivalent to the ratio of phase velocities in the two media, or equivalent to the reciprocal of the ratio of the indices of refraction*"

$$\frac{\sin(\alpha)}{\sin(\beta)} = \frac{c_1}{c_2} \tag{1.7}$$

where α is angle of incidence, β is angle of refraction, c_1 is the sound velocity in medium 1, and c_2 is the sound velocity in medium 2.

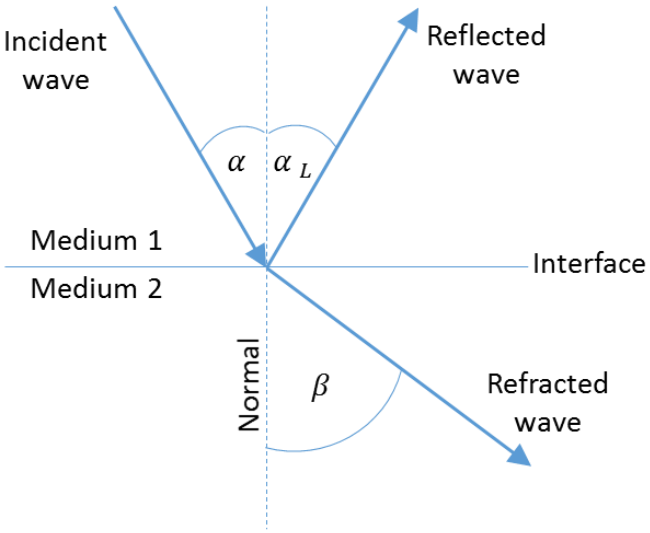

Fig. 1.4: Refraction and reflection of inclined waves.

Mode conversion can occur in certain cases, whereby longitudinal waves are converted to shear and vice versa. These modes of propagation have different propagation velocity, angles of reflection and refraction (as shown in Fig. 1.5), with longitudinal wave having a greater velocity than shear wave. Hence, it is refracted at a greater angle.

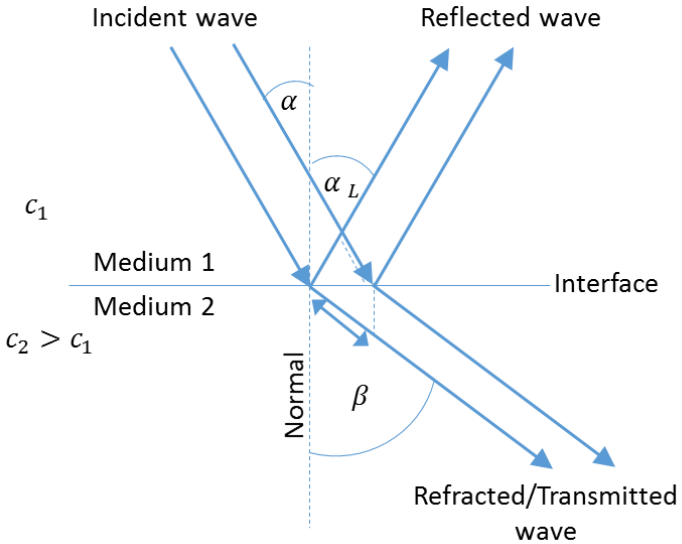

Fig. 1.5: Refraction and reflection of inclined waves during mode conversion.

The relationship between the incident, reflected and refracted waves is of critical importance when transmitting waves through multiple materials. The greater the difference in impedance between the materials the greater the dissipation effect and loss of energy. Under such situation,

couplers or matching layers are required to minimise these effects. Figures 1.6 and 1.7 describe the trend as a ratio of the impedance of the media changes. When *Rc* = 0, *Tc* = 1 and there is total transmission. When Z_1 is greater than Z_2, *Rc* tends towards 1 and the wave encounters a soft boundary with most of the waves reflected at angle of 180 degrees. On the other hand, when Z_2 is greater than Z_1, *R* tends towards -1 and the boundary is hard and almost no phase change occurs. When Z_1 is greater than Z_2, *Tc* tends towards 0 indicating that the acoustic impedance of the media is diverging.

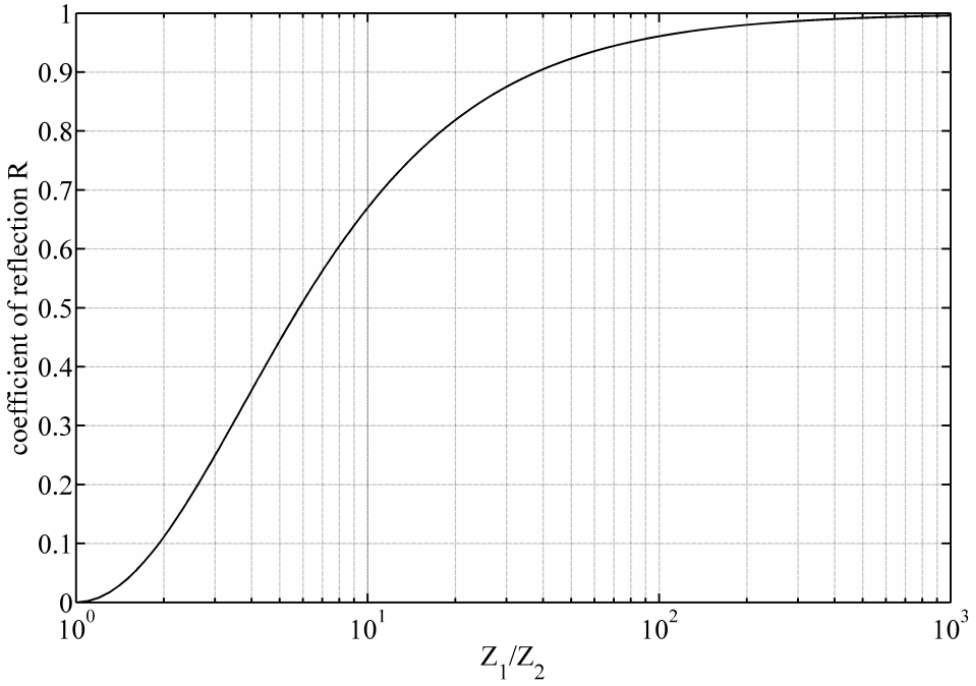

Fig. 1.6: Coefficient of reflection Rc as a function of the ratio $\frac{Z_1}{Z_2}$ *[9].*

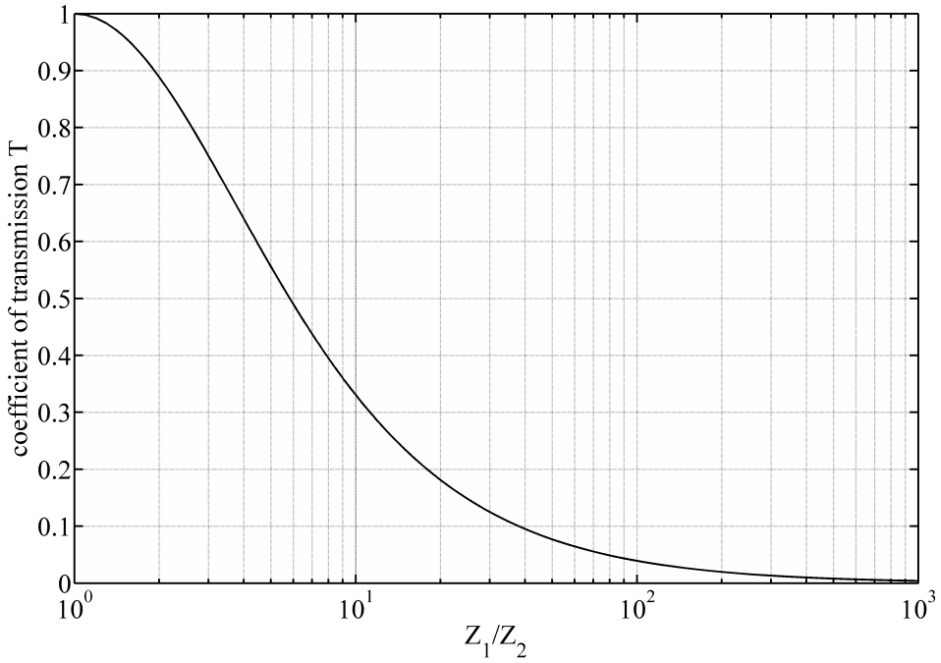

Fig. 1.7: Coefficient of transmission Tc as a function of the ratio $\frac{Z_1}{Z_2}$ [9].

1.2.3. **Ultrasonic Attenuation**

Attenuation or absorption [10] occurs in every material. It is defined as the gradual loss of energy and it affects the propagation of waves through a medium. Attenuation is an exponential function of the propagation distance in the medium. Attenuation is due to the transfer of energy from one particle to another. Friction and thermal conductivity occurs as a result of the mechanism of transference of energy. The energy within the vibrating particles is converted to thermal energy which weakens the wave as it travels through a medium.

In ultrasound, attenuation is measured as a reduction in intensity or amplitude of the ultrasonic wave as a function of the distance travelled along the medium, this is expressed as:

$$I_x = I_0 \cdot e^{-\mu x} \tag{1.8}$$

where I_x is intensity as a result of attenuation, I_0 is the intensity of input signal, μ is the coefficient of global attenuation and x is distance.

Note that dissipation is often referred to as "attenuation due to energy loss". The coefficient of global attenuation is the sum of the effect of energy loss due to molecular friction (μ_a) and

scattering (μ_s). The molecular friction depends on the frequency of the wave, temperature, viscosity and velocity of sound of the material, while scattering is dependent on the dimensions of the inclusion and the wavelength.

1.3 Guided ultrasonic waves

Longitudinal and shear waves are not the only propagation modes present in a medium. Other modes include; Stonley waves [11], which propagate along the interface between differing media and gravity waves [12] which propagates between two fluids having different densities. In solids, surface waves also known as Rayleigh waves [13] travel along the surface of a medium in the form of an elliptical motion of the surface particles changing into a circular motion as it progresses downwards within the medium. Lamb waves or plate waves can be found travelling in thin plates and Love waves [14] propagate within thin layers coated onto the surface of a medium.

There are many forms of such waves [15]; each dependent on the type of structure and how the energy is transmitted through the structure. Surface wave and interface wave are an example of waves guides transmitted along the boundaries of a medium. Rod, cylindrical, plate and rail waves are a few example of guided waves that propagate using the structure of the material. The complexity of the structure and interface of the material are attributes that determine the mode of propagation that can exist within it. Table 1.1 shows a few of the modes that exist within certain structures and interfaces.

Waves in Plates	***Waves in Rods***	**Waves in Interface**
Lamb waves (Axisymmetric & Anti-symmetric)	Longitudinal waves	Love waves
Flexural & Compressional waves	Flexural waves	Rayleigh waves
Shear waves	Torsional waves	Scholte waves

Table 1.1: Propagation modes of structure and interface specific waves.

Waves in plates and rods are often dispersive, the waves deform as they propagate and their velocity changes with frequency. The wave deformation can vary through the thickness of the material.

1.3.1. **Guided waves in Plates**

Lamb waves or plate waves can be used to describe the characteristics of waves travelling through a plate. They are extremely useful for detecting cracks and flaws in thin sheet and tabular materials. It is generated in a plate with free boundaries and as an infinite number of modes for both the axisymmetric (symmetrical) and anti-symmetric displacements for a specific thickness and acoustic frequency. The axisymmetric modes are also referred to as longitudinal waves because the displacement and propagation across the thickness of the plate is in the longitudinal direction as described in Fig 1.8. The antisymmetric waves propagate in a transverse mode via a shearing motion parallel to the plate's surface and perpendicular to the direction of propagation. This means that Lamb waves can travel via flexural and compressional motions either perpendicular or parallel to the surface [16].

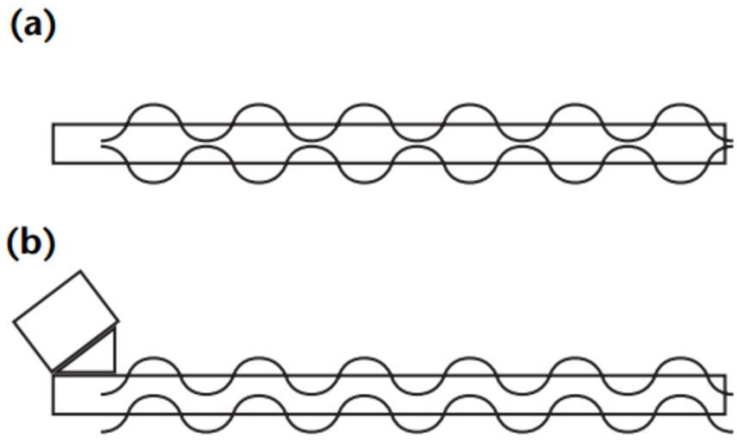

Fig. 1.8 Lamb wave propagating in plate [17]: (a) symmetric; (b) antisymmetric.

The infinite number of modes can be identified by their phase velocities as shown in the dispersion curve in Fig. 1.9. The dispersion curve describes the propagation characteristics and phase velocities as a function of the frequency multiplied by the thickness of the plates. The

labels, A0, A1, S0, S1 and so forth indicate the mode as either antisymmetric (A) or symmetric (S).

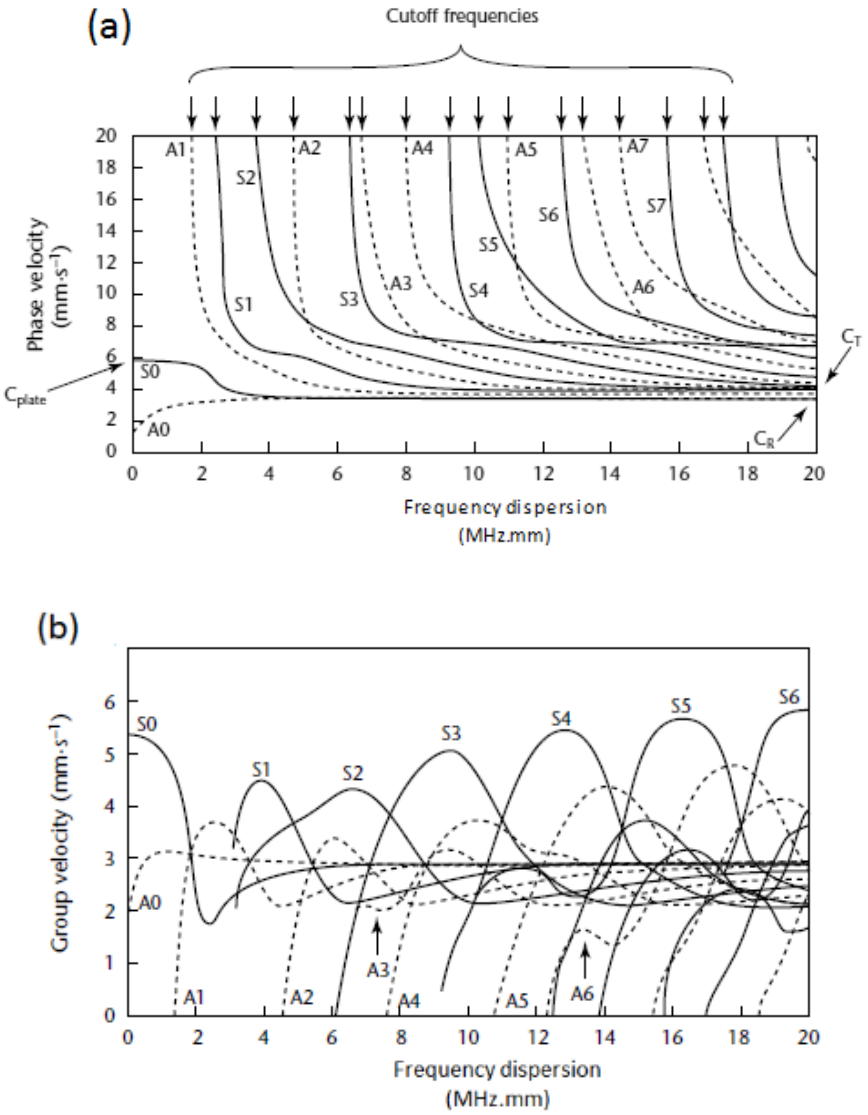

Fig. 1.9 Dispersion curve for an aluminium plate [17]: (a) phase velocity (b) group velocity

The incidence angle of the excitation wave determines which mode will be dominant. Specific Lamb waves can be generated if the phase velocity of the incident longitudinal wave is equal to the phase velocity for the required mode. Phase velocity of the incident longitudinal wave can be calculated by:

$$c_p = \frac{c_g}{sin\varphi} \tag{1.9}$$

where c_g is the group velocity of the incident longitudinal wave, c_p is the phase velocity of the incident longitudinal wave, and φ is the angle of the incident longitudinal wave.

1.3.2. **Guided waves in Rods**

When a wave is applied across a cylindrical structure such as a rod, the wave propagates axially along its length as shown in Fig. 1.10. This is because a solid rod can be considered as a stiff spring. The propagation of the wave produces lateral motion at right angle to the direction of wave propagation and since the surface is free, axial stress develops without any lateral stress occurring [18]. The lateral motion introduces inertial; which increases as the frequency increases. Spherical P-waves and S-waves excited at the loaded end of the rod travel a short axial distance (along the rod) propagating radially over the end where they are relieved by the free surface thereby creating surface waves. Hence, rod waves can be regarded as surface waves propagating along the free surface, extending radially into the rod and producing motion in a single direction across the surface of the rod.

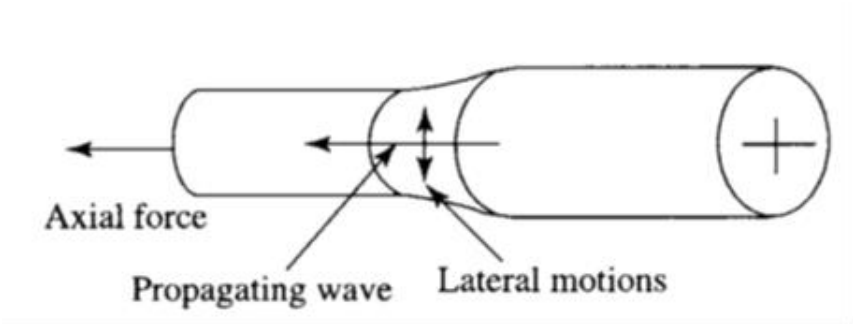

Fig. 1.10: Waves propagating along a rod [18]

If the wavelength is larger than the diameter of the rod, the surface waves extend across the entire diameter of the rod producing a plane wave of uniaxial stress which propagates along the rod. At shorter wavelengths the surface waves become independent surface waves staying close to the surface. But when the wavelength is equal to the cross section of the rod, guided waves are produced as shown in Fig. 1.11. Guided waves are along the rod axis, they are

confined and guided by the inner or outer boundaries of the rod depending on if they are hollow or solid.

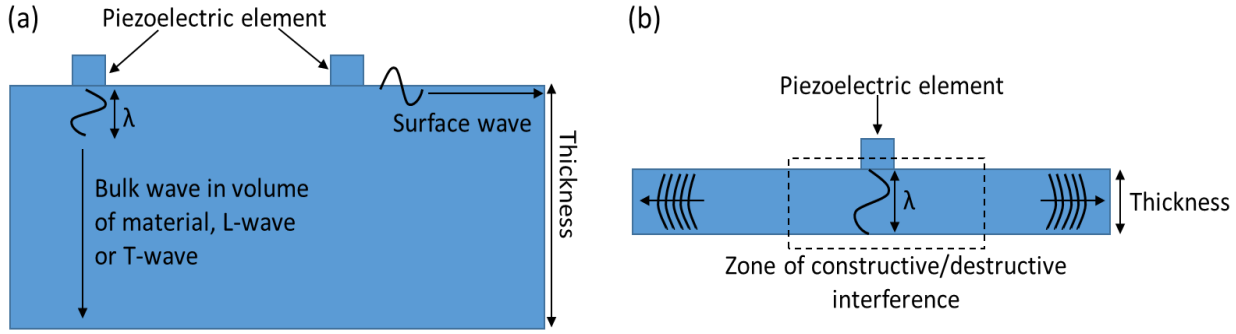

Fig. 1.11: (a) Diameter >> Wavelength (b) Diameter = Wavelength

Fig. 1.12 (a) and (b) below are dispersion curves showing the relationship between wave velocity and frequency for a steel rod with a 10 mm diameter. The dispersion curves illustrates three wave modes: torsional (T), longitudinal (L), and flexural (F). The velocity of the L- and F wave varies significantly with wave frequency, therefore, these waves are dispersive. The velocity of the fundamental torsional wave is constant and equal to the shear wave velocity of the rod material and is independent of frequency.

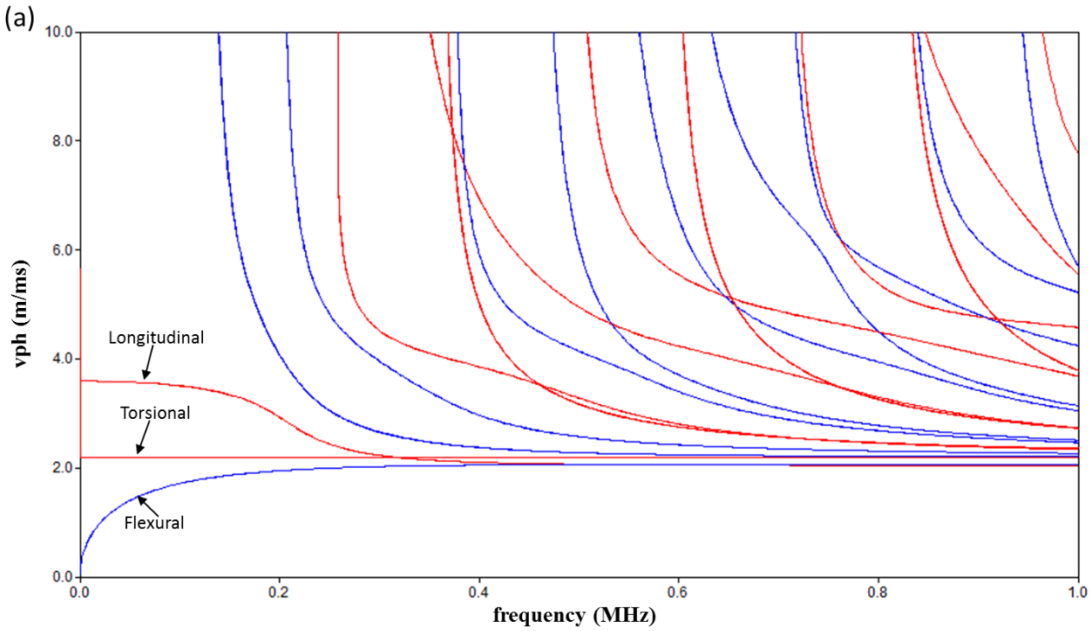

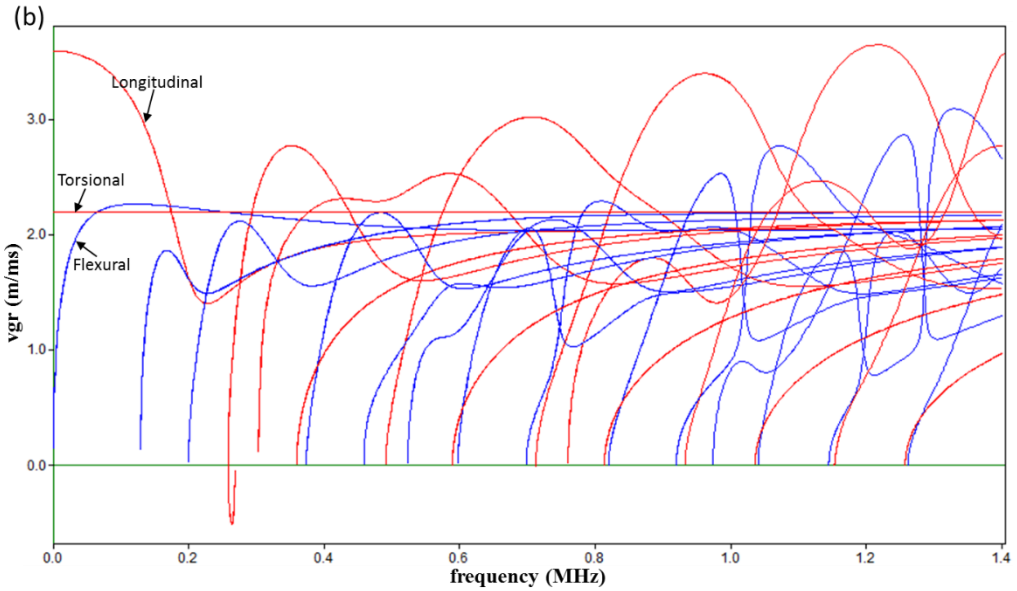

Fig. 1.12: Dispersion curve for a 10 mm diameter steel rod (a) phase velocity (b) group velocity [19].

1.4 Focussing Ultrasound for Medical Application

Ultrasound has many applications in medicine. Typically, when a person hears the term "ultrasound", it conjures an image of a doctor inspecting a foetus in the womb of a pregnant patient using an ultrasound device. This device consist of a transducer, signal generator, amplifier and a digital system for; focussing, processing and displaying the transmitted and received signals. While sonography (foetal imaging) is one of the most common application of medical ultrasound, there are several others uses in medical examinations, diagnostics and therapeutic treatment.

One aim of the research presented in this thesis is to produce high amplitude, wide bandwidth signals that could have a future application in therapeutic ultrasound. In this field, there is a need for high intensity focussed ultrasonic waves that provides a greater degree of focusing and higher focal power for applications such as ablation of tumours, treating hyperthermia, and the study of cavitation in liquids [20]. In ultrasound systems, the boundary between the nearfield and farfield (shown in Fig. 1.13) is of critical importance, beyond this region, interference effect is no longer viable and focussing of the beam cannot occur [21]. The near field is the region closest to the transducer where the acoustic pressure is a series of maxima

and minima, ending as a maxima at the near field distance (N) from the surface of the transducer. Distance N represents the natural focus of the transducer. Beyond distance N lies the far field region where the acoustic pressure gradually decreases to zero as the beam diameter widens resulting in energy loss and dissipation. The length of the near field region is a function of the frequency and diameter of the transducer as well as the acoustic velocity of the propagating medium.

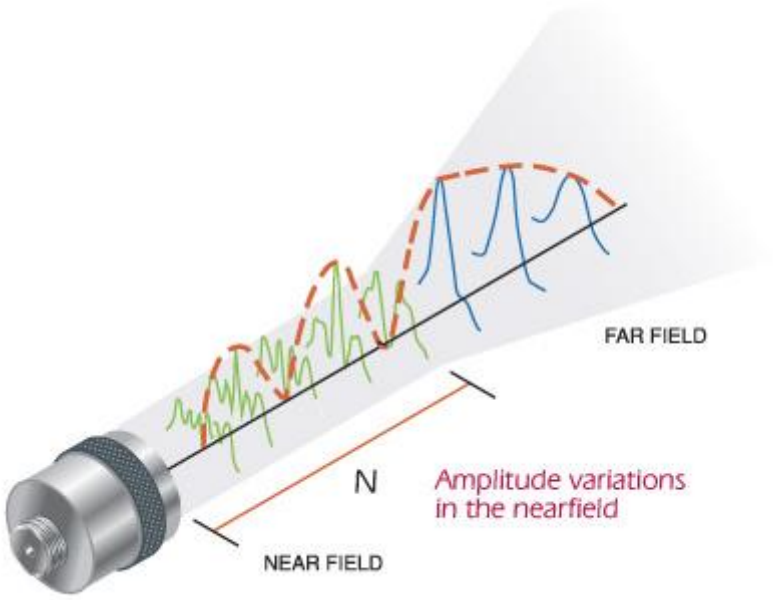

Fig. 1.13: Beam profile of a transducer highlighting the Near field and Far field regions [22].

1.4.1. **The transducers and coupling media**

A transducer is a device that converts one form of energy into another through the use of magnetostrictive or piezoelectric elements, for example. The application of an electric field across certain materials which are anisotropic (*i.e.* lacking centres of symmetry) causes a change in physical dimension known as the piezoelectric effect [23], quartz and tourmaline are common examples of such materials. The piezoelectric effect produces a connection between electric and dielectric phenomena; when the electric charges within the crystal lattice of such materials interact with the applied electric field it produces mechanical stress.

A piezoelectric transducer generates ultrasonic waves when driven by a sinusoidal electrical signal, the active elements deform in a corresponding fashion, producing a displacement of the face of the transducer. The resulting displacement radiates pressure waves into the medium in contact. The amount of energy radiated into the medium depends on the characteristic impedance at the interface between the medium and transducer. Energy reflected at the boundary travels back across the transducer to the opposite end producing an electromechanical coupling effect. There are a wide variety of transducer designs depending on its intended application. Medical ultrasound transducers or echo-scopic probes consist of one or more ultrasonic transducers such as linear probe, sectoral probe and convex probes. There are three essential components for any given transducer, these are: an active element (piezo-electric or piezo-composite material), a backing layer to assist with attenuation within the transducer and a wear plate to protect the active element. These are shown in Fig. 1.14.

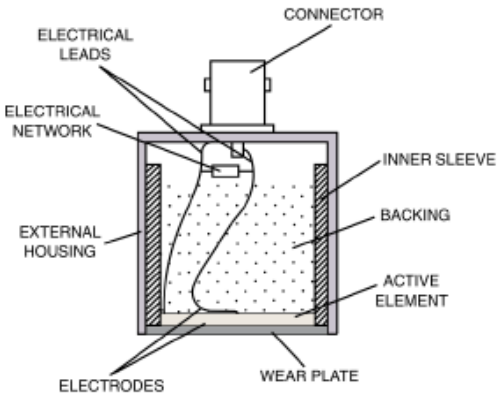

Fig. 1.14: The main components of a transducer [24]

Transducers are often constructed to operate at maximum efficiency of power generation when excited at a specific frequency. The frequency of the drive signal, particle velocity and thickness of the active element are interrelated. The transducer resonates with maximum amplitude when the frequency of the drive signal corresponds to a half wavelength thickness, this is referred to as the fundamental resonant frequency of the transducer. Other harmonics are achieved when driven at frequencies at which the thickness is equal to an odd integral number

of half its wavelength. At even integral number of half wavelengths, the transducer oscillates with minimal displacement.

1.4.2. **Velocity Transformers**

Velocity transformers [25] also known as ultrasonic horns are used to achieve greater performance and acoustic power when incorporated with a transducer. Velocity transformers are mechanical devices designed to have an impedance match with the transducer in order to magnify its intensity. This is attained by channelling the vibrations via a tapered structure. When the cross sectional diameter of the tapered end of the horn is less than half a wavelength, the particle velocity increases in an inverse proportion to the tapered diameter. This relation is expressed as:

$$\frac{v_i}{v_o} = \frac{d_o}{d_i} \tag{1.10}$$

$$\frac{I_i}{I_o} = \left(\frac{d_o}{d_i}\right)^2 \tag{1.11}$$

where I is intensity, d is the diameter of the taper, v is particle velocity and the suffixes i and o refer to the input and output planes, respectively.

It can be observed from equations 1.10 and 1.11**,** that the horn can be used to achieve higher particle velocity and ultrasonic intensity. For instance, if d_i = 30 mm and d_o = 1 mm and $d_i < \lambda/2$, therefore $v_o = 30v_i$ and $I_o = 900I_i$. The length of the horn determines its operating frequency, maximum output is attained when the length is equal to an odd integral of half wavelengths corresponding to the resonance frequency.

Fig. 1.15 shows a few examples of common ultrasonic horns. In the figure, the exponential taper (a) provides the best performance because the material is subjected to the smallest amount of stress and (c) is the easiest to construct, since it is made up of two cylinders, each of a quarter of a wavelength long and fabricated from a single piece of material [26]. The physical

properties of the material the horn is constructed from determines the maximum stress it can support and this affects the maximum particle velocity at the tip.

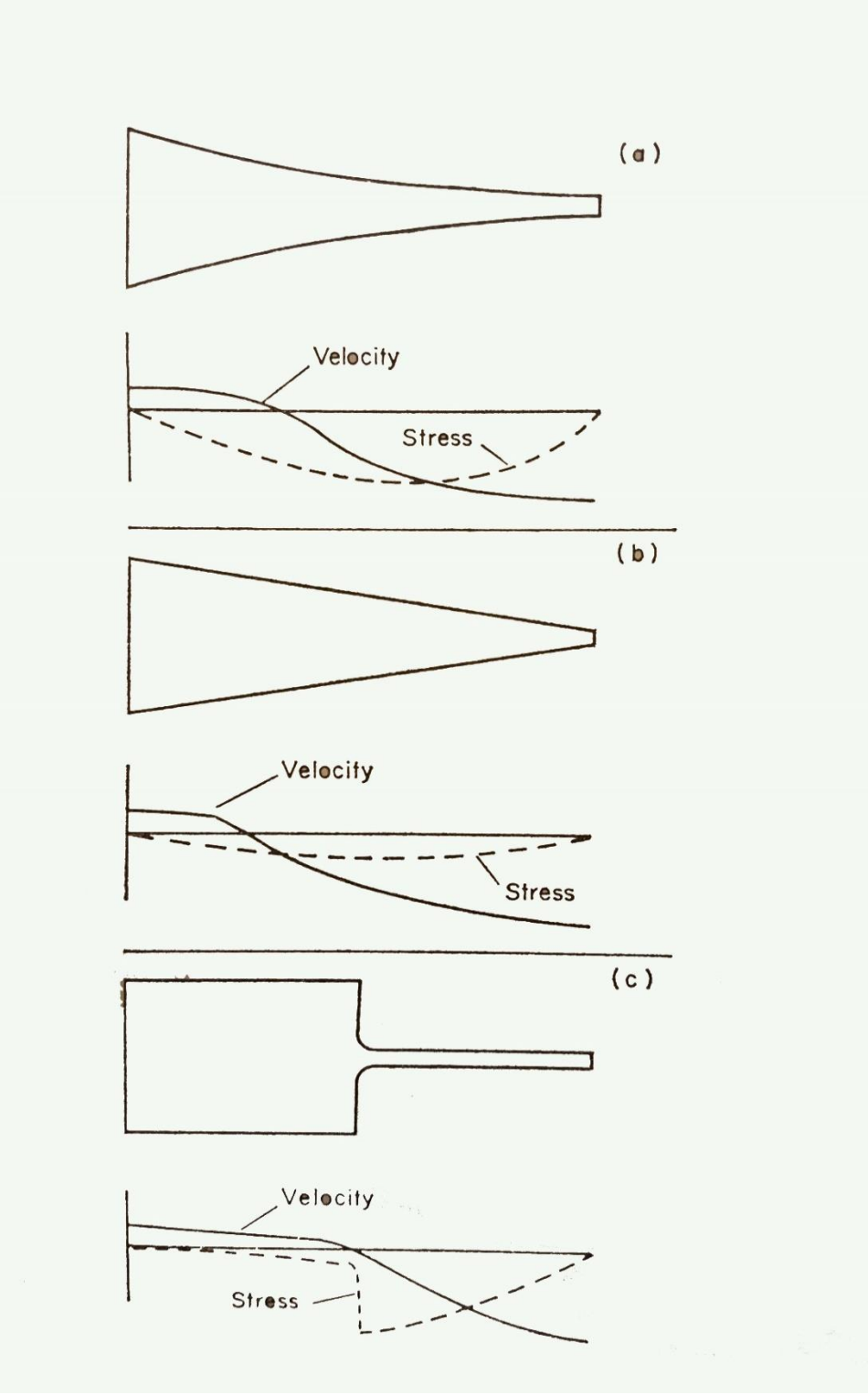

Fig. 1.15: Typical horn shapes, showing stress and velocity distribution [26]. (a) Exponential taper; (b) conical tapers; (c) stepped tapper.

1.4.3. **Focusing using a Transducer**

A transducer is conventionally defined as a focusing device if the width of the acoustic beam produced is reduced to a size smaller than the diameter of the transducer. A single transducer [27] is inflexible because it has a fixed focal length and focal pattern and has a slow scanning mechanism. Its focal length (*Rl*) and focal width (*wl*) can be derived using:

$$Rl = K_1 \left(\frac{Fd}{D}\right)^2 \tag{1.12}$$

$$wl = K_2 \frac{\lambda F}{D} \tag{1.13}$$

where *Fd* is the focal distance, λ is wavelength, and K_1 and K_2 are constants that depend on the aperture angle.

Therefore, if a standard curved 1.5 MHz transducer (often referred to as a "bowl transducer") with a 10cm diameter is used as High Intensity Focussed Ultrasound (HIFU) source to ablate tumours it will produce a focal area with a focal length of 10mm and focal width of 1mm. The dimensions of the focusing source; aperture diameter (*D*), focal distance (*Fd*) and wavelength (λ) determine the focal dimensions. This sharp focus is good because it leaves the surrounding tissues undamaged. However, the lateral width is too short and requires longer procedure time to treat large tumours. This limits the widespread use of therapeutic HIFU, for instance, the procedure required to ablate a tumour the size of 5 cm in a patient suffering from prostate cancer would take an average time of 149 minutes [28]. Making it difficult to treat cancers where the tumour is considerably larger than 5 cm in diameter.

The directivity and amplitude of an ultrasound beam may be tuned and reshaped by focusing, and using similar principles applied in optics. The wavelength of the ultrasound beam imposes restrictions on the dimension of the focal region, while the sharpness of the focus or focal length is established by the ratio of the aperture of the source to the wavelength as seen in

equations 1.12 and 1.13. There have been many studies conducted to enlarge the region of ablation involving techniques like cavitation enhancement [29] and algorithm optimisation for the focus pattern [30]. These techniques provide gains, however methods involving the use of acoustic lenses, focussed bowls, and curved transducers are more common in clinical application.

In recent years, other techniques such as the use of multi-frequency harmonics [31], the introduction of phased arrays [32], and the use of special transducer geometries [33] have all been shown to improve HIFU performance. In addition, various authors have proposed novel approaches using metamaterials [34] and discrete granular media [35] to achieve high amplitude focused ultrasonic beams. In the following Chapter the laws governing the techniques involving granular media will be presented as well as a review of a few approaches of this novel technique. This is done so that the research described in later chapters of this thesis can be put into context with possible future application to HIFU.

1.5 Thesis Outline

The following is a brief summary of the contents of the thesis; describing the work conducted on the development and characterisation of a new type of system which could be used in an acoustic lens.

Chapter 2 presents a review of the contact mechanics between spherical particles and the laws that govern them. It presents a detailed characterisation of the nonlinear propagation present in a chain of spheres and analytic solution which could be used to model a chain of spheres. It also contains a literature review on novel the techniques used to produce highly focussed ultrasonic beams.

Chapter 3 outlines the experimental approach used in this research. Furthermore, a full description of the analytical model used to validate the results from the experiments is provided. Nonlinear Normal Modes are used to explain the nonlinear dynamic motions of the modes found in a chain of finite length.

Chapter 4 demonstrates how to generate nonlinear solitary waves in a chain of granular spheres. Detailed characterisation of this form of propagation is provided.

Chapter 5 provides the results from experiments and predictive models illustrating the effect of varying factors such as sphere diameter and material properties.

Chapter 6 studies the relationship between applied excitation force and static pre-compression force. It shows how the propagation mode of the solitary wave can be transformed from linear to strongly nonlinear.

Chapter 7 provides a conclusion and recommendations for further work.

1.6 References

1. R.W. Hall, and J. Kresimir, (2001). The mathematics of musical instruments. The American Mathematical Monthly 108.4: 347-357.
2. G. Francis, (1883). Inquiries into human faculty and its development. Macmillan. 26-30.
3. W. D. O'Brien Jr, (1998). Assessing the risks for modern diagnostic ultrasound imaging. Japanese journal of applied physics 37.part 1: 2781-2788.
4. J. W. S. Rayleigh, (1945). The theory of Sound. Dover, New York: Vol. 1: 50-51.
5. J. F. Frederick, (1965). Ultrasonic Engineering. John Wiley & Sons, Inc. 100 -103.
6. R. Stoneley, (1924). Elastic waves at the surface of separation of two solid. Proceedings of the Royal Society of London. Series A, Containing Papers of a Mathematical and Physical Character, Vol. 116, 416-428.
7. B. R. Mace, (1984). Wave reflection and transmission in beams. Journal of Sound and Vibration 97.2: 237-246.
8. J. W. Shirley, (1951). An early experimental determination of Snell's law. American Journal of Physics, 19.9: 507-508.
9. H. S. Ribner, (1957). Reflection, transmission, and amplification of sound by a moving medium. The Journal of the Acoustical Society of America 29.4: 435-441.
10. S. Kociš and Z. Figura, (1996). Ultrasonic Measurements and Technologies, 1st ed. London: Chapman & Hall, 113-118.
11. R. Stoneley, (1924), Elastic waves at the surface of separation of two solids. Proceedings of the Royal Society of London. Series A, Containing Papers of a Mathematical and Physical Character, Series A, vol.116, 416-428.
12. E. E. Gossard and H. H. William, (1975). Waves in the atmosphere: Atmospheric infrasound and gravity waves-Their generation and propagation. Atmospheric Science, 2.
13. M. Hirao, Y. Sotani, K. Takami and H. Fukuoka, (1981). Love waves propagation in a solid with a coldworked surface layer. Journal of Nondestructive Evaluation, vol. 2, 51-55.
14. T. Toshiro, and D. L. Anderson, (1985). Lateral heterogeneity and azimuthal anisotropy of the upper mantle: Love and Rayleigh waves 100–250 s. Journal of Geophysical Research: Solid Earth 90 (B2), 1842-1858.
15. R. E. Collin, and H. Chang (1961). Field theory of guided waves. Physics Today, 14, 50.

16. I. A. Viktorov, (1967). Rayleigh and Lamb waves – Physical theory and Applications, Plenum Press, New York.
17. Lamb Waves: https://www.asnt.org/~/media/Files/Publications/Errata/3UT03p100.ashx (accessed: 20/02/15).
18. B. M. Lempriere, (2003). Ultrasound and elastic waves: frequently asked questions. Academic Press, 29 - 32.
19. Disperse Tool created by: Mike Lowe and Brian Pavlakovic (Licensed by Imperial College Consultants).
20. J. Vincenot, D. Melodelima, F. Chavrier, A. Vignot, A. Kocot, J. Chapelon, (2013). Electronic Beam Steering Used with a Toroidal HIFU Transducer Substantially Increases the Coagulated Volume, Ultrasound in Medicine & Biology, Volume 39, Issue 7, 1241-1254.
21. J. A. Jensen and N. B. Svendsen, (1992). Calculation of pressure fields from arbitrarily shaped, apodized, and excited ultrasound transducers. Ultrasonics, Ferroelectrics, and Frequency Control, IEEE Transactions on, 39(2), 262-267
22. Olympus: http://www.olympus-ims.com/en/ndt-tutorials/transducers/characteristics/ (Accessed: 12/01/2016)
23. B. Jaffe, (2012). Piezoelectric ceramics. Vol. 3. Elsevier.
24. NDT Resource Centre: https://www.nde-ed.org/EducationResources/CommunityCollege/Ultrasonics/EquipmentTrans/transducermodeling.htm (Accessed: 19/02/2015)
25. S. G. Amin, M. H. M. Ahmed, and H. A. Youssef, (1995). Computer-aided design of acoustic horns for ultrasonic machining using finite-element analysis. Journal of Materials Processing Technology 55.3: 254-260.
26. P.N.T. Wells (1997). Biomedical Ultrasonics. Academic Press
27. L. Ruibin, H. K. Hyung. J. M. Cannata, C. Gin-Shin, K. K. Shung, (2007). 10F-4 Self-Focused 1-3 Composite LiNbO3 Single Element Transducers for High Frequency HIFU Applications, In Ultrasonics Symposium (IUS). IEEE, 949-952.
28. T. Uchida, H. Ohkusa, Y. Nagata, T. Hyodo, T. Satoh, and A. Irie, (2006). Treatment of localized prostate cancer using high-intensity focused ultrasound. BJU international, 97(1), 56-61.

29. D. Melodelima, and D. Cathignol, (2004). Cancer treatment by ultrasound: increasing the depth of necrosis. Applied Physics Letters, 84(26), 5365-5367.
30. M. Lu, M. Wan, F. Xu, X. Wang, and X. Chang, (2006). Design and experiment of 256-element ultrasound phased array for noninvasive focused ultrasound surgery. Ultrasonics, 44, e325-e330.
31. R. Chopra, C. Luginbuhl, F. S. Foster, and M. J. Bronskill, (2003). Multifrequency ultrasound transducers for conformal interstitial thermal therapy, IEEE Trans. Ultrason. Ferroelectr. Freq. Control, vol. 50, no. 7, pp. 881–889.
32. X. Rongmin, S. Wende, C. Guoping, Z. Meidun (2001). A new-style phased array transducer for HIFU. Applied Acoustics; 63:957-964.
33. D. Melodelima, W. A. N'Djin, H. Parmentier, S. Chesnais, M. Rivoire, and J. Y. Chapelon, (2009). Thermal ablation by high-intensity-focused ultrasound using a toroid transducer increases the coagulated volume. Results of animal experiments. Ultrasound in medicine and biology, 35(3), 425-435.
34. S. Zhang, L. Yin, and N. Fang, (2009). Focusing ultrasound with an acoustic metamaterial network. Physical review letters, 102(19), 194301.
35. X. Jia, C. Caroli, and B. Velicky, (1999). Ultrasound propagation in externally stressed granular media. Physical Review Letters, 82(9), 1863.

CHAPTER 2: Nonlinear Waves in Hertz-type Granular Systems

2.1. Introduction

The propagation of ultrasound through particle chains has received a lot of recent interest, with potential applications in therapeutic ultrasound and biomedical imaging. This is due to the potentially non-linear nature of the propagation along the chain, which provides the ability to generate a signal with an increased frequency range. This form of wave propagation involves the study of solitary waves, which naturally occur in such chains of particles when the conditions are right. The concept of solitary wave propagation in particle chains has been a topic of growing interest in numerous fields of engineering and physics, such as; DNA double-strand dynamics in bioengineering [1], couples waveguide arrays and photorefractive crystals in nonlinear optics [2] and Bose-Einstein condensation in optical lattices in atomic physics [3].

Solitary waves can be thought of as propagating energy bundles. They possess interesting properties; solitons will pass through one another without interaction for example, and can travel long distances without changing their fundamental characteristics, and tend to travel along particle granular systems with these distinct characteristics. It is these characteristics which this research intends to exploit. These granular systems consist of discrete systems of particles in which the force-displacement attributes for each granular contact could be linear or nonlinear, *i.e.* the relationship between displacement and acceleration is nonlinear. These characteristics were first discovered by Nesterenko [4], who studied the case where there were no preloading force acting on the particles in the chain [5]. This required the chain to be arranged such that the particles are in light contact with one another, thereby restricting the oscillation of each particle so that its centre vibrates about its fixed starting position. When the chain is excited, the centre of each particle is displaced about its equilibrium point. If the input amplitude is sufficiently large, a separation (a pull and push behaviour) between

successive particles is created as the wave propagates along the chain, creating an "acoustic vacuum" or "sonic vacuum" [6]. As will be seen in this and later chapters, the relative motion of successive particles with nonlinear Hertzian contact between each other leads to some interesting properties. This Chapter thus considers Hertzian contact mechanics, the subsequent properties of solitary waves that can propagate in these chains and a review of several approaches used by other investigators.

2.2. Hertzian Contact Law

No solid is entirely rigid; hence, when two particles come into contact, they deform. The extent of the deformation is dictated by their physical properties; their elastic or viscoelastic properties, surface roughness, the interaction of their surface forces and the external load applied.

The problem of interest here is shown in Fig. 2.1. This has a chain (or column) of spheres in contact, to which a static force (f_0) is applied. A dynamic force (f_m) then introduces a vibration into the chain, and this is the signal which propagates along the chain, and which is modified by the interaction between each sphere in the chain. This interaction is known as Hertzian contact. In 1882, Hertz [7] provided the solution to the problem of two non-adhesive spherical particles. He evaluated two elastic spheres in contact with one another with a rigid wall on both ends providing an infinitely steep repulsion between the surfaces in contact as shown in Fig. 2.1. Under these conditions and assuming zero friction, Hertz deduced the area of contact and the stress attributed for a known compressive load, shown in column 1 of Fig. 2.2. He determined that two Hertzian solids would not adhere and could move freely when subjected to zero or negative loading. He further predicted that the dependence of displacement on applied force would be non-linear.

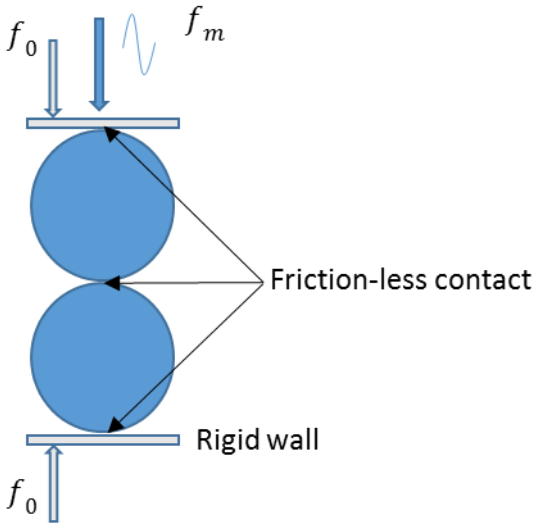

Fig. 2.1 Schematic diagram of a chain of spherical granules, subject to an applied static force f_0. A dynamic signal f_m creates acoustic propagation within the chain.

Johnson, Kendall and Roberts (JKR) [8] extended the Hertz theory to include two adhering spheres. These spheres stick together when in contact due to their finite surface energy. When the spheres adhere they possess greater contact area when subject to loading than predicted by Hertz. They demonstrated that the tensile stress is nearer to the boundary of the contact region and the compressive stress to be nearer to the centre (shown in column 2 in Fig. 2.2). To separate the spheres, a finite tensile load is needed and this depends on the radius of the spheres and their surface energy. As described in Fig. 3.2, JKR's theory predicts that the spheres would separate unexpectedly when the load reaches a critical tensile value and that there would be an infinite amount of tensile stress along the boundary of the contact zone making each surface bend at a right angle along this zone.

Derjaguin, Muller and Toporoc (DMT) [9] asserted that attractive forces between solids will have a finite range and would act in the region just beyond the contact area where the surfaces are but a short distance apart. DMT's theory assumes that surfaces deform as described by Hertz and are unaffected by surface forces. This eliminates the infinite stress distribution and gradient surface profile as aforementioned by JKR. Hence, DMT's theory predicted that the

solids (*i.e*. spheres) would separate when the contact area is reduced to zero and that the critical tensile value is $\frac{4}{3}$ greater than predicted by JKR.

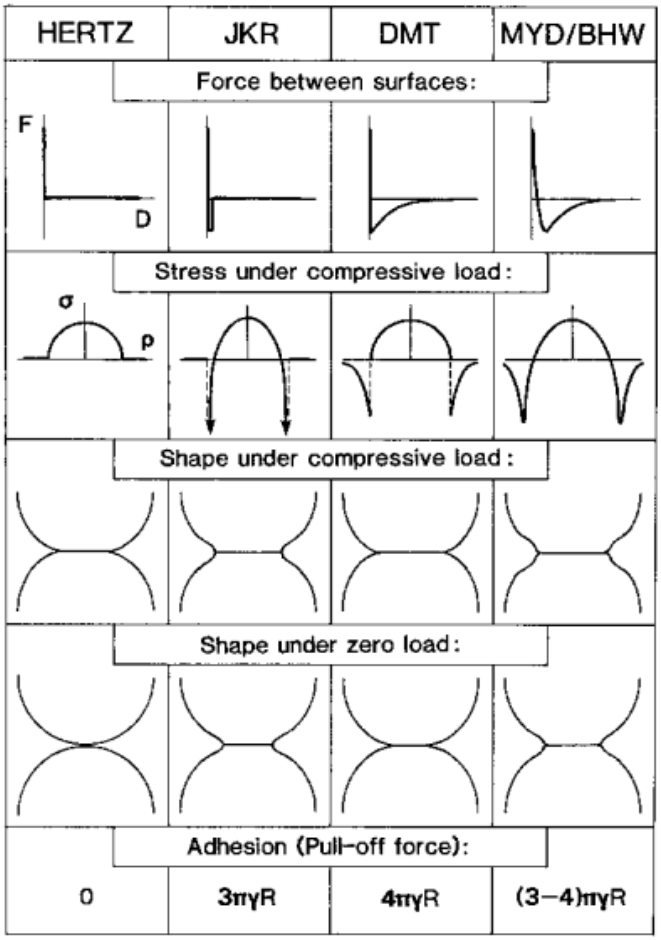

Fig. 2.2 Comparison of various theories on the deformation and adhesion of two elastic spheres [10], where γ is the surface energy.

Muller *et al*. (MYD) [11, 12] produced a theory that described the sphere-sphere interaction as a function of the separation between their respective surfaces. They stated that the stress distribution depended on the surface interaction which in turn depended on the shape of the deformation, which was determined when the stress distribution is known. This results in a nonlinear integral equation, when solved numerically predicted that the stresses are finite in all directions eliminating the right angle bend of the surfaces (column 4, Fig, 3.2).

2.2.1. **The Hertz Potential**

The Hertz potential considers the configuration and the initial conditions (loading) subjected to a particle chain. These are important factors that determine the properties of the solitary waves propagating along the chain. For example, the amplitude of the applied dynamic vibrational force (f_m) affects the velocity of propagation of the wave, while the static force (f_0) applied to the particles determines the regime: if propagation will be linear, weakly nonlinear or strongly nonlinear. These conditions are as follows:

- $f_0 \gg f_m$: When the compression force (f_0) is greater than the applied transient force (f_m), the chain acts like a continuous medium (a normal solid) producing a linear wave.
- $f_0 \approx f_m$: As the magnitude of f_0 approaches f_m, a weakly nonlinear wave in generated.
- $f_0 \ll f_m$: When f_0 is considerable less than f_m, propagation through the chain becomes highly nonlinear.

Strongly nonlinear solitary waves generated from weakly-compressed discrete systems or chains display different characteristics to those of weakly nonlinear systems. Under the conditions assumed by Nesterenko, the solitary waves that exist in such particle chains possess a finite and constant width that is highly dependent on the nature of the particle-particle interface but independent of the solitary wave amplitude, and a pulse speed lower than the bulk sound velocity of the particles the chain is composed of. It is these properties of nonlinear solitary waves found in discrete power law material that are of interest, where for an applied force (f_m), a spring constant (*k)* and particle displacement (δ) is described by:

$$f_m = k\delta^n \qquad for\ n > 1 \tag{2.1}$$

These properties can be further described using Hertz potential [13]; when compression is applied on two or more elastic objects in contact, they try to repel each other and this repulsion is in the form of potential energy, it increases as the compression increases. The energy transfer from a preceding particle to its succeeding increases gradually but as the repulsion increases

due to increasing length of particle chain, the energy required for the particle to remain in contact increases exponentially. These results in an exponential increase in the energy transferred from one particle to the next as the wave progresses through the length of the chain of particles.

The interaction of two spheres of radius R_1 and R_2 made of the same elastic material can be described using Hertz's law:

$$F = \frac{2Y}{3(1-\sigma^2)}\left(\frac{R_1 R_2}{R_1 + R_2}\right)^{1/2} [(R_1 + R_2) - (x_2 - x_1)]^{3/2} \tag{2.2}$$

where *F* is the Hertzian force between the particles, x_1 and x_2 are the centre coordinates of the spheres, σ denotes Poisson's ratio, and *Y* is the Young's modulus. The last term in this expression is the source of non-linearity, with a dependence to the power of 3/2.

The deformation (*r*) of the particles in terms of the overlap parameter or particle displacement (δ) associated with the contact area $\bar{r}$ must be defined before the potential energy generated as a result of the compression of two identical particles (*i.e.* spheres) as described by Hertz law [14] can be determined. The deformation can be expressed as:

$$r \sim \frac{\delta}{\bar{r}} \tag{2.3}$$

The pressure *P* experienced by each particle can be described as:

$$P = Yr = \frac{F}{\bar{r}^2} \tag{2.4}$$

Based on the geometry of spheres, we can write:

$$\bar{r}^2 \sim \delta \mathrm{R} \tag{2.5}$$

Therefore,

$$\mathrm{Y}\left(\frac{\delta}{\bar{r}}\right) \sim \frac{F}{\delta \mathrm{R}} \tag{2.6}$$

$$\mathrm{Y}\left(\frac{\delta}{R}\right)^{1/2} \sim \frac{F}{\delta \mathrm{R}} \tag{2.7}$$

and

$$F \sim YR^{1/2}\,\delta^{3/2} \tag{2.8}$$

It is important to point out the dependence in the form of $\delta^{3/2}$, where δ is the closest approximation of the sphere's centre. The power index of Hertz's law depends on the contact geometry as a result of the particle shape. Hertz used the power index $\frac{3}{2}$ to express an ideal spherical contact. This index is known as Hertz law index [15]. For particles with irregular contacts, the index may be higher and for those that compress a lot easier than two spheres, this index may be lower.

Using equation 2.8, the potential energy $V(\delta)$ of particles under Hertz force, can be expressed as follows:

$$V(\delta) \sim YR^{1/2}\,\delta^{5/2} \tag{2.9}$$

In a scenario involving particles made from different elastic materials, the distance between their centres when they are in slight contact is: $R_i + R_{i+1}$ where R_i denotes the radius of particle *i*. When the spheres are subject to loading, they overlap. The overlap parameter is defined as:

$$\delta_{i,i+1} \equiv R_i + R_{i+1} - (u_i - u_{i+1}) \tag{2.10}$$

where u_i is the displacement of particle *i*

The potential energy due to loading of the spheres as describes by the Hertz potential [16] is then expressed as:

$$V\left(\delta_{i,i+1}\right) = \frac{8}{15\left[\frac{1-\sigma_i^2}{Y_i}+\frac{1-\sigma_{i+1}^2}{Y_{i+1}}\right]}\sqrt{\frac{R_iR_{i+1}}{R_i+R_{i+1}}}\,\sigma_{i,i+1}^{\frac{5}{2}} \equiv a_{i,i+1}\delta_{i,i+1}^{\frac{5}{2}} \tag{2.11}$$

where $a_{i,i+1}$ represents the constants of elasticity (Y and σ) of the respective spheres and their radii.

Hertz law describes the compression force that is weaker than that applied due to harmonic springs for sufficiently small overlaps, which becomes steeper than the harmonic force as the overlaps becomes larger. This comparison is shown in Fig. 2.3

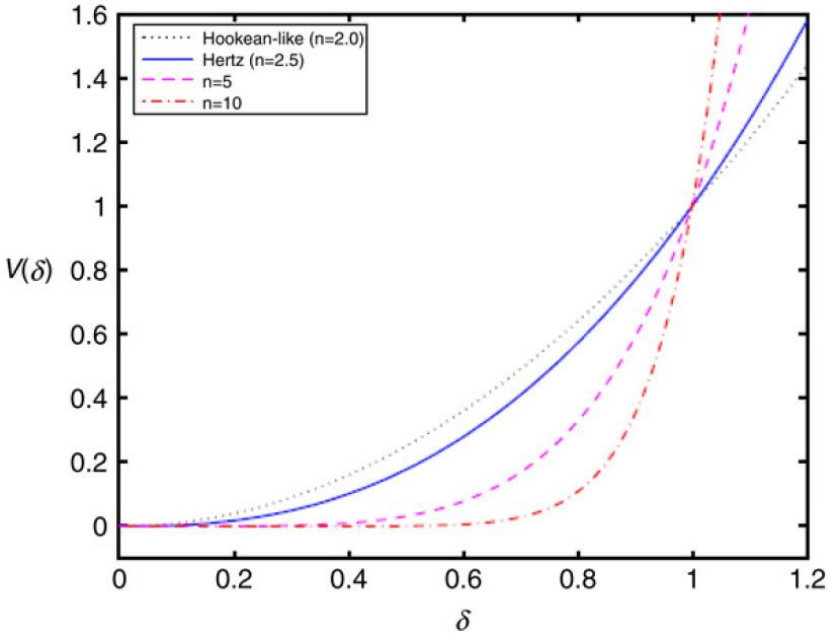

Fig. 2.3 Plot of Potential Energy $V(\delta)$ against overlap parameter δ. The dashed green line represents $V(\delta) \propto \delta^2$ (harmonic dependence) while the solid blue line represents $V(\delta) \propto \delta^{5/2}$ (Hertz dependence). The plot shows that the harmonic dependence is steeper than Hertz potential at small δ but at sufficiently larger δ Hertz Potential is steeper. The dashed pink and red lines n = 5 and n = 10 (n is the overlap between the particles in the chain) show how the potential steepens as n increases [17].

2.3. Solitary Waves in Granular Hertz-like Systems

A mass-spring system could be used as an analogy of a granular Hertzian system. It can be describe as a series of masses coupled by a spring with a known stiffness. An analytical solution for such a system can be derived by observing the equation of motion governing the dynamics of particle displacement. When expressed as a series of coupled nonlinear differential equation with an index $3/2$ of the Hertz's law, the equation of the motion of the particle is:

$$\ddot{u}_i = \frac{1}{2m\theta}\sqrt{\frac{a}{2}}\left\{[\delta_0 - (u_i - u_{i-1})]^{\frac{3}{2}} - [\delta_0 - (u_{i+1} - u_i)]^{\frac{3}{2}}\right\} \tag{2.12}$$

where m is the mass, θ is the effective Young's modulus associated with contact interactions, u_i is the displacement of the i[th] particle from its equilibrium position, and $\ddot{u}_i$ is its second derivative.,

To minimise the length of the equation; let's introduce an arbitrary parameter, say J_0, where

$$J_0 = \frac{1}{2m\theta}\sqrt{\frac{a}{2}} \tag{2.13}$$

When two identical elastic spheres of radius a are in contact and submitted to a static force f_0, the distance of approach δ_0 of their centres can be expressed as:

$$\delta_0 = \frac{2(\theta f_0)^{\frac{2}{3}}}{a^{\frac{1}{3}}}, \qquad where\ \ \theta = \frac{3(1-\sigma^2)}{4Y} \tag{2.14}$$

Substituting equation (3.13) into (3.14) gives:

$$\ddot{u}_i = J_0\left\{[\delta_0 - (u_i - u_{i-1})]^{\frac{3}{2}} - [\delta_0 - (u_{i+1} - u_i)]^{\frac{3}{2}}\right\} \tag{2.15}$$

Now use non-dimensionalised and normalised time $\quad \tau = w_0 t \Longrightarrow \mathrm{t} = \frac{\tau}{w_0}$ (2.16a)

and non-dimensional distance $\quad X = \frac{u}{a} \Longrightarrow \mathrm{u} = Xa$ (2.16b)

Introducing (3.16a & b) into equation (2.15), gives:

$$\frac{d^2u_i}{dt^2} = \frac{d^2(Xa)}{d\left(\frac{\tau}{w_0}\right)^2} = {w_0}^2 a\frac{d^2X}{d\tau^2}$$

$$= J_0\left\{[\delta_0 - (X_i a - X_{i-1}a)]^{\frac{3}{2}} - [\delta_0 - (X_{i+1}a - X_i a)]^{\frac{3}{2}}\right\} \tag{2.17}$$

$$w_0{}^2 a\frac{d^2X}{d\tau^2} = J_0\left\{\left[a\left(\frac{\delta_0}{a} - (X_i - X_{i-1})\right)\right]^{\frac{3}{2}} - \left[a\left(\frac{\delta_0}{a} - (X_{i+1} - X_i)\right)\right]^{\frac{3}{2}}\right\} \quad (2.18)$$

$$w_0{}^2 a\frac{d^2X}{d\tau^2} = J_0 a^{\frac{3}{2}}\left\{\left[\left(\frac{\delta_0}{a} - (X_i - X_{i-1})\right)\right]^{\frac{3}{2}} - \left[\left(\frac{\delta_0}{a} - (X_{i+1} - X_i)\right)\right]^{\frac{3}{2}}\right\} \quad (2.19)$$

$$remember\ J_0 = \frac{1}{2m\theta}\sqrt{\frac{a}{2}}.\ Hence\ the\ term\ J_0 a^{\frac{3}{2}}\ from\ equation\ 3.19\ becomes\ \frac{a^2}{2\sqrt{2}m\theta}$$

Therefore equation (3.20) becomes,

$$w_0{}^2\frac{d^2X}{d\tau^2} = \frac{a}{2\sqrt{2}m\theta}\left\{\left[\left(\frac{\delta_0}{a} - (X_i - X_{i-1})\right)\right]^{\frac{3}{2}} - \left[\left(\frac{\delta_0}{a} - (X_{i+1} - X_i)\right)\right]^{\frac{3}{2}}\right\} \quad (2.20)$$

From equation (2.12), it can be observed that no excitation term is present, incorporating an excitation term $f_m \sin(wt)$ into the equation gives:

$$\ddot{u}_i = \frac{1}{2m\theta}\sqrt{\frac{a}{2}}\left\{[\delta_0 - (u_i - u_{i-1})]^{\frac{3}{2}} - [\delta_0 - (u_{i+1} - u_i)]^{\frac{3}{2}}\right\} + \frac{f_m}{m}\sin(wt) \quad (2.21)$$

Solving the equation by performing the steps from equations (2.13) to (2.21), will give:

$$w_0{}^2 a\frac{d^2X}{d\tau^2} = \frac{a^2}{2\sqrt{2}m\theta}\left\{\left[\left(\frac{\delta_0}{a} - (X_i - X_{i-1})\right)\right]^{\frac{3}{2}} - \left[\left(\frac{\delta_0}{a} - (X_{i+1} - X_i)\right)\right]^{\frac{3}{2}}\right\} + \frac{f_m}{m}\sin(wt) \quad (2.22)$$

$$w_0{}^2\frac{d^2X}{d\tau^2} = \frac{a}{2\sqrt{2}m\theta}\left\{\left[\left(\frac{\delta_0}{a} - (X_i - X_{i-1})\right)\right]^{\frac{3}{2}} - \left[\left(\frac{\delta_0}{a} - (X_{i+1} - X_i)\right)\right]^{\frac{3}{2}}\right\} + \frac{f_m}{ma}\sin\left(\frac{w}{w_0}\tau\right) \quad (2.23)$$

$$if\ {w_0}^2 = \frac{a}{2\sqrt{2}m\theta}, \text{then equation (2.23) becomes:}$$

$$\frac{d^2X}{d\tau^2} = \left\{\left[\left(\frac{\delta_0}{a} - (X_i - X_{i-1})\right)\right]^{\frac{3}{2}} - \left[\left(\frac{\delta_0}{a} - (X_{i+1} - X_i)\right)\right]^{\frac{3}{2}}\right\} + \frac{f_m 2\sqrt{2}\theta}{a^2}\sin\left(\frac{w}{w_0}\tau\right) \qquad (2.24)$$

The system derived from the above series of equations is highly sensitive; the propagation of the wave changes depending on several factors such as the input frequency, the diameter and material properties of the spheres. An important parameter is the cut-off frequency, f_c, which represents the highest frequency that can exist in the chain, a consequence of the propagation mechanism (whereby the centres of the spheres move). The cut-off frequency specifies the upper limit within which the nonlinear behaviour for a given radius can be observed. The cut-off frequency, f_c can be calculated using the following expression:

$$f_c = \frac{1}{\pi}\sqrt{\frac{k}{m}} \qquad (2.25)$$

$$if, k = \frac{mg}{\Delta x}, and\ m = \frac{4}{3}\pi r^3\rho$$

Where: g is acceleration due to gravity, Δx is change in distance, m is mass, ρ is density and k is spring constant. Equation (2.25) then becomes:

$$fc = \frac{1}{\pi}\sqrt{\frac{mg/\Delta x}{4/3\ \pi a^3\rho}} = \frac{1}{2\pi}\sqrt{\frac{3mg}{\pi a^3 \Delta x\rho}} \qquad (2.26)$$

Let's consider a steel sphere with the following parameters: $m = 0.032\ kg,\ a = 1\ mm,\ \Delta x = 1\ mm, k = 1000\ kg/s^2,\ \rho = 7700\ kg/m^3\ and\ g = 10\ m/s^2$.

The cut-off frequency f_c within which the required behaviour can be observed is then 177.3 kHz.

The linear approximation of equation (2.12), obtained in the limit $|u_n - u_{n-1}|$, provides a linearized spring constant which takes into account the pre-compression force and material properties [18]. Hence, further narrowing the range of cut-off frequency to investigate:

$$k \equiv \left(\frac{\partial \delta_0}{\partial f_0}\right)^{-1} = \frac{3(af_0)^{\frac{1}{3}}}{4\theta^{\frac{2}{3}}} \tag{2.27}$$

$$f_c = \frac{1}{\pi}\sqrt{\frac{k}{m}} = \frac{3{f_0}^{\frac{1}{6}}}{4\pi^{\frac{3}{2}}\theta^{\frac{1}{3}}a^{\frac{4}{3}}\rho^{\frac{3}{2}}} \tag{2.28}$$

Using the same values for the steel sphere and $Y = 200\ GPa\ and\ \sigma = 0.30$ where, $\theta = \frac{3(1-\sigma^2)}{4Y}$

$$f_c = 101{,}953.04{f_0}^{\frac{1}{6}} \simeq 102{,}000{f_0}^{\frac{1}{6}}$$

Table 2.1 shows the dependence of cut-off frequency on applied static force.

$\boldsymbol{f_0}$ $(\boldsymbol{N})$	0.1	1	10	10^2	10^3	10^4	10^5	10^6
$\boldsymbol{f_c}$ $(\boldsymbol{Hz})$	69460	102,000	249,647	219,657	322,404	473,274	694,598	1,019,530

Table 2.1 Cut-off frequencies for various pre-compression using $f_c \simeq 102{,}000{f_0}^{\frac{1}{6}}$

Changing θ would change the value of f_c. Increasing θ decreases the effect of $\theta^{\frac{-1}{3}}$. Since, the Poisson's ratio for various materials have miniscule difference, changing this would have minimal effect. However, Young's modulus varies greatly from one material to another (as shown in Table 2.2) such that $\theta \propto 1/Y$.

Material	**Density (*Kg/m^3*)**	**Young's Modulus (*GPa*)**	**Poisson's Ratio**
Delrin	1410	3.5	0.30
Steel	7700	200	0.30
Tungsten Carbide	15630	530	0.31

Table 2.2 Physical properties for various materials.

Fig. 2.4 demonstrates the effect of varying the static pre-compression for different radii of a steel sphere. For the largest radius 1 mm, a big change in f_0 produces a smaller change in f_c. As the radius decreases from 1 mm – 0.1 mm, the effect of f_0 on f_c increases exponentially. A small increase in f_0 produces a large increase in f_c. This suggests that as the size of the sphere tends towards the sub-millimetre range, the system operates at a broader range of frequencies while systems with larger spheres operate over a narrower frequency range (with a lower cut-off frequency). In addition, Fig. 2.5, shows materials with various Young's modulus, where it can be seen that the denser the material or the greater the Young's modulus, the bigger the range of frequencies the chain of spheres can operate in.

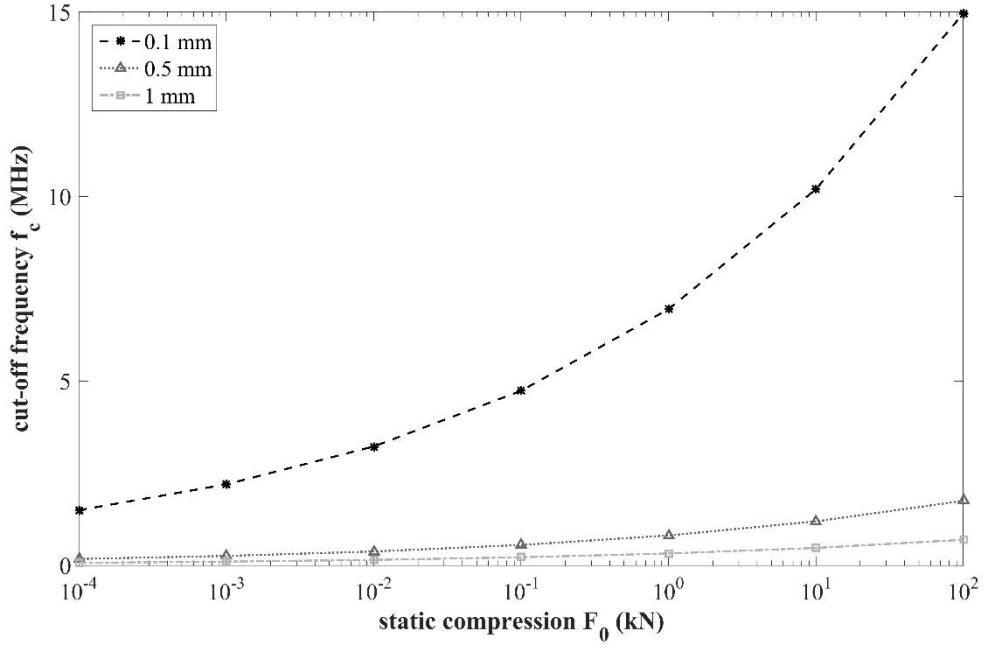

Fig. 2.4 Cuff-0ff frequency for different radii.

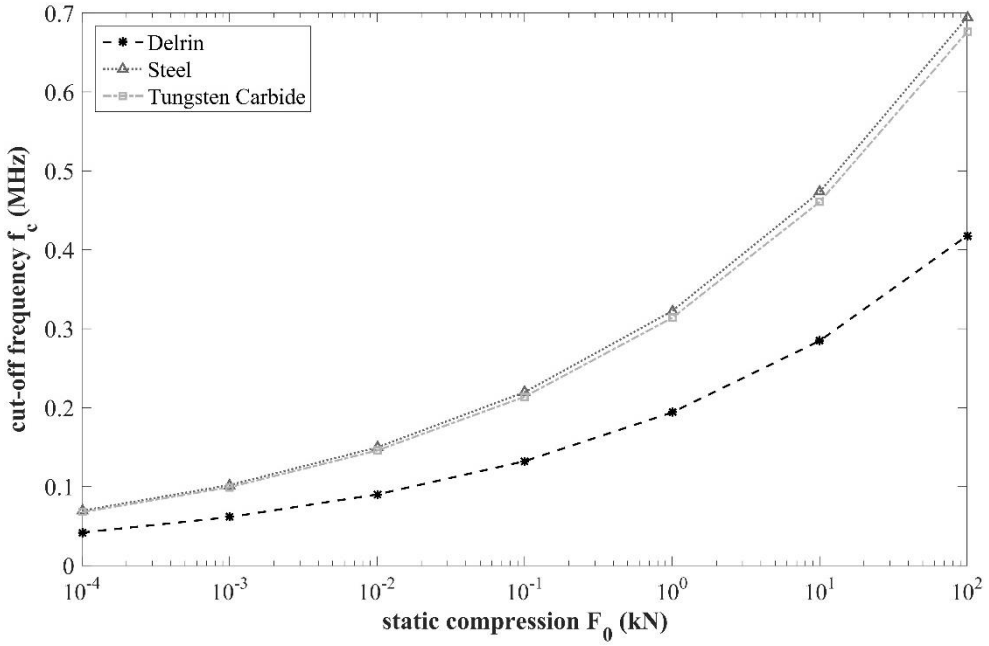

Fig. 2.5 Cuff-0ff frequency for different materials.

In 1983, Nesterenko [19] demonstrated that granular chains consisting of identical elastic spheres under Hertzian contact could support the propagation of solitary waves. He demonstrated that strong compressional waves (waves with an amplitude greater than the applied static compression) may propagate as solitary waves within the chain. Nesterenko's wave equation derived from Hertz law (equation (2.2)) for such a system is described as [20]:

$$u_{tt} = c^2 \left[\frac{3}{2} (-u_x)^{1/2} u_{xx} + \frac{a^2}{8} (-u_x)^{1/2} u_{xxx} - \frac{a^2}{8} \frac{u_{xx} u_{xxx}}{(-u_x)^{1/2}} - \frac{a^2}{64} \frac{(u_{xx})^3}{(-u_x)^{3/2}} \right] \tag{2.29}$$

where u is displacement and a is the initial distance between the particles of undisturbed system. This expression can be used to predict the type of solitary wave that would exist in long chains of spheres in Hertzian contact, and specifically treats the situation where there is no applied static force f_0 holding the spheres together, and where the chain is infinitely long (*i.e*. reflections from the ends of the chain are not considered). Under these conditions, the expression predicts that the spatial size of the solitary wave is independent of the amplitude of the solitary wave's velocity and the spatial size would be equal to five sphere diameters as shown in Fig 2.6; calculated for a long chain comprising of 1 mm diameter spheres

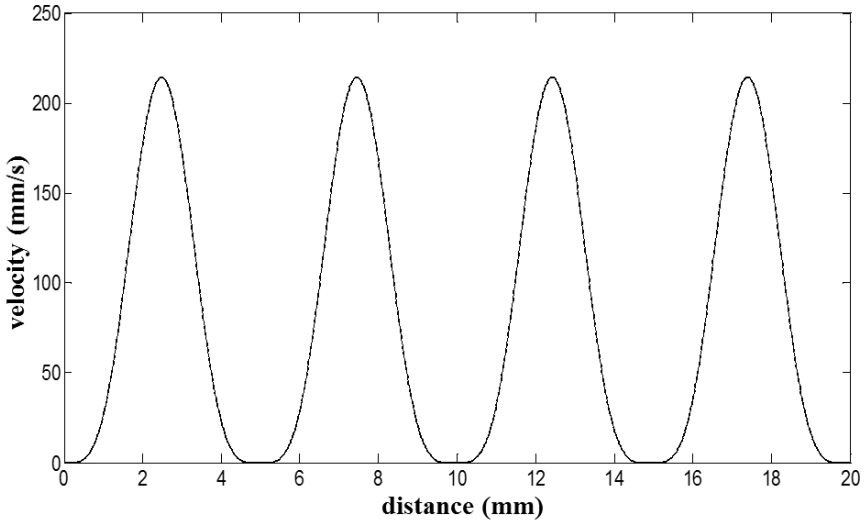

Fig. 2.6. Velocity profile of a solitary wave calculated for a 1 mm diameter chain of spheres using Nesterenko's solution.

Generating solitary waves requires both non-linearity and dispersion to exist, and in fact this is a natural occurrence within such chains. This prediction for long chains will not hold for the situation to be studied in this thesis, where the chains will be of finite length (up to a maximum of 10 for practical considerations). In these cases, reflections will occur within the chain, and these are likely to set up a situation, where normal modes (resonances) are established, this situation will be described in the next chapter.

2.4 Techniques of Generating Solitary Waves in Granular Chains

The following experiments describe some of the work reported at low frequencies, where the aim was to generate high amplitude impulses, and to measure their properties. These approaches have been shown to generate the special properties arising from non-linear Hertzian contact between successive spheres as described in earlier sections. It will be demonstrated that the result from such systems result in harmonic generation, and the ability to change sound velocity along the chain using applied static force.

2.4.1. One-dimensional Diatomic Periodic Chains

One-dimensional chains of particles arranged in accordance to Hertz's contact law are pertinent in investigating linear, weakly nonlinear and strongly nonlinear wave dynamics of chains composed of different particle-particle arrangements subjected to different conditions of loading and pre-loading [21]. An elastic diatomic chain can be constructed from the periodic arrangements of materials with different properties and masses, which may be initially compressed to produce linear wave or weakly compressed for nonlinear waves.

From an experimental perspective, this can be achieved by employing a system of one-dimensional nonlinear crystals consisting of periodic diatomic chains of stainless steel cylinder with alternating Polytetrafluoroethylene (PTFE) spheres. The elastic contact between the soft PTFE spheres and the rigid stainless steel cylinders produces a low elastic modulus that results to a frequency band-gap effect on the system, restricting the propagation of acoustic waves within the audible frequency range (20 – 20,000 Hz) for linear propagation [22].This assembly provides an easy change in behaviour from linear to strongly nonlinear by applying compressive force without altering the geometry of the system [23]. The setup shown in Fig. 2.7 consists of 18 stainless steel cylinders with height: 3.12 mm, diameter: 4.96 mm and mass: 0.485 g and 19 PTFE spheres of diameter: 4.76 mm and mass: 0.1226 g placed vertically in a PTFE cylinder with an inner diameter of 5 mm in an alternating sequence (sphere-cylinder-sphere). The stainless steel cylinder is used to ensure planar geometry of the contact area as described by Hertz contact law. A compression force of 2.38 N is applied on the chain using a ferromagnetic steel particle placed at the top of the chain. This produces an overlap parameter, $\delta = 7.34$ μm (*i.e.* decreases the distance between the centres of the particles).

Force amplitude readings can be measured using three piezoelectric sensors embedded in one stainless steel cylinder and two PTFE sphere at evenly spaced intervals (counting from the top;

positions 2, 14 and 17 in chain). A pulse is generated using a cylindrical striker made from Al_2O_3 with an impact velocity of 0.44 m/s.

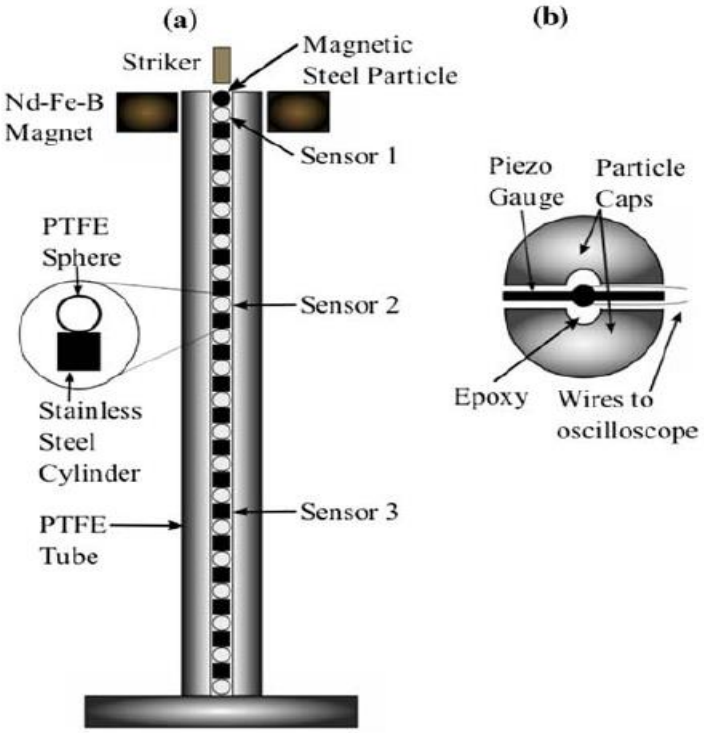

Fig. 2.7: A diagram of diatomic chain configuration. (a) The diatomic chain consisting of 18 stainless steel cylinders, 19 PTFE spheres, 3 piezoelectric sensors embedded inside the particles, 2 magnets and an alumina striker (b) An inset of a PTFE particle with an embedded sensor [23].

The results of the experiment in a nonlinear setup (without the use of the two Nd-Fe-B magnets) with a static force induced by gravitational preload and when the chain was struck with a PTFE striker of mass 0.62 g at 0.44 m/s is shown in Fig. 2.8. This impact created a single main pulse shown in Fig. 2.8 (a) and its frequency spectrum in Fig. 2.8 (b). The blue curve represents reading from the 1st sensor the green: 2nd second and the red: 3rd sensor.

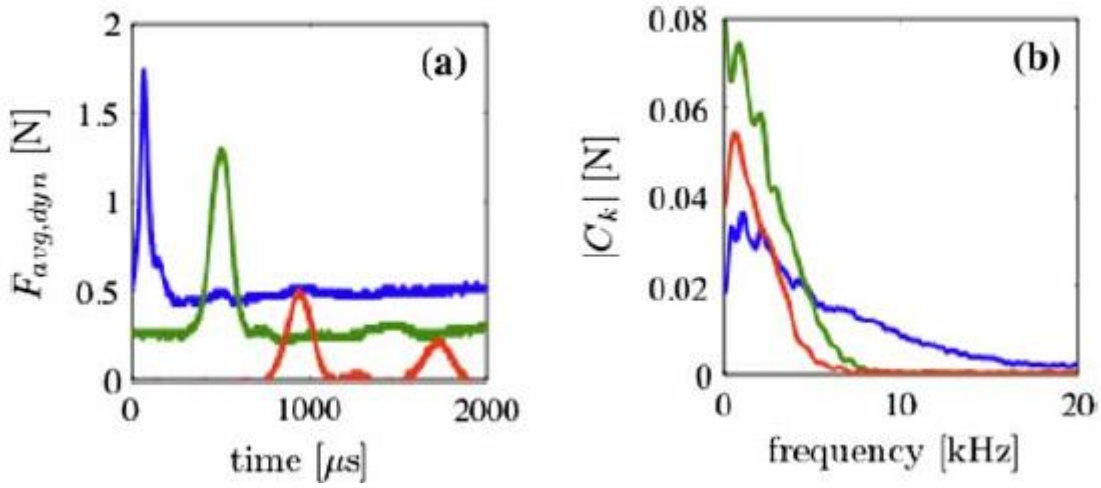

Fig. 2.8 Strongly nonlinear propagation with only gravity as static pre-compression using a striker of mass 0.61 g and an initial velocity of 0.44 m/s. (a) Shows the force against time behaviour observed at the 1st (blue waveform), 2nd (green waveform) and 3rd (red waveform) sensors. (b) Is the corresponding frequency response [23].

An average speed of 118 m/s was observed between the 2nd and 3rd sensors and time duration of 330 μs for the leading solitary wave at the 2nd sensor. The Fourier spectrum for the strongly nonlinear propagation Fig. 2.8 (b) is similar to that of Fig. 2.9 (b), because of the similar durations of the initial pulses. However, the speeds are different under the different mode of propagation (linear, weakly nonlinear and strongly linear) as shown in Table 2.3.

In both cases of nonlinear propagation the frequency spectrum tends towards lower frequencies with a more pronounced shift in the strongly nonlinear mode and a larger pulse width in the frequency versus time plot. This is due to amplitude attenuation that generates longer signal duration with the same spatial width.

Striker mass (g)	Weakly nonlinear pulse speed (m/s)	Strongly nonlinear pulse speed (m/s)
0.61	175	118
1.22	177	121
2.75	181	122

Table 2.3: A comparison of average speed of leading pulses between the 2nd and 3rd sensors.

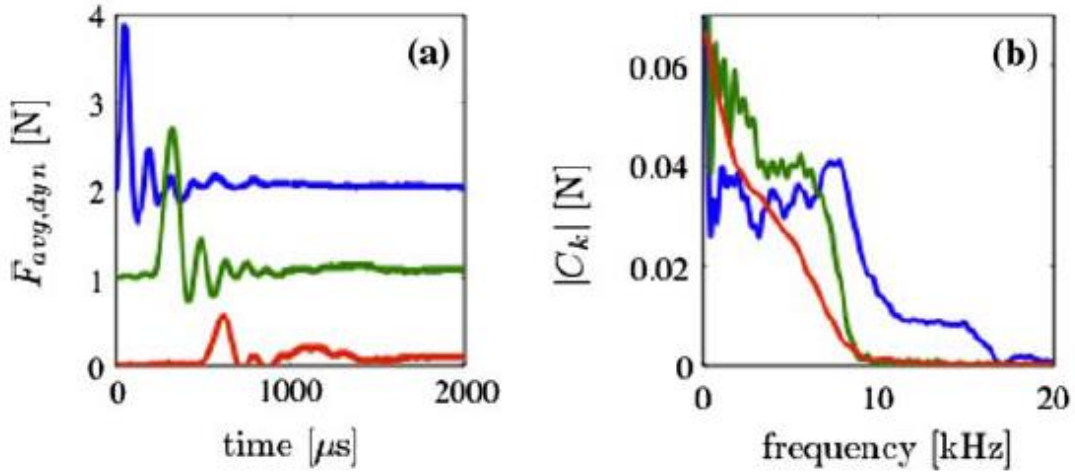

Fig. 2.9 weakly nonlinear propagation with a static force of 2.38 N using a striker of mass 0.61 g and an initial velocity of 0.44 m/s. (a) Shows the force against time behaviour observed at the 1st (blue waveform), 2nd (green waveform) and 3rd (red waveform) sensors. (b) Is the corresponding frequency response. [23].

2.4.2. **Heterogeneous Periodic Granular Media**

The use of chains containing periodic arrangements of dimer (two-mass) cell structures in a one-dimensional granular lattices is based on research performed by Nesterenko [24]. Spheres of different materials; stainless steel, bronze, PTFE, glass and rubber are used to vary the composition of the granular chains. This facilitates the ability to broadly vary the response of the system based on the elastic moduli, masses and Poisson ratios of the components. In contrast to chains that support traditional nonlinear solitary waves, these configuration features a double nonlinearity formed due to the nonlinear contact present between the particles and a zero tensile response to the contact [25].

The setup comprises of a dimer chain consisting of vertically aligned spheres in a guide made of four vertical rods of Garolite (a glass fibre reinforced polymer composite) in a square lattice, as seen in Fig. 2.10. The material of the spheres in each section (N1 and N2) differ. Each section consist of spheres of one type of material different from the other sections and repeated in an alternating pattern (N1-N2-N1-N2) with N1 and N2 having a fixed length between 1 and 5. With an arrangement of a few combination of material configuration (Steel: PTFE, Steel:

Rubber, Steel: Bronze and PTFE: Glass chains) and chain order; N1=1sphere:N2=1sphere (*i.e.* 1:1) containing 19 and 38 spheres with a diameter of 4.76mm. Three sensors are embedded within the chain of spheres and a fourth in the bottom wall of the frame. A striker is used to generate a pulse by dropping it on the chain from various heights.

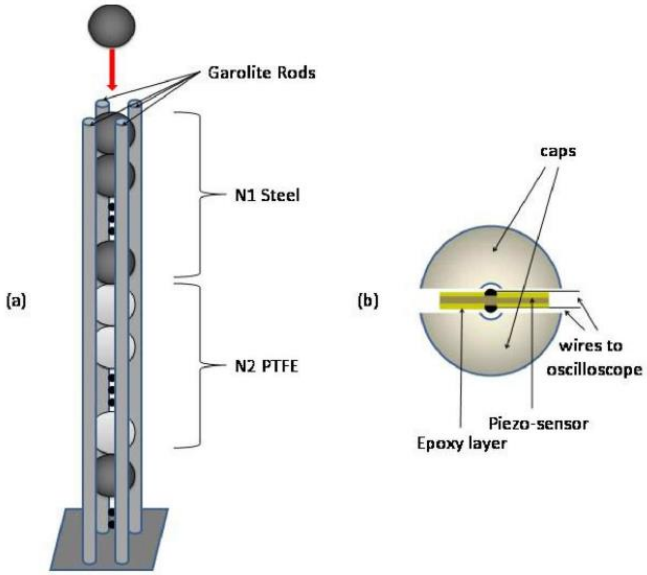

Fig. 2.10: (a) Experimental configuration for a dimer chain comprised of a periodic array of cells with N1 consecutive spheres of one material (e.g. stainless steel) and N2 of another material (e.g. Rubber). (b) Diagram of the composition of the sensors embedded in the sphere and wall. [25].

The results for the 1:1 dimers of steel: PTFE chain consisting of 38 spheres and steel: rubber chain with 19 spheres are shown in Fig. 2.11. The Figures show that the initial pulse develops into a solitary wave within the first 10 particles of the chain. With both chains supporting the formation of solitary-like-waves, however the inherently nonlinear elastic components in the steel: rubber chain is highly dissipative and the solitary waves are short lived (Fig. 2.11 (b)). In the steel: rubber chain the initial pulse is short and rapidly transformed into a slower and wider pulse unlike the narrower pulse in the steel: PTFE chain. The dissipation found in the steel: rubber chain dampens the propagation of the wave shortly after the 15^{th} sphere in the chain.

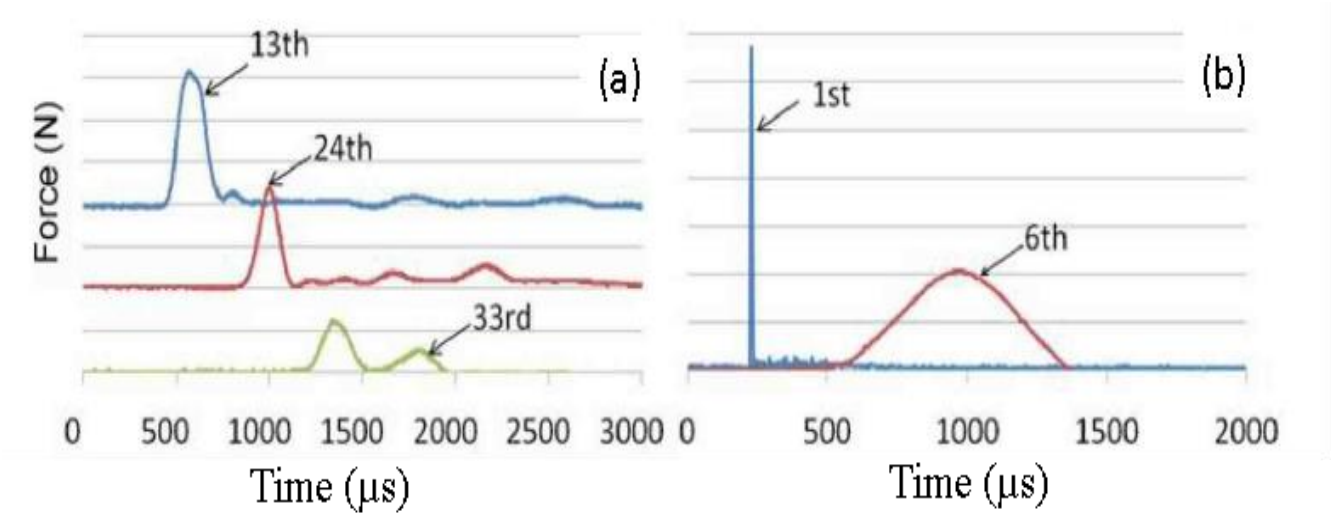

Fig. 2.11: Force against time for dimer chains containing (a) 1 stainless steel sphere alternating with 1 PTFE with a total of 38 particles (b) 1 stainless steel sphere alternating with 1 rubber sphere with a total of 19 spheres. The initial velocity of the striker is 1.37m/s on impact for both configurations. The y-axis scale is 2N per division for (a) and 20N per division in (b). The numbered arrows correspond to particles in the chain, in (a) and (b) the red curve corresponds to the 24th particle (PTFE) and 6th particle (steel) [25].

In a configuration comprising of steel: bronze (38 spheres) and PTFE: glass (34 spheres), two important characteristics were observed relating to the width and propagation speed of the pulse propagating along the chain. The speed was estimated by determining how long it took for the pulse to travel between the sensors embedded in the spheres. These values can be observed in Fig. 2.12. In Fig. 2.12 (a), the result for the steel: bronze chain struck using a steel sphere with an initial velocity of 1.21 m/s, generated a pulse speed of 499.2 m/s with a width of about 2.03 spheres. Fig. 2.12 (b) shows the results from the PTFE: glass which was struck with a glass striker with an initial velocity 1.17 m/s. In this case the pulse speed is significantly lower at 151.7 m/s with a width equal to 1.99 spheres.

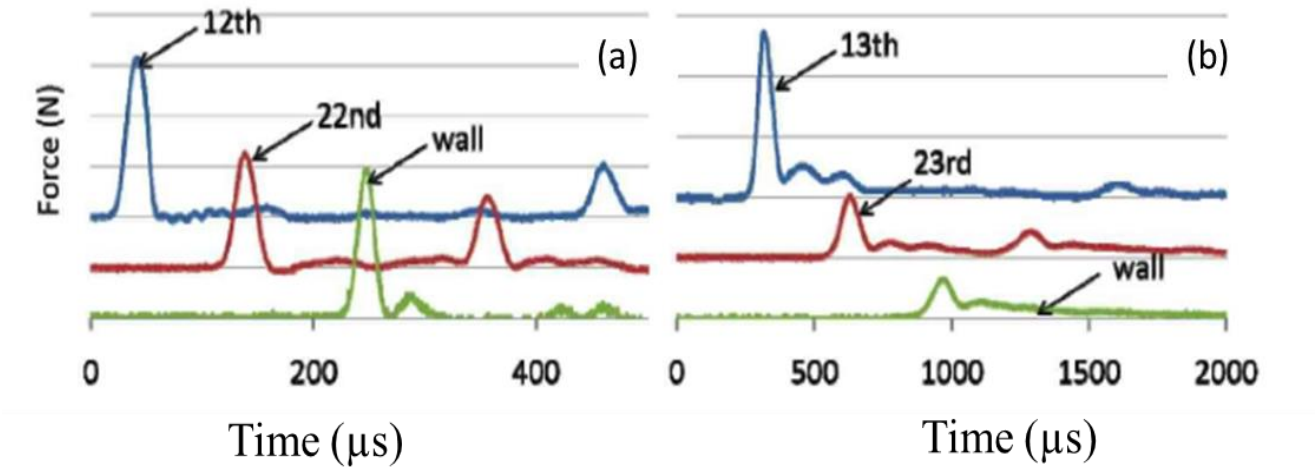

Fig. 2.12: Force against time for dimer chains containing (a) 1 steel sphere alternating with 1 bronze sphere with a total of 38 particles (b) 1 PTFE sphere alternating with 1 glass sphere with a total of 19 spheres. The y-axis scale is 5N per division for (a) and 20N per division in (b). The numbered arrows correspond to the sensor embed in the particles in the chain and the wall. [25].

Both configurations were reported to support the formation and propagation of nonlinear waves; however, some of the signal properties were different. This was reported to be due to the different physical properties (elastic moduli and Poisson ratios; shown in Table 2.2) of the material used. The widths were similar in both configurations, and the masses of the particles were also similar in each configuration (*i.e.* steel ≈ bronze), this showed that there was a relationship between the mass and the width in dimer chains.

Materials	**Mass (g)**	**Modulus E**	**Poisson Ration v**
Steel	0.45	193 GPa	0.3
PTFE	0.123	1.46 GPa	0.46
Rubber	0.08	30 MPa	0.49
Bronze	0.48	76 GPa	0.414
Glass	0.137	62 GPa	0.2

Table 2.4: Material properties.

2.4.3. **Multi-dimensional Array of Granular Chains for Focussing**

This was accomplished by using a nonlinear acoustic lens comprised of ordered arrays of granular chains [26]. The lens is made of aluminium with the dimension: 30.3 x 23 x 7.6 cm and containing 21 chains each consisting of 21 (9.5 mm diameter) stainless steel spheres (shown in Fig. 2.13). The topmost sphere of each chain was threaded with fishing line and secured to the case of the lens which was used to attach weights for applying compression. A 2.5 cm long screw was also embedded in the 1st sphere of each chain, this was aligned with an impacting plate with 21 holes to accommodate the 21 screws protruding from the spheres. An accelerometer was attached to the impacting rod to activate a high speed camera triggered 280 μs after impact. The camera acquired images at 300,000 samples per second.

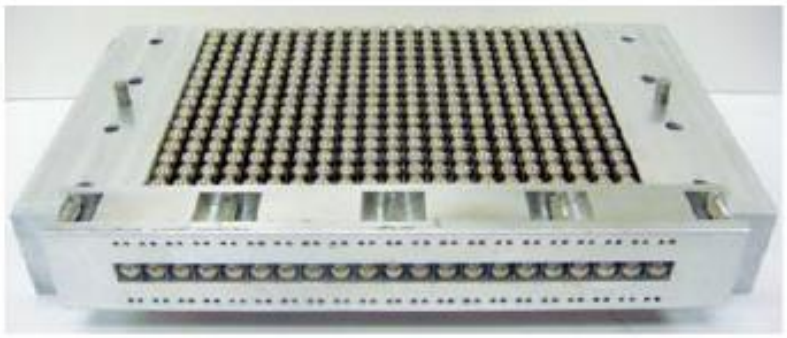

Fig. 2.13: Nonlinear acoustic lens consisting of 21 chains containing 21 steel spheres with density = 8100 kg/m3, Young's modulus = 195.6 GPa and diameter = 9.5 mm [26].

Each chain in the array was subjected to different static force such that an acoustic wave with a fixed phase incident on the acoustic lens produced transmitted waves with phase delays. The static force, f_0 and phase delays were chosen to ensure that the waves from each chain converged at a focal point, as illustrated in Fig. 2.14. Since, the phase velocity was determined by f_0, the distribution of f_0 could be selected to focus the acoustic energy into a sound bullet. The focusing depended on the lens's symmetry axis $f(x_1, y_1)$ when f_0 is symmetric about it (the dashed line in Figure 2.14) or off the symmetry axis $f(x_2, y_2)$; when f_0 is asymmetric (solid line).

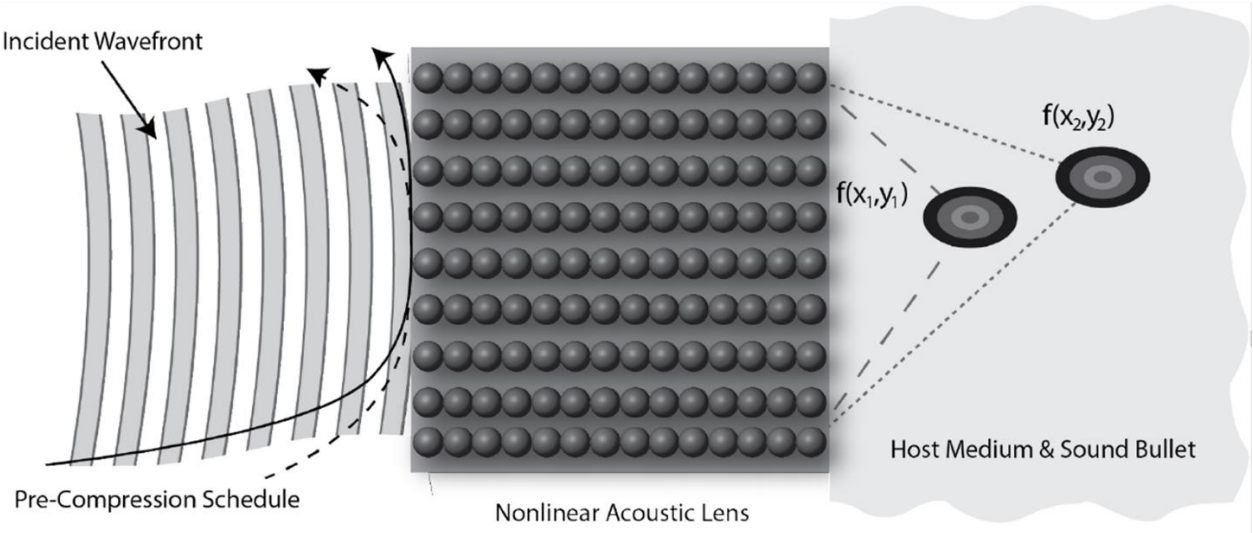

Fig. 2.14: Focusing of an acoustic lens [26].

When the impacting plate struck the lens at a velocity of 1m/s, an impulse was generated, illustrated in Fig. 2.15, the phase delay (Fig. 2.15 A) of the transmitted compact pulses after they were generated is shown Fig. 2.15 B and Fig. 2.15 C shows the focusing of the acoustic energy with a symmetric pressure distribution with one maximum and one minimum.

The generation of compact solitary waves was due to the nonlinearity and dispersion balance of the lens [27]. This property is retained even if the amplitude of the input is increased as long as the force deformation power is unaltered.

Therefore, the pressure amplitude of the sound bullets generated as a result of the constructive interference of the compact waves increased as the impact velocity increases. It was also observed that when a larger striker mass was used, a shock wave like propagation occurred within the lens (Fig. 2.15 D), instead of the solitary compact wave observed while using a smaller striker (Fig. 2.15 E).

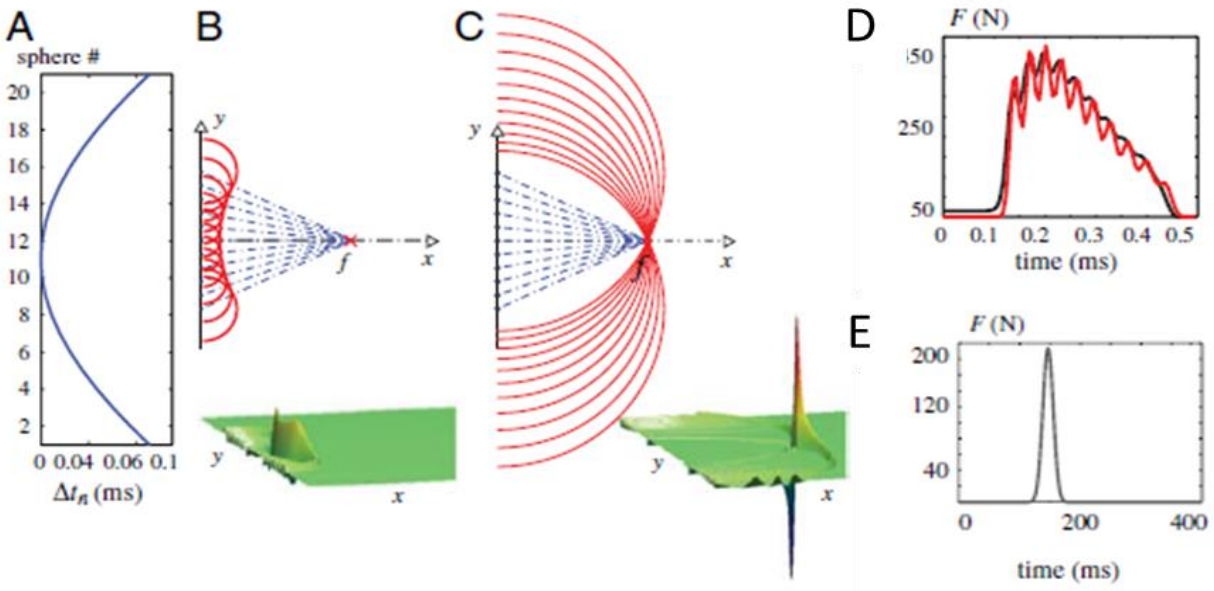

Fig. 2.15: (A) Time delay distribution required to achieve a focal point in air at x_f = 13 cm and y_f = 0cm, along the lens's symmetry. (B) The wave form generated shortly after striker impact, blue dashed line represent ray path and red indicates lines in constant phase. (C) Wave field as a result of the pressure when the acoustic energy collates at the focal point. (D) Shock like waves within the lens when a large mass striker is used. (E) Compact solitary waves generated when a smaller mass striker is used. [26]

2.5 Conclusions

This Chapter described the processes which occurs when a chain of spheres is subjected to negligible static pre-compression force, and excited using a forced vibration. It has been demonstrated that Hertzian contact leads to the creation of non-linear behaviour between successive spheres, which in turn leads to the creation of solitary waves, using the approach as described by Nesterenko [15]. The concept of cut-off frequency was introduced, indicating that the interesting propagation effects would only be expected at frequencies below a certain upper frequency limit, depending on the exact nature of the chain.

This Chapter has also demonstrated that the behaviour of propagating vibrational signals within non-linear granular chains is highly complex, with several parameters that could affect the signals that exist within these systems. Subsequent chapters of this thesis will aim to examine these parameters experimentally, using an ultrasonic high amplitude source to input forcing signals which should lead to the creation of nonlinear resonant modes. The characteristics of these behaviours were studied, and some interesting features were observed which are consistent with the analysis presented in this chapter.

Some relatively recent advances show potential for introducing some interesting possibilities. For example, granular chains have the ability to create interesting effects, such as bandwidth enhancement, due to the non-linear nature of interaction between each particle in the chain. They can also be used to produce a phased array. Research in granular chains has often been performed at low frequencies, as described in this Chapter. The research to be described in the following Chapters shows how propagation in granular chains at ultrasonic frequencies can lead to some very interesting behaviour, and which is likely to generate interest in many field of ultrasound, including HIFU.

2.6 References

1. M. Peyrard, (2004). Nonlinearity Dynamics and Statistical Physics of DNA. Nonlinearity 17(2):R1.
2. Y. S. Kivshar and G. P. Agrawal, (2003). Optical Solitons: From Fibers to Photonic Crystals. Academic Press, San Diego, California.
3. O. Morsch and M. Oberthaler, (2006). Dynamics of Bose-Einstein condensates in optical lattices. Reviews of modern physics, 78(1), 179.
4. A.N. Lazaridi, V.F. Nesterenko, (1985). Observation of a new type of solitary waves in a one dimensional granular medium. Journal of Applied Mechanics and Technical Physics, 26(3) 405–408.
5. V.F. Nesterenko, J. (1994). Solitary waves in discrete media with anomalous compressibility and similar to "sonic vacuum". Le Journal de Physique IV 4, 8-729.
6. V.F. Nesterenko, (1992): Nonlinear waves in “sonic vacuum”. Fizika gorenia i vzryva (in Russian) 28, 121.
7. H. Hertz, (1881). J. Reine Angew. Math. 92, 156.
8. K. L. Johnson, K. Kendall, and A. D. Roberts, (1971). Surface energy and the contact of elastic solids. In Proceedings of the Royal Society of London A: Mathematical, Physical and Engineering Sciences, 324, 301-313.
9. B. V. Derjaguin, V. M. Muller, and Y. P. Toporov, (1975). Effect of contact deformations on the adhesion of particles. Journal of Colloid and interface science, 53(2), 314-326.
10. R.G. Horn, J.N. Israelachvili, and F. Pribac, (1987). Measurement of the deformation and adhesion of solids in contact. Journal of colloid and interface science, 115(2), 480-492.
11. V. M Muller, V. S. Yushchenko, and B. V. Derjaguin, (1980). On the influence of molecular forces on the deformation of an elastic sphere and its sticking to a rigid plane. Journal of Colloid and Interface Science, 77(1), 91-101.
12. V. M Muller, V. S. Yushchenko, and B. V. Derjaguin, (1983). General theoretical consideration of the influence of surface forces on contact deformations and the reciprocal adhesion of elastic spherical particles. Journal of Colloid and Interface Science, 92(1), 92-101.
13. H. Hertz, J. Reine. Angew (1881). Math. 92, 156.
14. E. Falcon, Ph.D. Thesis, (1997).´L Universite Claude Bernard – Lyon I.

15. V. F. Nesterenko, (2001). Dynamics of Heterogeneous Materials. New York, USA: Springer-Verlag.
16. A.E.H. Love, (2003). A Treatise on the Mathematical Theory of Elasticity, Dover, New York.
17. S. Sen *et al*. (2008). Solitary waves in the granular chain. Physics Reports 462, 21–66.
18. Coste, C., Falcon, E., & Fauve, S. (1997). Solitary waves in a chain of beads under Hertz contact. Physical Review E, 56(5), 6104.
19. V. F. Nesterenko, (1983). Propagation of nonlinear compression pulses in granular media, Journal of Applied Mechanics and Technical Physics, 24(5), 733–43.
20. V. F. Nesterenko, (1994). Solitary waves in discrete media with anomalous compressibility and similar to. Le Journal de Physique IV, 4(C8), C8-729.
21. C. Daraio, V. F. Nesterenko, E. Herbold, S. Jin, (2005). Strongly nonlinear waves in a chain of Teflon beads. Physical Review E, 72, 016603.
22. A. T. Alastalo, J. Kiihamaki, and H. Seppa, (2006). Microelectromechanical delay lines with slow signal propagation. Journal of Micromechanics and Microengineering, 16(9), 1854.
23. E. B. Herbold, J. Kim, V. F. Nesterenko, S. Y. Wang, and C. Daraio, (2009). Pulse propagation in a linear and nonlinear diatomic periodic chain: effects of acoustic frequency band-gap. Acta Mechanica, 205(1), 85-103.
24. V. F. Nesterenko, (2001). Dynamics of Heterogeneous Materials (Springer, New York), 1–136.
25. M. A. Porter, C. Daraio, E. B. Herbold, I. Szelengowicz, P. G. Kevrekidis, (2008). Highly nonlinear solitary waves in periodic dimer granular chains. Physical Review E, 77(1), 015601.
26. A. Spadoni, C. Daraio (2010). Generation and control of sound bullets with a nonlinear acoustic lens. Proceedings of the National Academy of Sciences, 107(16), 7230-7234.
27. V. F. Nesterenko, (1983). Propagation of nonlinear compression pulses in granular media. Journal of Applied Mechanics and Technical Physics, 24(5):733–43.

CHAPTER 3: Solitary Waves in Finite Length Chains

3.1. Introduction

The approach of producing nonlinear waves presented in this thesis is a new departure in terms of periodic structures; by introducing a chain of spheres of finite length excited using a sinusoidal tone-burst, a highly tuneable device is created. This system of a chain of spheres has the ability to generate high amplitude ultrasound that has the potential to radically improve the targeting and destruction of tumours. To the knowledge of this author, the use of a high amplitude sinusoidal tone-burst input from an ultrasonic horn has not been investigated before as an input into such structures at ultrasonic frequencies.

The approach relies on nonlinear propagation through a chain of spheres arranged in series, such that the motion of the spheres is restricted to a single plane and are in Hertzian contact with one another. This creates a nonlinear acoustic system similar to those described is Chapters 2 and 3. The nonlinear nature of the Hertzian contact between the spheres is dependent on the relative values of the oscillating applied force (f_m) and static pre-compression (f_0). Thus, if:

- $f_m \ll f_0$, the chain acts like a continuous medium (a normal solid) producing a linear wave.
- $f_m \approx f_0$, a weakly nonlinear wave in generated.
- $f_m \gg f_0$, propagation through the chain becomes highly nonlinear.

When f_m is considerably larger than f_0, the effect of nonlinearity is thus at its greatest. This nonlinearity would be expected to lead to the generation of broader bandwidth signals and the generation of harmonics. Hence, the concept is that input of a high amplitude signal, from a source such as an ultrasonic horn, would lead to some interesting results in terms of increased bandwidth. The exact nature of these signals needed to be established experimentally, and also

the presence of solitary waves needed to be determined. The effects of factors such as the size, shape and the number of spheres within the chain was also of interest.

This Chapter looks at this process by showing the results from some preliminary experiments. The construction of the apparatus, and some typical waveforms generated by the system, are presented. This experimental work was performed by the present author, and contributed experimentally to a collaboration between the University of Warwick, the University of Leeds and University College London, funded by the Engineering and Physical Sciences Research Council (EPSRC). The preliminary results from this work were published in a recent paper [1]. The theoretical modelling that is also described below was developed as part of this research programme by a postdoctoral researcher. It is presented here briefly, as it will be used to compare predictions with experimental results throughout the rest of the thesis, so as to confirm the observed experimental behaviour in finite-length chains of spheres.

A discussion of non-linear normal modes (NNM) – the resonances that can occur in chains of finite length is presented thereby demonstrating the need to extend Nesterenko's theory. NNM describes the relative motions of the spheres and confirming the existence of sonic vacuum experimentally in a chain of finite length. The Chapter then concludes with experimental observations of the nonlinear normal modes using a high-speed camera, to show that the expected modes are present in the system developed in this research.

3.2. Experimental Arrangement

3.2.1. Basic Design

The basic approach is shown in Figure 3.1. An ultrasonic horn was used to produce high amplitude displacements into a chain of spheres, which had to be held in some form of cylindrical holder. With the horn touching one end of the chain, a small pre-compression force $F_0$was created, as well as an oscillating signal f_m, in this case at 73 kHz. The vibration at the far end of the chain was then measured using a vibrometer.

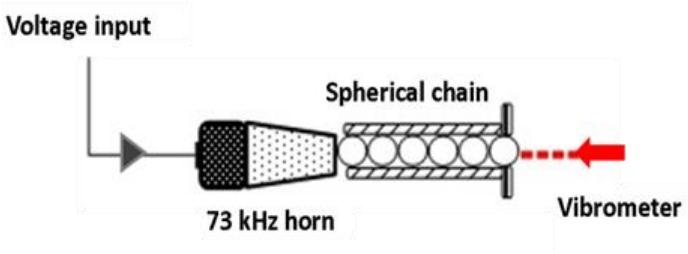

Fig. 3.1 The basic design.

The success of this experiment depended upon some careful experimental design. The first point is that the oscillating input amplitude had to be as high as possible, so that substantial non-linearity could occur. This was why a transducer with a horn incorporated was chosen; it was capable of providing amplitudes of vibration in excess of 1 μm at maximum output, at a frequency of 73 kHz, although there were also other higher frequencies available at lower amplitude. The spheres had to be contained within a holder, which allowed them to be held in a straight line against an exit plate containing a hole. This annular plate was needed, in order to measure the vibration that resulted at the output of the chain. It was decided to use an additive manufacturing method known as Micro-stereolithography (MSL) to create the holder. Finally, a vibrometer was chosen for measuring the output waveform. This gave a particle velocity waveform as output, and was used to compare the waveforms recorded at the last sphere to those of the vibration of the horn tip used as the input to the first sphere. A more detailed diagram of the setup used in the experiments is illustrated in Fig. 3.2.

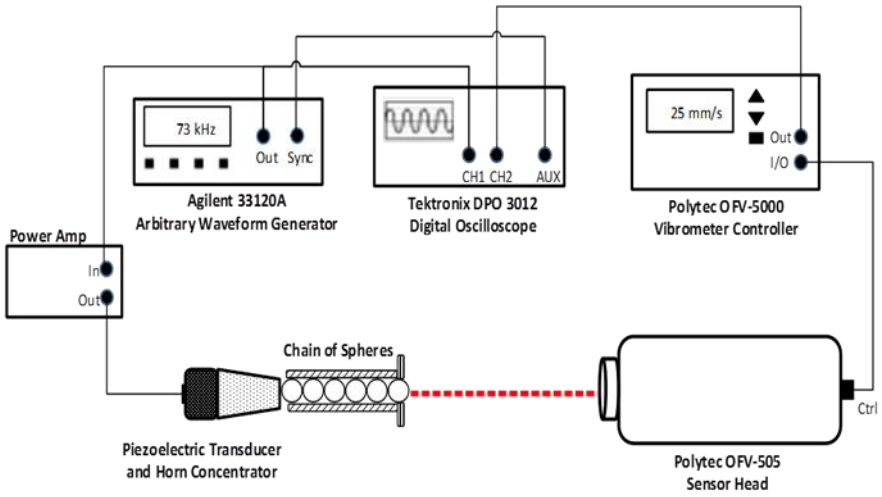

Fig. 3.2. Schematic diagram of the experimental setup.

The first sphere was excited harmonically by a longitudinal ultrasonic horn, operating at 73 kHz, shown in Fig. 3.3. The ultrasonic horn was driven by a high voltage tone-burst signal using an Agilent 33120A function/Arbitrary waveform generator and a power amplifier which produces an output of 160 V peak to peak from an input source of 10 V peak to peak, with a load bandwidth and impedance of 10 kHz – 500 kHz and 50 Ω respectively. Both the horn and the chains of spheres were clamped rigidly onto an optical translation stage, and a micrometre was used to position the horn against the first sphere to produce as little force as possible. The last sphere in the chain was held in place using an annular aperture, allowing detection of the particle velocity waveform at the output via a Polytec laser vibrometry system. The tone-burst duration and amplitude of the drive voltage signal could both be adjusted.

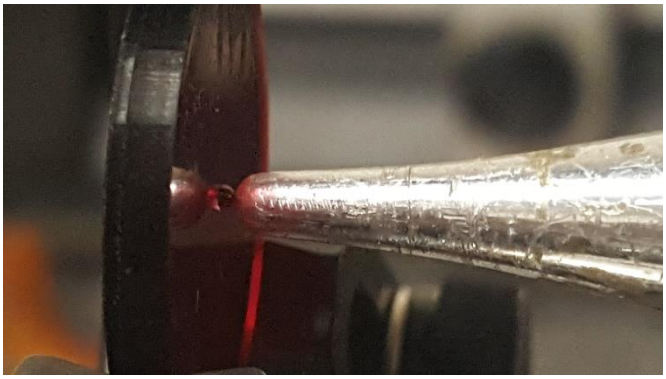

Fig. 3.3. Image of the Horn's tip in contact with the 1st sphere in a cylindrical holder.

The ultrasonic motion of the horn tip at full power, for drive voltage tone-bursts of 20 cycles and 45 cycles in duration, are shown in terms of waveform (v_m) and frequency spectrum in Fig. 3.4 respectively. Both show a prominent peak at 73 kHz, with only a small amount of harmonic content from the vibration of the horn.

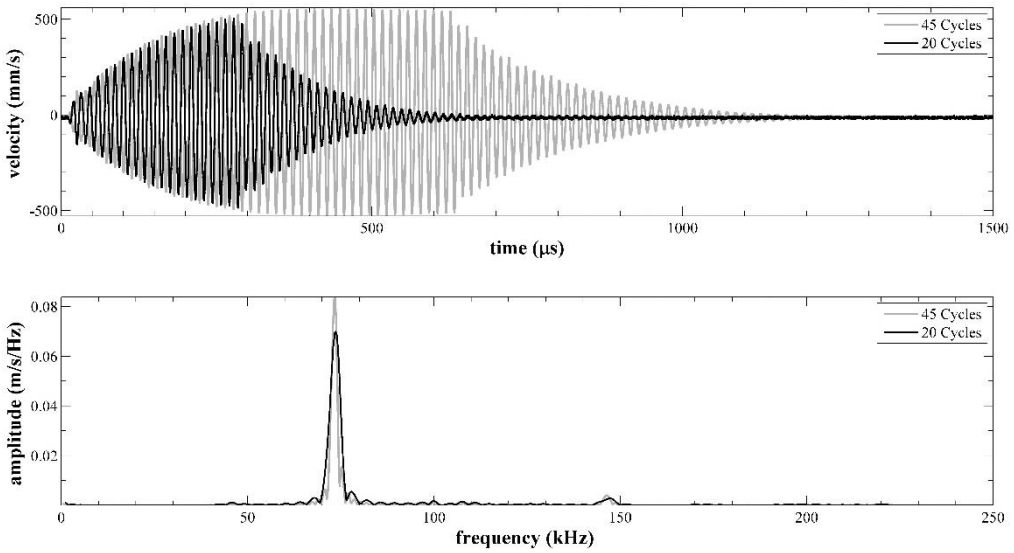

Fig. 3.4. Waveforms (top) and Spectra (bottom) of a 20 and 45-cycle tone burst at 73 kHz.

The tip of the horn was carefully positioned in a fashion that ensured as light and minimal a contact with the first sphere in the chain. The chain of ball bearings were held horizontally within the additively-manufactured cylinder channel with the annular wall end aperture smaller than the diameter of the spheres, which allowed the laser vibrometer to measure the resulting signal viewed and saved using a digital oscilloscope. Both optical translation stages for the transducer and chain of spheres were rigidly fastened onto a steel base plate. The base plate was then screwed onto the optical bench. The base plate provided an approximation of a cradle thereby reducing the vibration loop in the system. The rods used to clamp the chain of spheres and ultrasonic horn could not be shorter than 7 cm. Although shorter rods minimised the vibration loop, they produced a negative effect of introducing high frequency vibrations into the output of the system, while rods longer than 10 cm coupled low frequency vibration into the output.

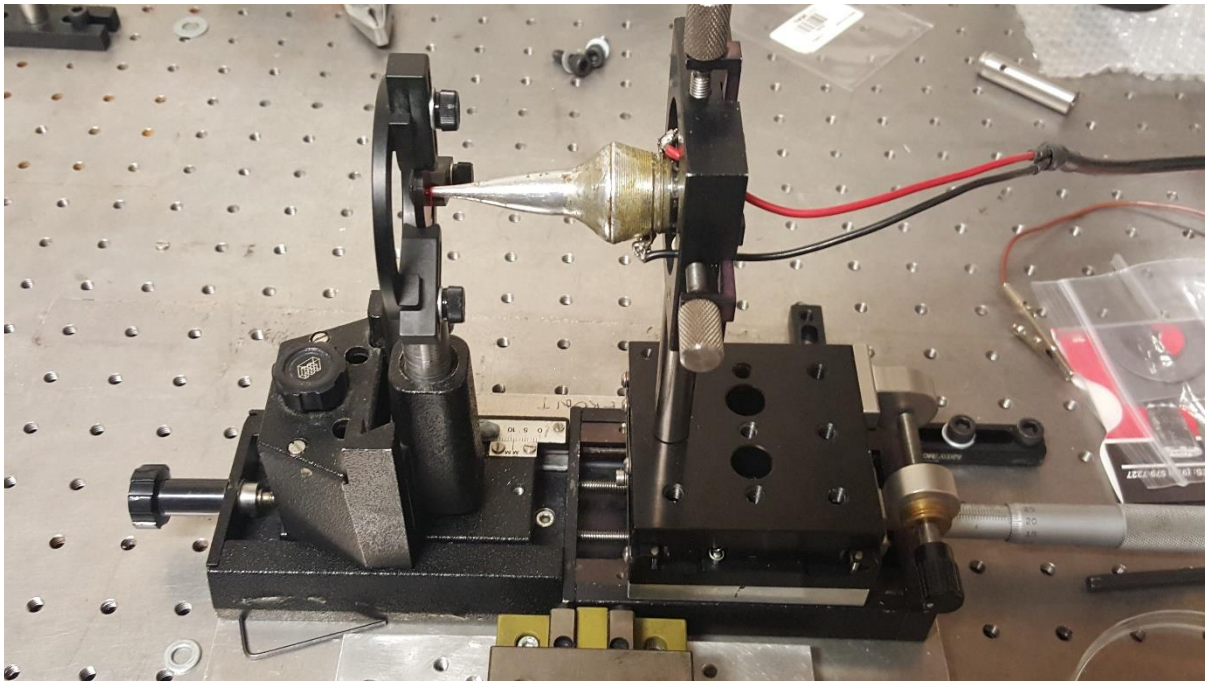

Fig. 3.5. Picture of the experimental setup showing the arrangement of the transducer and chain of spheres mounted on a translation stage.

If the arrangement of the system was too stiff or heavily-damped, more energy was required from the input vibration to trigger the conditions necessary for the creation of the solitary waves. Although the system arrangement shown in Fig 3.5 looks simple, careful design of the arrangement with the optimum material for the clamps (using metal optical clamps produced varied results), holders, and lengths of the rods was required. This arrangement enabled consistently repeatable results. The system could be easily dismantled and reassembled and it would generate solitary waves with the same characteristics without having to selectively tune for an optimum set of input parameters each time.

Microstereolithography (MSL) provided the best technique to fabricate the channels used to encase the chain of spheres. MSL provided a build resolutions around the 20 μm range when compared to methods such as fused deposition modelling and selective laser sintering. The holder and its fabrication process will be described in more detail below. The cylindrical

holder containing the spheres was loaded horizontally instead off vertically because when vertically stacked the effect of gravity from the transducer and spheres produces pre-compression in the system. This variation and others will be described in later sections and chapters.

3.2.2. **Details of the Ultrasonic Horn's Output**

Fig. 3.6 shows the image of a 25 mm diameter dual element contact transducer incorporated with an exponential taper horn concentrator with a length of 48 mm and 2 mm diameter at the tip. The horn was used to achieve greater performance and acoustic power from a transducer with a resonance frequency of 73 kHz. The horn produced a peak to peak particle velocity, v_m of approximately 1,000 mm/s when driven at 73 kHz for a duration of 20 cycles at a maximum voltage of 162 volts. Reducing the voltage produced a linear decreases in the particle velocity of the horn as illustrated in Fig. 3.7.

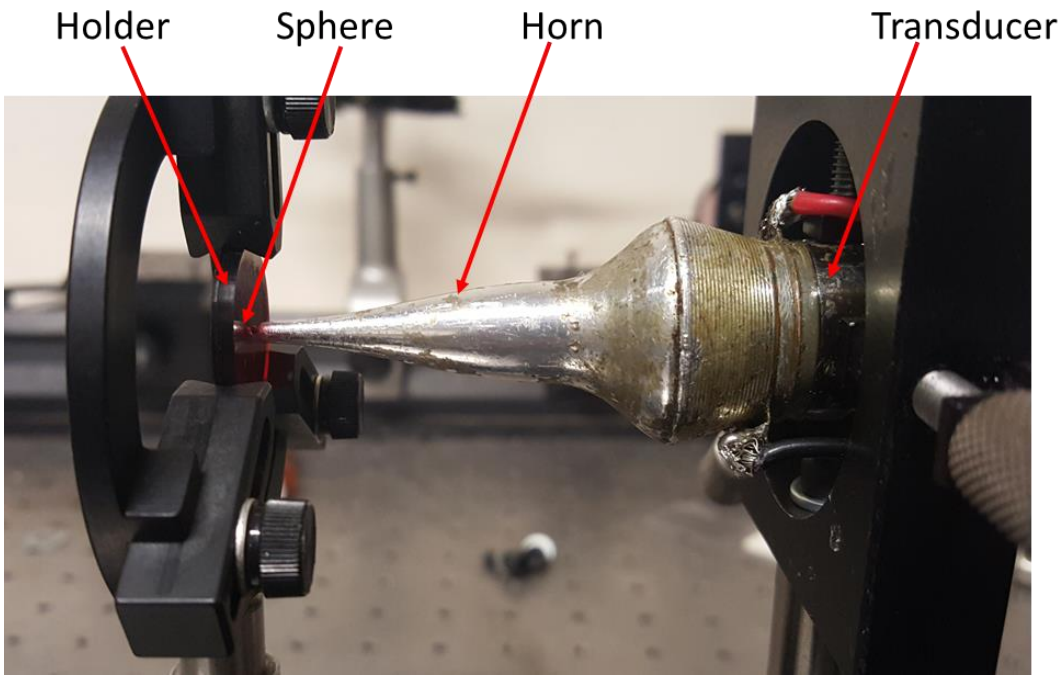

Fig. 3.6. Picture of the Transducer and Horn.

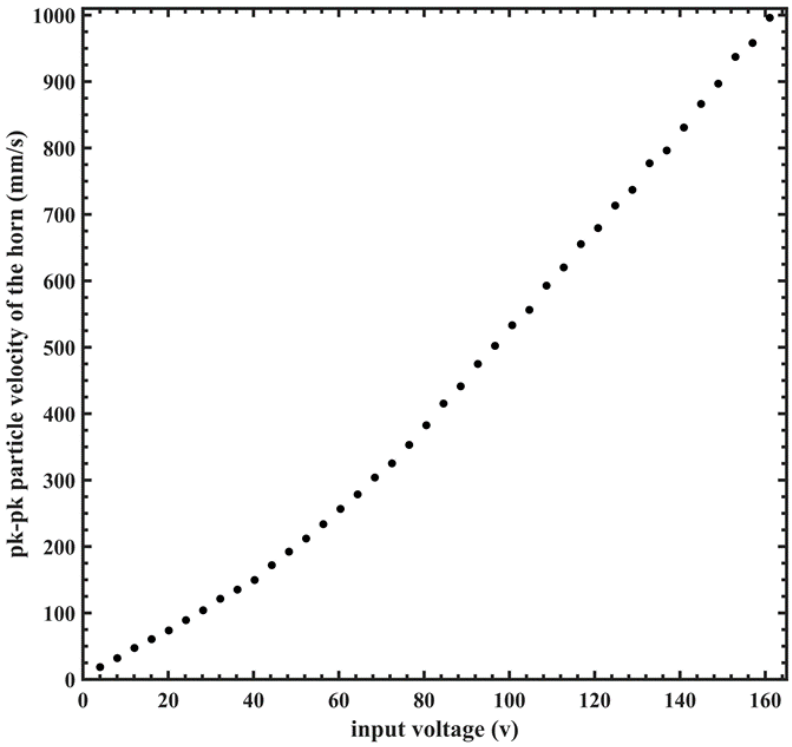

Fig. 3.7. Peak to peak velocity of the horn at 73 kHz for a duration of 20 cycles and various drive voltages.

The horn produced the largest magnitude of particle velocity when operating at its resonant frequency of 73 kHz. It was also capable of functioning at other frequencies between 43 and 203 kHz. Some frequencies within this range produced insufficient amplitudes and high attenuation, as such, the frequencies used in this research were carefully. Fig. 3.8 shows a few of these frequencies.

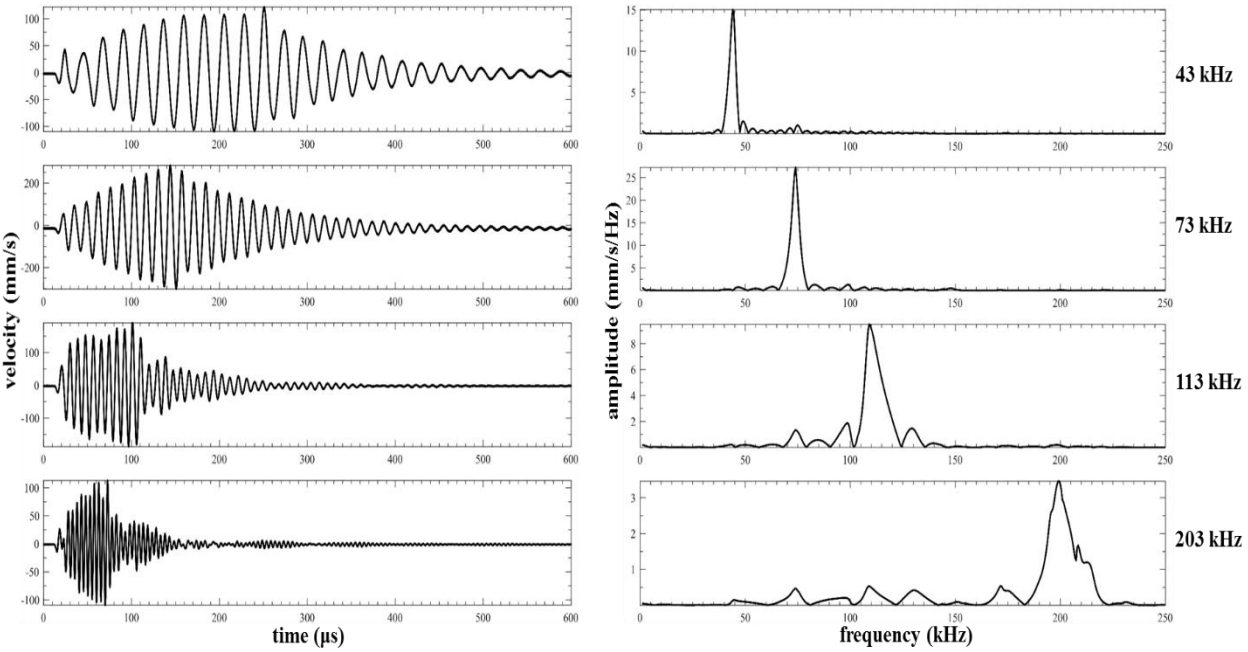

Fig. 3.8. Waveforms (left) and Spectra (right) of a various drive frequencies for a duration of 10 cycles.

3.2.3. **Use of Microstereolithography (MSL) to Fabricate the Holder**

Microstereolithography is a micro-manufacturing technique that utilizes UV radiation to construct 3D structures by solidifying resin layer by layer [2]. The resulting sample is cured to bind the chemical compounds on the surface; then rinsed with isopropanol to remove any uncured resin and post cured in a UV flash box. The MSL system used to fabricate the cylindrical holders was a high resolution EnvisionTEC Perfactory 3 Digital Shell Printer (DSP), capable of resolutions down to 20 µm in the X and Y plane and can achieve as little as 25 µm in Z plane [3]. The system illustrated in Fig. 3.9 was composed of a LED light engine with spectra output maxima at 365 nm, a DMD projector, focusing optics, 45^{o} mirror, resin tray and a linear stage. The DSP was capable of building up to 40 shells within 3 hours with a build envelope of 21 mm x 27 mm x 130 mm.

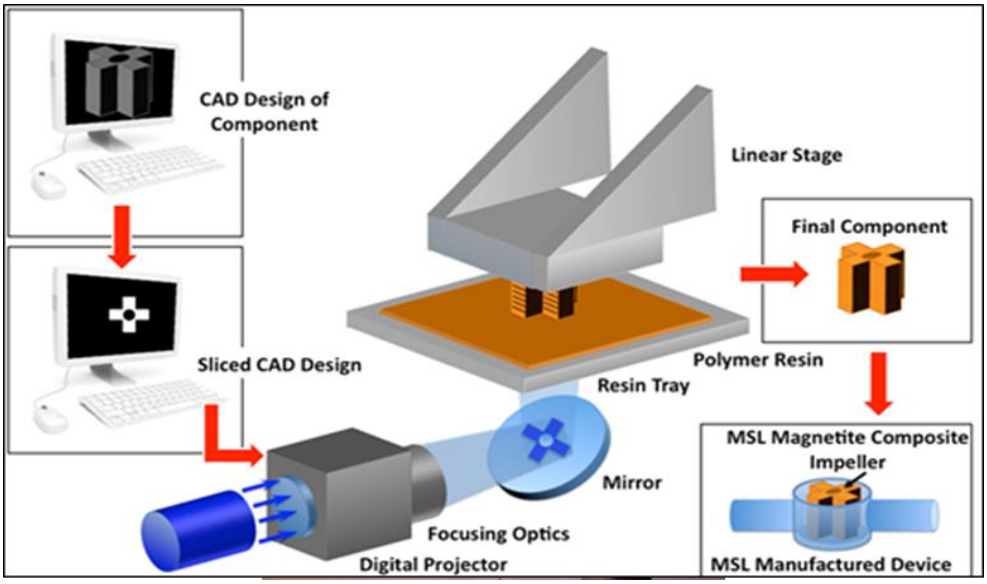

Fig. 3.9. Overview of the MSL system [3].

The desired structures for all the holders were designed using OpenScad and converted to .STL file format for fabrication. The fabrication process was performed in a room with filtered ambient light to avoid premature polymerization of the materials. The resin used to construct the device was EnvisionTec R11 with a 25 µm voxel depth. The R11 resin was composed of an acrylic oligomer, cross-linking agents, a photo-initiator and dye to prevent over curing of the resin. The mechanical properties of the resultant solid material are given in Table 3.1. For these studies, the holders were manufactured from photo-sensitive acrylic resin. Variation of the material of the holder were also studied, the effects of these will be discussed in later chapters. The design specification of a few of the holders manufactured are shown in Fig. 3.10. The shape, length and diameter of the inner radius were varied depending on the situation investigated.

Compressive Modulus (GPa)	**Young's Modulus (GPa)**	**Density (kg/m^3)**	**Velocity of Sound (m/s)**
4.3	3	1235	2100

Table 3.1 Physical properties of R11 resin with force applied parallel and perpendicular to fabricated layers.

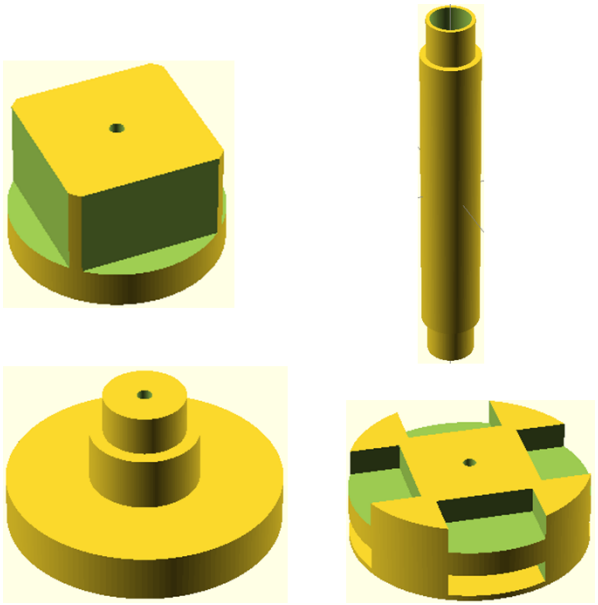

Fig. 3.10. CAD design of various holders used in the experiments.

Fig. 3.11 shows the design of a typical holder that would contain six spheres of 1 mm diameter. For this holder, the channel has a diameter of 1.10 mm from the input end (top), which ran down the length of the cylinder for 5.35 mm. A 10% tolerance in diameter was used to ensure that the spheres moved freely without sticking to the walls; minimising the effect of friction.

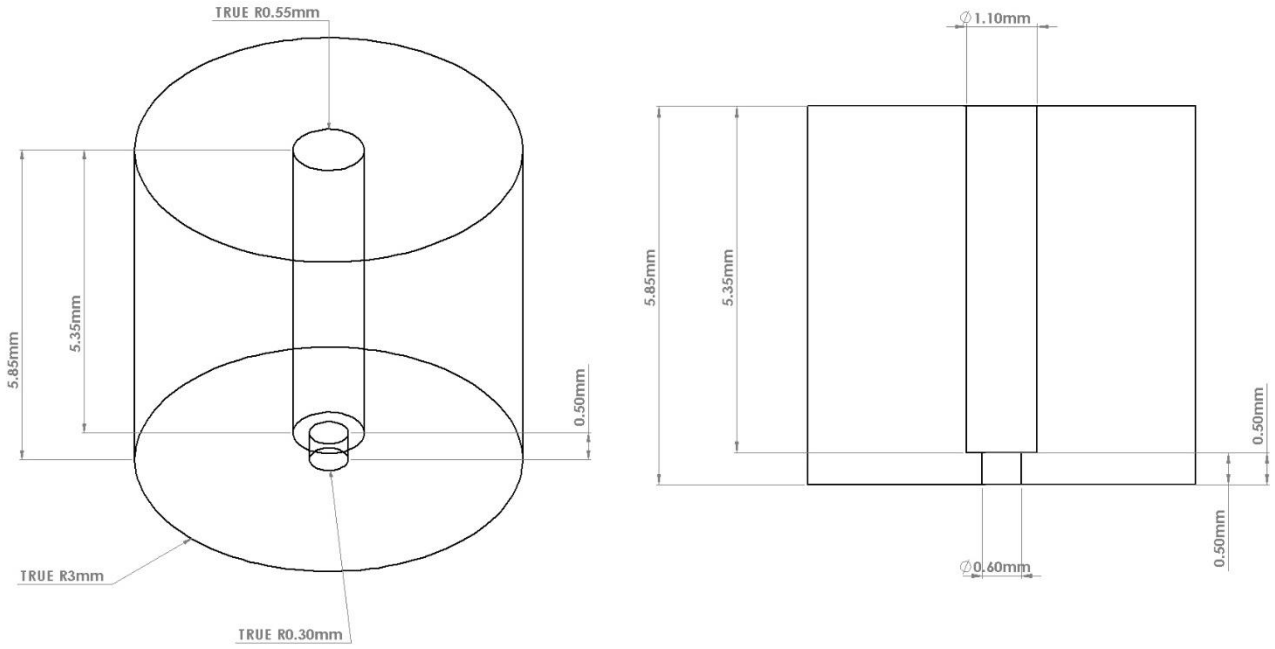

Fig. 3.11. CAD design highlighting the main features of the cylindrical holder.

As stated earlier, the bottom end was in the form of an annulus with a narrower exit diameter, allowing the chain of spheres to be held in place while allowing some part of the final sphere to be visible to the vibrometer. Looking from the bottom a hole can be observed with a diameter of 0.6 mm and it runs for a length of 0.5 mm. This end serves as the annular wall preventing the spheres from falling out and restricting its motion. It was observed that the solitary wave pulses of interest could not be obtained in holders with walls thicker than 0.5 mm.

For a cylinder containing six spheres, the total length of the holder was 5.85 mm, this is shorter than 6 mm, the length of six 1mm spheres. This was designed this way to ensure that the transducer was only in contact with the 1st sphere in the chain, which protruded beyond the front surface of the holder. The ensured that signals travelled through the chain, and not through the holder material directly.

The shape and length of the holder could be varied easily using the MSL technique, so as to accommodate various different sphere sizes, chain lengths, and methods of attaching the holder to the optical bench used to align the horn, holder and vibrometer. A few of the samples fabricated are shown in Fig. 3.12. The dimensions vary depending on the optical clamps used and the number of spheres required for the experiments. However, the inner dimension (i.e. the channel containing the spheres) was always constant.

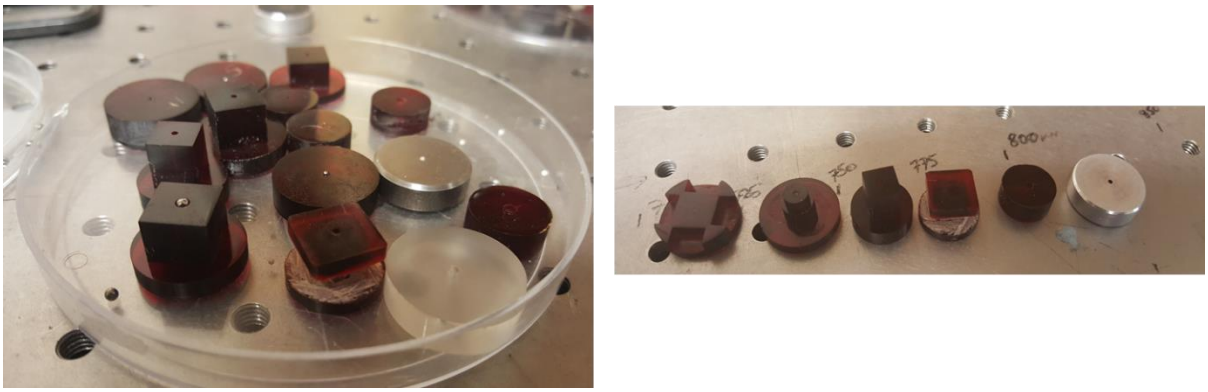

Fig. 3.12. CAD design of various holders used in the experiments.

Several design specifications were investigated, one of which involved carbon fibre rods embedded in the channel of the holder, as shown in Fig. 3.13. The design philosophy was to ensure that the spheres were only in contact with rods and not with the holder. This would reduce the area of contact, hence reducing the effects of friction. However, this arrangement did not produce any noticeable difference in the results but it increased the complexity of the arrangement.

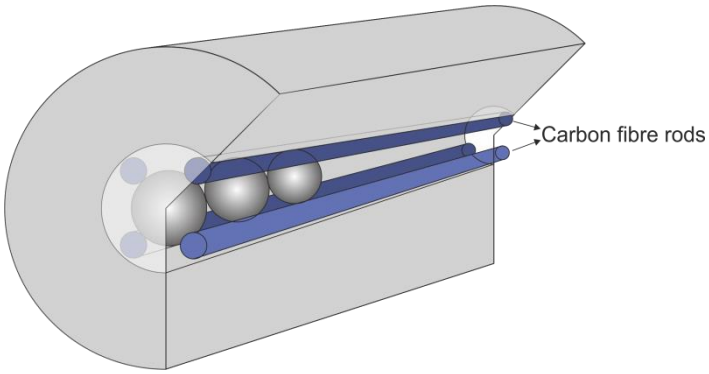

Fig. 3.13. Design of a cylindrical holder with 4 carbon fibre rods inserted in its channel.

3.3. Some Preliminary Experimental Results

In this Section, some typical results are shown, which illustrate the type of behaviour which can be obtained, provided all conditions are correctly adjusted. As will be described in later Chapters, the exact nature of the output is highly dependent upon many different factors – the exact nature of the input waveform and its amplitude, the value of the pre-compression force, the number, material and size of the spheres used, and the holder characteristics.

However, the main aim of this work was to try and establish solitary wave behaviour, so as to transform input tone-burst signals into a different form, hopefully wide bandwidth transients with a high amplitude. It was found that it was necessary to get just the right conditions for this to occur. This will be described in greater detail in later chapters. If the conditions are right, it

was found that this effect could be seen. These types of waveforms are the first examples ever published, and were included in a journal paper and a conference proceedings [4].

An example of the type of results that could be obtained is shown in Fig. 3.14. In each case, the input and output signals are shown together as the amplitude from the horn was gradually increased. The input signal from the horn is shown in grey, and the output from the last sphere of a chain of six chrome steel with 1 mm diameter is shown in black, in both cases obtained using the vibrometer. In this scenario the chain of spheres are subjected to negligible static pre-compression (f_0) and driven using a tone-burst voltage drive input of 20 cycles at 73 kHz. The four waveforms in Fig. 3.14 demonstrate the type of behaviour that could be supported by the system as the amplitude of the applied force (f_m) was increased (or as the peak to peak particle velocity amplitude from the vibrometer (v_m) was increased from 152 mm/s to 937 mm/s). This increase in input amplitude highlights the effect of the relationship between f_m and f_0. By keeping f_0 constant and changing f_m (or v_m), the gradual evolution of the solitary wave pulses can be demonstrated, from when the system switches from being linear to being weakly nonlinear and finally to strongly nonlinear.

The most obvious change in characteristic of the input and output waveform can be observed when v_m increases from 152 mm/s to 378 mm/s. At low input amplitudes (152 mm/s), the input and output have similar time-domain characteristics in terms of periodicity, with the output being smaller in amplitude as expected. At 378 mm/s, the periodicity of the waveforms loses its synchronicity, and features with a different periodicity start to appear. Finally, as f_m increases further to 937 mm/s, impulses appear that have a totally different periodicity to those present in the input. These are the solitary wave impulses that were the target of these studies, and they begin to emerge due to the strongly nonlinear contacts between the spheres and also as a result of multiple reflections with the chain.

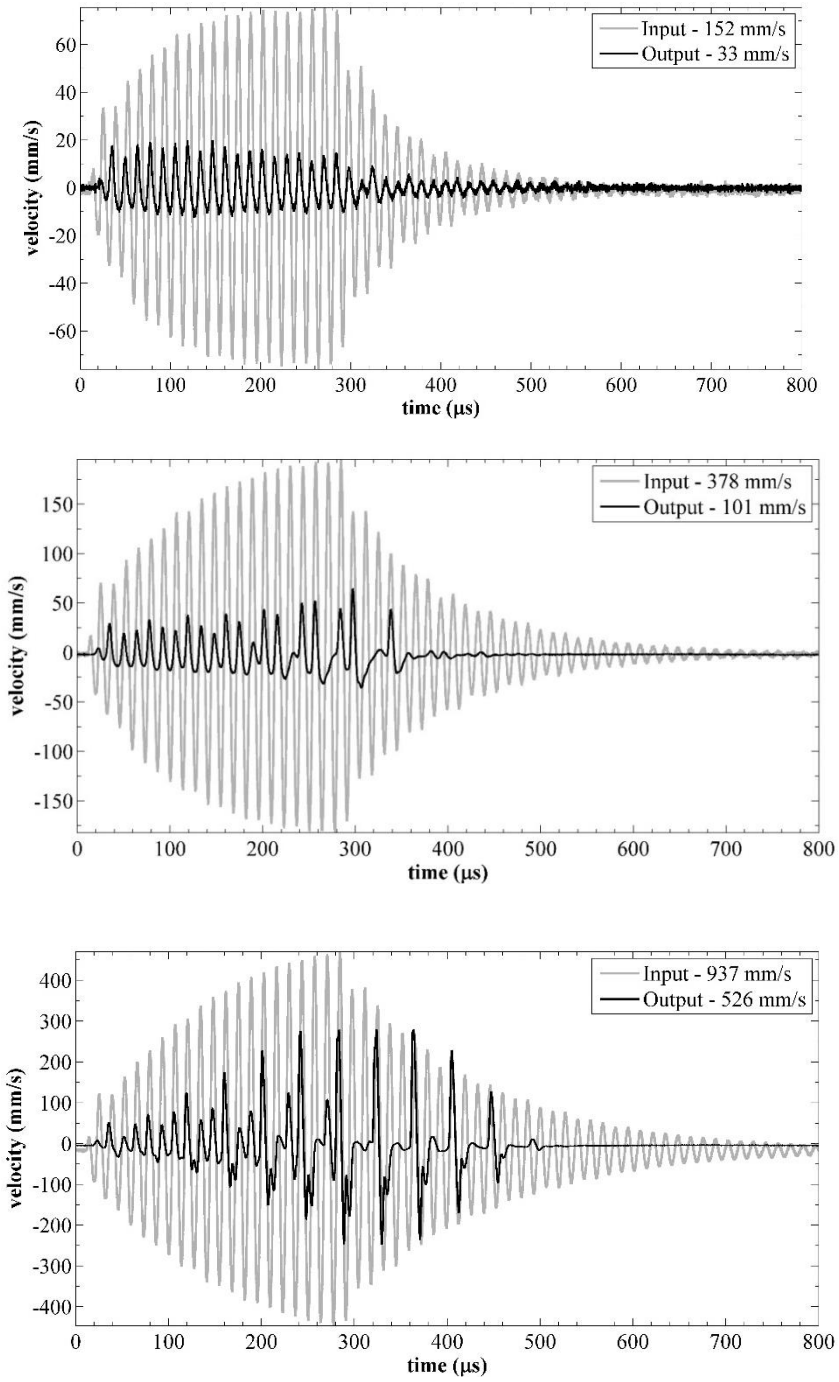

Fig. 3.14. Velocity waveforms of the transducer/horn as Input and chain of 6 spheres as Output signal. The input and output particle velocity amplitudes (v_m) *are given in each case.*

3.4. Theoretical Modelling - Extending Nesterenko's Solution

3.4.1. Background

This thesis is primarily concerned with experimental measurements of finite-length chains of spheres, and the study of how non-linearity changes the waveforms that are produced within them. Earlier Chapters gave some background on the propagation of waves in chains, and

described the concepts of solitary waves. The experimental waveforms of Fig. 3.14, when analysed more fully in later Chapters, will indeed show these characteristics. It is also important, though, to compare the results to theoretical modelling. This allows the effect of different parameters (input signal, sphere properties *etc*.) to be studied, and also means that the predictions can be compared to experiment, so as to increase some of the understanding of what is happening.

As discussed earlier, this theory was developed as part of an EPSRC-funded research programme, to which the results presented in this thesis were the experimental contribution. As part of the collaboration, equations were developed by Dr Jia Yang which could be used to predict the characteristics of a particular chain of spheres, which all members of the research consortium could use. It is this theory that is presented below.

3.4.2. **Theoretical Equations**

Predictions of behaviour need solutions to the wave equations that describe wave propagation in chains. Nesterenko [5] described a solution based on Hertz law to predict the dynamic behaviour of the last sphere within a chain of spheres. The equation is as follows:

$$u_{tt} = c^2 \left[\frac{3}{2} (-u_x)^{1/2} u_{xx} + \frac{a^2}{8} (-u_x)^{1/2} u_{xxx} - \frac{a^2}{8} \frac{u_{xx} u_{xxx}}{(-u_x)^{1/2}} - \frac{a^2}{64} \frac{(u_{xx})^3}{(-u_x)^{3/2}} \right] \tag{3.1}$$

In Nesterenko's equation, u is displacement which includes the initial displacement responsible for the closest approach of δ_0. a is the initial distance between the particles of undisturbed system and c is the propagation velocity.

His model is the starting point for development of a more comprehensive theory that will be described below. However, the model doesn't take into consideration the effect of the following:

1. Dissipation/damping phenomena: due to friction, material differences between the transducer and sphere and viscoelastic behaviour of the spheres.
2. The presence of a non-negligible pre-compression force
3. Reflection within the chain: Nestrenko's assumption of a chain of infinite length means that reflection doesn't occur
4. The solution only accounts for one form of contact (*i.e.* contact between adjacent spheres).

Due to the experimental design these factors cannot be ignored. The arrangement involved multiple forms of contact (horn-to-sphere, sphere-to-sphere and sphere-to-wall), and a chain of finite length as shown in Fig. 3.15.

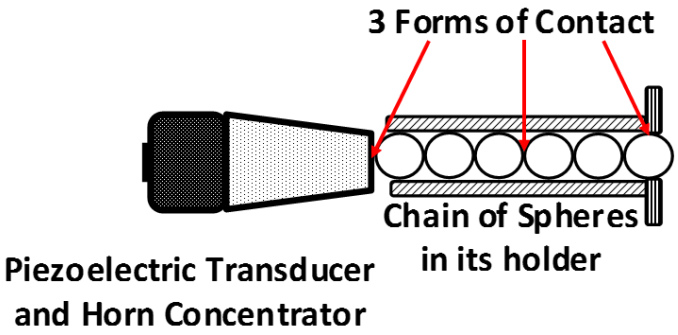

Fig. 3.15 Schematic diagram of the experimental arrangement.

The first sphere in the chain was in contact with the planar face of the horn; the last sphere was assumed to be in contact with a fixed planar wall (although in practice this has an opening to allow measurement of the vibration of the last sphere in the chain). The planar surfaces of these two boundaries are, in fact, modelled as spheres with radii in the limit tending to infinity.

To account for these factors, equation (3.1) can be expanded to describe each of the three forms of contact (horn to first sphere, between two spheres, and between the last sphere and the far wall). The result is the following set of equations:

The dynamic equation of motion for the first sphere in contact with the transducer is given as:

$$m\frac{d^2u_1}{dt^2} = \frac{2\sqrt{R}}{3}\left[2\theta_l(\delta_{0l} + u_0 - u_1)^{3/2} - \frac{\theta_m}{\sqrt{2}}(\delta_0 + u_1 - u_2)^{3/2}\right] + Q\left(\frac{du_0}{dt} - \frac{du_1}{dt}\right)H(\delta_{0l} + u_0 - u_1) - Q\left(\frac{du_1}{dt} - \frac{du_2}{dt}\right)H(\delta_0 + u_1 - u_2)\,. \quad (3.2)$$

Here, u_0 is the excitation generated by the transducer, and u_1 is the displacement of the first sphere. δ_{0l} is the initial static displacement caused by the pre-compression applied to the chain. θ_l and θ_m are effective elastic constants, defined below. Q was the term used to describe the linear viscous damping between neighbouring spheres and it was used to model the inherent dissipation which aroused in the experiments. Damping is considered only when the spheres were in contact; hence, a Heaviside function *H* was used to denote when this contact is lost, and goes to zero when this happens [5].

The dynamic equation of motion between the spheres, from the second to the penultimate sphere is given as:

$$m\frac{d^2u_i}{dt^2} = \frac{\sqrt{2R}}{3}\theta_m\left[(\delta_0+u_{i-1} - u_i)^{3/2} - (\delta_0 + u_i - u_{i+1})^{3/2}\right] + Q\left(\frac{du_{i-1}}{dt} - \frac{du_i}{dt}\right)H(\delta_0 + u_{i-1} - u_i) - Q\left(\frac{du_i}{dt} - \frac{du_{i+1}}{dt}\right)H(\delta_0 + u_i - u_{i+1}) \quad (3.3)$$

Finally, the dynamic equation of motion for the last sphere and the end wall is:

$$m\frac{d^2u_N}{dt^2} = \frac{2\sqrt{R}}{3}\left[\frac{\theta_m}{\sqrt{2}}(\delta_0 + u_{N-1} - u_N)^{3/2} - 2\theta_r(\delta_{0r} + u_N)^{3/2}\right] + Q\left(\frac{du_{N-1}}{dt} - \frac{du_N}{dt}\right)H(\delta_0 + u_{N-1} - u_N) - Q\frac{du_N}{dt}H(\delta_{0r} + u_N) \quad (3.4)$$

where θ_l and θ_r are the effective Young's moduli associated with contact interactions. Note the negative values of the force terms involving successive spheres in Equations (3.2 – 3.4) imply that the relevant neighbouring spheres have lost contact and the terms are then set to

zero; additionally the damping term involving the Heavyside function H then becomes inactive.

The values relating to the material property can be derived using:

$$\frac{1}{\theta_l} = \frac{1-\sigma_l^2}{Y_l} + \frac{1-\sigma_s^2}{Y_s}, \qquad \theta_m = \frac{Y_s}{1-\sigma_s^2} \qquad \frac{1}{\theta_r} = \frac{1-\sigma_r^2}{Y_r} + \frac{1-\sigma_s^2}{Y_s} \tag{3.5}$$

where Y_l is Young's modulus and σ_l is Poisson ratio of the transducer. Y_r and σ_r are that of the end wall; Y_s and σ_s are associated with the spheres; and m is the mass of each sphere.

The initial displacements under a known static force F_0 are given as:

$$\delta_{0l} = \left(\frac{3F_0}{4\sqrt{R}\theta_l}\right)^{2/3} \qquad \delta_0 = \left(\frac{3F_0}{\sqrt{2R}\theta_m}\right)^{2/3} \qquad \delta_{0r} = \left(\frac{3F_0}{4\sqrt{R}\theta_r}\right)^{2/3} \tag{3.6}$$

where δ_{0l} is the distance between the tip of the transducer and the centre of the first sphere; δ_0 is the distance between the centres of neighbouring spheres and δ_{0r} is the distance between the centre of the last sphere and the wall/base of the holder.

The model predicts the displacement of the centre of each sphere from its equilibrium position ($u_1, u_2, \ldots, u_i$) for a given input displacement waveform (u_0). The input displacement waveforms were obtained experimentally from the horn using the laser vibrometer at the desired sinusoidal tone-burst.

3.4.3. **Illustration of the Predictions from the Model**

The behaviour of the resulting output signals from the two scenarios described in the dynamic equation of motion given in equation (3.1) and equations (3.2 – 3.6) differ greatly. Here, it is possible to show some general features to demonstrate these differences. (Note that predictions of the results shown earlier in Fig. 3.14 are presented in Chapter 4, where the exact modelling conditions needed are mentioned). In each case, a MATLAB script was written to evaluate these equations. This MATLAB code is attached in Appendix A1. As an example, examining

a situation where a chain of six chrome steel ball bearings with material properties and input conditions shown in Tables 3.2 and 3.3 are used in each scenario. The input was a sine-wave tone burst of constant amplitude.

No. of Spheres	Radius (mm)	F_0 (N)	Frequency (kHz)	Amplitude (μm)	No. of Cycles
6	0.5	0.009	73	1.0	20

Table 3.2 Input conditions used for the predictions of Fig. 4.16.

	Density (kg/m^3)	Young's Modulus (GPa)	Poisson's Ratio
Sphere	7833	201	0.3
Transducer	7833	210	0.3
Wall	1235	3	0.35

Table 3.3 Physical properties of the materials used for the predictions of Fig. 3.16.

The resulting time waveforms that were predicted from the two equations are shown in Figs. 3.16(a) and (b), for a tone-burst with a time duration of 900 μs. The waveform in Fig. 3.16(a) was generated using Nesterenko's equation, while that in Fig. 3.16(b) was from the "*modified*" equation which takes into account the three forms of contact and viscous damping (0.276 Ns/m). Note that a small amount of static pre-compression was used in both scenarios. This not only ensures that the spheres are all in light contact but also mimics the force applied when the transducer is in contact with the first sphere. In the time waveform of Fig 3.16(a), a trail of pulses can be observed. The trail begins with two individual pulses which appear to be evenly spaced but by the arrival of the third this pattern collapses and the succeeding signals appear to be stochastic with no discernible pattern, and with a lack of periodicity. However, once damping and the end conditions via contacts with the horn and wall were introduced, the resulting waveform changes drastically (Fig. 3.16(b)). A trail of periodic pulses emerges, with a periodicity observed in the pulses in the time waveform that corresponds to a frequency of 24 kHz (approximately 1/3rd of the input frequency of 73 kHz) similar to those observed in the experiment (Fig. 3.16(c)). As will be shown in the next Chapter, this is no accident – it

represents the creation of a nonlinear normal mode of vibration and the creation of sub-harmonics via non-linear behaviour.

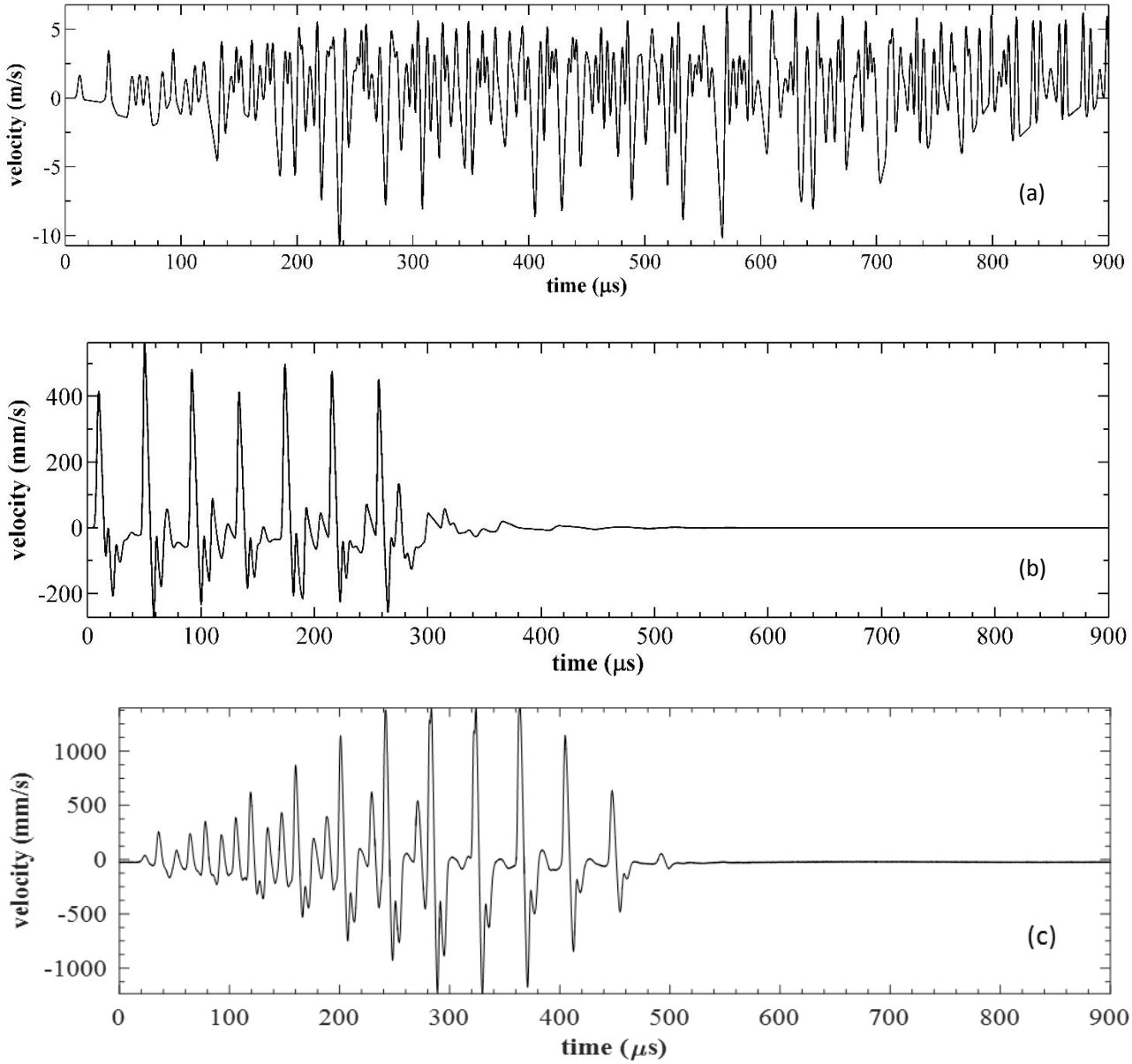

Fig. 3.16: Output time waveform predicted for the conditions of Tables 3.2 and 3.3 from (a) Nesterenko's unmodified equation (3.1), (b) the three forms of contacts as given in equations (3.2 – 3.6), modified Nesterenko's equation and (c) experiment.

This demonstrates that Nesterenko's prediction for a chain of infinite spheres does not hold for situations studied in this thesis, where reflection and dissipation occur to generate and establish resonances within a system of spheres. The modified equation (Fig. 3.16b) is a closer match to

the results from the experiment (Fig. 3.16c), as such the model described in equations (3.2 – 3.4) will be used and compared to results of the experiments.

Now, let's compare the differences between using a sinusoidal continuous wave to a tone-burst as the input stimuli. Again, using the parameters found in Tables 3.2 and 3.3, the waveform in Fig. 3.17 was obtained. In general, similar characteristics to the waveforms in Fig. 3.16 can be observed. However, it can be noticed that the waveform loses its periodicity between 300 μs – 500 μs. Within this region there appears to be an over-saturation of energy resulting in a loss in the balance between dispersion and non-linearity, this balance is credited with the formation of the solitary pulses. Meaning that there is an optimum range for the number of cycles that could be used for the tone-burst for a set of chain.

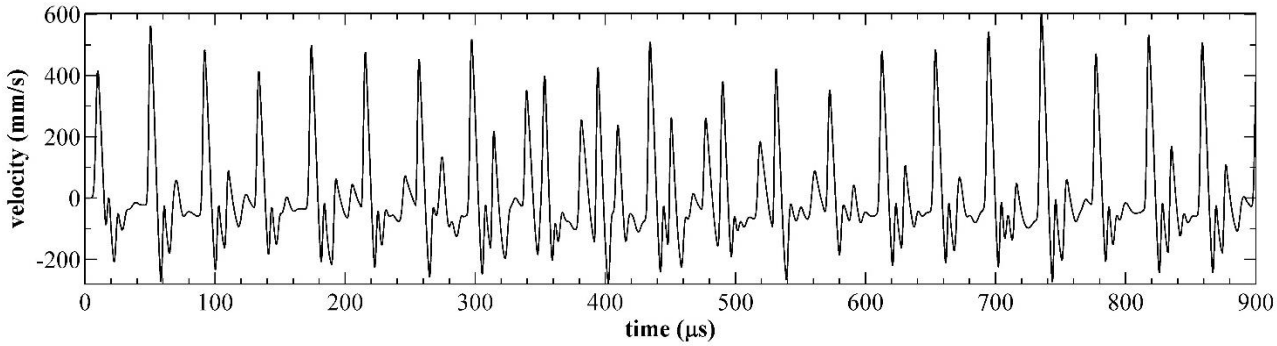

Fig. 3.17. Output time waveform from 'modified' Nesterenko's equation which accounts for the three forms of contacts as given in equations (3.2 – 3.6) when using a continuous sine wave.

It will be seen in the following Chapters that the shape of the spheres, the dimensions of the spheres, the details of the contact between neighbouring spheres, the transducer and wall, their physical properties and the characteristics of the input signal all have an effect of the regime of propagation within the granular chain. This variations present difficulties and propose several questions about how solitary waves may be generated within the system proposed. The following sections and chapters will attempt to provide answers on the phenomena that arise from this variation.

3.5. Nonlinear Normal Modes (NNM)

Nonlinear normal modes (NNM) are effectively resonances of systems which contain non-linear elements and can be used to demonstrate the dynamic motion of the spheres with the chain as described earlier using Nesterenko's long chain approximation. They represent synchronous time periodic motions which occur when an entire system vibrates in an equi-periodic fashion [6]. This synchronicity makes all the co-ordinates of the system reach a maxima, minima and pass through zero in unison (*i.e.* at the same instant in time). This behaviour occurs in free oscillators, where a supplementary system models the excitation to extend the equations of motion. This excitation is an additional state to the system producing an additional degree of freedom (DOF) with a known response. The majority of the descriptions in the literature (*e.g.* Lyapunov [7], Rosenberg [8]) deal with low order lumped mass systems with a few DOFs such as the system shown earlier in Fig. 2.1. This system can be represented as a nonlinear oscillator consisting of two identical masses connected by three cubic stiffness as illustrated in Fig. 3.18.

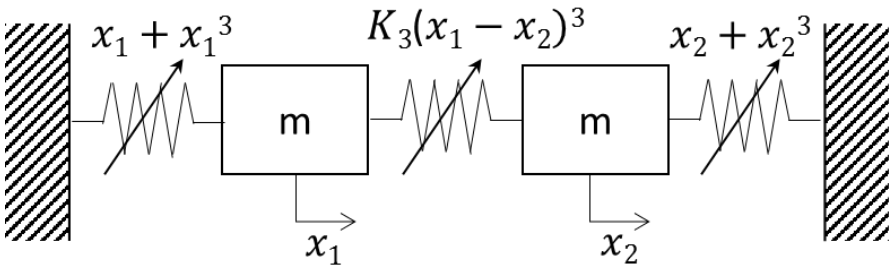

Fig. 3.18 A simple 2-dof mass–spring system.

This system is governed by the equations of motion:

$$\ddot{x}_1 + x_1 + x_1^3 + K(x_1 - x_2)^3 = 0$$
$$\ddot{x}_2 - K(x_1 - x_2)^3 + x_2 + x_2^3 += 0 \tag{3.7}$$

Contrary to linear systems, nonlinear oscillators exhibit complex behaviours. Such behaviours include: nonlinear mode localisation, bifurcations, internal resonances, chaos, saturation, and sub-harmonics and super-harmonics of the original forcing frequency.

In the work of Vakakis *et al*. [8] the discussion of NMMs was focussed on homogeneous dynamic systems, such as a chain composed of finite number of spherical granular particles. Jayaprakash and Vakakis [9] extended the definition of NNM by showing that the condition of synchronicity was not valid under certain modes of the chain of spheres. When the granular chains are under Hertzian contact with fixed boundary conditions and subjected to no pre-compression force (f_0), they become a highly complex and tunable dynamic system. This illustrates the importance of the boundary conditions which are not present in Nesterenko's long chain approximation. Depending on the pre-compression applied, it could be either weakly or strongly nonlinear. In such a system the non-linear normal modes (NNMs) appear as travelling waves due to the effect of separations between successive spheres. They further explain the dynamics of a system with negligible to no pre-compression as smooth when the neighbouring spheres are in contact and non-smooth when separation occurs between spheres. Non-smoothness is due to the loss of Hertzian contact when the distance between successive spheres is greater than twice the radius. The separation and collision of the spheres in addition to their Hertzian interaction provides an added effect to the strong nonlinearity of the system.

Since the system lacks compression and sphere separation occurs (zero in extension), *k* is a nonlinear coefficient in the force (*F*) – displacement (*d*) relationship governing the Hertzian interaction between successive spheres:

$$F = \begin{cases} kd^{3/2}, & d < 0 \\ 0, & d \geq 0 \end{cases} \tag{3.8}$$

This system was characterised by Nesterenko [10] as an ‘acoustic vacua’ or ‘sonic vacuum’ (discussed in section 3.3) because the propagation of sound (*i.e.* linear acoustic waves) is impossible due to the sphere separation when there was no static pre-compression force applied. In this system the spheres do not oscillate individually about the zero position but are non-synchronous and highly asymmetric.

3.6. Comparison of NNM properties to experiment and simulation

3.6.1. The predictions of Jayaprakash *et al.* [11]

The discussion in this section compares the numerical results of Jayaprakash *et al*. [11] to a set of experiments performed on a similar granular system, as part of the current research. This comparison was performed to demonstrate the dynamic motion of a finite chain of spheres which is in part due to the existence of the boundary conditions, hence, necessitating the need to expand on Nesterenko’s theorem. Firstly, Jayaprakash’s system and numerical method is described. In their system a chain consisting of a finite number of spheres was considered, the spheres were placed between rigid walls, with no gaps existing between the spheres and walls while in equilibrium position (Fig. 3.19).

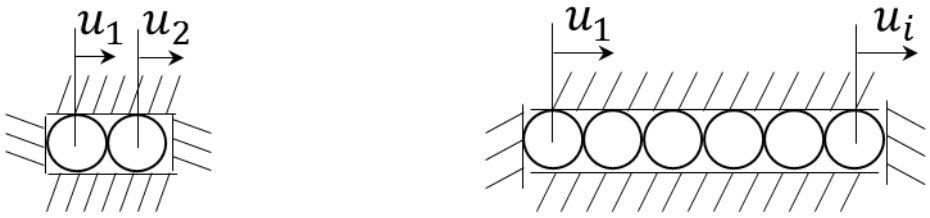

Fig. 3.19 Schematic diagram of spherical granular systems under Hertz contact.

Under Hertzian contact between the spheres and the walls, the kinetic (KE) and potential (PE) energies of the chain of spheres were given as follows for a two-sphere system:

$$KE = \frac{1}{2}m(\dot{u}_1^2 + \dot{u}_2^2) \tag{3.8}$$

$$PE = \frac{2}{5}\frac{Y(2a)^{\frac{1}{2}}}{3(1-\sigma^2)} * \left[(-u_1)_+^{\frac{5}{2}} + (u_2)_+^{\frac{5}{2}} + (u_1 - u_2)_+^{\frac{5}{2}}\right] \quad (3.9)$$

The (+) subscript in the expression above denotes that the term in the bracket is non zero. The equation of motion for each sphere can be derived from Lagrange's equation:

$$\ddot{u_1} = A\left[\left((-u_1)_+^{\frac{3}{2}} - (u_1 - u_2)_+^{\frac{3}{2}}\right)\right] \quad (3.10)$$

$$\ddot{u_2} = A\left[\left((-u_2)_+^{\frac{3}{2}} + (u_1 - u_2)_+^{\frac{3}{2}}\right)\right] \quad (3.11)$$

$$where;\ A = \frac{Y(2a)^{\frac{1}{2}}}{[3m(1-\sigma^2)]} \quad (3.12)$$

The displacements are non-dimensionalised using the following normalisations:

$$X = \frac{u}{a},\ \ \tau = \frac{t}{2a/C}\left(\frac{\pi(1-\sigma^2}{\sqrt{2}}\right)^{-1/2}\ and\ C = \sqrt{\frac{Y}{\rho}}$$

Hence, the equation of motion in its normalised form is:

$$\ddot{X_1} = (-X_1)_+^{\frac{3}{2}} - (X_1 - X_2)_+^{\frac{3}{2}} \quad (3.13)$$

$$\ddot{X_2} = (-X_2)_+^{\frac{3}{2}} + (X_1 - X_2)_+^{\frac{3}{2}} \quad (3.14)$$

Jayaprakash's numerical model detected three periodic solutions; in-phase NNM, out-of-phase NNM and sub-harmonics. Out-of-phase NNM is a synchronous oscillation and in-phase is an asynchronous oscillation. In Fig. 3.20 (two sphere chain case), the two spheres pass through their equilibrium point at different moments in time. Because of this characteristic of non-synchronicity and energy transfer within the chain of spheres, Jayaprakash defined a NNM as

a *"time-periodic oscillation where the bead oscillations possess identical frequencies but are not necessarily synchronous" [11]*.

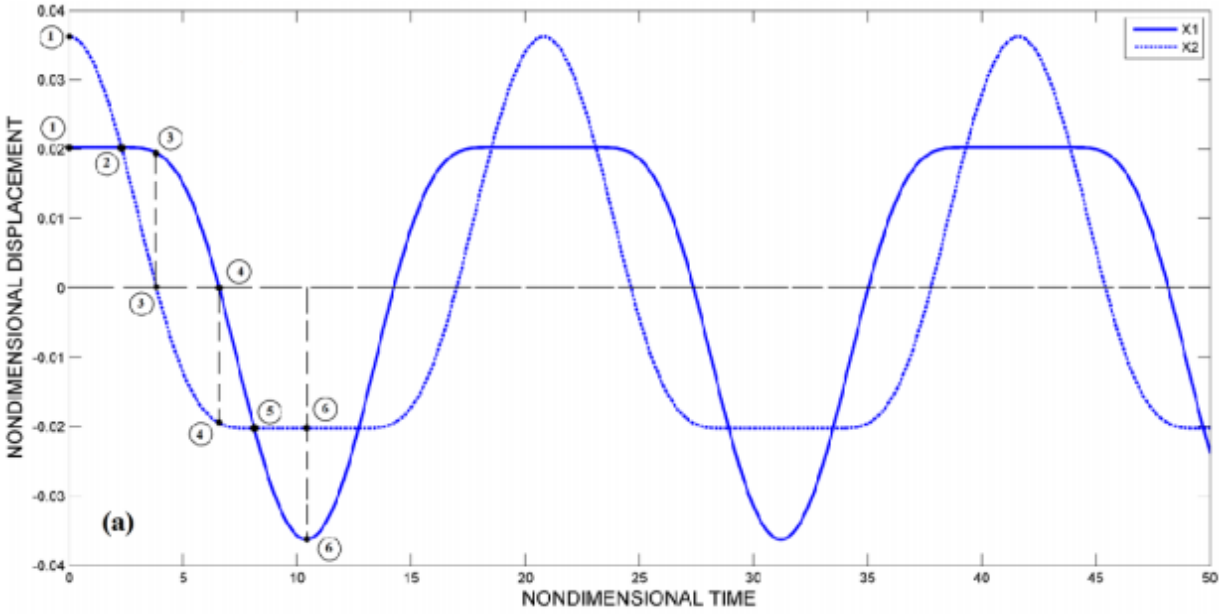

Fig. 3.20 The in-phase NNM for the two-bead granular system (X1: sphere 1 and X2: sphere 2) [11].

At point 1 in Fig. 3.20, the energy in the system becomes elastic due to the interaction between the wall and the second sphere (X_2) while, the first sphere (X_1) remains motionless but displaced from its equilibrium position. At the next time interval, point 2, the spheres collide with one another and begin interacting. At point 3, the second spheres moves away from the wall passing through its equilibrium position. When the first sphere interacts with the wall and passes through its equilibrium position at point 4, the second sphere would at that point have transferred all its energy to the first sphere and would be entering a motionless state. Proceeding to point 5, the second sphere is stationary and offset from its equilibrium position and the cycle repeats again. From point 2 to 5, the two spheres are interacting (in contact) with each other while at point 1, when the spheres are out of contact and the 1st sphere is in contact with the wall, the energy of the system is entirely in the form of elastic potential. This highlights the complex and asymmetric oscillation taking place within the chain of spheres when oscillating in an in-phase to out-of-phase periodic motion as part of a NNM.

When the length of the system is extended by an *nth* number of spheres, the behaviour remains similar to a two-sphere system, with the nth sphere system possessing domains where the spheres are motionless and displaced from their equilibrium positions. The system also produces high non-synchronicity sphere oscillations. The significant difference between this and a two-sphere chain is the sequence of detachment and loss of contact both between the spheres, and between the last sphere and the rigid wall. When an excitation is introduced to the system, the two end spheres possess opposite velocities and the central sphere(s) remain motionless acting as a virtual wall. When the one of the end spheres interacts with the wall, it oscillates with an amplitude twice greater than the amplitudes of the other spheres and neighbouring spheres oscillate in an out-of-phase mode.

3.6.2 Experiments using a high-speed camera to observe NNMs

Experiments were constructed to evaluate the complex dynamic motion of a chain of four 1 mm chrome steel spheres. The experiments involved using a High speed camera (Schimatzu HPV1) to capture the motion of a chain of four spheres (Fig. 3.21). The high speed camera offered up to one million frames per second at a resolution of 312 x 260-pixel for a maximum of 100 frame storage. In the experiment, the chain was excited at one end using a continuous sinusoidal displacement at a frequency of 40 kHz. This arrangement was similar to those investigated by Jayprakash *et al.* [11], the difference being:

- The material properties of the two end walls differ. In the system shown in Fig. 3.21, the transducer to the left acts as a pseudo wall and it is made from steel while the other wall is made from an acrylic material.
- The system in Fig. 3.21 was subjected to the effect of friction, dissipation and damping.

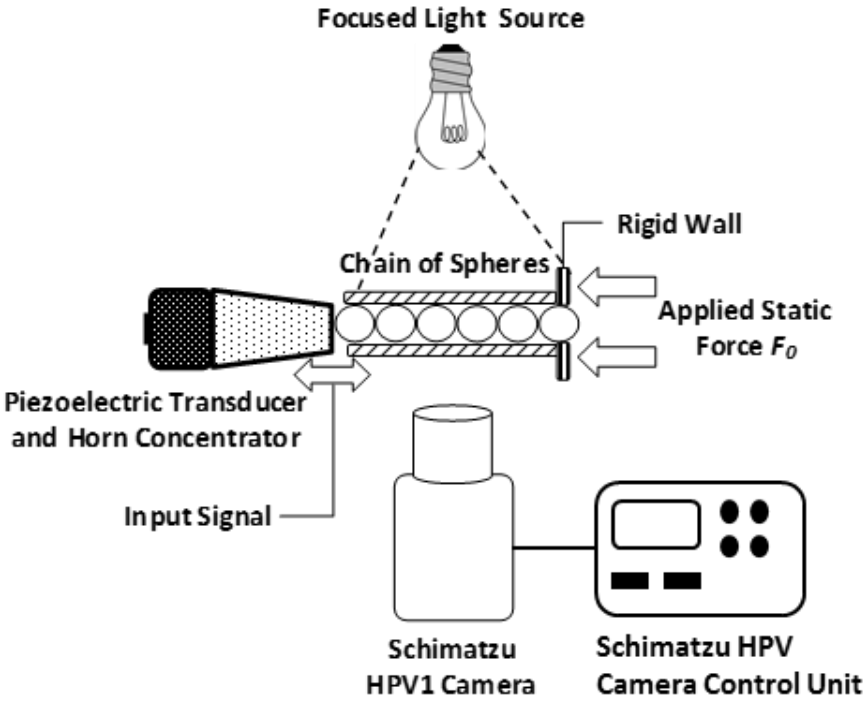

Fig. 3.21 Schematic Diagram of experimental setup.

In Fig. 3.21 and 3.22, four spheres and their respective regions of contact were viewed through a slit in the sphere holder. The transducer was rigidly fixed to a position while the sphere holder was mounted on a micrometre optical translation stage. The stage was used to adjust the amount of pre-compression on the chain of spheres by approaching or backing away from the transducer.

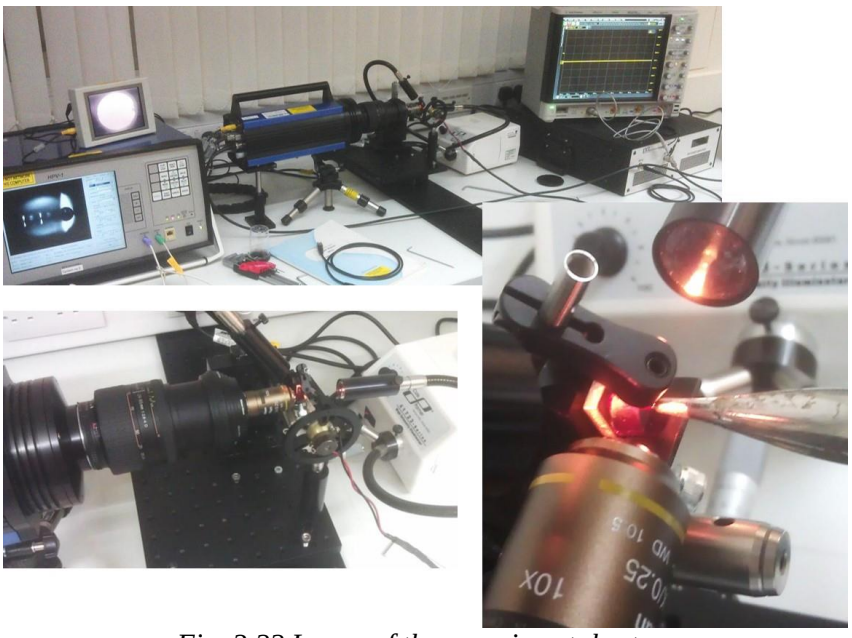

Fig. 3.22 Image of the experimental setup.

Fig. 3.23 shows an image from the camera at time zero, when the spheres were all in contact and at rest at their equilibrium positions. The image shows all 4 spheres with their region of contact highlighted. When the spheres loose contact, the section marked as: Gaps between spheres becomes broader and more distinct, this will be shown in the later figures.

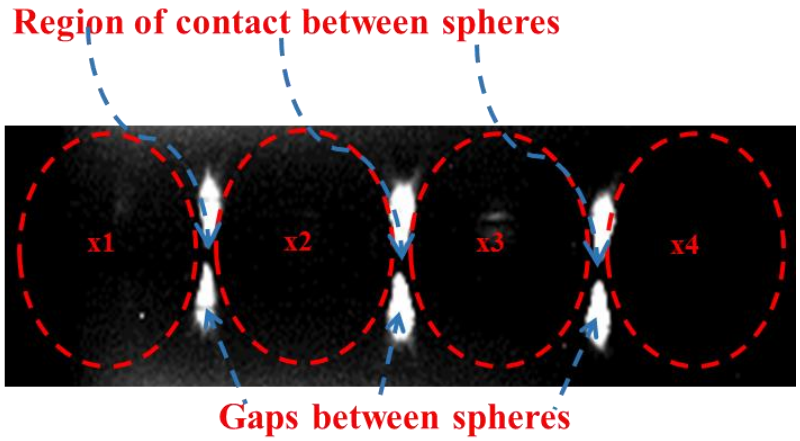

Fig. 3.23 Image from the high speed camera showing the chain of 4 spheres highlighting the area of contact and gaps between successive spheres.

In-phase NNM: This mode can be observed in the series of images in Fig. 3.24, special attention should be paid to the regions between the white shape highlighted as 'Region of contact between spheres' and 'Gaps between spheres' in Fig. 3.23. As the gaps between the spheres in series of images are viewed from left to right and top to bottom, the region of contact between the spheres expand and in some cases shrink thereby merging the two gaps into one. When the gaps between two successive spheres merge that means the spheres have lost contact.

At time zero just before excitation, all spheres were at their equilibrium position in contact with each other when subjected to negligible pre-compression force. Soon after, the energy in the system becomes elastic due to the interaction between the transducer and the 1st sphere while, the other spheres (x2, x3 & x4) remain motionless but shifted from its equilibrium position. At the next time interval; time 1, the spheres collide with one another and begin interacting until they attain a balance between nonlinearity and dispersion. At time 2, the

fourth sphere moves towards the wall passing through its equilibrium position and separating from sphere 3, while all other spheres remain in contact. The 4th sphere regains contact with sphere 3 as it moves away from the wall once again passing through its equilibrium position at time 3. By time 4, the 3rd sphere (x3) would have transferred all its energy to the 2nd sphere and is entering a motionless state. While at time 4 the 2nd sphere is interacting with the 1st and loses contact with the 3rd and would be entering a motionless state. Proceeding to time 5, at this moment, the first sphere is displaced towards the transducer and the potential energy is being converted to kinetic while the 2nd to 4th spheres remain stationary but offset from their equilibrium position. Then at time 6, the cycle repeats in a reverse order starting with 1st sphere. From time 2 to 5, the spheres are interacting with one another in a push-pull fashion while at time 1, when the 4th sphere is out of contact and the 1st sphere is in contact with the transducer, the energy of the system is entirely in the form of elastic potential. This highlights the complex and asymmetric oscillation taking place within the chain of spheres when oscillating in an in-phase periodic motion. The four spheres pass through their equilibrium point at different moments in time. This was in agreement with the system of Jayaprakash *et al.* [11], with characteristics of non-synchronicity and energy transfer within the chain of spheres which matches their definition of NNM as a *"time-periodic oscillation where the bead oscillations possess identical frequencies but are not necessarily synchronous".* This asynchronous oscillation is shown in Fig. 3.24.

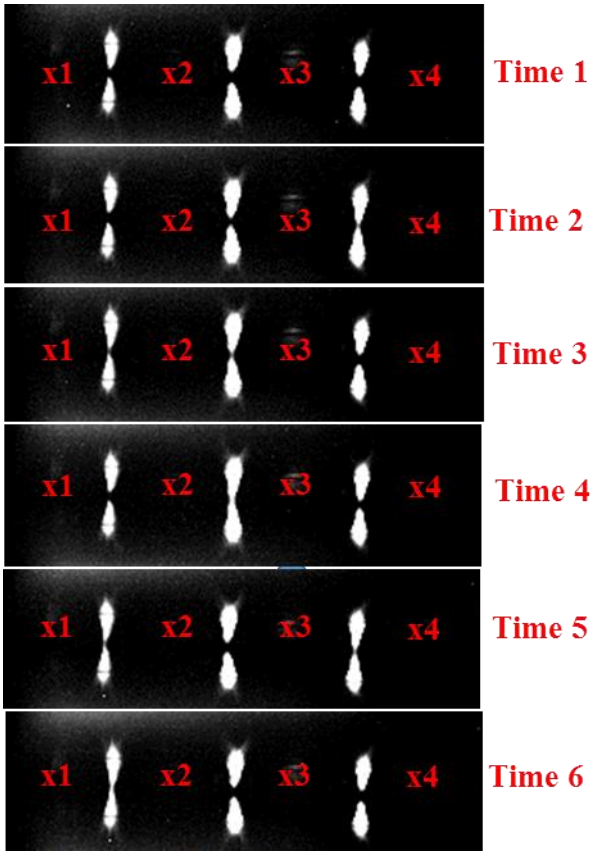

Fig. 3.24: Illustration of the asynchronous (in-phase) behaviour of NNMs, as observed in experiments with the high-speed camera.

Domains within the oscillation present a pattern of separation between the beads, the transducer and the rigid walls where some spheres remain motionless but offset from their initial positions until a motion in the reverse direction is executed. As suggested by Jayaprakash, this feature of high non-synchronicity bear a resemblance to a traveling wave moving back and forth with the chain of spheres.

Out-of-phase NNM: This mode corresponds to a synchronous and symmetric motion within the chain of spheres and was realised when pre-compression was introduced to the chain of spheres. In this case there are no silent modes or motionless states for each sphere. The spheres oscillate in a [near] synchronous mode with the ability to tune the synchronicity by adjusting the pre-compression. By increasing the pre-compression, the state changes from a condition where 2 central spheres (x2 and x3) are oscillating at the same time period while the 2

outermost (x1 and x4) vibrate at the same frequency which is different from the other 2 spheres. In this phase, the energy in the form of elastic potential is shared by the two end spheres (x1 and x4) due to their interaction with the transducer and the wall. As time progresses they pass through their initial positions transferring their energy to the 2 central spheres causing them to separate and then collide with spheres 1 and 2 and the cycle begins again. This is illustrated in Fig. 3.25.

Increasing the pre-compression produces an effect where they soon begin to vibrate under a [near] uniform synchronicity. Introducing further pre-compression such that the chain becomes a continuous medium (a state where the pre-compression is sufficiently greater than the applied force) causes no oscillation or separation in any of the spheres. This is as would be expected from the work of Jayaprakash *et al*. [11], and demonstrates that the expected NNMs were present in the experimental chain of steel spheres.

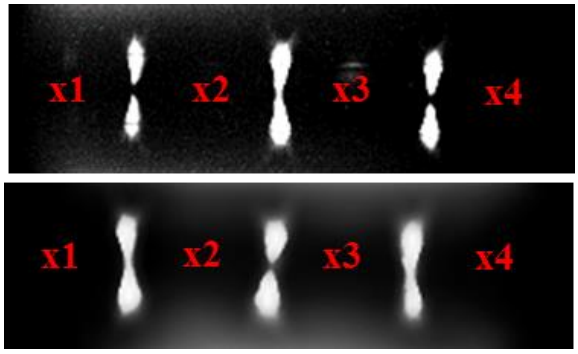

Fig. 3.25: Illustration of Synchronous (out-of-phase) behaviour of NNMs, as observed in experiments with the high-speed camera.

3.7. Conclusions

This Chapter has described the apparatus used to generate non-linear solitary waves in chains of spheres, and it has been shown that this can be achieved. Furthermore, the processes of modelling the system of chain of spheres by expanding Nesterenko's solution to include reflection, damping and by defining functions for the contacts between the spheres, transducer and wall has been described. It was shown in both cases that predictions are for the creation of a set of impulses, which are derived from strongly nonlinear behaviour within the chain. The agreement between theory and experiment for a 20-cycle tone-burst at 73 kHz also shows that the experimental arrangement was able to produce some very interesting phenomena – the creation of impulses from a sine-wave tone-burst.

For the case where the chains are of finite length, the possibility then exists for the creation of non-linear normal modes (NNMs). These were predicted by Jayaprakash *et al*. [11], and their properties were confirmed in this Chapter by an experiment using a high-speed camera to observe the motion of individual spheres in a chain.

The following Chapters will describe this process in much more detail, and present an analysis of the results to show an understanding of the mechanisms present.

3.8. References

1. D.A. Hutchins, J. Yang, O. Akanji, P. J. Thomas, L.A.J. Davis, S. Freear, S. Harput, N. Saffari and P. Gelat, (2015). Evolution of ultrasonic impulses in chains of spheres using resonant excitation, Europhysics Letters (EPL), 109, 54002.
2. B., Laurence, A. Bertsch, and P. Renaud, (1999). Microstereolithography: a new process to build complex 3D objects. International Society for Optics and Photonics 808-817.
3. envisionTec: Perdactory 3 Digital Shell Printer. URL: http://envisiontec.com/envisiontec/wp-content/uploads/2012/12/Machine-P3-DSP.pdf [15 July 2013].
4. D.A. Hutchins, J. Yang, O. Akanji, P. J. Thomas, L.A.J. Davis, P. Gelat, N. Saffari, S. Harput, and S. Freear, (2015). Generation of Impulses from Single Frequency Inputs Using Non-linear Propagation in Spherical Chains. Physics Procedia, 70, 131-134
5. V. F. Nesterenko, (1983). Propagation of nonlinear compression pulses in granular media. Journal of Applied Mechanics and Technical Physics, 24(5), 733-743.
6. A. F. Vakakis, and R. H Rand, (1992). Normal modes and global dynamics of a two-degree-of-freedom non-linear system—I. Low energies. International Journal of Non-Linear Mechanics, 27(5), 861-874.
7. A. Lyapunov, (1907). Probleme generale de la stabilité du mouvement. In Annales de la faculté des sciences de Toulouse, vol. 9, 203–474
8. C. H. Pak, and R. M. Rosenberg, (1968). On the existence of normal mode vibrations in nonlinear systems. Quarterly of Applied Mathematics, 26, 403–416.
9. A. F. Vakakis, L. I Manevitch, Y. Mikhlin, V. Pilipchuck, A. A. Zevin, (1996). Normal Modes and Localization in Nonlinear Systems. Wiley, New York.
10. V. F. Nesterenko, (2001). Dynamics of Heterogeneous Materials. New York, USA: Springer-Verlag.
11. K. R. Jayaprakash, Y. Starosvetsky, A. F. Vakakis, M. Peeters, and G. Kerschen, (2011). Nonlinear normal modes and band zones in granular chains with no pre-compression. Nonlinear Dynamics, 63(3), 359-385.

CHAPTER 4: Effects of Chain Characteristics on Solitary Wave Propagation

4.1. Introduction

Systems comprising of granular chains possess the ability to increase the bandwidth of an ultrasonic signal. This ability is due to the strongly nonlinear Hertzian contact between neighbouring spheres [1]. The dynamic response of said system is governed by a combination of the effects of dispersion, dissipation and nonlinearity, resulting in the propagation of solitary waves along the chain of spheres [2 – 4]. In chapters 3 and 4, equations for the nonlinear dynamic motion of the spheres were derived along with predictions using Nesterenko's solution (and an extended version of the solution) to illustrate the characteristics of the solitary waves [5]. The high degree of tunability of a system containing a chain of spheres was also demonstrated in [6].

Most of the experimental work performed to date concerning solitary wave propagation along a chain of spheres has involved the use of relatively low ultrasonic frequencies, large spheres with diameters greater than 4 mm and a striker as the stimulus used to excite the chain of spheres. The cut-off frequency (described in Chapter 2) limits the upper frequency of the solitary wave that can propagate within a chain containing spheres with a certain diameter. Therefore, higher frequencies require smaller spheres or spheres with a high Young's modulus. Furthermore, little work appears to have been performed experimentally to establish whether higher frequencies and non-impulsive waveforms could be used in chains of finite length. This formation of resonances within chains of small spheres (less than 4 mm) using sinusoidal tone-burst excitation is of particular interest in this research. This is due to the fact that the cut-off frequency would increase, allowing higher frequencies to travel along the chain. Moreover, a high amplitude sinusoidal input might lead to strongly-nonlinear behaviour, and the creation

of some interesting effects. This would then allow some biomedical applications to possibly use these interesting waveforms.

As explained in Chapters 2 and 3, resonances would be created in the form of Non-linear Normal Modes (NNMs) in such chains of finite length. Jayaprakash *et al*. [7] examined similar chains which had fixed boundary conditions, and predicted a set of NNMs which resemble a traveling wave propagating back and forth along the finite granular chain. These were also observed in a two-sphere experimental system [8]. These systems are highly sensitive to their input conditions, in terms of the relation between f_m and f_0, the material and dimensions of the spheres used and the boundary conditions. Despite this, the predictions are that interesting effects could occur.

This chapter explores the effect of using small spheres with a radius of 0.5 mm, with excitation at high amplitudes using an ultrasonic horn at a frequency of 73 kHz. This was performed on various chain lengths subjected to various input waveform parameters. As was shown in Chapter 4, the result is that a tone-burst can be transformed into a set of impulses. This Chapter investigates further the factors which govern the creation of these pulses. Discrete dynamic equations of motion for chains of spherical oscillators were also used to predict the signal development and propagation in such chains, for comparison to the corresponding experimental results.

4.2. Experimental Results and Comparison to Model.

Experiments were performed on a series of chain configurations consisting of 1 mm diameter spheres subjected to the minimum static pre-compression achievable using the experimental arrangement described. The set of experiments involved varying: the length of the chain, the number of cycles of the drive waveform (*i.e.* the duration of the input signal) and the amplitude of the velocity of the input signal v_m at 73 kHz. The results in this section will discuss the

behaviour of the system of chain of spheres as these factors were varied, and give comparisons between the experiments and analytical results. Fig. 4.1 shows a set of input signals produced by the horn at 73 kHz for a drive voltage containing 20 and 45 cycles. Signals between these two limits will be used in the following to drive one end of the chain. The FFT of the waveform at the horn tip (bottom) shows the resonance of the horn at 73 kHz and another, at 146 kHz indicating the presence of some limited harmonic content within the horn. In fact, the vibrometer was used to record the output of the horn for a range of input voltage amplitudes, so that the output at the far end of the chain could be compared to the input. In addition, the input waveform could be used as the input to the theoretical model for the prediction of solitary wave impulses. This allowed proper comparison of the predictions from the theory to the results from the experiments.

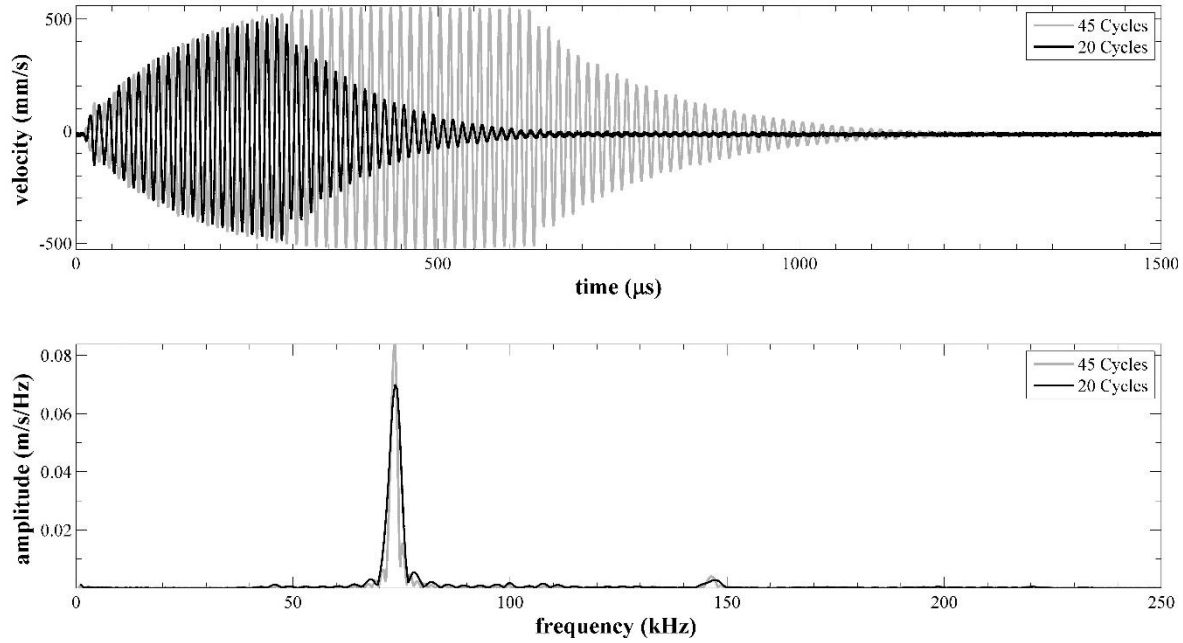

Fig. 4.1. Waveform (Top) and spectrum (Bottom) of the motion of the vibrating horn tip, as measured using a vibrometer. Excitation was a tone-burst of 20 cycles (black) and 45 cycles (grey) at 73 kHz.

In the following sub-sections, results are shown for selected lengths of chains containing the 1mm diameter chrome steel spheres. The first sub-section describes general results obtained by varying the length of the chain. This is then followed by detailed results from a chain

containing 10 spheres, which illustrates the phenomena that tend to occur as the amplitude and duration of the tone-burst from the horn is changed. The results were also compared to the theory, and some conclusions drawn concerning the type of behaviour observed. This is then followed by results from other lengths of chain and a discussion of how chain length affects the results. As will be seen, only certain chain lengths show solitary wave behaviour and the formation of distinct impulses.

4.2.1. **Effects of changing the chain length**

Experiments were performed on a wide range of chain lengths (over the range 2-10 spheres), for various amplitudes and duration of the 73 kHz drive signal from the horn. It was discovered that only certain lengths of chain produced the behaviour of interest – the creation of a set of solitary wave impulses from a tone-burst input. Also, it was found that the resultant signals were highly dependent on the characteristics of the input signal in each case, in terms of its duration and amplitude at 73 kHz. Fig. 4.2 (waveform) and Fig. 4.3 (FFT) both illustrate this. They contain a series of results obtained from these experiments, in each case, the time duration and amplitude of the input were adjusted in order to get the best possible output in terms of impulse generation. In all cases, it can be observed that the chain attempts to transform the input sinusoidal signal of the transducer (Fig. 4.1) into periodic pulses with the period of the pulses getting narrower and sharper as the number of spheres increased. This was achieved more effectively for certain situations; for 2, 3, 6 and 10 spheres, where the chain achieves the balance between non-linearity and dispersion, the result is the generation of solitary wave impulses. For 4, 5, 7, 8, 9 and 11 (only 5, 7 and 9 being shown in Fig. 4.2), the system fails to achieve the solitary wave impulses, showing that the appropriate conditions necessary to setup the waves haven't been met. It further illustrates that the system is sensitive to the number of spheres, the duration and frequency of the input. The combination of all these factors (in 5, 7 and 9) could present an effect whereby the spheres were not resonating

individually/independently but as a series of lumps of spheres. Presenting a situation unlike those established in 3 or 6, here, the wave propagating through the chain of 5 or 7 spheres could be more of a guided wave than a solitary. There wasn't a single set of parameters which worked for all chain lengths. The main point is that 2, 3, 6 and 10 spheres were of the correct length for the input frequency used, with fine-tuning of the input amplitude and duration, solitary waves are generated.

Fig. 4.2 also suggests that the maximum amplified voltage (160 V) used to drive the transducer and horn was sufficiently greater than the pre-compression force resulting from the light touch of the tip of the horn with the first sphere. The voltage applied to the transducer for the 2-sphere case was the same as that used for the 10-sphere and all others in-between. As mentioned, there wasn't a universal set of parameters that worked for all the chain lengths. For each scenario at 73 kHz the duration of the input signal had to be tuned to the correct range of cycles to attain the pulses. For 2 spheres this was at 5 cycles, 10 cycles for 3, 20 cycles for 6 & 7 and 45 cycles for 10 spheres. However, for 4, 5, 7, 8 and 9 spheres, it was difficult to establish solitary wave pulses at any duration of the input.

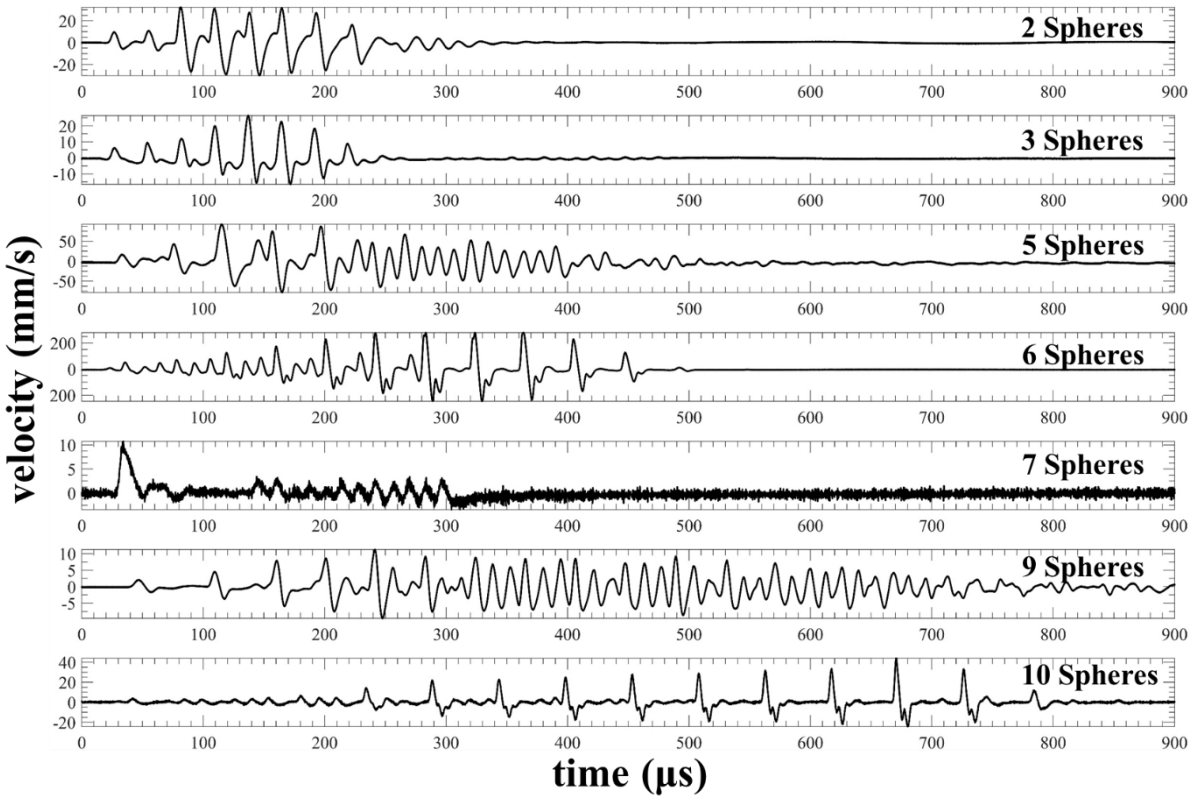

Fig. 4.2. A series of waveforms obtained from the experiments for various chain lengths and input duration at 73 kHz.

The spectra corresponding to the waveforms of Fig. 4.2 are shown in Fig. 4.3. The first observation that can be made is that a regular set of resonances appear when the solitary wave impulses are present in the time waveform. These are represented in the spectra in the form of both sub-harmonics and harmonics. In the chain lengths shown where impulses are not genereated efficiently, these sub-harmonics can also be observed (in chains containing 5, 7 and 9 spheres). The trend that can be observed is; 1 sub-harmonic in 3-sphere chain, 2 in 6-sphere and 3 in 10-sphere chain, between 3 and 6 spheres, the number of sub-harmonics is trying to change from 1 to 2. Similarly, between 6 and 10 spheres, it attempts to change from 2 to 3 sub-harmonics. Following this trend, it is expected that the 5-sphere chain shouldn't have a greater number of sub-harmoncis than those present in the 6-sphere however, it contains just as many sub-harmonics as the 10-sphere chain but less distinct and so do the 7 and 9-sphere cases. This further suggests that there is a set of conditions required to estabilish the resonant mode which

permits the propagation of non-linear solitary wave pulses. The number of sub-harmonics and harmonics present depends on the number of spheres - as the number of spheres increases so do the number of sub-harmonics and harmonics. In the 2 and 3 sphere cases there was a single sub-harmonic, for 6 spheres there were two sub-harmonics and three sub-harmonics were observed for 10 spheres. The resolution of the spectrum increases has the number of spheres increase producing a sharpness and narrowing of the frequency peaks. Further details into the characterics of each chain lengths will be presented in following sections.

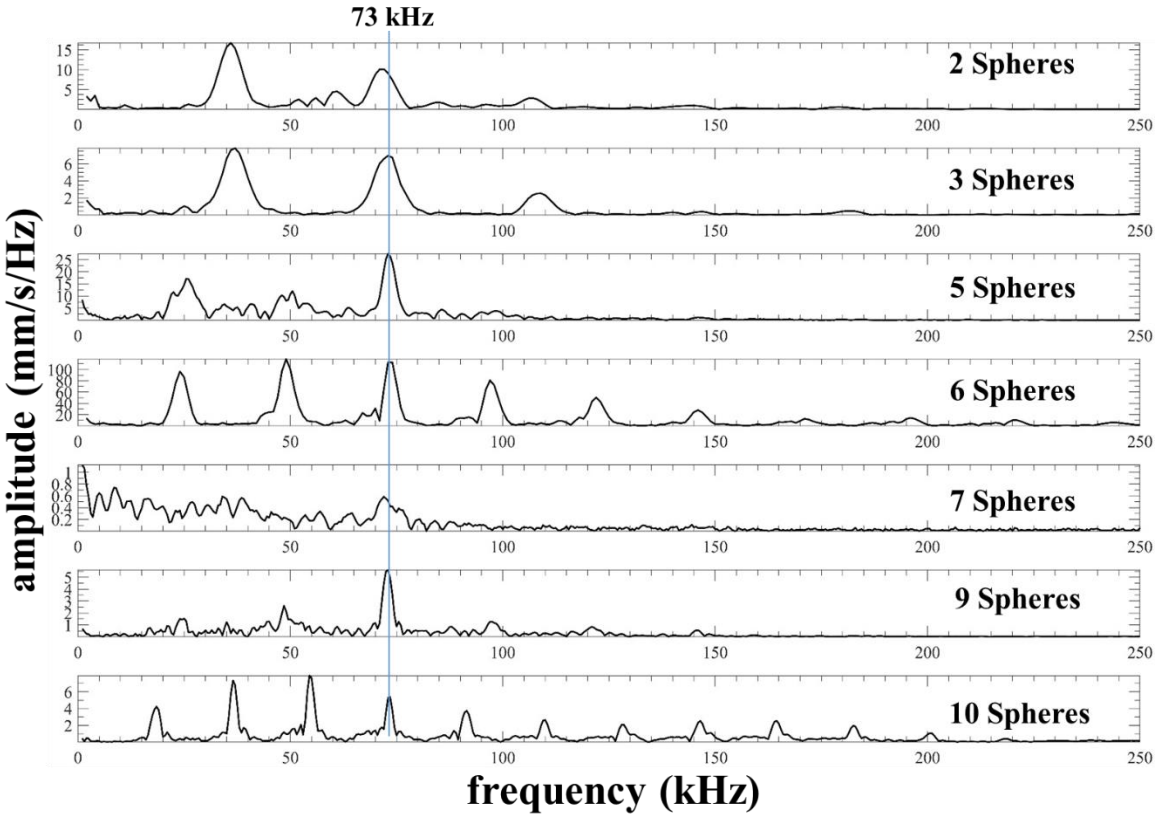

Fig. 4.3. A series of spectrums for various chain lengths and input duration at 73 kHz obtained from the experiments.

4.2.2. **Detailed results for a 10-Sphere Chain**

A 10-sphere chain was found to give a good response in terms of solitary wave generation, and so the results for this system are presented here in some detail. Fig. 4.4 shows the experimental results as the input peak to peak particle velocity amplitude (v_m) from the horn was gradually increased from 33 mms^{-1} to 1,081 mms^{-1} using a 45-cycle voltage signal excitation. At low amplitudes of the input signal (v_m = 33 - 151 mms^{-1}), the output signal obtained from the last

sphere within the chain displayed characteristic similar to those of the horn (Fig. 4.1). The corresponding spectrum shows a similar frequency content to that from the horn, with the dominant peak at 73 kHz and a smaller peak at 146 kHz, which is more prominent at v_m = 151 mms^{-1}.

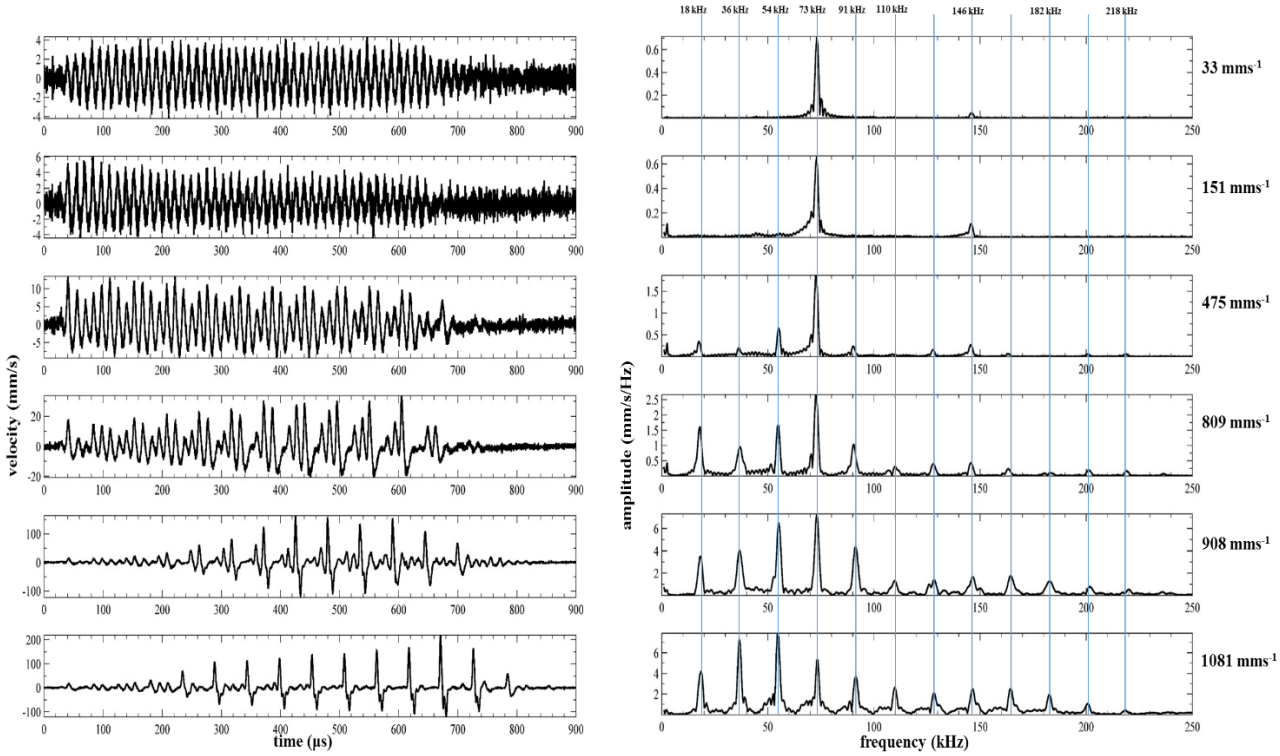

Fig. 4.4. Waveform (left) and frequency spectrum (right) of the output from a 10-sphere chain excited using a 45 cycle tone-burst from an ultrasonic horn at 73 kHz.

As the amplitude, v_m of the input signal increases from 475 to 809 mms^{-1}, the time waveform begins to transform into groups of periodic signals with a periodicity different to those the input signal. This periodicity is illustrated in the spectrum as regularly spaced peaks at frequencies higher and lower than the input frequency of 73 kHz. As v_m increases further, the transformation is complete and the periodic pulses become more obvious in the time waveform. At the maximum input amplitude (1,081 mms^{-1}), a set of distinct regularly spaced pulses can be observed. The frequency spectrum contains three sub-harmonics with the lowest frequency peak occurring at 18 kHz, which is approximately a quarter of the input frequency 73 kHz. This frequency (18 kHz) corresponds to the periodicity of the pulse in the time waveform,

which was 55μs. It can also be seen that the input frequency of 73 kHz is no longer the most dominant peak within the spectrum.

By windowing a section of the waveform between 655 – 695 μs, a single pulse can be isolated for $v_m = 1081$ mms^{-1} as shown in Fig. 4.5. The frequency spectrum for this single pulse shows that each of these periodic pulses contain a wide bandwidth, with components at frequencies greater than 200 kHz.

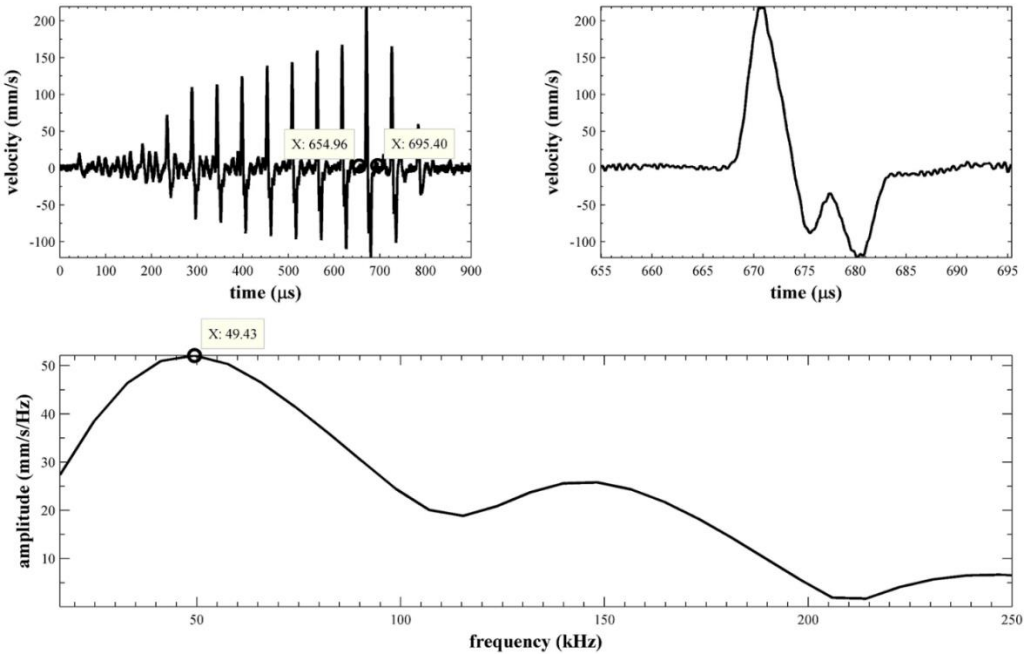

Fig. 4.5. Waveform of the entire waveform (top-left), waveform of the windowed pulse (top-right) and frequency spectrum (bottom) of the windowed pulse of the output from a 10-sphere chain excited using a 45 cycle tone-burst from an ultrasonic horn at 73 kHz at maximum amplitude of 1081 mms^{-1}.

The output signal is highly dependent on the duration of the input signal, which in turn is controlled by the number of the cycles of the tone-burst. The duration also affects the input signal's peak to peak amplitude, v_m, such that the longer the duration, the greater the value of v_m. This is illustrated in Fig. 4.6, which shows the waveforms and spectra for 20, 30, 40, 45 and 50 cycles. At 20 and 30 cycles, the pulses were not fully formed and their corresponding spectral peaks were indistinct. As the number of cycles increase, the periodic pulses begin to emerge and the peaks become more distinct within their spectra. However, at 50 cycles and

greater the pulses change to a set of double pulses and the resolution of the spectrum become duller suggesting that the optimum number of cycles lie between 45 and 50 cycles.

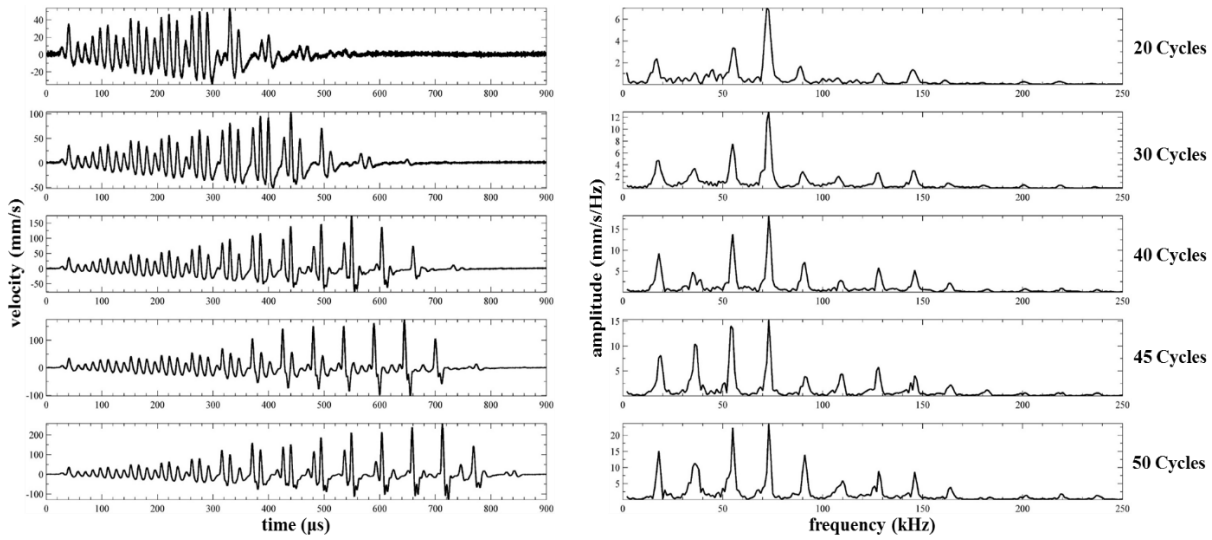

Fig. 4.6. Waveforms (left) and Spectra (right) showing the effect of changing the number of cycles in the drive waveform for a 10-sphere.

The above results for a 10-sphere chain can now be compared to theoretical predictions of the model, so as to confirm the expected behavior. The predicted results for the 10-sphere chain are shown in Fig. 4.7 for a 45-cycle input at amplitudes v_m= 33, 475 and 1,081 mms^{-1}. The predicted waveforms show similar trends to those from the experiments, with additional harmonics and sub-harmonics appearing in the frequency spectrum. A pre-compression force $f_0 = 0.032$ N and viscous damping coefficient $Q = 0.32$ Ns^{-1}m was used in the model to account for the effect of damping present in the experiment. Note that a zero pre-compression force did not produce an output signal with the desired features, showing that a finite value is needed to produce the desired effect (the result of higher pre-compression forces is discussed in a later chapter). A pre-compression of 0.032 N produced a result closest to that of the experiment. The predicted waveform and corresponding spectrum for v_m = 33 mms^{-1} (Fig. 4.7 (top)) contain features that agree with those observed in the experiments (Fig. 4.4), that is; a waveform with an envelope similar to that of the horn and two peaks at 73 kHz and 146 kHz. When v_m = 1,081 mms^{-1} (Fig. 4.7 (bottom)) the output contains strongly periodic nonlinear

solitary wave pulses with a spectrum containing three sub-harmonics and peaks separated by a quarter of the 73 kHz input frequency.

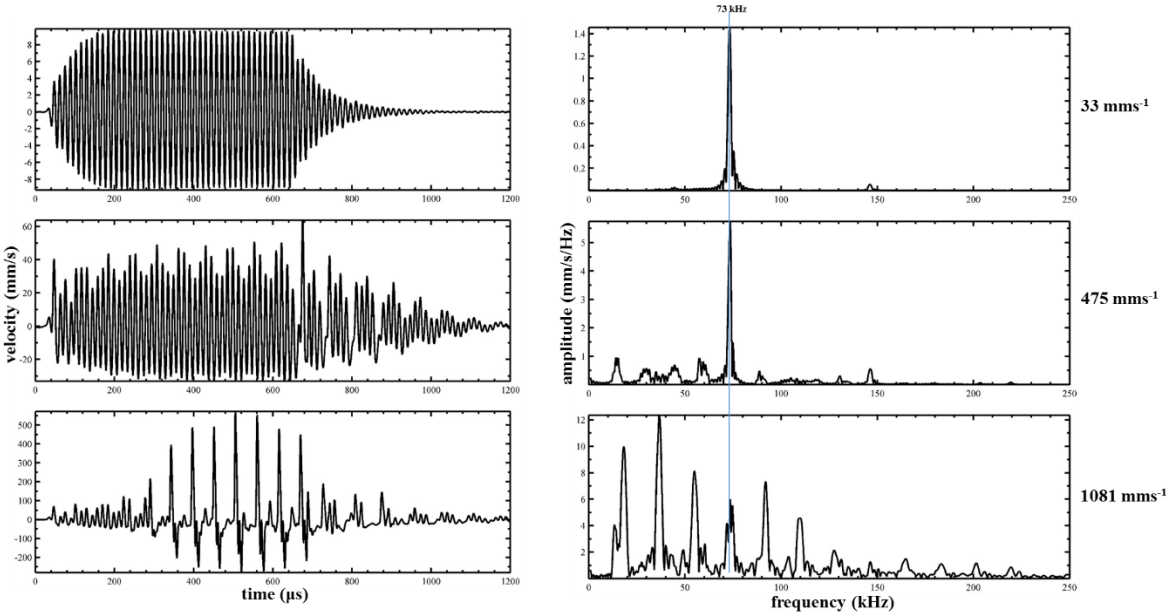

Fig. 4.7. Model prediction for a 10-sphere chain using an input of 45-cycle tone burst from an ultrasonic horn at 73 kHz. Waveforms (left) and Spectra (right) at various input amplitudes.

Fig. 5.8 illustrates how the solitary waves form as they propagate along the chain from the first sphere (Fig. 4.8 (a)) to the tenth sphere (Fig. 4.8 (d)) over time. The predictions depict a similar trend across all ten spheres; a region of relatively low velocity for the first few 100 µs which is required to build or pump energy to form the solitary pulses. These pulses are maintained for a certain time duration, before the spheres reach a resting point or silent zone. At this point, the energy from the sphere is transferred to its neighbouring sphere and a loss in contact occurs between the spheres. As the solitary wave propagates along the chain, the pulses become slower and their periods become larger. By the tenth sphere the pulses are more defined. This is due to the effect of reflection, which gives the pulses a smooth bipolar appearance unlike those in preceding spheres.

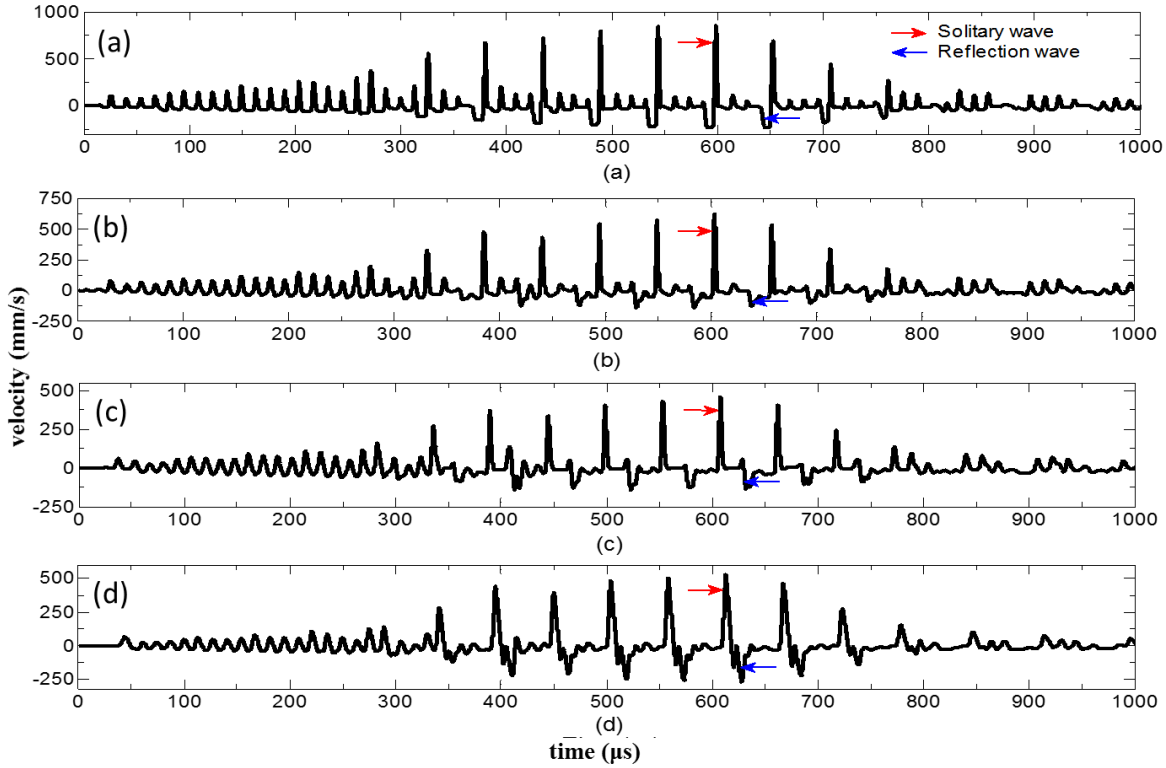

Fig. 4.8. Predicted waveforms of individual spheres within a chain of 10 spheres for (a) the first sphere; (b) the fourth sphere; (c) the seventh sphere; (d) the tenth sphere. Red arrows show the direction of propagation away from the input, and blue arrows show direction of the reflected signal [9].

The corresponding theoretical spectra in Fig. 4.9 show the presence of harmonics, and also highlight the effect of the broadening pulse period. As the period increases from the first sphere to the tenth sphere, the number the number of higher harmonics reduces while the amplitude of the lower harmonics increases. In the spectrum of the 1st sphere, the harmonic content extends beyond 300 kHz but by the 10th sphere a reduction as occurred and the content is slightly above 200 kHz.

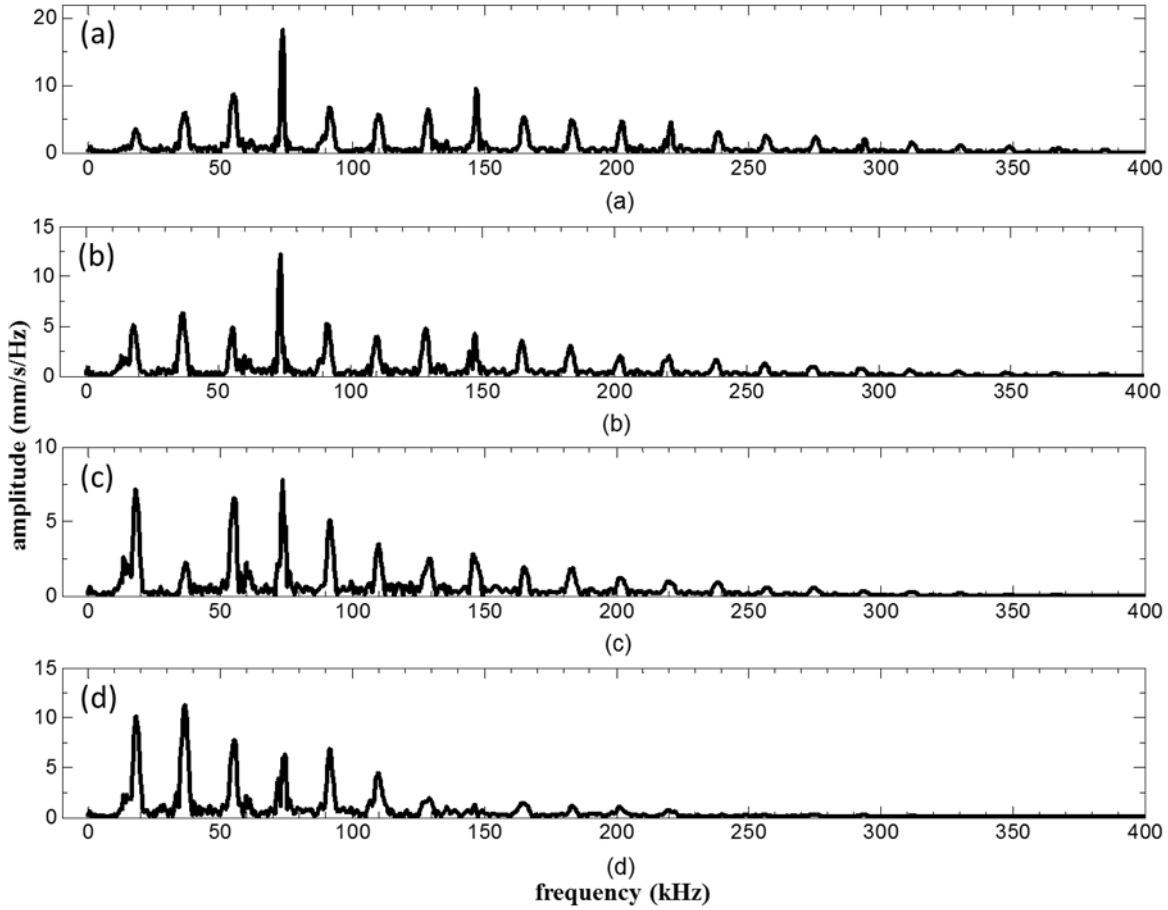

Fig. 4.9. Predicted spectra of individual spheres within a chain of 10 spheres for (a) the first sphere; (b) the fourth sphere; (c) the seventh sphere; (d) the tenth [9].

The theory has thus been able to show how these solitary wave impulses form, and how the waveform varies along the chain. The result in both theory and experiment was that the signal at the 10^{th} sphere was in the form of a periodic waveform, containing solitary wave impulses, with a spectrum possessing a set of regularly-spaced distinct frequency components. These effectively represent the non-linear normal modes (NNMs) of the system. The assumption of a small compression force in the theory was reasonable, as this cannot be avoided in practice, and resulted a good agreement with experiment. There must be some small pre-compression force due to the positioning of the horn against the first sphere. Also, there is likely to be damping in the system due to the acrylic holder.

4.2.3. Results for other chain lengths where solitary wave impulses were observed

A. 6-Sphere Chain

Here, a similar analysis to that presented earlier for the 10-sphere case is presented. The outputs from a chain of six spheres excited using a 20-cycle tone-burst signal via the horn while varying the amplitude is shown in Fig. 4.10. Due to the shorter length of the chain (when compared to the 10-sphere chain) less energy is required by the system to transform the sinusoidal input wave to the solitary wave pulses which are evenly spaced apart. At low amplitudes, a weakly nonlinear behaviour was observed defined by multiple small peaks in the spectra and a saw tooth-like trail of wave in the time waveform. As v_m tends towards its maximum amplitude of 937 mms^{-1}, the period or separation of the pulses increases in the time waveform and the peaks in the spectrum introduced to the system due to the nonlinearity of the contacts between the spheres become more prominent. The periodicity of the pulses was 41 µs which corresponded to the first peak in the spectrum at 24 kHz, which was approximately a third of the input frequency. (Note that this is different to that seen for the 10-sphere case, where the period was longer and corresponded to a quarter of the input frequency). All the main frequency peaks were integer multiples of the first peak (24 kHz) and two sub-harmonic peaks can be observed.

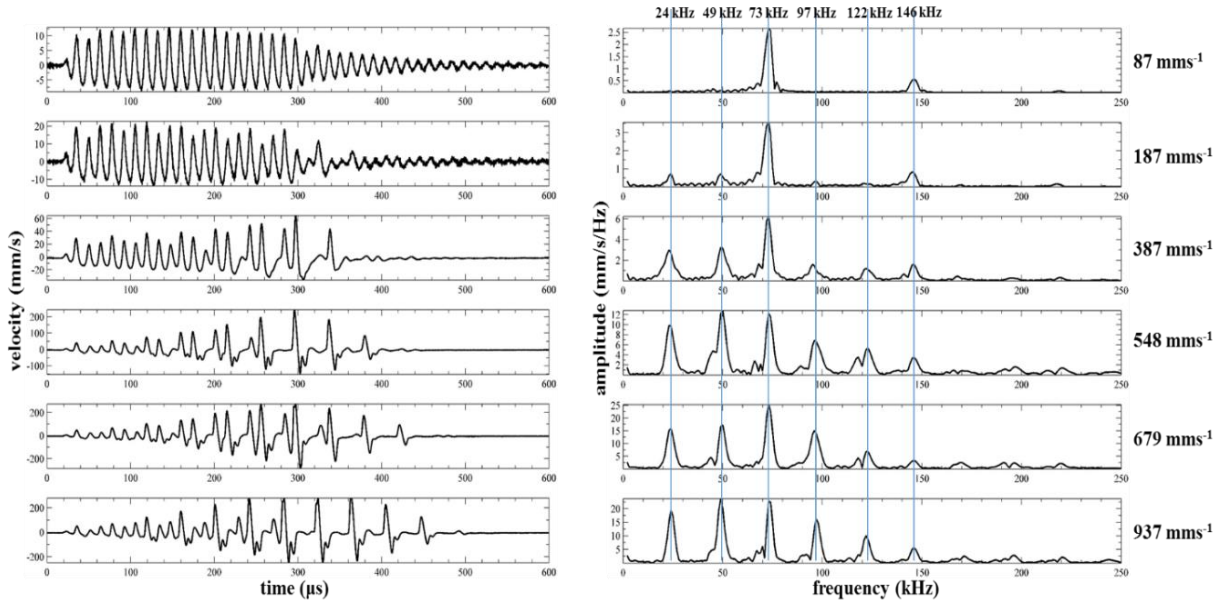

Fig. 4.10. Waveform (left) and frequency spectrum (right) of the output from a 6-sphere chain excited using a 20-cycle tone-burst from an ultrasonic horn at 73 kHz.

Windowing a section of the waveform between 299.66 µs and 341.48 µs for the maximum peak to peak amplitude of 937 mms^{-1}, allows a single pulse to be studied as shown in Fig. 4.11. The frequency spectrum for this single pulse shows that each of these periodic pulses contain a wide bandwidth with frequencies greater than 150 kHz.

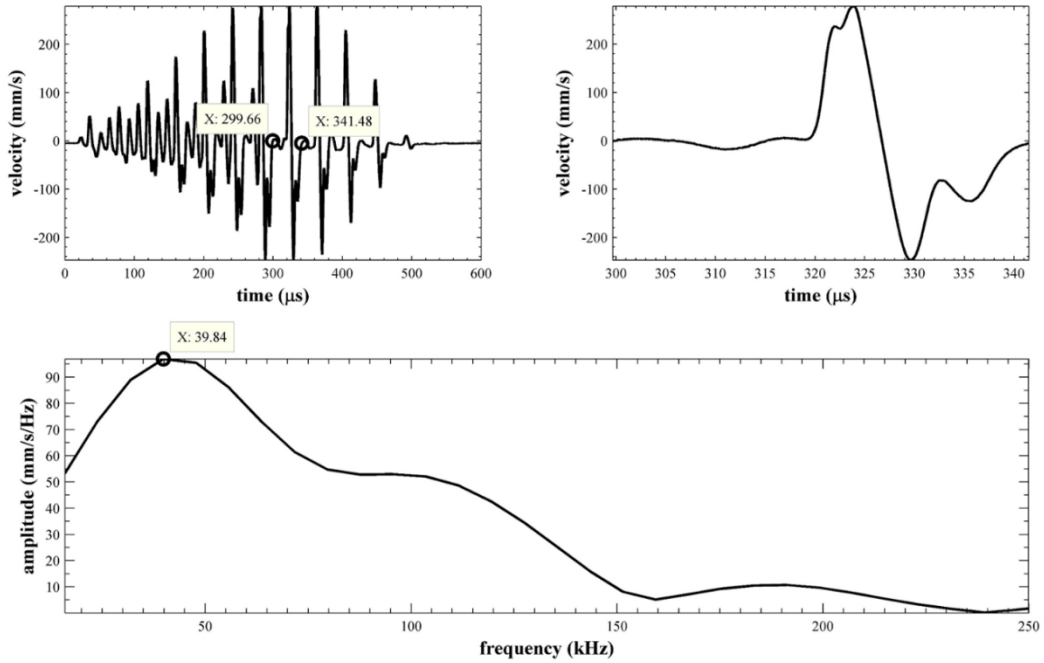

Fig. 4.11. Waveform of the entire waveform (top-left), waveform of the windowed pulse (top-right) and frequency spectrum (bottom) of the windowed pulse of the output from a 6-sphere chain excited using a 20 cycle tone-burst from an ultrasonic horn at 73 kHz at maximum amplitude of 937 mms^{-1}.

As expected the experiments showed that there was also a dependency on the duration of the excitation signal as demonstrated in Fig. 4.12 for 1, 4, 10, 20 and 30-cycle excitations. At 1 and 4-cycle, the spectra peaks of the two sub-harmonic peaks were beginning to take form but still relatively indistinct. As the duration increased to 10 cycles, the periodic pulses begin to emerge and the resolution of the spectra improves. The optimum result was noted to be at 20 cycles, here the spectra peaks were fully formed with the sub-harmonic peaks having larger amplitudes than the input frequency of 73 kHz. When the input signal's duration was increased to 30 cycles, the amplitudes of the harmonics and sub-harmonics decreased relative to the input frequency of 73 kHz and the pulses became less distinct in the time waveform.

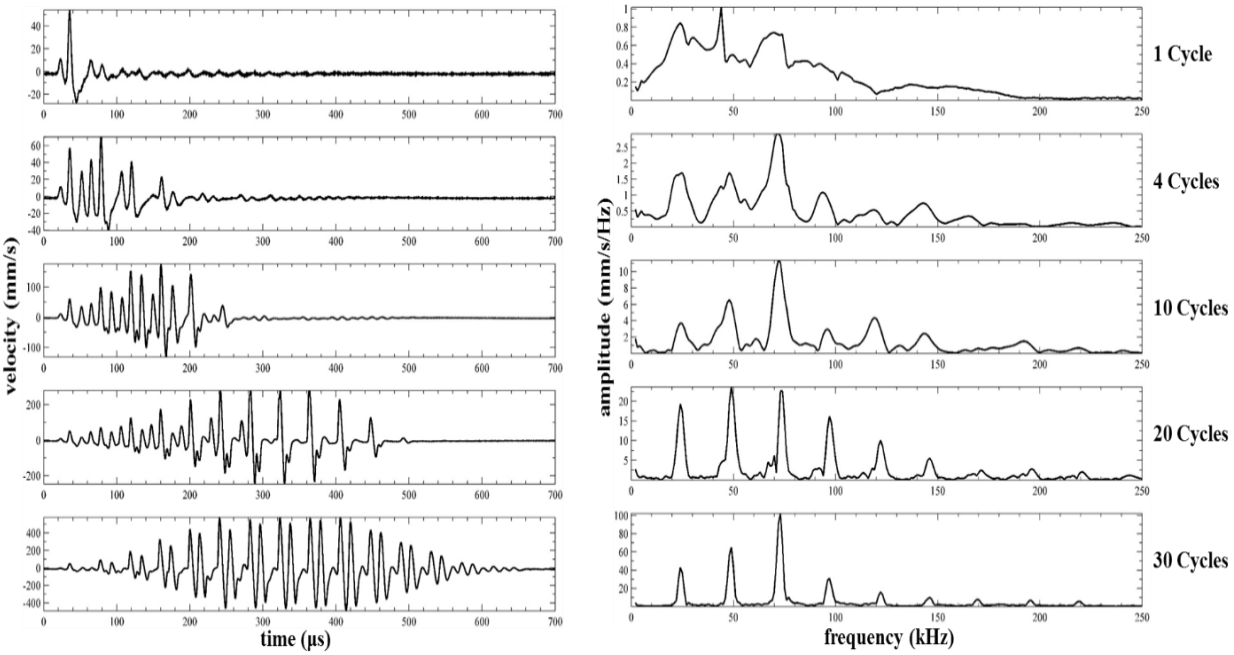

Fig. 4.12. Waveforms (left) and Spectra (right) showing the effect of changing the number of cycles in the drive waveform for a 6-sphere.

The predicted waveforms shown in Fig. 4.13 were generated when a small amount of pre-compression force $f_0 = 0.03894$ N was introduced to the system. For this amount of compression, the model produced small initial displacements for the spheres: $\delta_{0l} = 0.024$ μm; $\delta_0 = 0.03$ μm and $\delta_{0r} = 0.28$ μm.

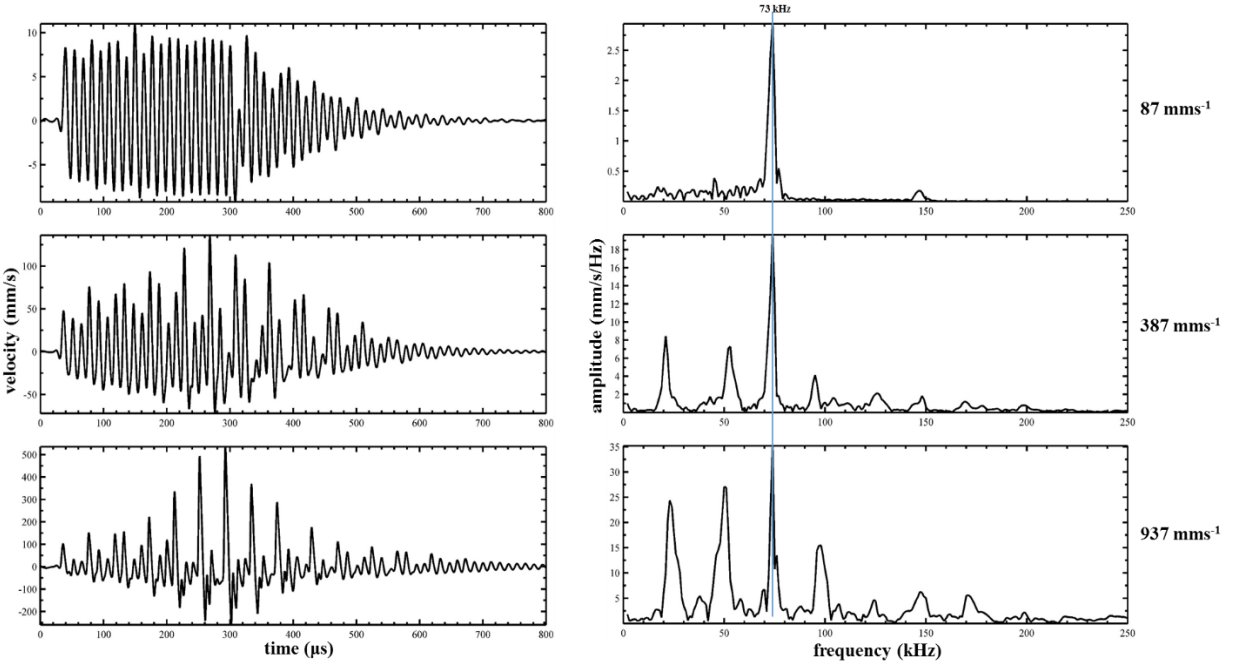

Fig. 4.13. Model prediction for a 6-sphere chain using an input of 20-cycle tone burst from an ultrasonic horn at 73 kHz. Waveforms (left) and Spectra (right).

The features of the predicted result for an input amplitude of 87 mms^{-1} were in agreement with those observed experimentally in Fig. 4.10. The time waveform contained a signal with similar features of those of the input from the ultrasonic horn. At an intermediate amplitude of 387 mms^{-1} the output was transformed to a weakly nonlinear signal. Similarly at high amplitude (937 mms^{-1}), when the output is strongly nonlinear, the main features shown in the experiments can be observed to be present in the predicted results. The distinct periodic pulses were predicted with the same spacing in time as seen in the experiment, and the spectrum contained two sub-harmonics and peaks separated by a third of the input frequency (73 kHz).

B. 2-Sphere and 3-Sphere Chains

These two lengths behaved in a similar way, with the 3-sphere case producing solitary wave impulses which were slightly more obvious. In this section results are thus shown only for the 3-sphere chain.

For the chain comprising of three spheres, the output waveforms and spectra are shown in Fig. 4.14 for an excitation with a duration of 10 cycles. Just like in the chain comprising of six and ten spheres, the time waveform and spectrum of the lowest amplitude (22 mms^{-1}) excitation resembles that of the output of the horn in Fig. 4.1 with a peak at 73 kHz and a minute peak at 146 kHz. As the amplitude tended towards its maximum v_m, the solitary pulses began to form and finally at the maximum amplitude of 591 mms^{-1} the pulses had become prominent and the corresponding spectrum contained the expected harmonics and sub-harmonics. At this amplitude, the dominant peak was a single sub-harmonic at 36 kHz, which was approximately half of the input frequency of 73 kHz. This sub-harmonic corresponded to the spacing of the peaks in the spectrum and also to the period of the pulses in the time waveform. The trend seen from 10 to 6 spheres has thus continued.

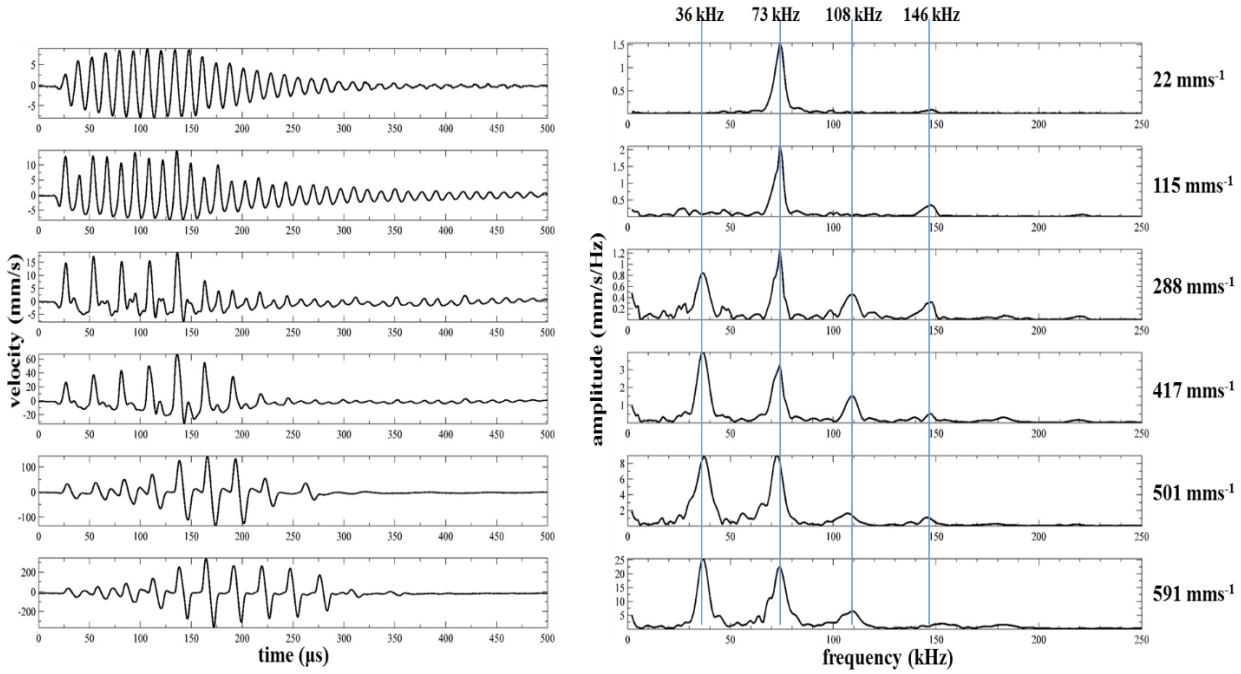

Fig. 4.14. Waveform (left) and frequency spectrum (right) of the output from a 3-sphere chain excited using a 10-cycle tone-burst from an ultrasonic horn at 73 kHz.

Windowing a section of the waveform between 150.77 µs and 178.10 µs, isolates a single pulse for the maximum peak to peak amplitude of 591 mms^{-1} as shown in Fig. 4.15. The frequency spectrum for this single pulse shows that each of these periodic pulses contain a wide bandwidth with frequencies greater than 100 kHz.

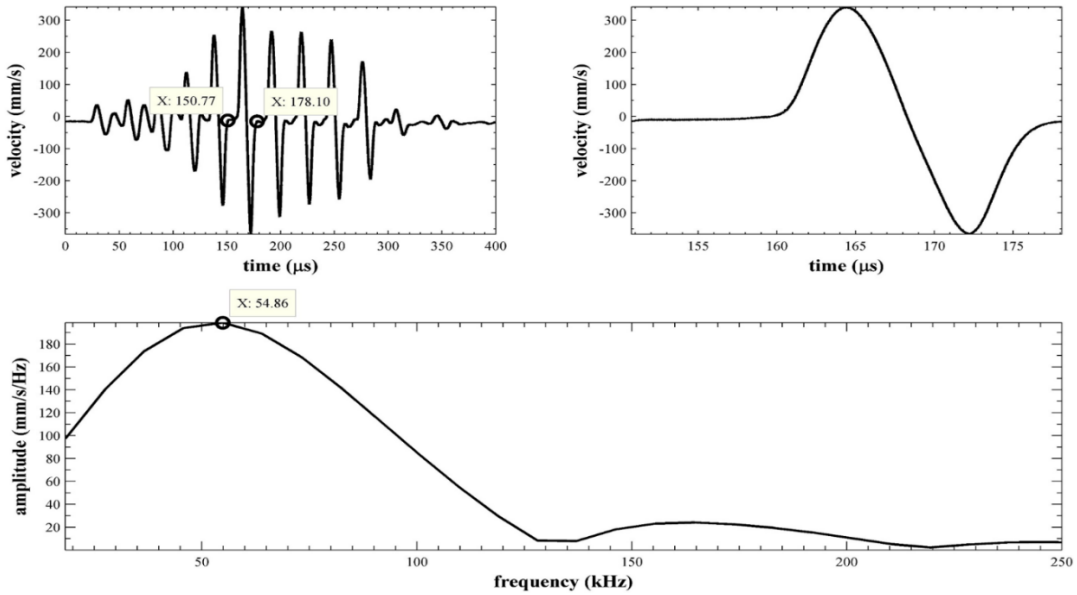

Fig. 4.15. Waveform of the entire waveform (top-left), waveform of the windowed pulse (top-right) and frequency spectrum (bottom) of the windowed pulse of the output from a 3-sphere chain excited using a 10 cycle tone-burst from an ultrasonic horn at 73 kHz at maximum amplitude of 591 mms^{-1}.

The duration also affects the input signal's peak to peak amplitude, v_m, the longer the duration, the greater the value of v_m. This was illustrated in Fig. 4.6 for the chain of ten 1 mm spheres. Fig. 4.16 shows the waveforms and spectra for 5, 10, 15, and 20 cycles. At 5 cycles, the pulses weren't fully formed and their corresponding spectral peaks had a broad frequency resolution. As the number of cycle increases, the periodic pulses become more pronounced and the first three harmonic peaks become better defined with greater amplitudes. As a result of this, the energy from the lesser peaks at 145 kHz and above has been distributed to the larger peaks and they begin to fade. At 15 cycles, the lesser peaks at 145 kHz and above re-emerge in the spectrum resulting in a reduction it the amplitudes of the dominant peaks. In the time waveforms, the period of the pulses is narrower and the trail of pulses is less obvious. When the duration was further increased to 20 cycles the pronounced periodic pulses become more obvious, the resolution of the peaks within the spectra is sharper. However, the number of harmonic peaks in the spectra is fewer and similar to those present in the 10-cycle excitation.

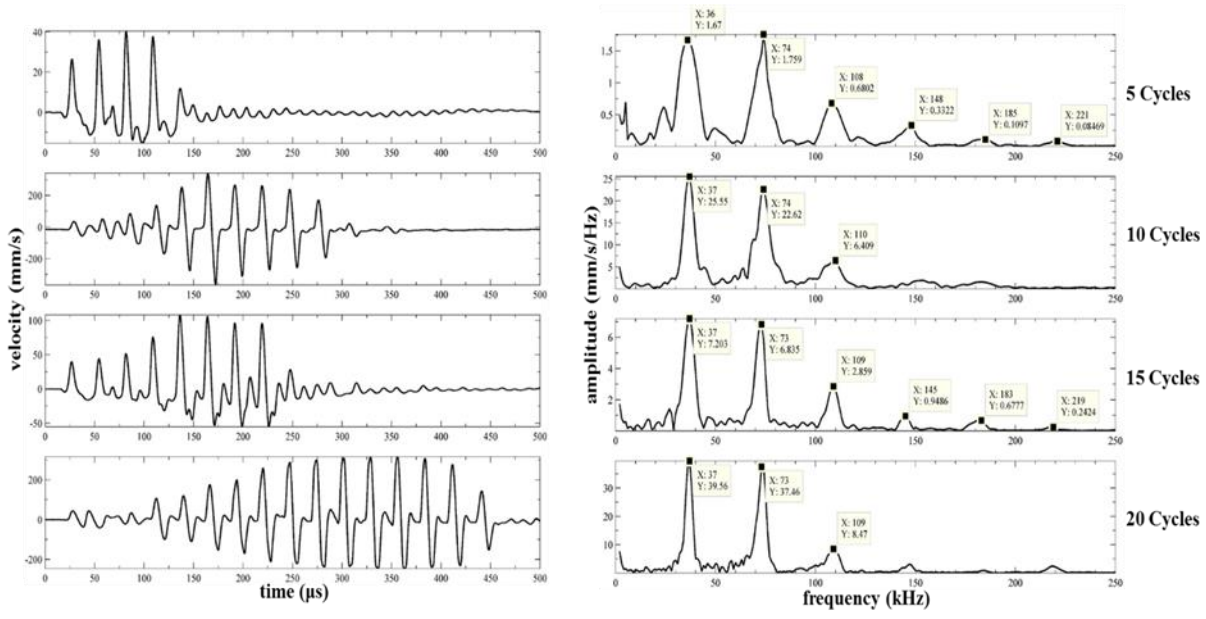

Fig. 4.16. Waveforms (left) and Spectra (right) showing the effect of changing the number of cycles in the drive waveform for a 3-sphere.

Results from the model again match those observed experimentally. The predicted result for a 3-sphere chain is shown in Fig. 4.17 for a 10-cycle input at amplitude of 591 mms^{-1}. The

waveform has a similar trend to those from the experiments (Fig. 4.16) with the input signal modified to contain additional harmonics in the frequency spectrum. A pre-compression force $f_0 = 0.$ 0.02 N and viscous damping coefficient $Q = 0.23$ Ns^{-1}m was used in the model to account for the effect of damping and the slight pre-compression present in the experiment. The predicted waveform and corresponding spectrum for v_m = 591 mms^{-1} contain features that agree with those observed in the experiments, that is; a waveform with strong periodic nonlinear solitary wave pulses and a spectrum containing one sub-harmonic and peaks separated by a spacing which was half of the input frequency (73 kHz).

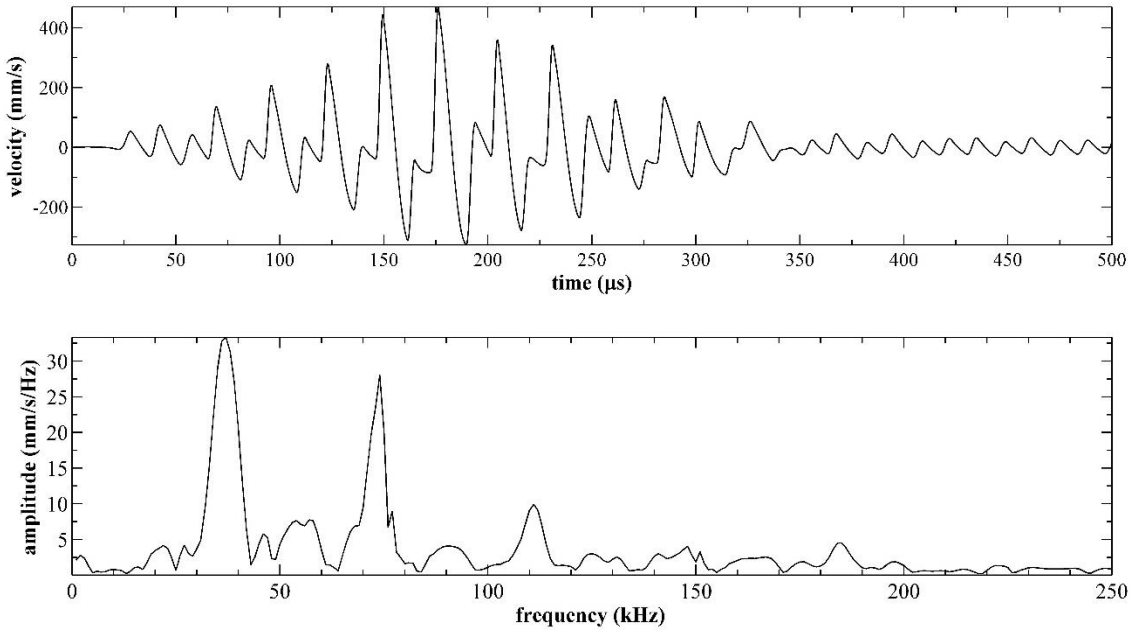

Fig. 4.17. Model prediction for a 3-sphere chain using an input of 10-cycle tone burst from an ultrasonic horn at 73 kHz and v_m =591 mms^{-1}. Waveforms (top) and Spectra (bottom).

C. Comparison between 3, 6 and 10-Sphere chains

In all three cases, a train of pulses with regular periodicity were present which corresponded to harmonics and sub-harmonics within the spectra. These regularly-spaced resonant peaks were characterised by being present at integer fractions of the input frequency (73 kHz): a quarter for 10-sphere chain (18 kHz), a third for 6-sphere chain (24 kHz) and half for the 3-sphere

chain (36 kHz). In each case, the value of the first sub-harmonic was equal to the distribution of the peaks in their respective spectra and the periodicity in the time waveform.

It was also evident that the longer chain length resulted in a wider bandwidth at the maximum input signal level, with sharper peaks in the spectrum and pronounced pulses in the time waveform. This was confirmed when a FFT was performed on an individual pulse for each chain length.

It was found that an increase in the peak to peak amplitude of the input signal did not produce a linear response to that of the particle velocity measured at output as shown in Fig. 4.18. Initially, at low input amplitudes, the peak to peak particle velocity of the output were proportional to that of the input (region 'A' in Fig. 4.18) acting in a linear fashion. Beyond this initial stage, the output amplitude for 3, 6 and 10-sphere rapidly increased until reaching a threshold or saturation point. At this point the amplitudes become more erratic (more evident in the 10-sphere case) and soon begin to diminish. This behavior is similar to those of a finite-amplitude resonant system in which sub-harmonic generation is involved such as those observed in bubble dynamics [10].In this region exist the non-linear regime; B and C for weakly non-linear and strongly non-linear propagation respectively.

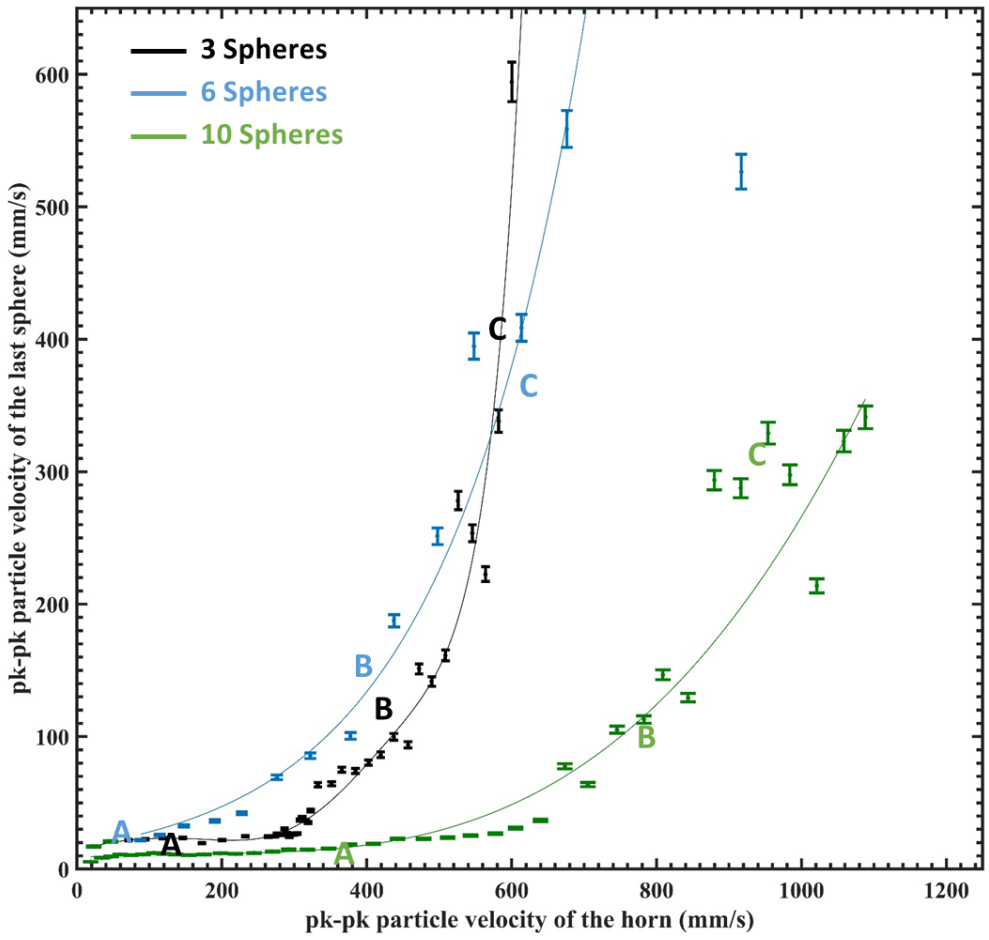

Fig. 4.18. Dependence of output pk-pk amplitude on that of the input, as measured by the vibrometer in chains containing 3, 6 and 10 spheres. A: Strongly nonlinear regime, B: Weakly nonlinear and C: tending towards linear.

4.2.4. 5 and 9-Sphere Chains

Chain lengths consisting of 5 and 9 spheres were found to possess weakly non-linear solitary waves for an input frequency of 73 kHz.

A. 5-Sphere Chain

Fig. 5.19 shows the experimental results of varying the duration of the excitation signal between 10 and 30 cycles at an input frequency of 73 kHz. At 10 cycles the chain consisting of five spheres produced a train of pulses which corresponds to a weakly non-linear behaviour, the pulse travel for a short duration and then collapse. The spectrum for 10 cycles displays multiple harmonics with characteristics similar to those present in the 6-sphere case. This was presented in the form of two large sub-harmonics which were not has evenly spaced as those

observed in the 3, 6, and 10-sphere chains. Increasing the duration to 20 cycles produced a worse result with the train of pulses devolving rapidly after creation with the chain resonating in a mode which allows the transmission of guided waves. The peaks in the spectrum were less distinct with the appearance of other lower harmonics. At 30 cycles, the waveform becomes unstable and the peaks within the spectra completely lose the distribution attained in the 10-cycle scenario. This behaviour was also predicted by the model shown in Fig. 5.20 for a 10-cycle input.

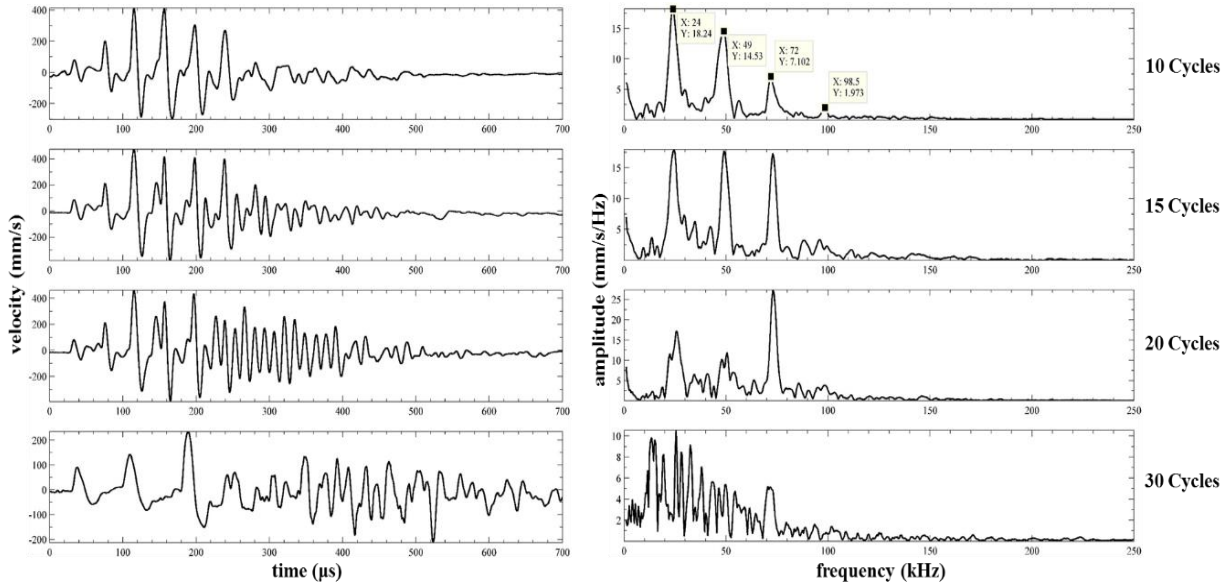

Fig. 4.19. Waveforms (left) and Spectra (right) showing the effect of changing the number of cycles in the drive waveform for a 5-sphere.

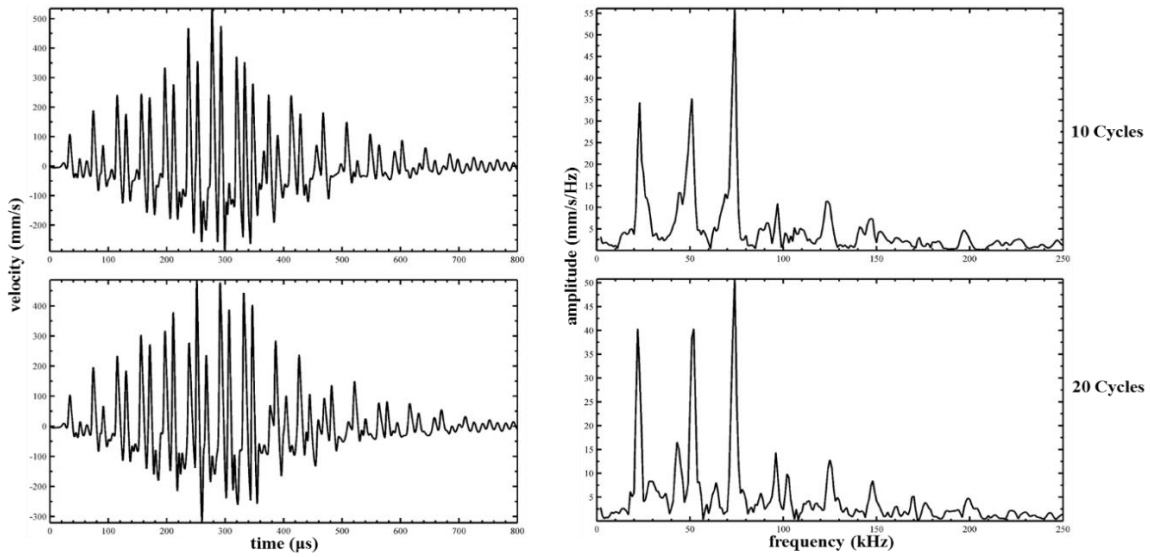

Fig. 4.20. Model prediction for a 5-sphere chain using an input of 10 and 20-cycle tone burst from an ultrasonic horn at 73 kHz and v_m =591 mms^{-1}. Waveforms (left) and Spectra (right).

B. 9-Sphere Chain

Similar to the 5-sphere chain, the 9-sphere also attempts to produce the strongly non-linear solitary wave but soon after it establishes the pulse it collapses to a weakly non-linear wave as shown in Fig. 4.21

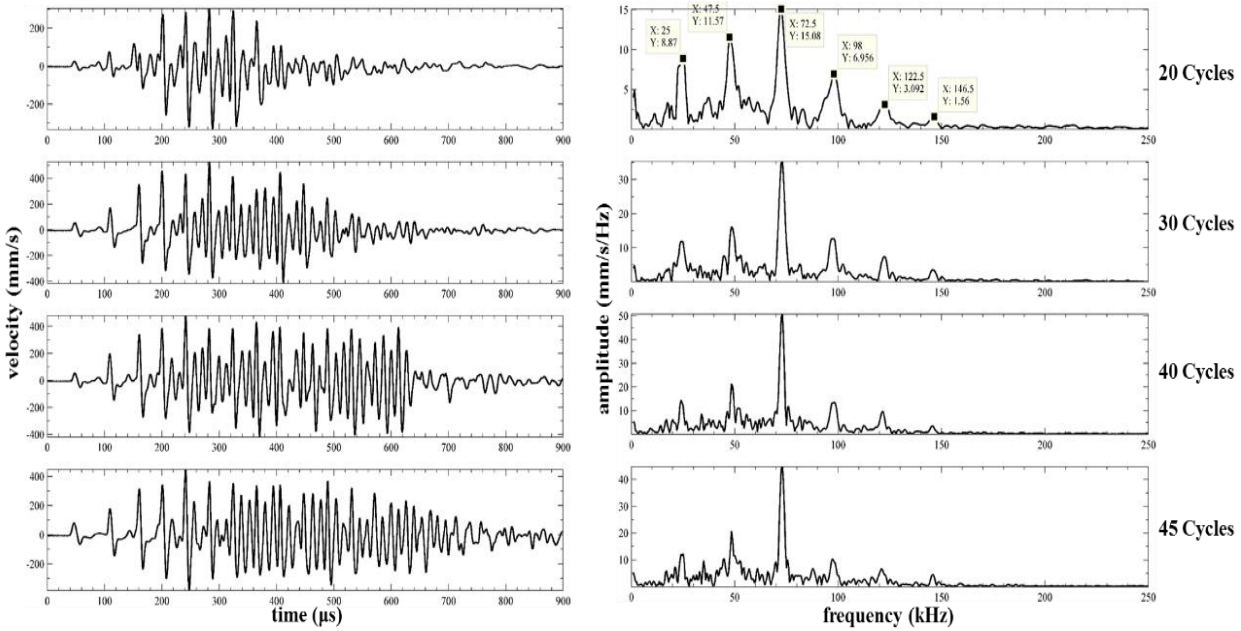

Fig. 4.21. Waveforms (left) and Spectra (right) showing the effect of changing the number of cycles in the drive waveform for a 9-sphere.

Just like in the case of the 6-sphere, the system produces multiple harmonic peaks with two sub-harmonic peaks at 25 and 45 kHz. It struggles to maintain the even distribution found in 3, 6 and 10 sphere chains with the resolution of the time wave getting progressively worse as the duration of the input signal increases. A similar behaviour was observed in the results from the model shown in Fig. 4.22. In both situations (experiment and simulation), there are other resonances present, which appears to be the chain of spheres attempting to shift the frequencies to attain some form of integer fraction of the input frequency.

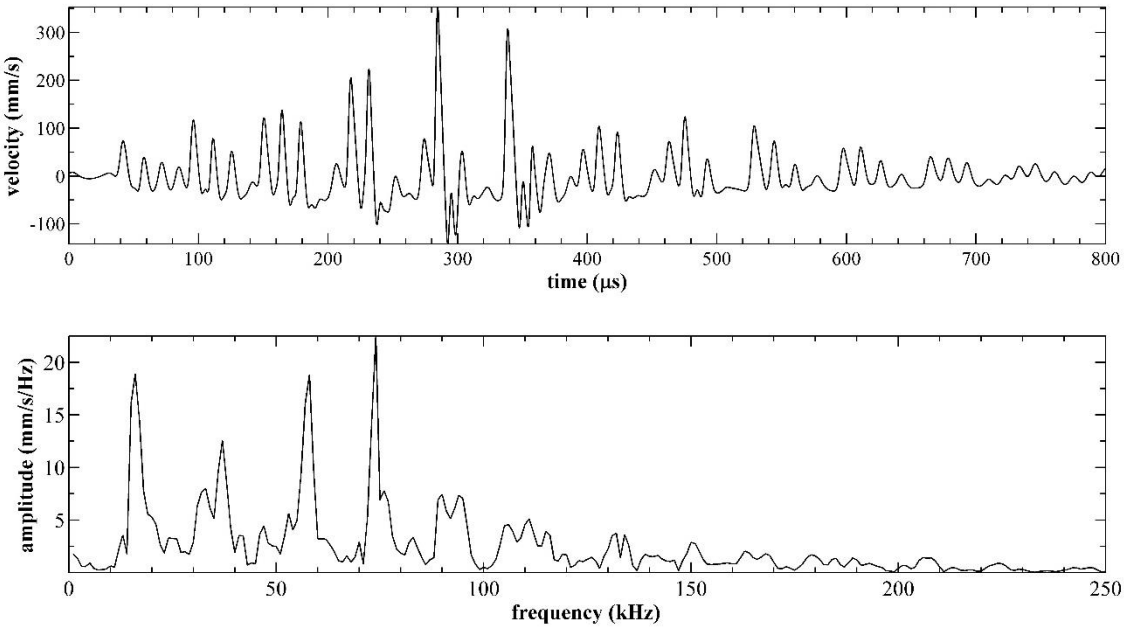

Fig. 4.22. Model prediction for a 9-sphere chain using an input of 20-cycle tone burst from an ultrasonic horn at 73 kHz and v_m =937 mms^{-1}. Waveforms (top) and Spectra (bottom).

4.3. Conclusions

This chapter has demonstrated the effects that occur when high amplitude input signals were used to excite resonant chain of spheres. At high amplitudes, strongly nonlinear behaviours were observed which were due to the non-linear interaction between the spheres. Given the right amplitude and duration of the input sinusoidal tone-burst, nonlinear resonant modes can be triggered with the chain. This produces harmonics and sub-harmonics of integer fractions of the input frequency, effectively creating a series of solitary wave pulses with characteristics that were highly sensitive to state of the chain and input parameters. This type of strongly nonlinear behaviour were only observed in chain lengths containing 2, 3, 6 and 10 chrome steel spheres for a 73 kHz input frequency. This suggests that only certain chain length of this material at this frequency can permit this form of resonant behaviour. It appears that there is a transition between the number of harmonics; both lower and higher as the length of the chain increases. It is possible that this resonant mode only occurs when an integer number of half wavelengths can exist within the chain, hence, permitting the transition of one half wavelength from 2 – 3 spheres, two half wavelength from 5 – 6 spheres and three half wavelength from 9 – 10 spheres. It is also possible that using a fraction of the chain length instead of a whole number would permit the existence of the desired mode (i.e. using a chain length of 5.3 mm instead of 5 mm).

Modelling the nonlinear dynamic motion of the spheres confirmed the behaviours observed in the experiments. The same features and trends were seen in the model when appropriate damping and pre-compression were used. The model also showed a similar degree of sensitivity to the chain structure and input parameters.

The results were consistent with the content of previous Chapters, where the background to solitary wave behaviour in chains of finite length were discussed. Here, it was explained that a

chain of spheres would resonate at certain frequencies. This was a complicated process, as propagation is dispersive and non-linear along the chains. But previous analysis has shown that resonances in the form of Non-linear Normal Modes (NNMs) would be expected in such chains [7]. The spectral peaks observed in certain chain lengths are examples of these modes. It should be noted that this appears to be the first time that this behaviour has been observed. It is the subject of a published journal paper [11], plus two others that have been submitted for publication [9, 12].

It can be seen from the above that the creation of these NNMs, and the train of impulses that result, are very sensitive to the conditions of the chain. They only appear when there is a very small pre-compression force between the spheres. This is just the condition needed for the creation of strongly non-linear interactions between the spheres, where the force holding them together statically is smaller than that caused by the ultrasonic applied signal. The effect of increasing applied static force is considered in the next Chapter, as well as the use of different sphere sizes, materials and input frequency.

4.4. References

1. V. F. Nesterenko, (1983). Propagation of nonlinear compression pulses in granular media. J. Appl. Mech. Tech. Phys. 24, 733–43.
2. C. Coste, E. Falcon, S. Fauve S, (1997). Solitary waves in a chain of beads under Hertz contact, Physical Review E 56, 6104-6117.
3. S. Sen, J. Hong, E. Avalos, R. Doney, (2008). Solitary waves in a granular chain, Physics Reports 462, 21-66.
4. R. S. Mackay, (1999). Solitary waves in a chain of beads under Hertz contact, Phys. Lett. A. 251, 191-192.
5. V. F. Nesterenko, (2001). Dynamics of Heterogeneous Materials, Springer-Verlag, New York.
6. C. Daraio, V. F. Nesterenko, E. Herbold, S. Jin, (2006). Tunability of solitary wave properties in one-dimensional strongly nonlinear phononic crystals, Phys. Rev. E. 73, 026610.
7. K. R. Jayaprakash, Y. Starosvetsky, A. F. Vakakis, M. Peeters, and G. Kerschen, (2011). Nonlinear normal modes and band zones in granular chains with no pre-compression, Nonlinear Dyn, 63: 359-385.
8. C.M. Donahue, P.W.J. Anzel, L. Bonanomi, T.A. Keller, and C. Daraio, (2014). Experimental realization of a nonlinear acoustic lens with a tunable focus, Applied Physics Letters, 104: 014103.
9. J. Yang, D. A. Hutchins, O. Akanji, P. J. Thomas, L. A. J. Davis, S. Harput, P. Gelat, S. Freear, and N. Saffari, (2015). An analysis of solitary wave impulses in granular chains using ultrasonic excitation. [Accepted August 2015 for publication in Physics Procedia].
10. A. Eller and H. G. Flynn, (1969). Generation of subharmonics of order one-Half by bubbles in a sound field, J. Acoust. Soc. Am. 46, 722.
11. D.A. Hutchins, J. Yang, O. Akanji, P. J. Thomas, L.A.J. Davis, S. Freear, S. Harput, N. Saffari and P. Gelat, "Evolution of ultrasonic impulses in chains of spheres using resonant excitation), EPL,109, (2015) 54002.
12. D. A. Hutchins, J. Yang, O. Akanji, P. J. Thomas, L. A. J. Davis, S. Freear, S. Harput, N. Saffari and P. Gelat, Ultrasonic propagation in finite-length granular chains, submitted August 2015 to Ultrasonics journal.

CHAPTER 5: Investigation of Parameters Affecting Propagation

5.1. Introduction

Solitary wave pulses in finite lengths of spherical chains subjected to minimal pre-compression force were generated using a narrowband ultrasound source in Chapter 4. At sufficient amplitudes of the input sinusoidal signal, sub-harmonics and harmonics of the input signal were generated as non-linear modes of the system of spheres with the presence of trains of strongly nonlinear pulses. These characteristics of strongly nonlinear waves have also been observed in chains consisting of Teflon beads [1], double power-law materials [2], and in granular dimer chains [3].

This chapter will demonstrate that the system investigated in this research supports the generation of nonlinear solitary waves; both weakly and strongly for various input frequencies and chain configurations (*i.e.* different materials, sphere radii and input frequencies). Previous work in is this field of study was primarily performed using an impulse from a striker as the excitation method, and as such there are presently no studies on how a chain of granular particles respond to various frequencies. Using a system composed of either 3 or 6 spheres (shown to support the formation of strongly nonlinear solitary waves at an input signal of 73 kHz in Chapter 5), the effects of using an input signal between the frequency ranges of 40 – 150 kHz will be described. Furthermore, the behaviour of the system to changes such as the diameter of the sphere, the material of the sphere and holder will be demonstrated in this chapter. Table 6.1 shows the physical properties of the materials used in this study for different spheres (Chrome-steel, Delrin, Synthetic Sapphire and Tungsten Carbide) and the holder (R11, Perspex, Aluminium and Steel). Due to the scope of this research and its goal of producing a prototype nonlinear acoustic lens for possible clinical use, sphere diameters above 2 mm were considered too large to implement in the experiments. Limitations in the fabrication method

(MSL) used to produce the R11 holders restricted the optimal minimum inner diameter of the holder to 1 mm. Going below this produced holders with a non-uniform channel, which was critical to the alignments of the centre of the spheres. It was possible to machine holders with sub-millimetre channels from other materials used in this study. However, it was discovered that of all the materials used, only R11 provided the physical properties essential to produce the train of pulses. This will be demonstrated in this chapter.

Material	***Density (kgm^{-3})***	***Young's Modulus (GPA)***	***Longitudinal Sound Speed [approx.] (ms^{-1})***
R11	*1235*	*2.45*	*2100*
Delrin	*1420*	*3.2*	*2430*
Perspex	*1190*	*2.76*	*2700*
Aluminium	*2600 – 2800*	*70 – 79*	*5500*
Chrome-Steel	*7833*	*210*	*4228*
Steel	*7750 – 8100*	*190 – 210*	*5790*
Synthetic Sapphire (Ruby)	*3980*	*345*	*5000*
Tungsten Carbide	*15800*	*530 – 700*	*6665*

Table 5.1 Physical properties of the materials used.

5.2. Results for sphere diameters where solitary wave pulses were observed

Using the experimental setup described in preceding chapters, experiments were performed on a chain consisting of three chrome-steel spheres of different diameters for various amplitudes and duration of the 73 kHz sinusoidal drive signal. The output waveforms and spectra for a 3-sphere chain of 2 mm diameter are shown in Fig. 5.1 for an excitation with a duration of 10 cycles. As previously observed in Chapter 4, at the lowest amplitude (22 mms^{-1}) excitation the

time waveform and spectrum resembles that of the output of the horn with a peak at 73 kHz and a smaller one at 146 kHz. In this situation, the propagation is closer to those found in a linear regime. As the amplitude increases to 115 mms^{-1}, the regime switches to weakly non-linear and the nonlinear pulses begin to emerge in the time waveform accompanied by two sub-harmonic peaks present at 25 and 48 kHz in the spectrum. Further increments of the amplitude produces sharper and more defined periodic waves; suggesting a strongly nonlinear regime. In the frequency spectrum the energy from the input frequency peak (73 kHz) is fed to the sub-harmonic peaks which grow to become more prominent than the input frequency.

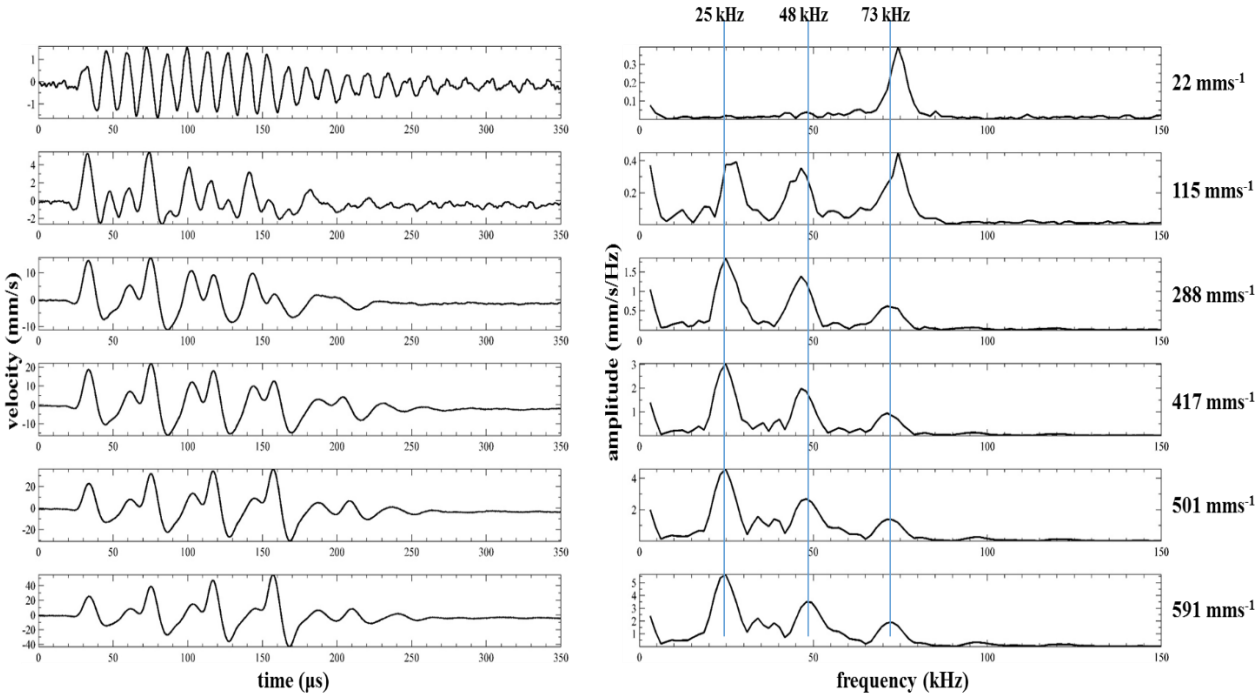

Fig. 5.1. Waveforms (left) and frequency spectra (right) of the output from a 3-sphere chain of 2 mm diameter (chrome-Steel) excited using a 10 cycle tone-burst from an ultrasonic horn at 73 kHz.

Changing the duration of the 73 kHz input signal from 10 to 20 cycles produces better resolution in the waveforms and frequency spectrum as shown in Fig. 5.2. The waveforms and frequency peaks are both narrower and more distinct. Increasing the input signal duration to 30 cycles produces a decrease in the effectiveness of pulse creation. The time waveforms become more chaotic and although the peaks in the spectrum become narrower, there were larger side-lobes present which could be as a result of interference from other resonances within the

system. This is a similar behaviour to those observed in Chapter 4.2 when the duration of the input signal was varied, the system responds better to a specific number of cycles.

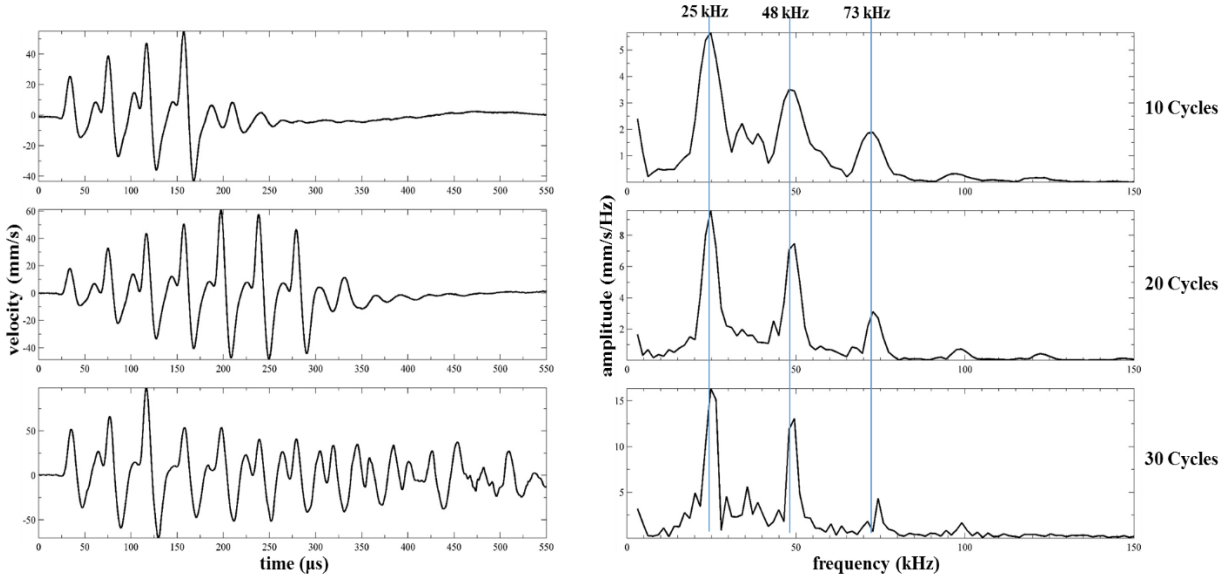

Fig. 5.2. Waveforms (left) and spectra (right) showing the effect of changing the number of cycles in the drive waveform for a 3-sphere of 2 mm diameter.

Fig. 5.3 shows a comparison between a chain of three 1 mm diameter and a chain of three 2 mm diameter sphere for a duration of 10 cycles of a 73 kHz input signal. In both situations the number of nonlinear interfaces were the same but the dimensions were different. This difference is apparent in the waveforms and spectra. The results of the two configurations produced a train of solitary waves of which the 1 mm diameter had an elongated or longer train of pulses with approximately three times the maximum amplitude peak to peak velocity of the 2 mm diameter chain. The periodic pulses of the 2 mm diameter chain were broader; having a periodicity of 40.2 μs while those of the 1 mm chain had a periodicity of 26.4 μs. This translated to two sub-harmonics (25 and 48 kHz) and harmonics peaks spaced approximately 25 kHz from one another for the 2 mm diameter. In the results for the 1 mm diameter chain, there were more harmonics present of which there was only a single sub-harmonic peak at 37 kHz with successive harmonics spaced approximately 37 kHz apart. The results indicate that as the

sphere size (and as a result overall length) increases most of the amplitude of the frequency content shifts from the higher harmonics to lower harmonics.

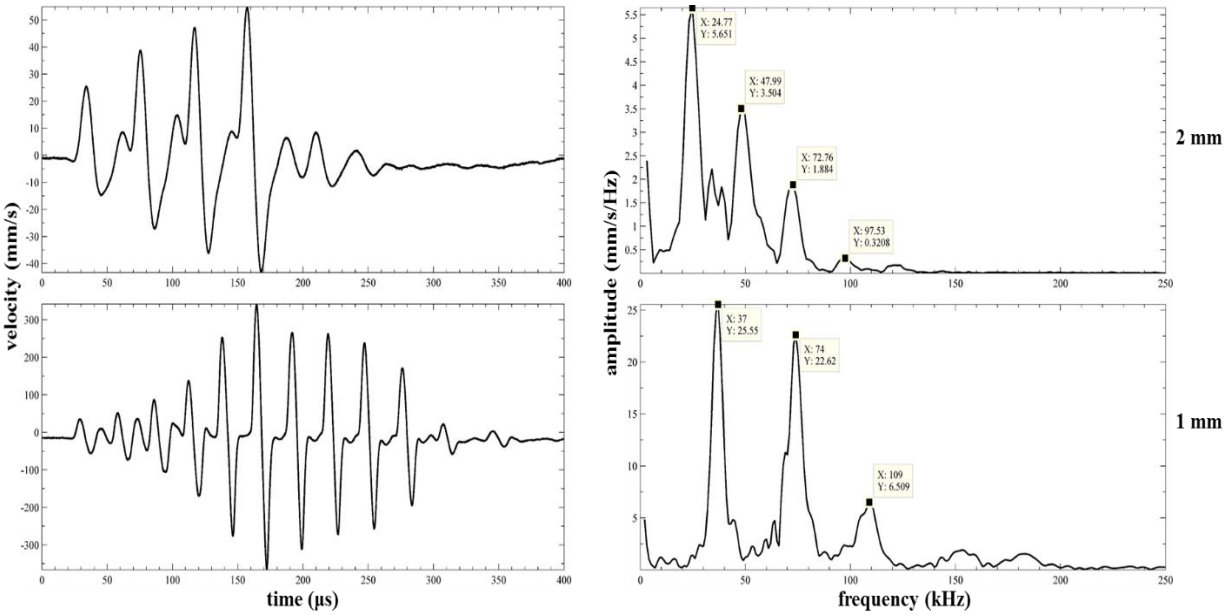

Fig. 5.3. Waveforms (left) and spectra (right) obtained from the experiments on a 3 x 2 mm chain (top) and a 3 x 1 mm chain (bottom) at an input duration of 10 cycles.

Comparing the results from a configuration of 2 mm diameter, 3-sphere chain to a 1 mm diameter 6-sphere chain excited using an input signal duration of 20 cycles in both cases, illustrated in Fig. 5.4. A similar behaviour was observed in both situations, once the resonant modes were excited, pulses are seen in the time waveform and distinct frequency peaks appear in the spectrum at the same frequencies: 25 and 48 kHz. All other subsequent harmonics are spaced approximately 25 kHz apart with the 6-sphere chain having more harmonics present. The results of the two configurations produced a train of solitary waves with similar periodicity of approximately 40.2 μs. The pulses found in the 6-sphere (1 mm) chain pulses were narrower with more distinct features when compared to the 3-sphere (2 mm) chain. The train of pulses were also longer with a peak to peak amplitude velocity approximately 23 times larger than that of the 3-sphere chain and the individual pulses were narrower with more distinct features. However, the amplitudes of the sub-harmonics for the 3-sphere chain is considerably larger than the input frequency (73 kHz) when compared to those found in the 6-sphere chain where

the amplitudes of the sub-harmonics are relatively the same amplitude as the 73 kHz peak. The radius and number of interfaces were different, with the chain composed of 1 mm spheres having twice as many as those found in the 2 mm sphere chain, however both systems have the same chain length suggesting that the overall length of the chain and diameter are the dominant factors in determining the periodicity of the resultant solitary wave pulses, but that energy loss in the longer chain reduces output amplitudes.

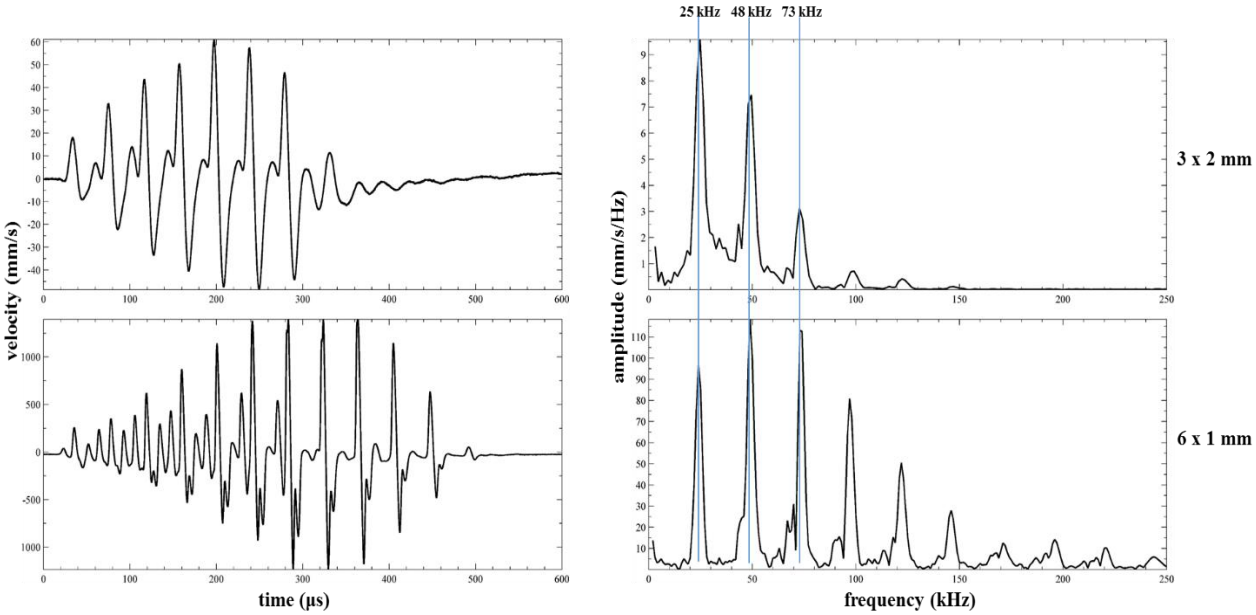

Fig. 5.4. Waveforms (left) and spectra (right) obtained from the experiments on a 3 x 2 mm chain (top) and a 6 x 1 mm chain (bottom) at an input duration of 20 cycles.

The results for the theoretical model correlate to those of the experiments, in terms of the trend in the number of sub-harmonics and harmonics. Fig. 5.5 shows the predicted waveforms and spectra for a 3-sphere chain with diameters ranging from 0.25 mm to 3 mm excited using an input signal of 73 kHz for a duration of 10 cycles. From top (0.25 mm) to bottom (3 mm), observing the spectra only, and from 73 kHz (highlighted in the figure) to 800 kHz. It can be seen that the number of harmonics decreases. At 0.25 mm diameter, the chain contained a wide bandwidth, with components at frequencies greater than 700 kHz. By 3 mm, the frequency component was less than 50 kHz. Now observing from the bottom (3 mm) to the top (0.25

mm), from the highlighted frequency at 73 KHz to 0 Hz. It can be observed that the number of sub-harmonics decreases as the diameter decreases. This trend is similar to those observed in the experiments in Chapter 4.2 were the number of harmonics increases as the length of a chain of 1mm diameter spheres was increased. The accompanying time waveforms show that the pulses become broader and the train of pulses become more elongated as the diameter increases.

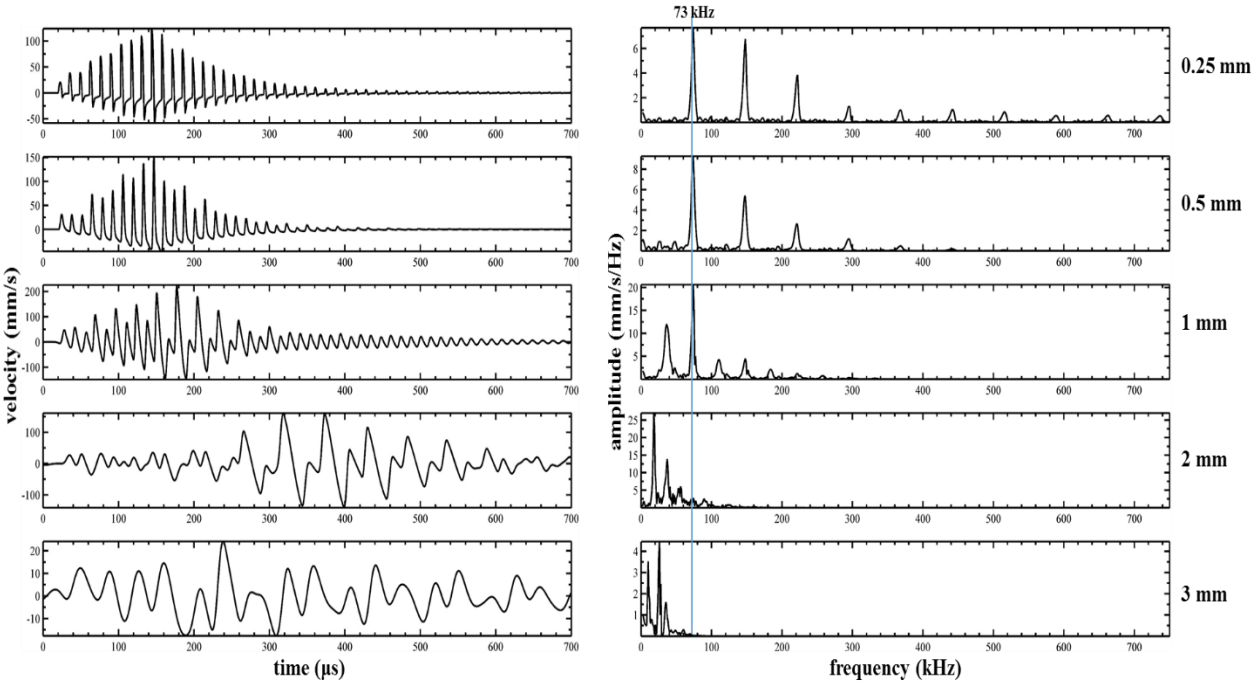

Fig. 5.5. Theoretical model prediction for a 3-sphere chain with various diameters using an input of 10-cycle tone burst from an ultrasonic horn at 73 kHz. Waveforms (left) and Spectra (right).

Increasing the diameter of the spheres to 4 mm produces undesirable effects as shown in the results from the experiments and model in Fig. 5.6. Following the trend described above, the pulses are considerably broader in the time waveform, and there are no harmonic peaks present at 73 kHz and above, only sub-harmonics are present.

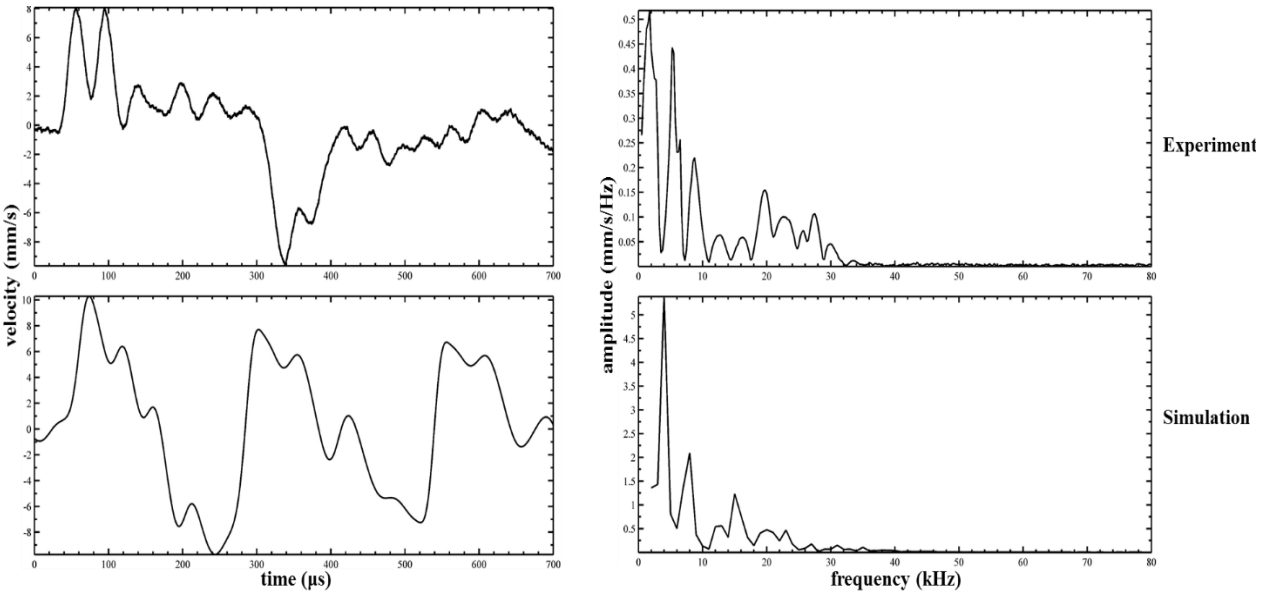

Fig. 5.6. Experiment (top) and theoretical model prediction (bottom) for a 4 mm diameter 3-sphere chain using an input of 15-cycle tone burst from an ultrasonic horn at 73 kHz. Waveforms (left) and Spectra (right).

5.3. Effects of changing the sphere material

The result of using Delrin and tungsten-carbide as the material of a chain of three 1mm diameter spheres is shown in Figs. 5.7 (a) and (b) respectively. This produced results similar to those observed in the same length and diameter of the chrome steel chain described in Chapter 4. The results displayed in Fig. 5.7 were generated from a 10-cycle input excitation at 73 kHz at various peak to peak input velocity (v_m). For both Delrin (Fig. 5.7 (a)) and tungsten-carbide (Fig. 5.7 (b)), waveforms and spectra with similar characteristics can be observed. At low input amplitudes, a weakly nonlinear behaviour was detected. This was denoted by the presence of frequency peaks at 73 kHz and 146 kHz, as found in the input signal's spectrum. In the time domain, the waveforms have an envelope also similar to that of the sinusoidal input tone-burst where the sine waves rapidly builds up then gradually attenuates. As v_m tends towards 591 mms^{-1}, the pulses become broader and their periodicity increases and a sub-harmonics is formed in the spectra. At the maximum v_m of 591 mms^{-1}, the sub-harmonic and harmonics were fully formed in both cases and the waveform had no trace of the sinusoidal pulses. What is interesting here was that the nonlinear solitary pulses emerged at low amplitudes for the chain made of tungsten-carbide. By v_m = 115 mms^{-1}, the solitary pulses and accompanying subharmonics were on display while this behaviour wasn't exhibited in the chain of Delrin spheres until higher amplitudes (when v_m = 417 mms^{-1}). Chrome-steel also required less peak to peak velocity amplitude for sub-harmonics to emerge in its spectrum. In fact by v_m = 115

mms^{-1}, there were small signs of the sub-harmonic peaks, although these peaks were not as distinct as those in tungsten-carbide at the same amplitude.

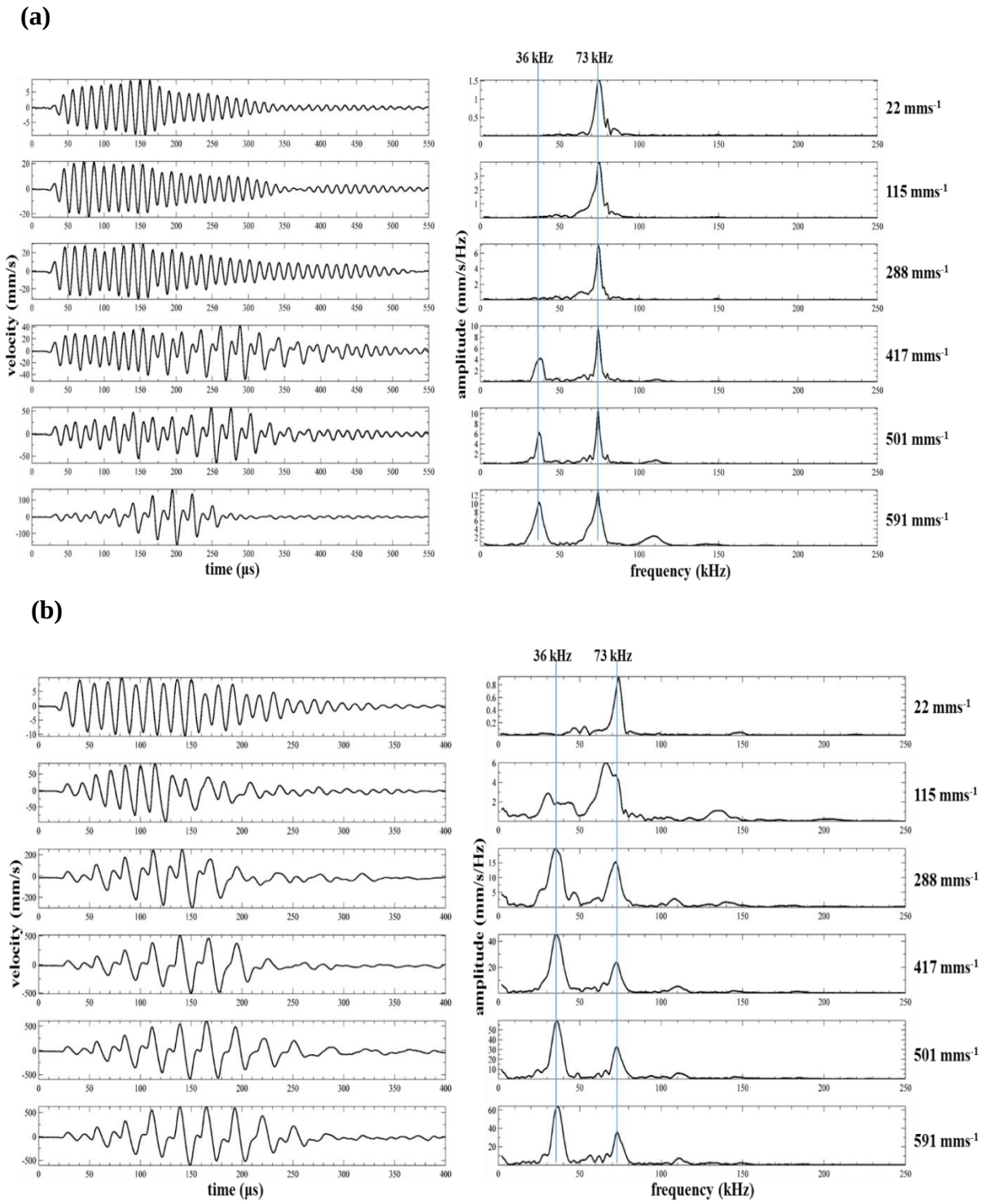

Fig. 5.7. Waveform (left) and frequency spectrum (right) of the output from a chain of 3 spheres of 1 mm diameter excited using a 20 cycle tone-burst from an ultrasonic horn at 73 kHz. (a) Delrin spheres (b) Tungsten Carbide spheres.

This suggest that for the same input parameter and experimental setup, the denser the material the less energy would be required to form the nonlinear behaviour for a chain of six 1 mm diameter spheres subjected to slight compression force. In other words, less damping and absorption/energy loss occurs in a chain composed of materials with high Young's modulus and low internal losses.

Experiments were also performed on a chain of three, 1 mm spheres composed of synthetic sapphire (ruby), and the results are shown in Fig. 5.8. Although tungsten carbide has a higher Young's modulus, sapphire is an oxide mineral with a high level of hardness but a much lower density (less than half of chrome steel). This resulted in a divergent in behaviour from those exhibited in Delrin, chrome-steel and tungsten-carbide. Observing the physical and acoustic properties of sapphire does not present an obvious reason to justify this difference in behaviour.

Material	***Density (kgm^{-3})***	***Young's Modulus (GPA)***	***Sound Speed (ms-1)***	***Z (MRayls)***
Delrin	*1420*	*3.2*	*2100*	*3.5*
Chrome-Steel	*7833*	*210*	*4228*	*45.4*
Synthetic Sapphire (Ruby)	*3980*	*345*	*5000*	*19.9*
Tungsten Carbide	*15800*	*530 – 700*	*6665*	*105.1*

Table 5.2 Physical and acoustic properties of the sphere materials used.

The results in Fig. 5.8. illustrate an entirely different resonant behaviour. The sinusoidal waveforms present at low amplitudes are transformed to saw tooth like waves as the amplitude was increased. The corresponding spectra shows no sub-harmonics present, however, the smaller harmonic peak at 146 kHz grows as energy is pumped into it as the input peak to peak

velocity amplitude was increased. Comparing all four materials: Delrin, chrome steel, tungsten carbide and synthetic sapphire (Fig. 5.9), it was evident that chains of spheres composed of the 1st three materials support the formation of strongly non-linear solitary waves while only weakly nonlinear behaviour was present in sapphire. As the density and Young's modulus increased from Delrin to tungsten carbide, the amplitudes of the sub-harmonic frequency peaks also increased. This resulted in the sub-harmonic peaks being the most dominant frequency peak in tungsten carbide.

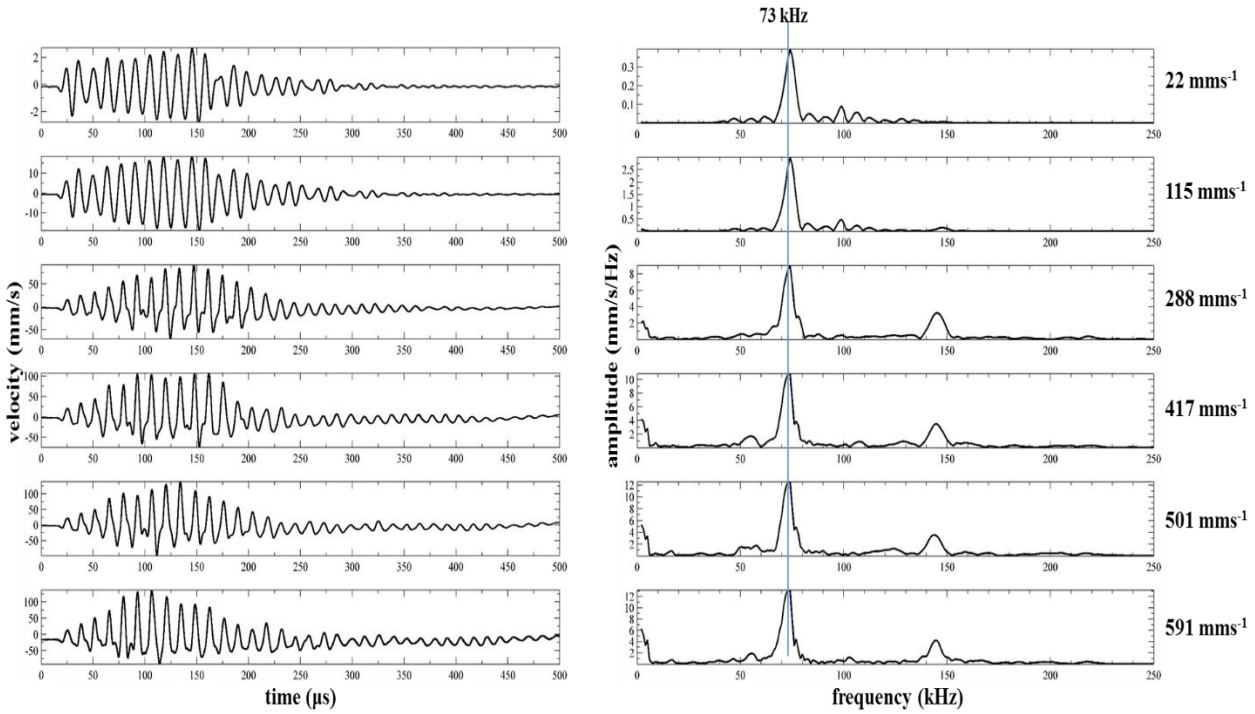

Fig. 5.8. Waveform (left) and frequency spectrum (right) of the output from a chain of 3 (1 mm) Synthetic Sapphire (Ruby) spheres of 1 mm diameter excited using a 10 cycle tone-burst from an ultrasonic horn at 73 kHz.

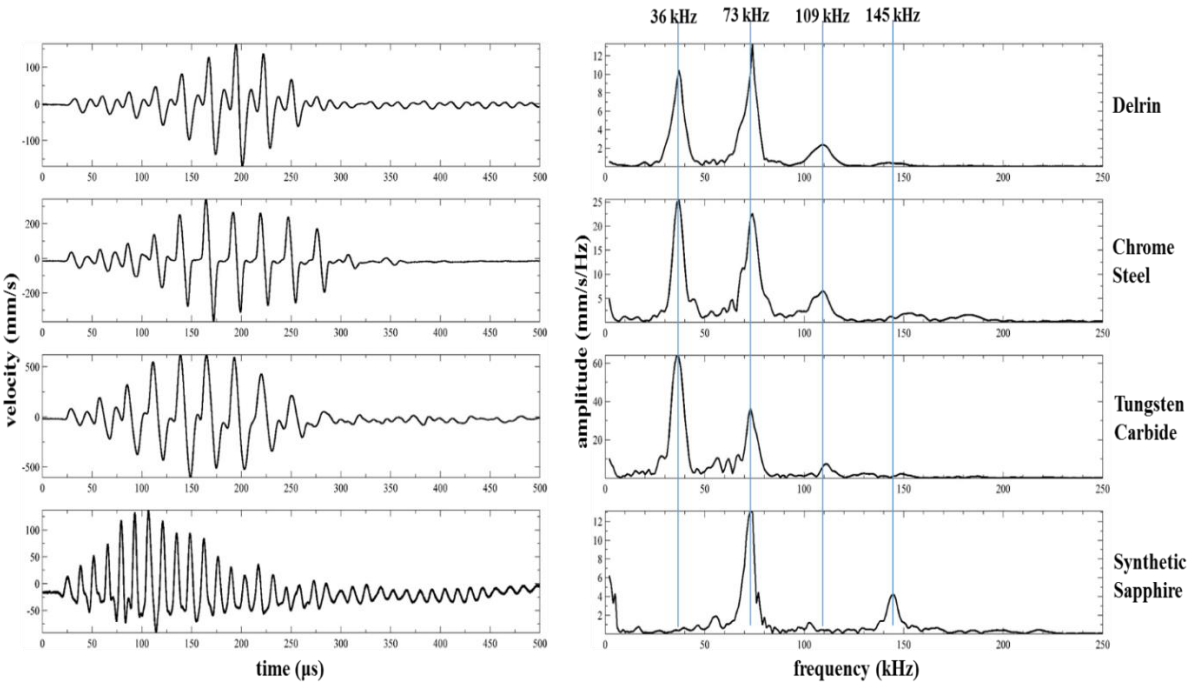

Fig. 5.9. Waveforms (left) and spectra (right) obtained from the experiments on a 3-Sphere (1 mm) chain of various material at an input duration of 10 cycles.

The waveforms predicted by the theoretical model are shown in Fig. 5.10 for the chain of 3 spheres for the different materials. The predictions produced a similar number of sub-harmonics as those observed experimentally. For Delrin, chrome steel and tungsten carbide, there was a single sub-harmonic peak at approximately 36 kHz which wasn't present in the spectrum of the chain composed of sapphire. The periodic pulses were present in the predicted results although not as distinct as those observed in the experiment. There appears to be more energy present in the harmonic peaks in the predicted result of the chain of tungsten carbide spheres. In this case, the amplitude of the sub-harmonic is less than that of the 73 kHz peak.

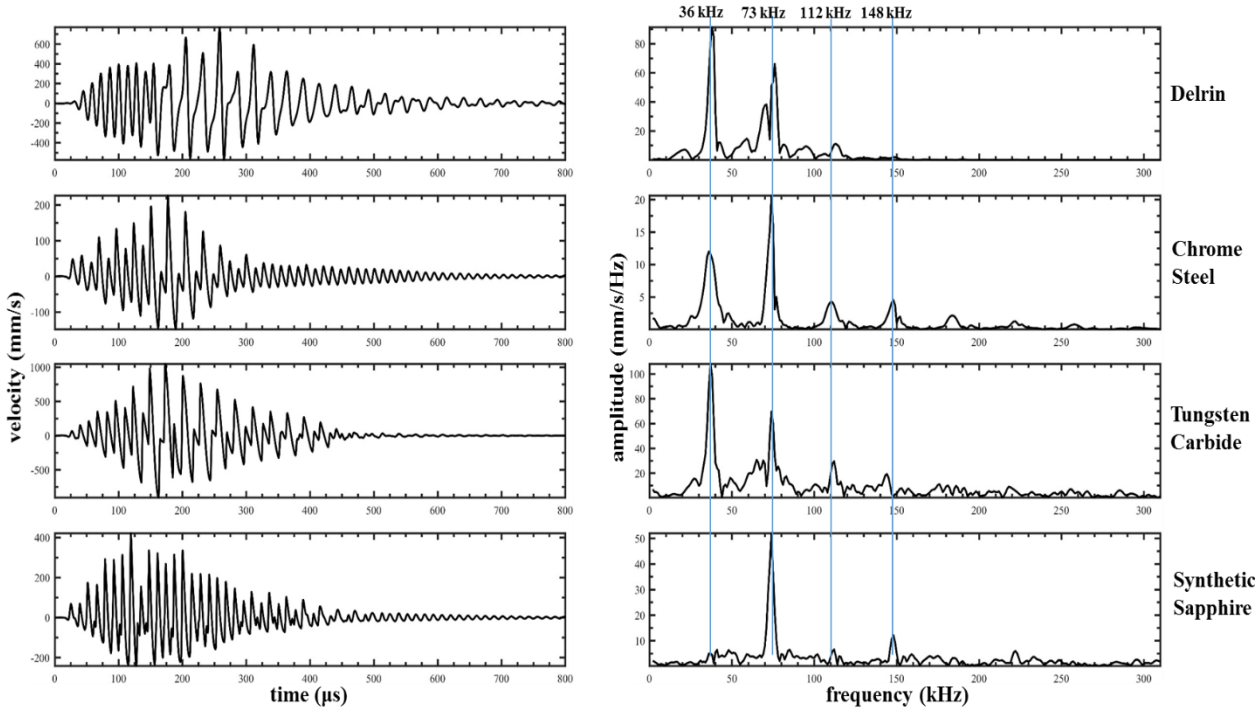

Fig. 5.10. Predicted theoretical waveforms (left) and spectra (right) obtained from the model on a 3-Sphere (1 mm) chain of various material at an input duration of 10 cycles.

5.4. Effects of changing the holder material

Changing the material of the holder effectively changes the nature of the contact between the last sphere and the wall (*i.e.* the holders' annulus). A chain of six chrome-steel spheres of 1 mm diameter were encased in Perspex, Steel, Aluminium and R11. The chain was subjected to slight compression from an ultrasonic horn producing an amplified excitation signal at 73 kHz for a duration of 20 cycles. The results of these experiments are shown in Fig. 5.11 and the predicted results from the theoretical model for the same situations are shown in Fig. 5.12. The features of the predicted results were found to correlate with those observed in the experiments. Sub-harmonics were generated in the spectrum of both acrylics; Perspex and R11 while there were none present in the metallic holders; steel and aluminium. The use of Delrin produced a broadening of the bandwidth, which could be due to damping. When metallic holders (steel and aluminium) were used, there were no sub-harmonics present and the dominant effect was the creation of higher harmonics of the input frequency which is a characteristic of nonlinear

systems. Only with R11 holder did the system truly exhibit a strongly nonlinear behaviour with the existence of both sub-harmonics and higher harmonics.

It is clear from Chapter 4 that the reflected wave travelling back from the last sphere contributes to the solitary wave pulses, aluminium and steel holders have a similar acoustic impedance to the chrome steel spheres which would result in no reflected waves. While Perspex and R11 have lower acoustic impedance to the spheres producing a greater degree of reflected waves to occur.

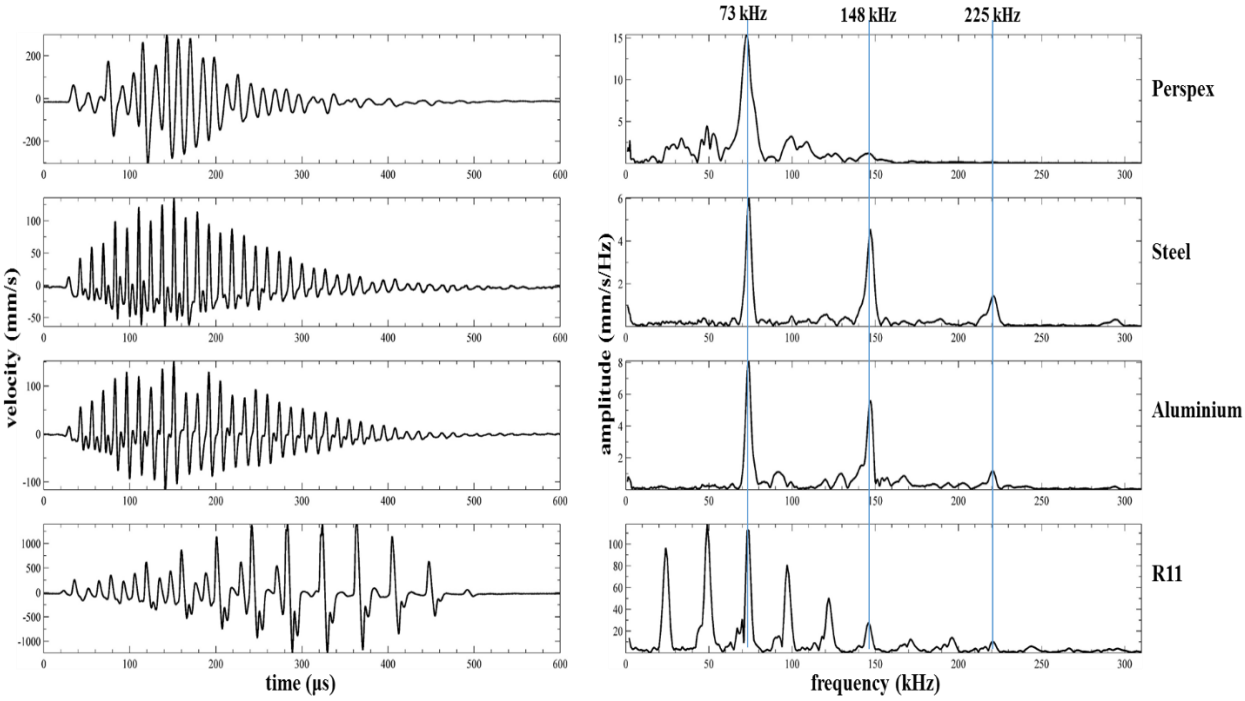

Fig. 5.11. Waveforms (left) and spectra (right) obtained from the experiments on a 6-Sphere chrome-steel (1 mm) chain enclosed in holders of various material at an input duration of 20 cycles.

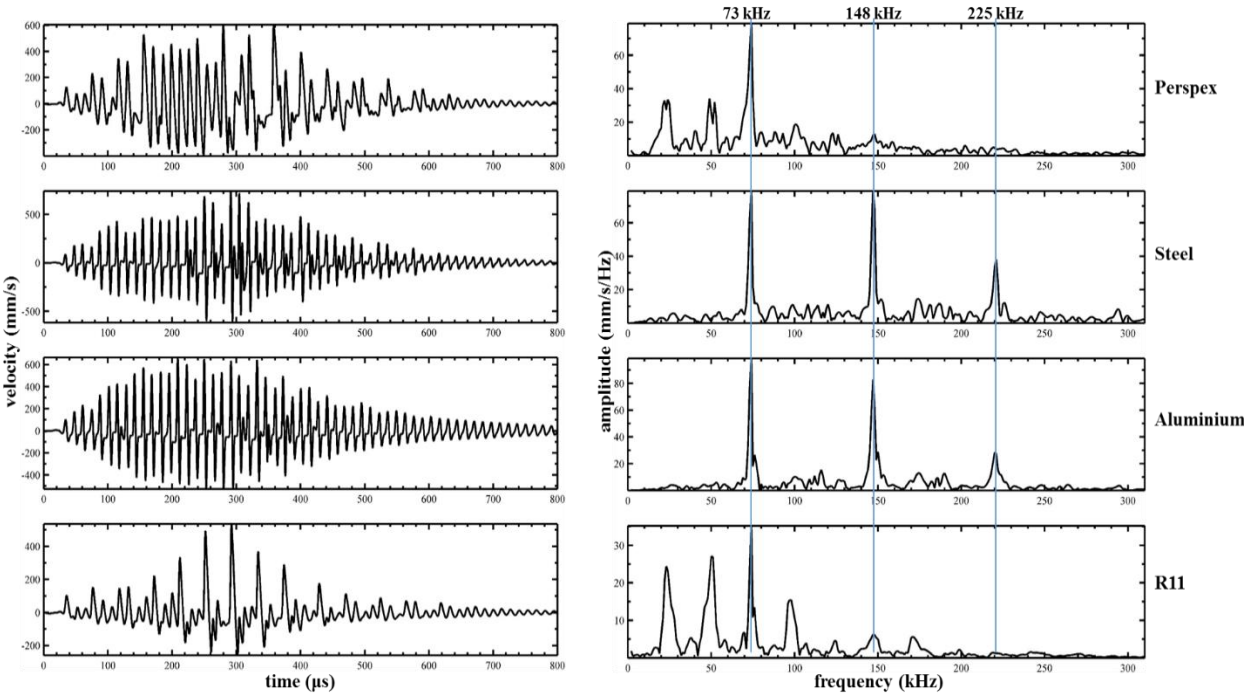

Fig. 5.12. Predicted theoretical waveforms (left) and spectra (right) for a 6-Sphere chrome-steel (1 mm) chain enclosed in holders of various material at an input duration of 20 cycles.

5.5. Effect of changing the input Frequency

Experiments were performed on a wide range of excitation frequencies on a chain of 3 chrome steel spheres in a R11 holder for an input duration of 10 cycles. The range of frequency were from 43 to 143 kHz dictated by the centre frequency (73 kHz) of the transducer used. Going in either direction of this range produced insufficient v_m which resulted in a scenario were $f_m \approx f_0$ and the system response was weakly nonlinear at best. Fig. 5.13 shows a series of output waveforms and spectra from the experiments. It was observed that only certain frequencies produced the strongly nonlinear behaviour of interest: the creation of a set of solitary wave impulses from a tone-burst input.

For all frequencies, it can be observed that the chain attempts to transform the input sinusoidal signal of the transducer (Fig. 5.14) to periodic pulses with the period of the pulses changing at certain frequencies. This was achieved more effectively for certain frequencies; for 43, 73, 83, 113, 123 and 133 kHz, as in these cases the chain achieves the balance between non-linearity

and dispersion, the result being the generation of solitary wave impulses. For the other frequencies, the system fails at achieving the solitary wave pulses, demonstrating that the required conditions necessary to setup the waves haven't been adequately fulfilled. It further illustrates that the system is sensitive to the frequency of the input signal, indicating that the interesting propagation effects would only be expected at certain frequencies, depending on the exact nature of the chain.

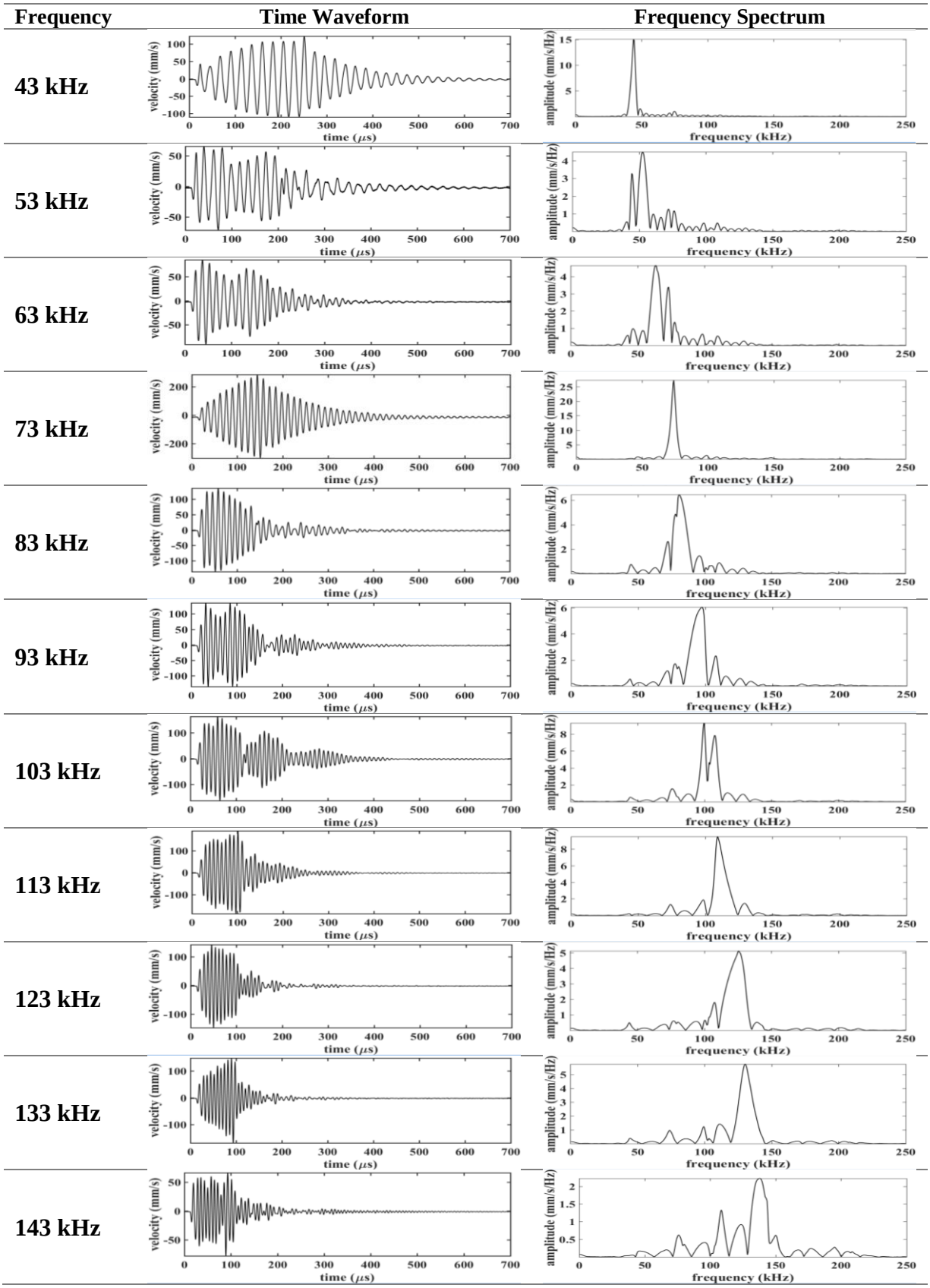

Fig. 5.13. Waveforms (left) and spectra (right) for the input excitation used in the experiments for the 3-Sphere (1 mm) chain at various input frequencies for an input duration of 10 cycles.

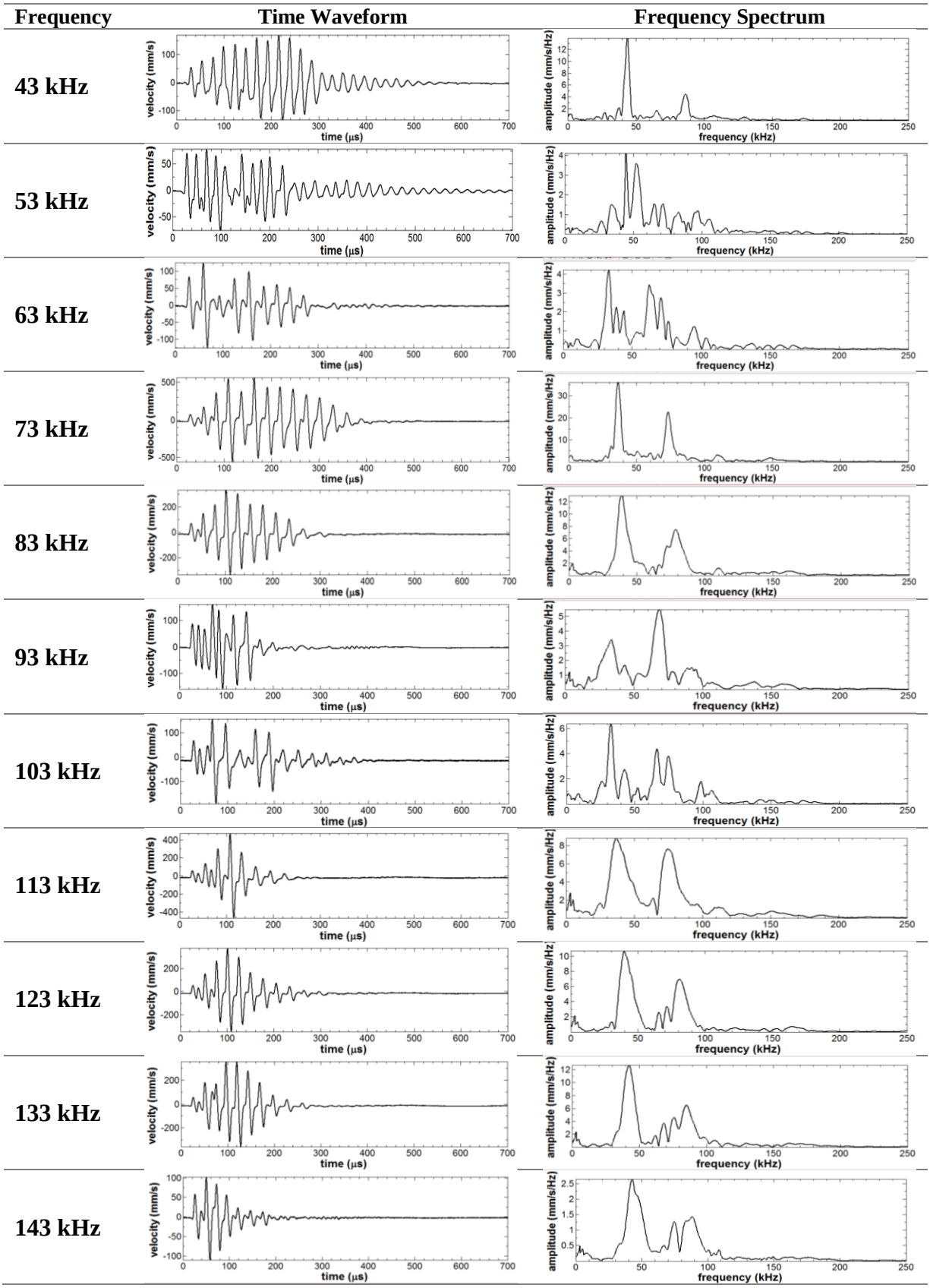

Fig. 5.14. Waveforms (left) and spectra (right) obtained from the experiments on a 3-Sphere (1 mm) chain using various input frequencies for an input duration of 10 cycles.

5.6. Conclusions

This chapter demonstrated the effects of changing the following features in the experimental setup:

- The diameter of the sphere
- The material of the sphere
- The material of the holder
- The frequency of the input excitation signal

At diameters below 4 mm strongly nonlinear behaviours were observed, whereas increasing the diameter beyond this produced undesired results with no trace of the nonlinear periodic pulse in the signal. Between 1 and 3 mm, the presence of sub-harmonics were detected with the number of sub-harmonics increasing from a single peak for a chain of three 1 mm spheres to two frequency peaks in the chain composed of three, 2 mm spheres. The chain containing 3 spheres of 2 mm diameter chain possessed the same periodicity as the chain of six 1 mm chain even though the number of nonlinear interfaces resulting from the Hertzian contacts of the spheres were twice as many as those in a chain of three 2 mm diameter sphere. This suggest that the number of nonlinear interfaces isn't linearly proportional to the number of sub-harmonics detected in the chain but may be related to distance the solitary wave has to propagate. It does suggest, however, that the length of the chain (or diameter of the sphere) is the important factor. The predicted results showed that at sub-millimetre diameters the sub-harmonics had been replaced by multiple harmonics effectively increasing the frequency components towards the mega-Hertz range. Again as the distance the solitary wave had to propagate decreased, so did the number of sub-harmonics detected.

Changing the material of the spheres to Delrin, chrome steel and tungsten carbide produced a similar profile across all three materials. Each material produced higher harmonics and a sub-harmonic of integer fractions of the input frequency, effectively creating a series of solitary

wave pulses with characteristics that were highly sensitive to state of the chain and input parameters. The amplitude of the sub-harmonic peak grew and became larger than the input frequency (73 kHz) as the density and Young's modulus increased. It was observed that chains of spheres composed of Delrin, chrome steel and tungsten carbide materials supported the formation of strongly non-linear solitary waves while anomaly sapphire produced a resonant mode different to the others which could not be explained using its physical or acoustic properties.

Changing the material of the holder generated varying results. Less dense acrylic materials such as Perspex and R11 generated an effect which led to the presence of sub-harmonics and harmonics within a chain of six 1 mm spheres. Unlike the case of R11 were strongly nonlinear behaviour was present, Perspex produced a weakly nonlinear behaviour when subjected to similar conditions. This was because Perspex and Delrin have a lower acoustic impedance to the chrome steel spheres, hence, resulting in reflected waves which is required to generate the nonlinear solitary pulses observed. On the other hand, the metallic holders made from Steel and Aluminium with a better acoustic match to the spheres, hence no reflection, produced an effect which eliminated all sub-harmonics replacing them with multiple high harmonic spaced at intervals of the input frequency of 73 kHz; a similar behaviour to any nonlinear system.

Varying the frequency of the input signal produced an effect were the strongly nonlinear behaviour was only observed at certain excitation frequencies: 43, 73, 83, 113, 123 and 133 kHz. All of these effects serve to demonstrate the sensitive nature of the system and how the chains may be tuned to produce waveforms with specific characteristics and frequency components by way of generating desired sub-harmonics and/or harmonics.

5.7. References

1. C. Daraio, V. F. Nesterenko, E. Herbold, S. Jin, (2005). Strongly nonlinear waves in a chain of Teflon beads, Physical Review E. 72, 016603.
2. E. B. Herbold, V. F. Nesterenko, (2007). Solitary and shock waves in discrete strongly nonlinear double power-law materials, Applied Physics Letters, 90, 261902.
3. K.R. Jayaprakash, Y. Starosvetsky, A.F. Vakakis, (2011). A New Family of Solitary Waves in Granular Dimmer Chains with No Pre-compression, Physical Review E. 83, 036606.

CHAPTER 6: Effect of Pre-compression on Chain Behaviour

6.1. Introduction

Several parameters were varied in Chapters 4 and 5, and it was shown that impulses with different properties could be generated. One area of interest is the generation of a nonlinear acoustic lens with a tuneable focus, which would need the time delay along a chain to be varied. Spadoni [1] demonstrated that the speed of solitary waves along a chain could be altered by applying pre-compression force, provided the conditions of the chain are appropriate, leading to the concept of sound bullets. Sound bullets are generated from the superposition of the output signals from multiple neighbouring chains with their individual spheres subjected to Hertzian contact. Results from Chapters 4 and 5 demonstrated that piezoelectric actuation via a horn structure could be used to generate solitary waves in a column of chain of ball-bearings under minimal pre-compression (f_0). The resultant effects were found to be dependent on the characteristics of the applied transient force (f_m) (*i.e.* the peak to peak amplitude velocity), the diameter of the spheres, the length of the chain of spheres and so forth.

In this chapter, the effects of changing the relative values of static pre-compression f_0 will be examined while f_m is kept constant at its maximum. This effect will demonstrate the behaviour of the chain as it transitions form highly nonlinear (when; $f_m >> f_0$) to weakly nonlinear (when; $f_m \approx f_0$). In other words, a transition in characteristics from an interaction between granular media to those found in a bulk material is expected, together with a change in the speed of propagation along the chain.

The technique used to determine the time of flight and the maximum intensity of the resultant waveforms will be described. Measuring the time of flight is important for developing a device composed of arrays of chains capable of producing sound bullets that can be controlled by

introducing differences in phase between each chain output, which could arise from having an array comprising of chains of varying length, physical properties or pre-compressions. Hence, it is crucial to accurately determine the time of flight for each individual chain. Wavelet decomposition provides the ability to decompose a waveform into multiple levels with precise information in the time and frequency domains. This provides better resolution and identifies features suppressed by noise.

6.2. Wavelet Analysis

There is a difference between wavelet analysis and an FFT: a Fourier series maps a one-dimensional function of a continuous variable into a sequence of one dimensional coefficients which is localised in frequency only, whereas a wavelet expansion maps the function into an array of two dimensional coefficients. This two dimensional depiction allows localisation of the signal in time and frequency simultaneously (in a similar way to a musical score where the location of the notes signifies when the timbre occurs). The discrete wavelet transform (DWT) is given as [2]:

$$DWT_{\psi}f(j,k) = \int_{-\infty}^{\infty} f(t)\psi_{m,n}^{*}(t)dt \tag{6.1}$$

where $\psi_{m,n}$ is the dilated and translated style of the main wavelet $\psi(t)$, the asterisk denotes a complex conjugate and *m* and *n* are positive integers.

$$\psi_{m,n}(t) = 2^{-m}\psi(2^{m}t - n) \tag{6.2}$$

The wavelet algorithm decomposes the signal into multiple levels of approximated (cA1, cA2 …) and detailed (cD1, cD2 …) coefficients. The first two levels are illustrated in Fig. 6.1, h and g in the figure represent low-pass and high-pass decomposition filters. In the first level of decomposition, the original signal is filtered using both filters, afterwards, it is sub-sampled by a factor of 2. This produces two coefficients of the original signal, cA1 and cD1. This process

is then repeated over several levels producing outputs of multiple coefficients with different frequency bands displayed in time domain.

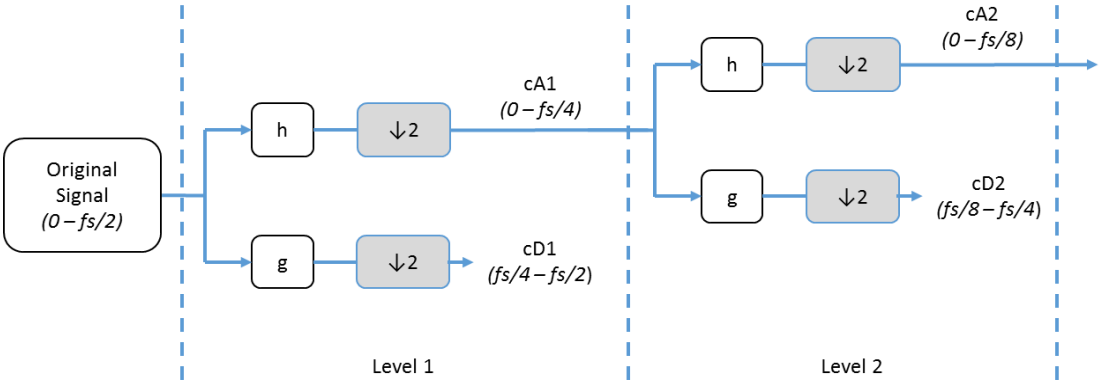

Fig. 6.1. The first 2 levels of the wavelet decomposition.

A six-level decomposition was applied to the results of the experiments (shown in Fig. 6.2) on the chain of 6 spheres discussed in Chapter 5 for both the input and output signals. This number of levels was sufficient, considering the low input frequency of the transducer (73 kHz) and the sampling rate of 100 MHz used during the experiments. Figs. 6.3 and 6.4 are a selection of the decomposed waveforms for the input signal and the resulting output from a chain of spheres (Fig. 6.2). In these two figures, A6 represents an approximated component of the signals from a level 6 decomposition. D4 – D6 are detailed components from levels 4 – 6 of the decomposition, with each corresponding to different frequency bands. These bands are D4: 3.125 – 6.25 MHz, D5: 1.563 – 3.125 MHz, D6: 781 kHz – 1.56 MHz, A6: 0 – 781 kHz. As expected the decompositions D4, D5 and D6 shown in Fig. 6.4 produced noisy signals for frequencies greater than 780 kHz, suggesting that the original signal from the 73 kHz transducer does not contain energy at this high a frequency. However, a signal was detected in the frequency range 781 kHz – 1.563 MHz (D6) for the chain of spheres. This suggests that the system of chain of spheres excited using a tone-burst at 73 kHz can produce frequency components ten folds greater than its input frequency.

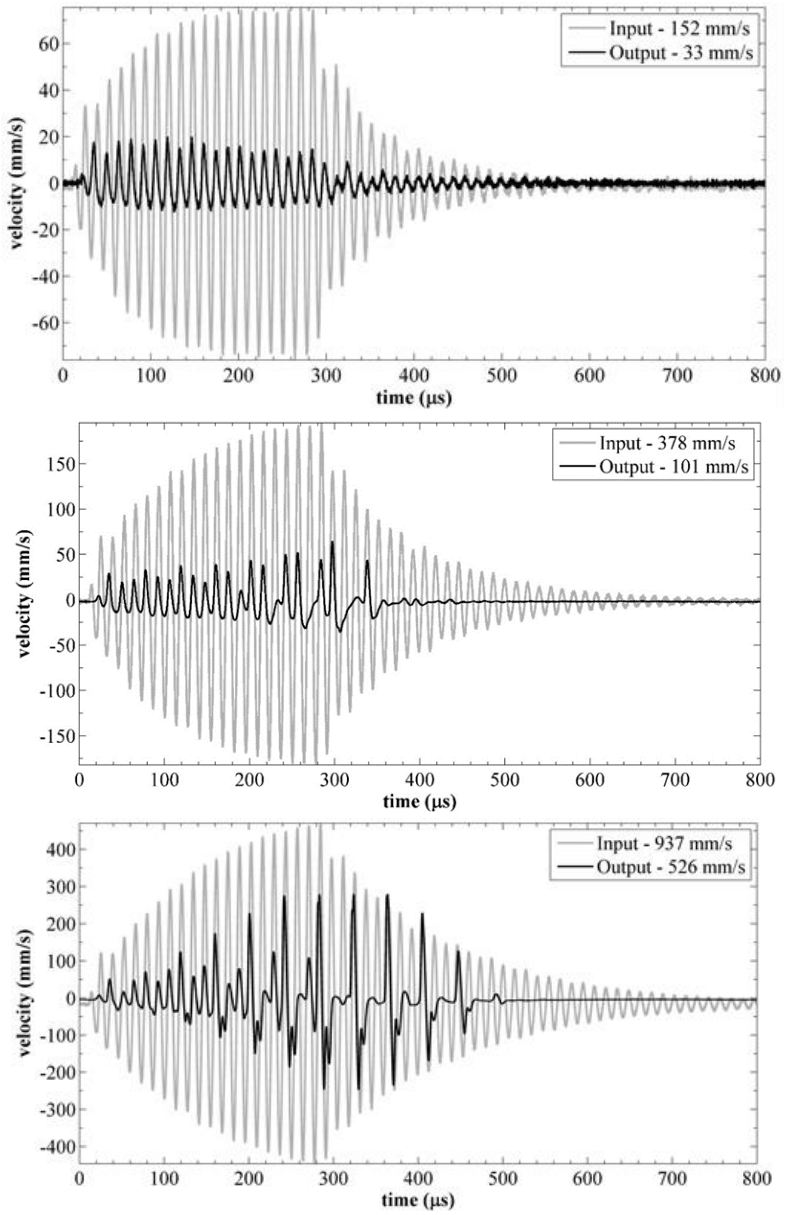

Fig. 6.2. Input (grey) and Output (black) signals for a chain of 6 spheres as the input amplitude was increased from 152 to 937 mm/s. The legends show the peak to peak particle velocity of the input and output signals.

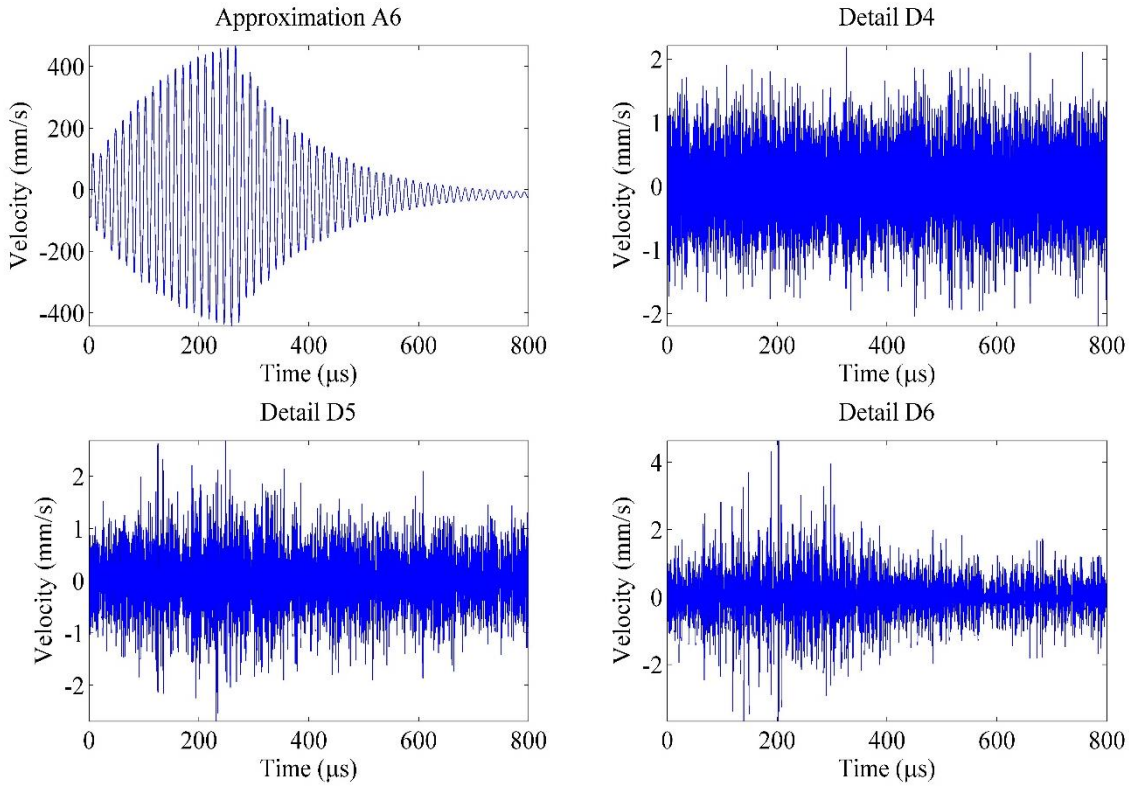

Fig. 6.3. A selection of the decomposed waveforms for the transducer (v_m = 937 mm/s).

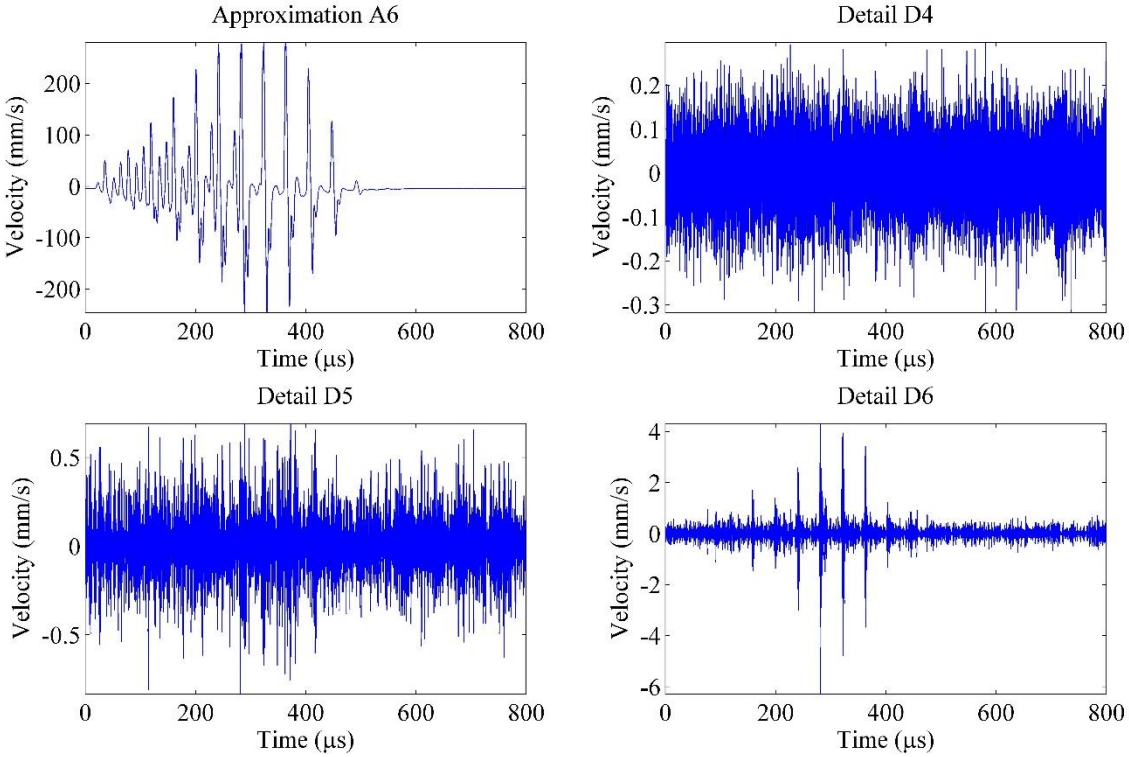

Fig. 6.4. A selection of the decomposed waveforms for a chain of 6 spheres (v_m = 526 mm/s).

The A6 approximation of the wavelet decomposition provides the ability to estimate the time of flight. This feature provides an enhanced signal to noise ratio when compared to the original signal. Using the A6 approximation makes it is easier to determine the first arrival of the signal in the waveform. Fig. 6.5 shows a magnified view of the first arrival/peak of the input from the transducer (left figure) and the output from the chain of spheres (right). The time of flight was estimated by subtracting the time of the first arrival of the chain of spheres from that of the transducer giving 8.76 μs (23.1 μs – 14.34 μs) as the time of flight and a propagation velocity of 685 mm/s for a chain of six 1 mm spheres.

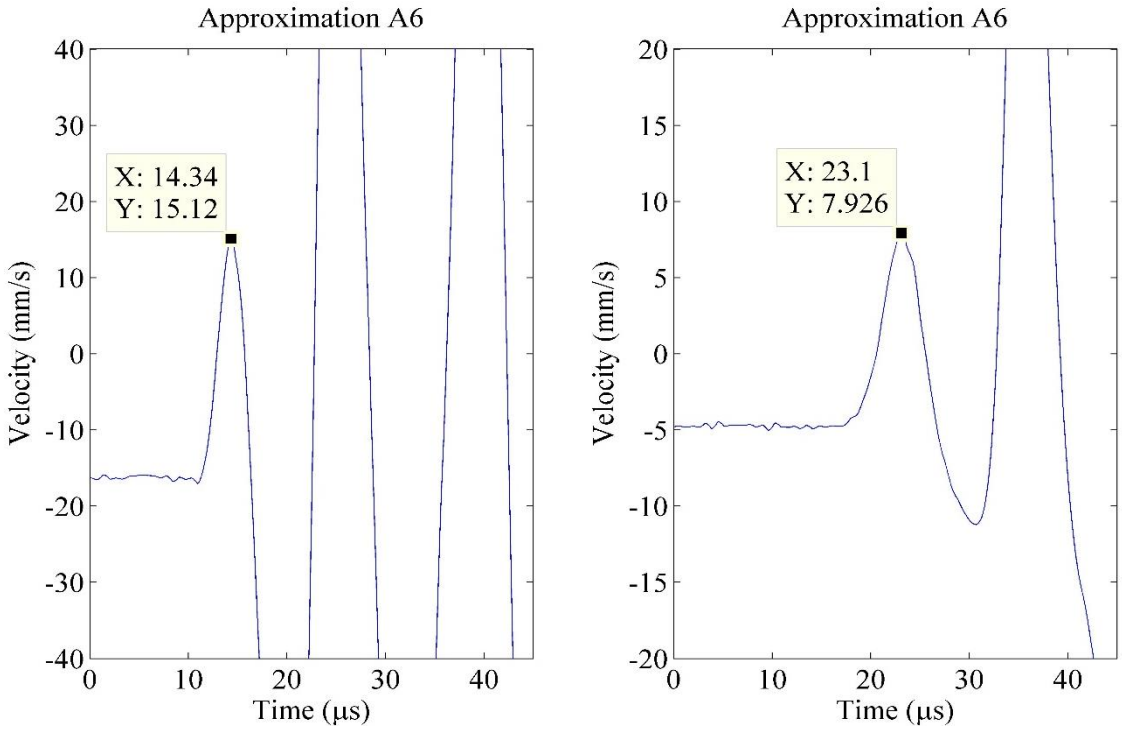

Fig. 6.5. Magnified view of the first arrival/peak of the input from the transducer (left figure) and the output from the chain of spheres (right) from the A6 decomposition at v_m = 937 m/s and 526 m/s.

The decomposed waveform (Fig. 6.6) for the chain of spheres excited by a low amplitude signal with a peak to peak particle velocity of 152 m/s illustrates that the output signal does not contain any energy at D6 frequency, suggesting that the signal is weakly nonlinear. It also worth noting that the propagation velocity for this signal increases to 713 m/s (time of flight: 8.41 μs) as shown in Fig. 6.7

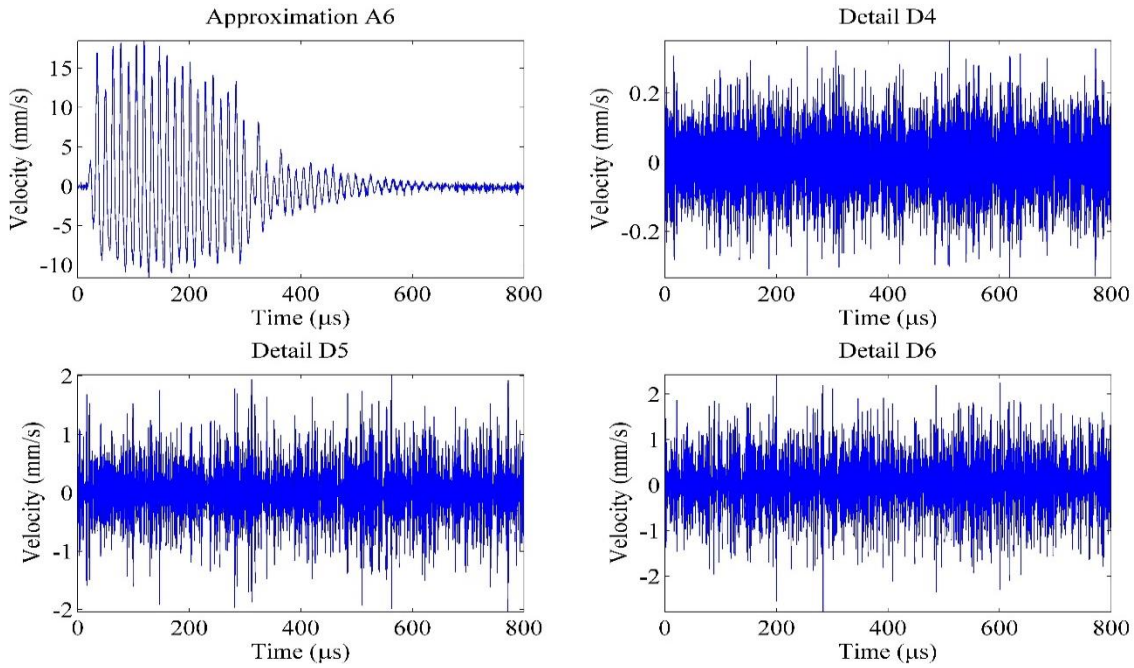

*Fig. 6.6. A selection of the decomposed waveforms for a chain of 6 spheres (**V_m** = 33 mm/s).*

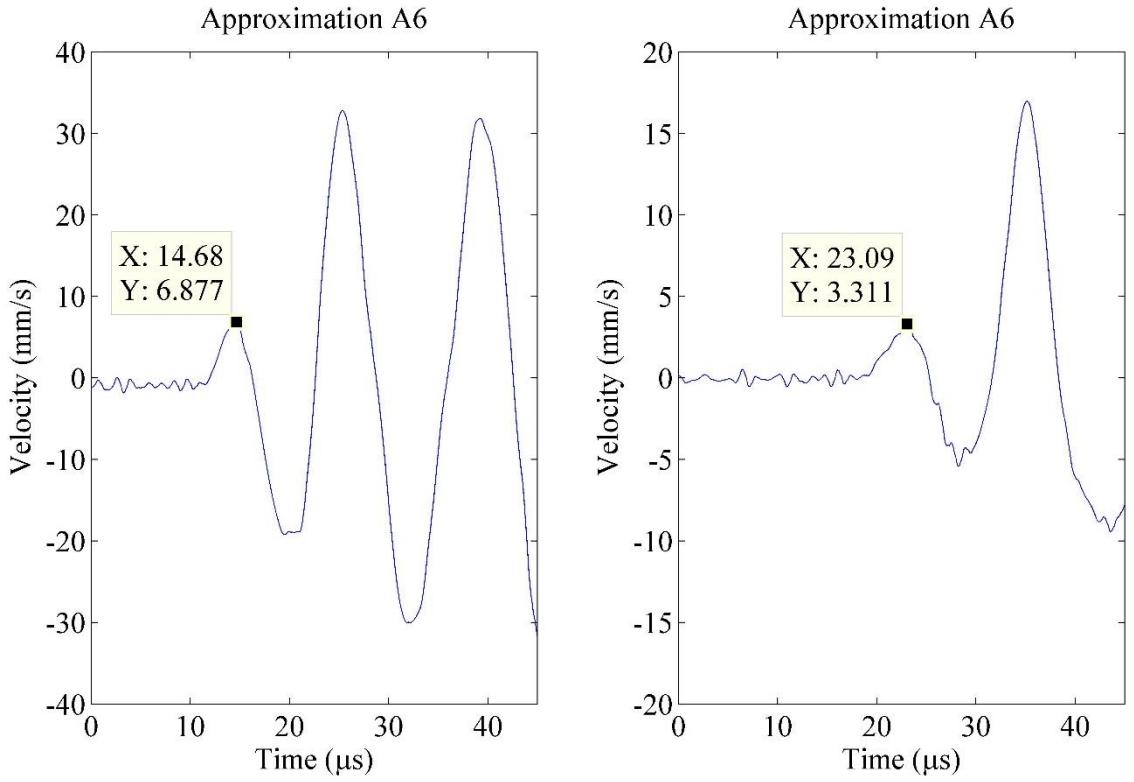

Fig. 6.7. Magnified view of the first arrival/peak of the input from the transducer (left figure) and the output from the chain of spheres (right) from the A6 decomposition at v_m = 152 m/s and 33 m/s.

The correlation coefficients for the input excitation signal and output signals for the chain of spheres for the different peak to peak particle velocity (v_m) are shown in Table 6.1, where A0

represents the original unprocessed signals. This shows that as the amplitude of the input signal increases, the correlation coefficients decreases. This suggests that at the low input velocity amplitude of 33 m/s, the output signal exhibits a weakly nonlinear behaviour, but at higher amplitude the nonlinear effects are greatly enhanced producing solitary waves.

6.3. Experimental Setup

There were many complexities involved in creating a stable experimental arrange that could provide a controlled and varied amount of pre-compression on the chain of spheres. Previous studies [1] using controlled pre-compression consisted of chains of 10 mm diameter spheres with a hole drilled down their centre. A fishing line was knotted at on end, passed through the hole and at the other end of the line weights were hung and used to vary the pre-compression on the chain. For the experiments described in this chapter such a method could not be applied on spheres of 1 mm diameter, as the force would be too great. Therefore, a stylus displacement probe or profiler [3], usually used for measuring surface topography, was modified to act as a mechanism of applying controlled pre-compression force, f_0 onto the chain of spheres. The schematic diagram of the profiler is shown in Fig. 6.8. The probe consists of three main parts; an electromagnetic force actuator, a differential capacitive sensor and a leaf spring suspension system.

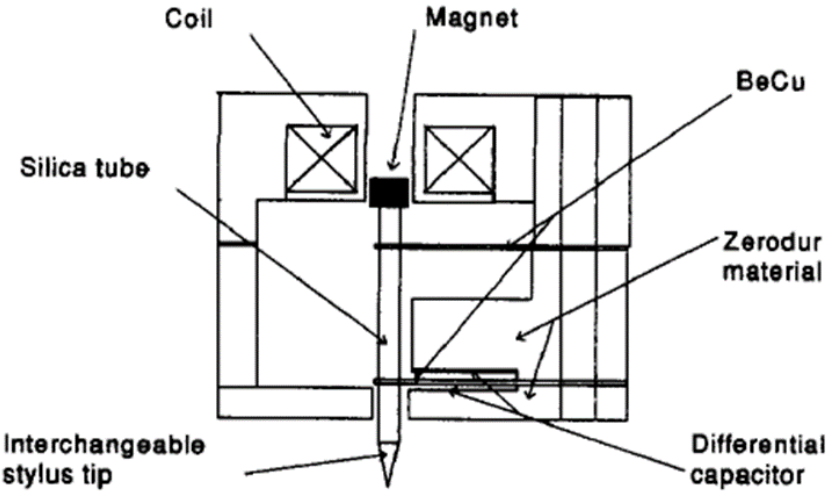

Fig. 7.8. Schematic diagram of force displacement probe/profiler [3].

Typically, the profiler is used to measure force variations arising from the deflection of the probe's ligaments as it travels along the surface of a sample [4]. The deflection of the probe's tip is measured via electrodes and the differential capacitive sensor. To achieve the required function as a controlled mode of applying pre-compression, the current that passes through the force actuator consisting of a solenoid coil and a magnet was varied. The interaction of the magnetic field of the coil and magnet generated a force on the magnet which is directly proportional to the current applied. Since the magnet had its poles aligned along the axis of the solenoid coil and the base of the magnet was attached to the probe, the probe and stylus experienced a co-linear force which was proportional to the current applied along the coil.

Using a specially designed current drive, the force actuator was used to provide a calibrated static contact force at a neutral position. Positioning the probe accurately, the force on the 60 mm long, 1.5 mm diameter stylus resulting from the magnet was controlled by varying the drive current. An overview of the pre-compression assembly is shown in Fig. 6.9. The profiler was mounted onto an aluminium platform with its stem clamped onto a Rank Taylor Hobson Talysurf 5 to support the magnet and coil placed directly above the stylus.

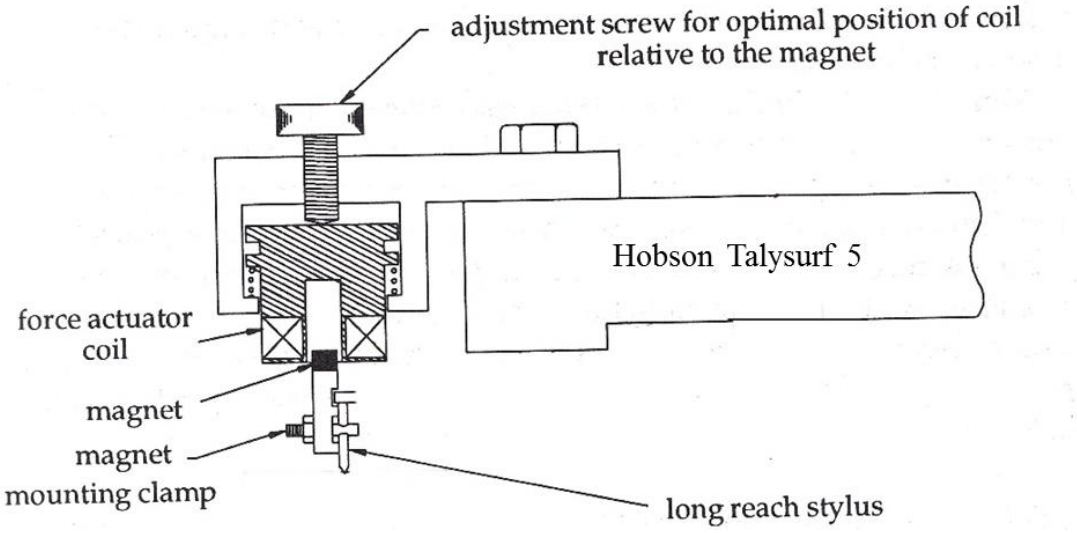

Fig. 6.9. Schematic representation of the stylus pre-compression mechanism [5].

The coil assembly was held in place by brackets clamped using screws right above the magnet. Spring mounts with adjustable screws were used to hold the coil in place, while, the screws provided fine adjustments to position the magnet and coil assembly in an optimum position. This arrangement was adequate because the force applied by the rig (stylus-magnet-coil) was independent of small displacements; therefore, small vibrations within the system did not couple into the measurement loop [5].

The Talysurf provided the means to carefully and accurately position the tip of the stylus onto a fulcrum or lever made of aluminium. The fulcrum was used to apply pre-compression directly on the chain of spheres as shown in Fig. 6.10. The length from the point where the stylus was in contact with fulcrum was equal to the point where the sphere was also in contact with the fulcrum, to achieve a one-to-one correlation between the force from the stylus on the fulcrum and that exerted by the fulcrum on the sphere. The fulcrum was designed to be light and strong enough not to deform from the force exerted on it. It also had a circular hole to accommodate the last sphere which protruded out of the annulus of the holder, the hole was smaller than the diameter of the sphere (approximately 0.3 mm) and also smaller than the circumference of the widest section of the sphere protrusion. This ensured that there was a gap between the holder and the fulcrum. The pre-compression system provided electrically selectable static force in the range of 0.01 mN to hundreds of mN. The rest of the experimental setup remained the same; a 73 kHz transducer and horn concentrator as input connected to an amplified function generator, a laser vibrometer and oscilloscope to capture the resulting waveform of the chain of spheres encased in an acrylic holder (as described in Chapter 4).

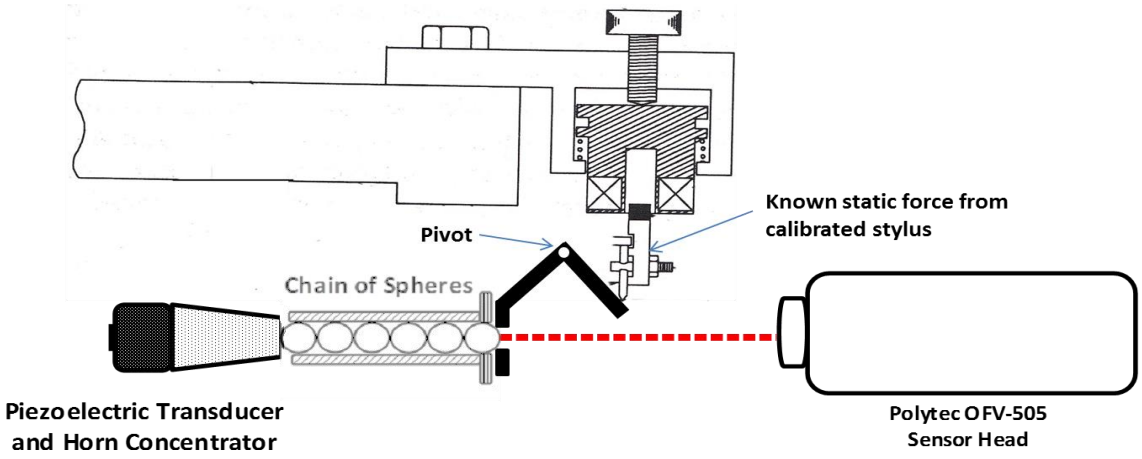

Fig. 6.10. Schematic diagram of the modified experimental setup for the application of known static pre-compression force (f_0).

6.4. Experimental Results and Comparison to Model.

The experiments in this chapter were performed on chains containing 3, 6 or 10 chrome steel spheres with a diameter of 1 mm. As described in Chapter 4, each chain length subscribes to a specific duration or number of cycles of input tone-burst to trigger and build the train of solitary waves. However, unlike the experiments and setup found in Chapter 4 where the last sphere was in contact with an acrylic wall, here, an aluminium fulcrum was used as both the wall and as a means of applying pre-compression force. In the following sub-sections, the results for these length of chains (3, 6 and 10 spheres) containing 1 mm diameter chrome steel excited using the 73 kHz horn concentrator will be presented for 10, 20 and 45 cycles subjected to various pre-compressions. The results were also compared to the theory, and some conclusions drawn concerning the type of behaviour observed. It will be observed that as the pre-compression increases the behaviour in terms of time of flight and propagation velocity tends towards that of a bulk material as the motion and the separation between each individual sphere is increasingly restricted. The time of flight will be determined using wavelet analysis as previously described.

6.4.1. **Detailed results for a 3-Sphere Chain**

For the chain comprising of three spheres, the output waveforms and spectra are shown in Fig. 6.11 for an input of 10 cycles at maximum input amplitude (v_m = 591 mms^{-1}) from the horn. The minimum force, f_0 is that with no additional pre-compression forces on the chain other than those resulting from a light contact of the horn and the fulcrum (estimated to be about 0.01 N or 10 mN by comparison to modelling predictions); note that this could not be estimated experimentally. At this minimum pre-compression, the non-linear periodic pulses were present in the time waveform. The shape of these pulses was different from those presented in Chapter 5. This was due to a change in the boundary conditions - unlike the arrangements in Chapter 5, where the end wall was made of an acrylic material, here the wall is formed of an aluminium material (*i.e.* the fulcrum) thereby, creating an acoustic match in terms of impedance value. This altered the shape of the waveform however the general characteristics remains; the pulses are periodic and the spectrum contains a dominant sub-harmonic peak at 36 kHz with side-lobes. The time of flight estimated using wavelet analysis was 2.58 μs with a propagation velocity of 1,163 ms^{-1}. As f_0 increases, the amplitude of the harmonic peaks in the spectra begin to reduce, the period of the pulses become narrower and the propagation velocity decreases to 718 ms^{-1} at $f_0 = 28$ mN. By 52 mN, the envelope of the time waveform starts to resemble that of the input signal from the horn with a peak at 73 kHz and a smaller one at 146 kHz. At this point the propagation velocity as increased back to 1,007 ms^{-1} and tending towards that of a continuous medium. Finally, at 220 mN the waveform and spectrum resembles that of the input signal, shown in Fig. 6.12. An elongation of the time waveform can be observed as well as a resonant signal at 73 kHz. The system has thus become weakly nonlinear, with f_0 being of the same order of magnitude as the input signal f_m, with pre-compression reducing the ability of spheres in the chain to move relative to each other, decreasing non-linearity, and suppressing the presence of the solitary wave impulses.

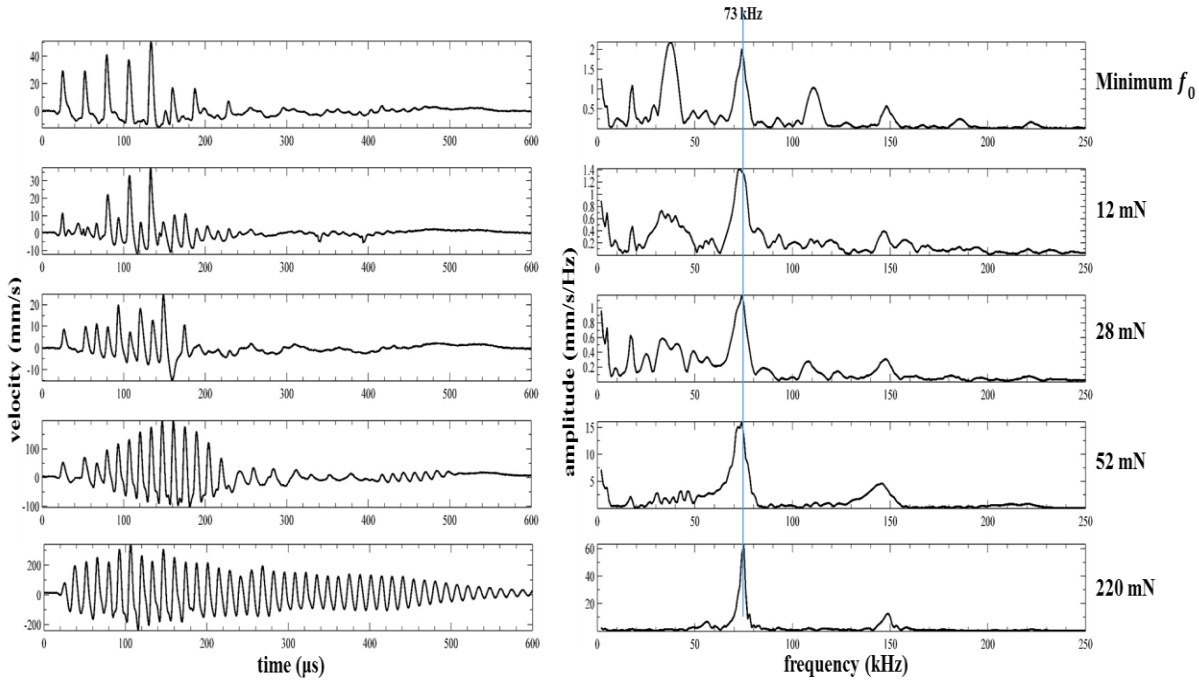

Fig. 6.11. Waveform (left) and frequency spectrum (right) of the output from a 3-sphere chain excited using a 10-cycle tone-burst from an ultrasonic horn at 73 kHz ($\boldsymbol{v_m}$ = 591 mms^{-1}) subjected to various pre-compression force.

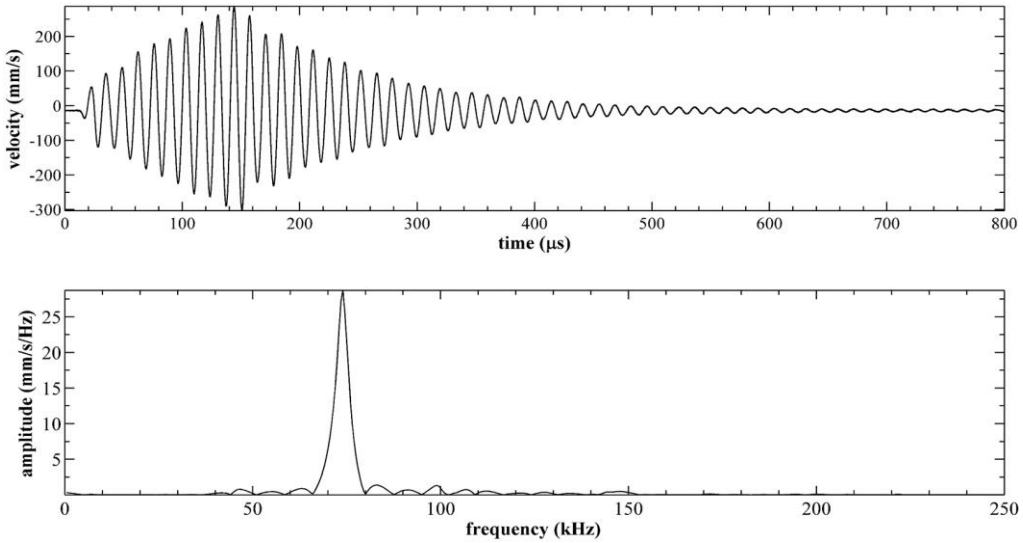

Fig. 6.12. Waveform (Top) and spectrum (Bottom) of the motion of the vibrating horn tip, as measured using a vibrometer. Excitation was a tone-burst of 10 cycles at 73 kHz ($\boldsymbol{v_m}$ = 591 mms^{-1}).

Increasing f_0 beyond 220 mN causes misalignment of the spheres creating a contact similar to those illustrated in Fig. 6.13. The misalignment occurs because the inner diameter of the holder is 10% wider than the diameter of the spheres to reduce surface friction. The resulting

waveforms when this misalignment takes place are shown in Fig. 6.14. Instead of the waveform looking further like that of the input, it becomes distorted and takes on additional characteristics which at present are not relevant to this research.

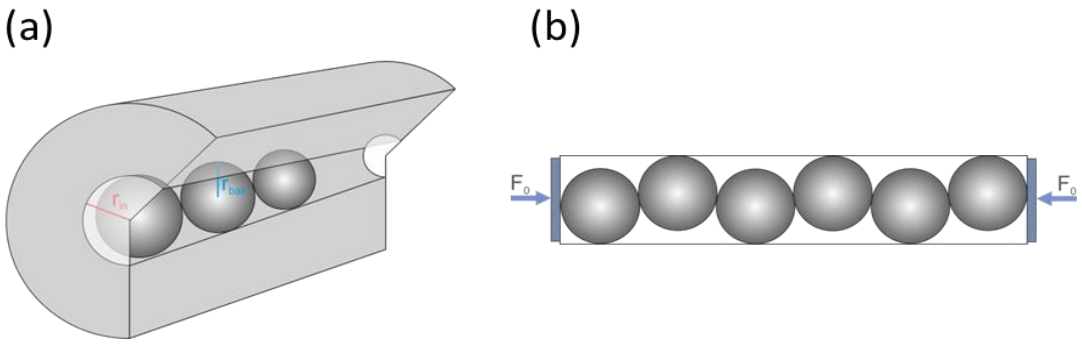

Fig. 6.13. Cross sectional view of the holder before misalignment (b) Misalignment of ball bearings under pre-compression.

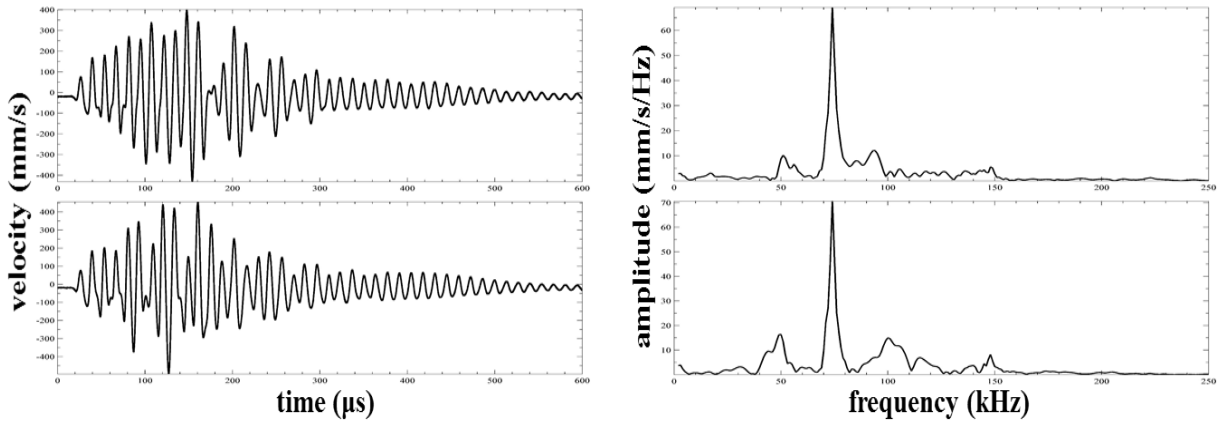

Fig. 6.14. Waveform (left) and frequency spectrum (right) of the output from a misaligned 3-sphere chain excited using a 10-cycle tone-burst from an ultrasonic horn at 73 kHz (v_m = 591 mms^{-1}).

The results from the experiments (Fig. 6.11) were compared to those from the theoretical predictions shown in Fig. 6.15. The predicted results produced similar trends, however, the propagation velocity increased in a linear fashion, from 495 ms^{-1} for 50 mN to 971 ms^{-1} for 500 mN. As the pre-compression force increases the period of the pulses become narrower in the time waveform and the harmonics begin to fade. The main differences between the model and the experiment can be observed within the spectra; in the experiments there was a sub-harmonic peak at 36 kHz and a smaller peak or side-lobe at 18 kHz. In the result of the simulation there

are also two sub-harmonic peaks at 46 kHz and 27 kHz. For f_0 = 50 mN the peaks are conjoined but at f_0 = 70 mN peaks become separated. It is suspected that the discrepancies and the slower velocity at 50 mN was due to the contact between the last sphere and the combined walls of the acrylic holder and aluminium fulcrum. This combination of walls were not accounted for in the model.

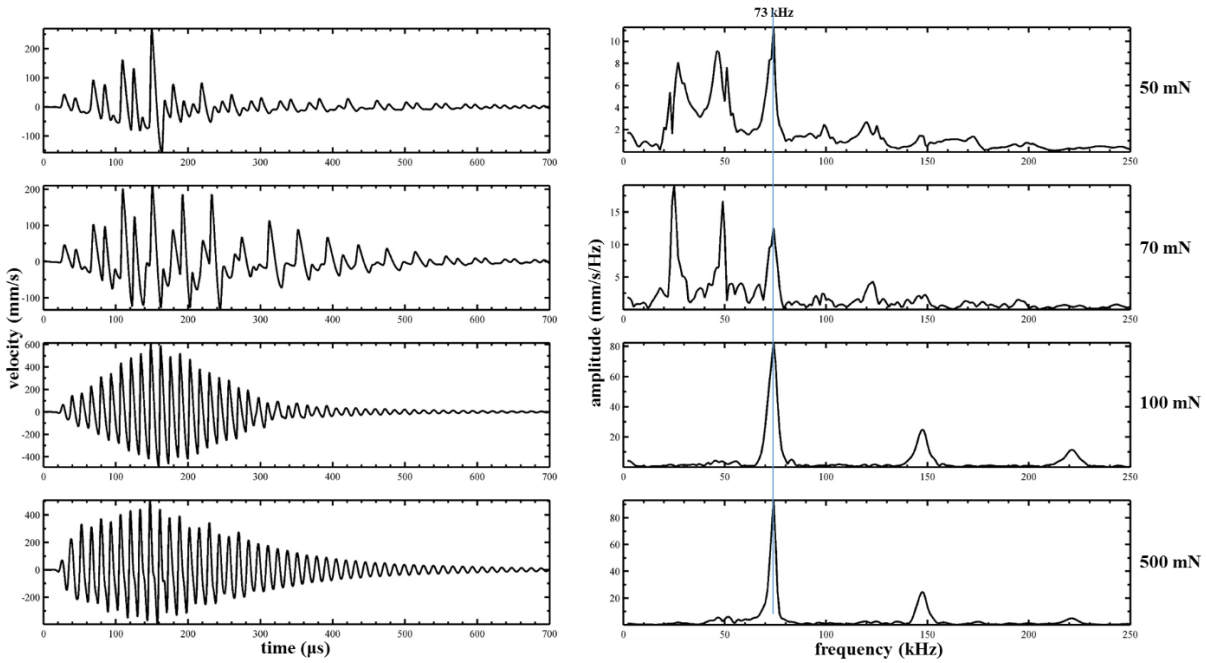

Fig. 6.15. Model prediction for a 3-sphere chain using an input of 10-cycle tone burst from an ultrasonic horn at 73 kHz. Waveforms (left) and Spectra (right) at various pre-compression force.

To minimise the effects of the combined wall (acrylic and aluminium), an acrylic ring was fused to the fulcrum ensuring that the last sphere was no longer in direct contact with the aluminium fulcrum. The results of the experiment using the modified fulcrum produced waveforms more representative of those illustrated in Chapter 4 (Fig. 4.14), these are shown in Fig. 6.16 below. In this experimental setup, the nonlinear solitary periodic pulses are more apparent in the time waveform. In the spectra, there is a single sub-harmonic peak which is equal to the periodicity of the pulses in the time waveform. Similarly, the time of flight and propagation velocity decreases in a linear fashion as f_0 increased. The train of pulses in the time waveform becomes narrower with their periods getting shorter. The amplitude of the sub-

harmonic peak at 36 kHz also decreases as the values of f_0 increases. At the minimum pre-compression force when strongly nonlinear behaviour was detected, the propagation velocity was 458 ms^{-1}, at f_0 = 36 mN, it became 482 ms^{-1} and by f_0 = 209 mN the signal had transitioned to a weakly nonlinear state, with the velocity increases to 556 ms^{-1} with the envelope of the time waveform appearing closer to that of the input signal. This indicates that there is a fine balance between applied force/displacement and static pre-compression in granular chain systems, with the latter being a dominant controlling feature. This is consistent with other studies in granular chains [6], where stiffening of the chain resulted in a weakly nonlinear behaviour, and the generation of weak harmonics.

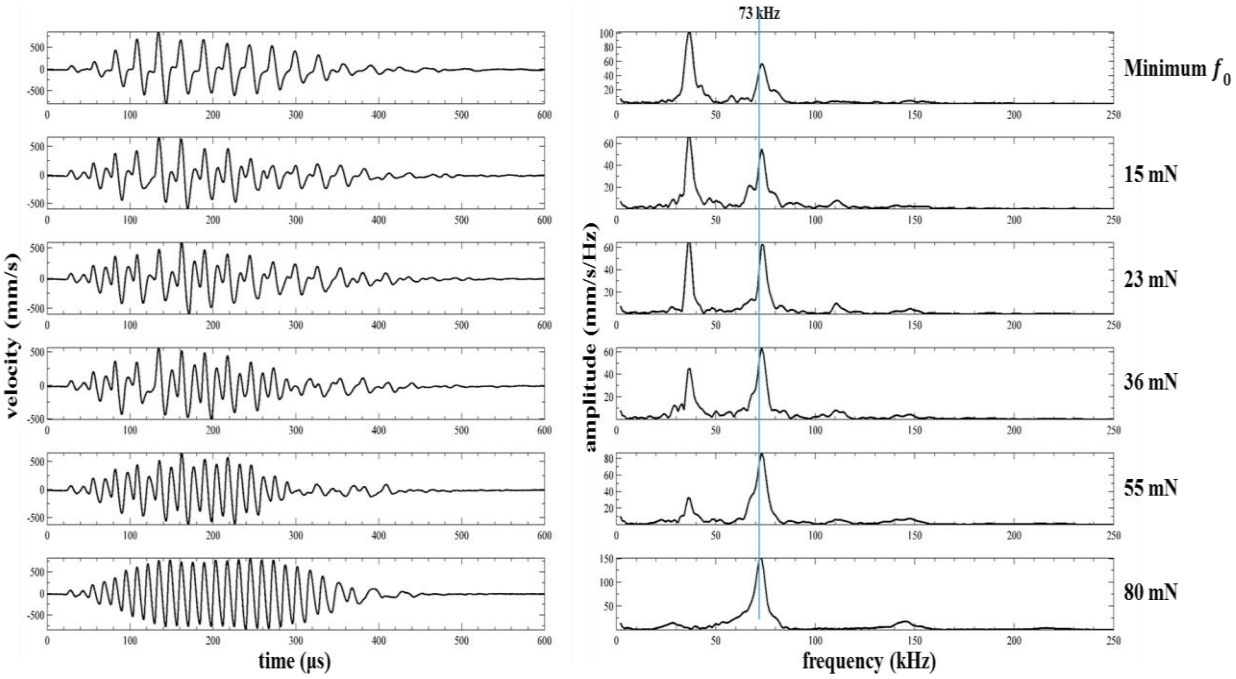

Fig. 6.16. Waveform (left) and frequency spectrum (right) of the output from a 3-sphere chain excited using a 10-cycle tone-burst from an ultrasonic horn at 73 kHz ($\boldsymbol{v_m}$ = 591 mms^{-1}) and using the modified fulcrum to vary the pre-compression.

By changing the viscous damping coefficient from 0.32 to 0.23 Nsm^{-1} for the theoretical model, the results in Fig. 6.17 were obtained. These predicted results are a close match to those of Fig. 6.16 using the modified fulcrum. The waveforms obtained when the chain was subject to a pre-compression force from 20 – 40 mN contained periodic pulses that got

narrower. This was accompanied by a single sub-harmonic frequency peak at 37 kHz which faded as the pre-compression was further increased.

Consider now the propagation velocity of the solitary wave pulses along the chain. Although there was an initial decrease in propagation velocity at low applied static pre-compression forces, the value rose from 543 to 1,038 ms^{-1} as the pre-compression force increased from 20 to 500 mN. Note that the shapes of the experimental and theoretical curves are similar in Fig. 6.17, with an initial rapid change in propagation velocity at low applied static forces (below 50 mN), but with a levelling off at intermediate values, before increasing again. The curve demonstrates the transition of the system from strongly nonlinear to weakly and as it tends towards a linear regime with all its sub-harmonica suppressed. This change in regime is highlighted with the letters A (strongly nonlinear), B (weakly) and C (tending towards linear) in Fig. 6.18. The difference between modelling and experiment could be due to many different factors (such as alignments and dissipation in the experiments), noting that the experiment was highly sensitive to input conditions. It can still be seen though that the propagation velocity increased with applied static pre-compression in a characteristic way. This big change would allow the use of this system to introduce significant time delays between chains, and hence possible future use in an array for focussing.

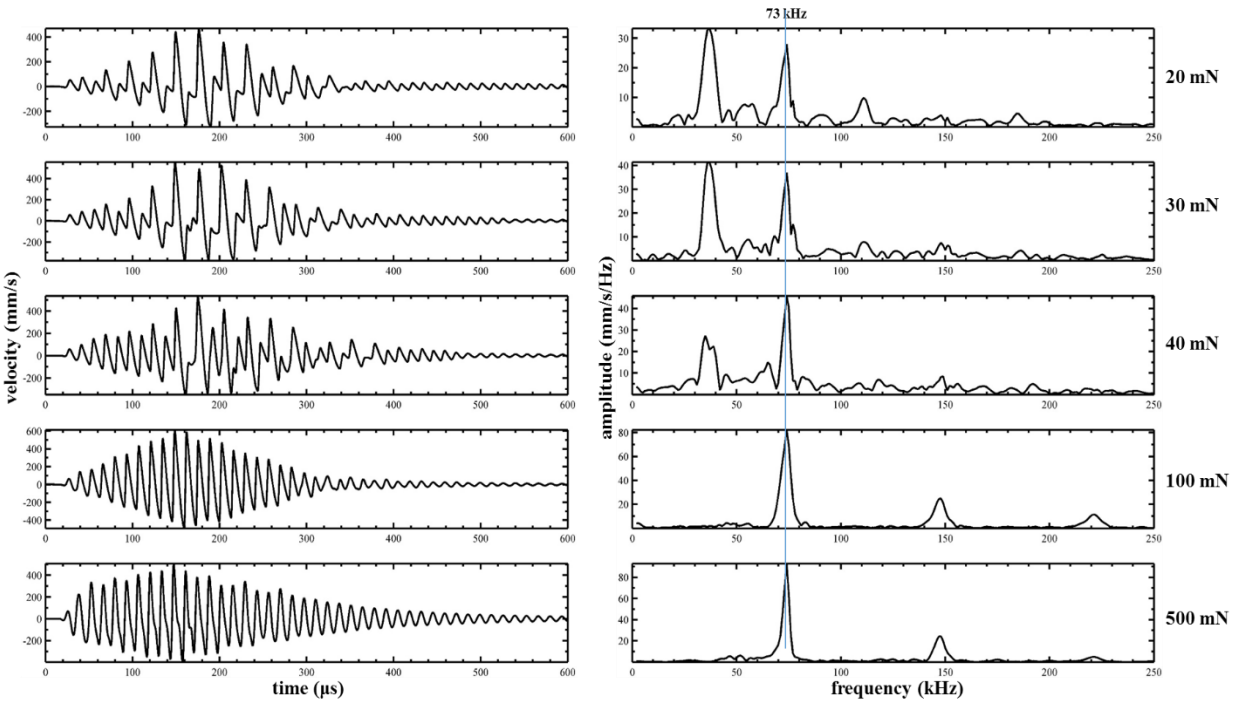

Fig. 6.17. Model prediction for a 3-sphere chain using an input of 10-cycle tone burst from an ultrasonic horn at 73 kHz. Waveforms (left) and Spectra (right) at various pre-compression force (damping = 0.23 Nsm^{-1}).

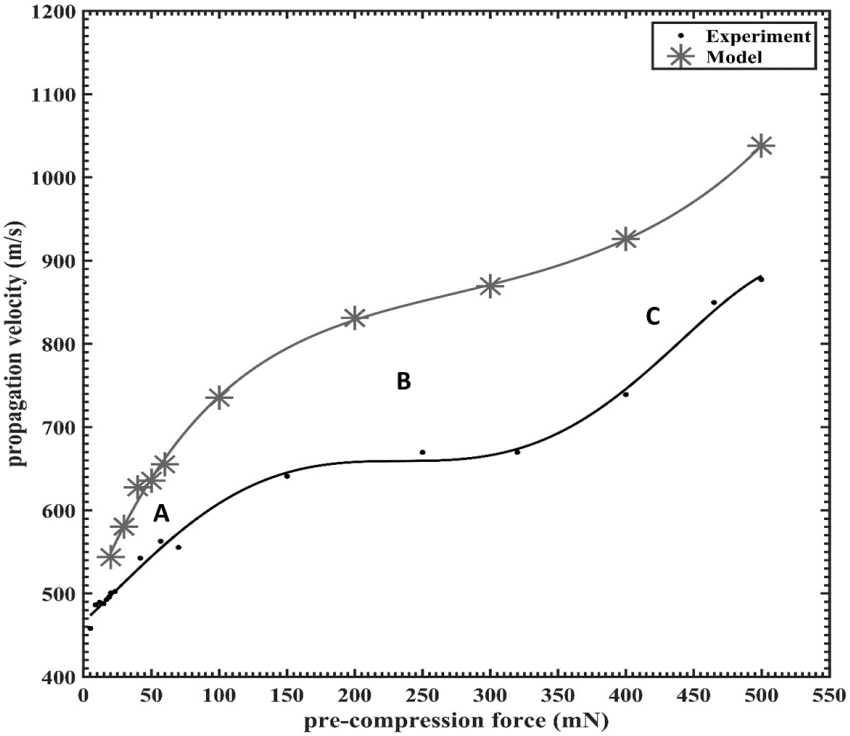

Fig. 6.18. Propagation velocity from the experiment using the modified fulcrum and modelling predictions (damping = 0.23 Nsm^{-1}) for a 3-sphere chain excited by an input of 10-cycle tone burst from an ultrasonic horn at 73 kHz at various pre-compression force.

6.4.2. **Results for 10 and 6-sphere Chains**

A. Results from a 10-Sphere Chain

The output waveforms and spectra for the chain containing 10 spheres using the combined acrylic and aluminium wall (unmodified fulcrum) are shown in Fig. 6.19 for an excitation with a duration of 45 cycles and a peak to peak amplitude velocity, v_m of 1,081 mms^{-1} subjected to various pre-compression force. At the minimum pre-compression, a train of saw-tooth pulses were observed with the frequency spectrum containing a single sub-harmonic peak at 37 kHz. At this level of pre-compression the time of flight was 24 μs with a propagation velocity of 415 ms^{-1}, the three sub-harmonics peaks previous observed (in Chapter 4) at 18, 36 and 54 kHz were no longer present. As f_0 was increased to 28 mN, two sub-harmonics emerged at 30 and 45 kHz while the peak at 37 kHz was supressed. The velocity of the time waveform at this compression was 395 ms^{-1}.

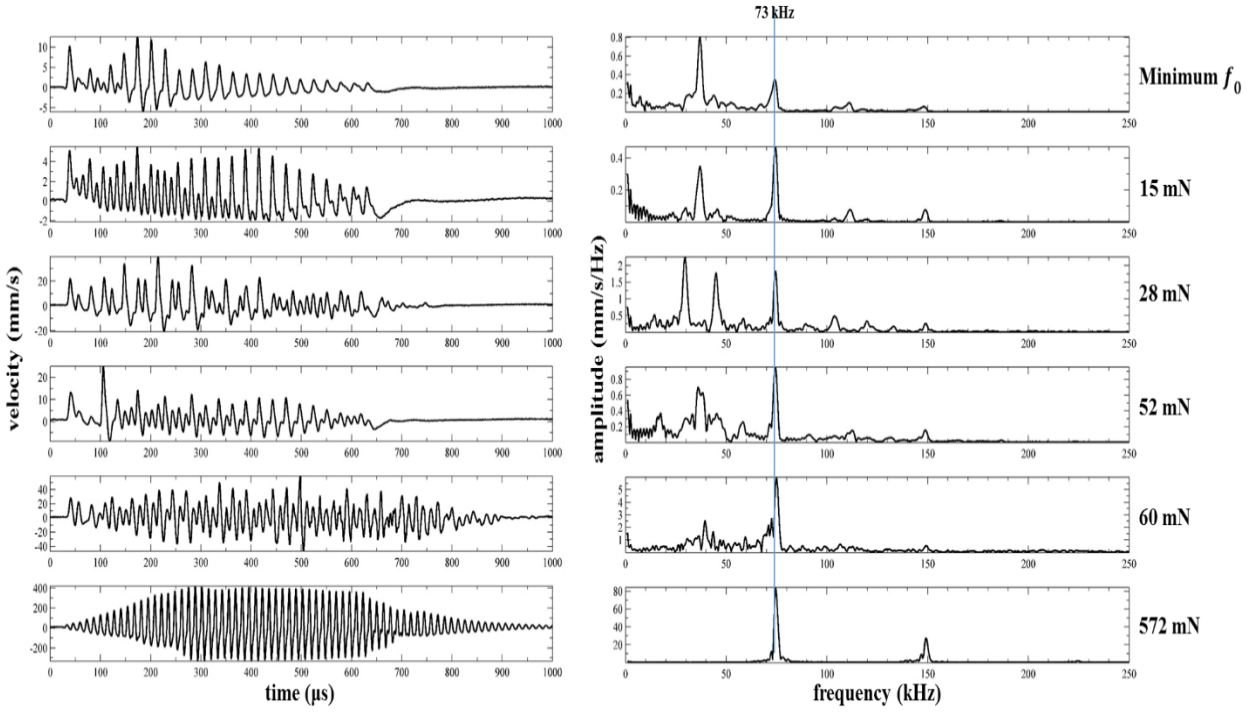

Fig. 6.19. Waveform (left) and frequency spectrum (right) of the output from a 10-sphere chain excited using a 45-cycle tone-burst from an ultrasonic horn at 73 kHz (v_m = 1081 mms^{-1}) and using the unmodified fulcrum to vary the pre-compression.

As f_0 was further increased to 52 mN, the train of periodic pulses began to form at the end of the time waveform this was accompanied by the three previously mentioned sub-harmonic peaks at approximately 18, 36 and 54 kHz in the spectrum. The propagation velocity of the time waveform was 386 ms^{-1}. By 572 mN, the propagation velocity had increased to 546 ms^{-1} and the envelope of the time waveform resembled that of the input signal (Fig. 6.20). Within the spectrum, all the sub-harmonic peaks had been suppressed with the remaining peaks found at 73 and 146 kHz which was similar to the spectrum of the input signal. Just like the case of the 3-sphere chain when the unmodified fulcrum was used, the propagation velocity decreases just before the wave transforms from strongly nonlinear to weakly nonlinear, but in this case it is much more obvious. This change in regime is highlighted as B (strongly nonlinear) and C (weakly nonliear) in Fig. 6.21, the region A (also encircled in the figure), is a state where the system is uncontrollable. The instability in this region may be a result of a drift in magnitude of the pre-compression applied suggesting that the level of pre-compression is the region is unreliable or it could be that the effect of a balance between nonlinearity and dispersion as yet to occur.

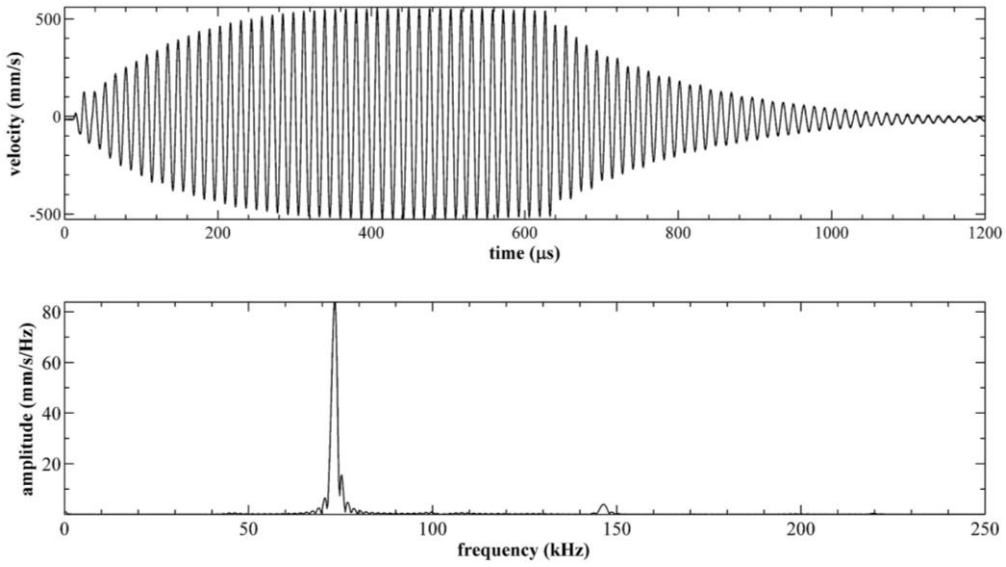

Fig. 6.20. Waveform (Top) and spectrum (Bottom) of the motion of the vibrating horn tip, as measured using a vibrometer. Excitation was a tone-burst of 45 cycles at 73 kHz (v_m = 1081 mms^{-1}).

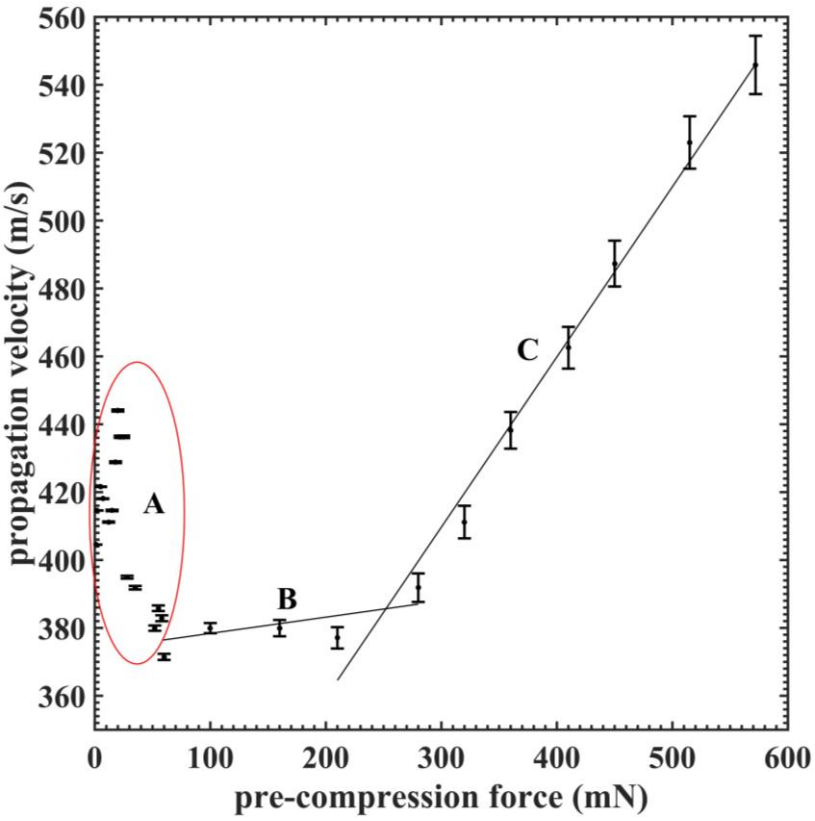

Fig. 6.21. Propagation velocity from the experiment using the unmodified fulcrum for a 10-sphere chain excited by an input of 45-cycle tone burst from an ultrasonic horn at 73 kHz at various pre-compression force.

The theoretical predictions of the model shown in Fig. 6.22 displayed different waveforms and spectra from those of the experiments. In the spectra of the predicted results from f_0 = 10 mN to 40 mN there were three sub-harmonic peaks present at 18, 36 and 56 kHz. The energy fed to these peaks were transferred to those of 73 and 146 kHz as the compression reached 50 mN. The propagation velocity also increased from 348 ms^{-1} to 385 ms^{-1} as f_0 increased to 50 mN. Again, this mismatch between the characteristics of the predicted and experimental results was attributed to the boundary conditions further highlighting the sensitive nature of the nonlinear chain of granular particles.

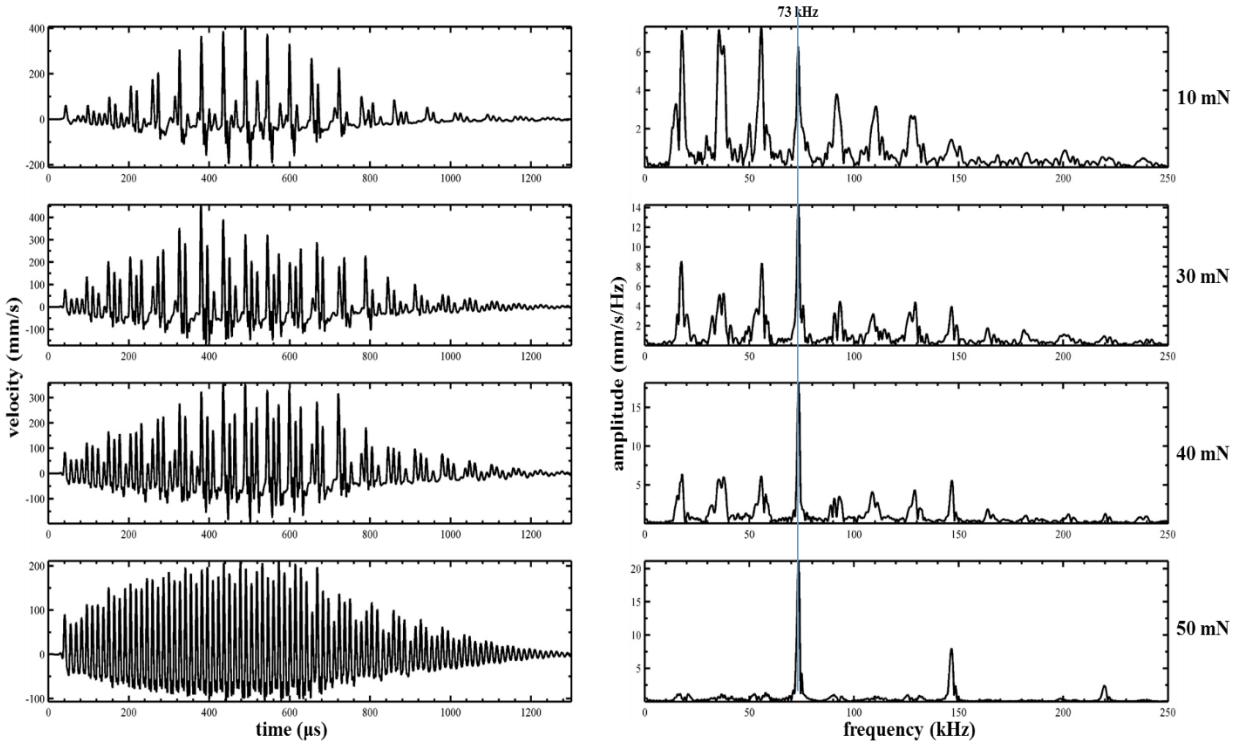

Fig. 6.22. Model prediction for a 10-sphere chain using an input of 45-cycle tone burst from an ultrasonic horn at 73 kHz ($\boldsymbol{v_m}$ = 1081 mms^{-1}). Waveforms (left) and Spectra (right) at various pre-compression force.

The 10-sphere chain was then subjected to pre-compression using the modified fulcrum which was fused with a ring made of acrylic R11 resin. The results from this experiment are shown in Fig. 6.23. It was observed that the 45-cycle tone-burst input signal was no longer sufficient to maintain the train of nonlinear pulses. The nonlinear pulses collapsed shortly after they were triggered as seen in the time waveform. In the spectrum, the three sub-harmonics witnessed in the predicted results were present although indistinct and with small amplitudes.

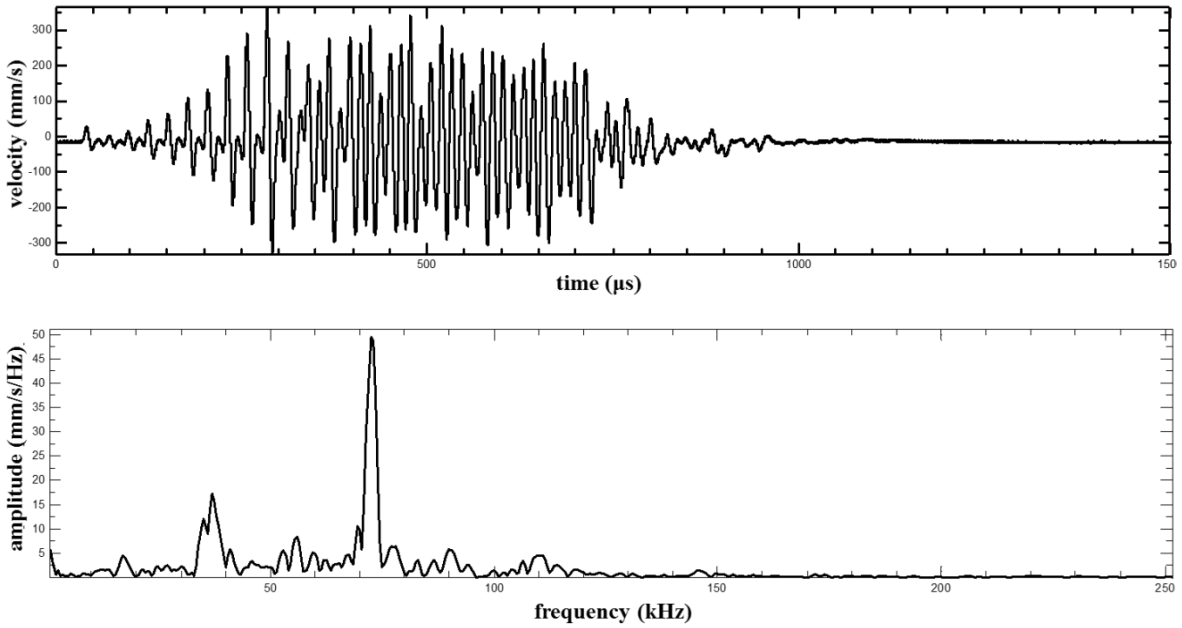

Fig. 6.23. Waveform (top) and frequency spectrum (bottom) of the output from a 10-sphere chain excited using a 45-cycle tone-burst from an ultrasonic horn at 73 kHz ($\boldsymbol{v_m}$ = 1081 mms^{-1}) and using the modified fulcrum at minimum pre-compression.

In an attempt to re-establish and maintain the train of nonlinear pulses, different durations of the input tone-burst were used, and it was noted that the system only responded to a 10-cycle input signal as illustrated in Fig. 6.24. The periodic pulses were present in the time waveform when subject to the minimum pre-compressions. However, the waveforms were shorter with longer periods when compared to the narrow pulses generated using a 45-cycle input signal in Chapter 5 or those of the predictive model. These broader pulses resembled those of the 3-sphere chain (also excited using a 10-cycle tone-burst) were accompanied by a single sub-harmonic at 37 kHz approximately half of the input frequency. By the time f_0 had increased to 15 mN, the periodic pulses in the waveform were narrower with a propagation velocity of 528 ms^{-1} and was accompanied by two additional but indistinct sub-harmonic peaks at 19 and 54 kHz in the spectrum. At 28 mN the velocity had increased to 536 ms^{-1} with the sub-harmonic peaks were fully formed at 19, 37 and 54 kHz as observed in the predicted waveforms and those introduced in Chapter 5 excited by a 45-cycle input signal. When f_0 was increased to 300 mN, the periodic pulses and accompanying sub-harmonic no longer existed with the waveform

and spectrum resembling those of the input signal. At this point the propagation velocity was 719 ms^{-1}.

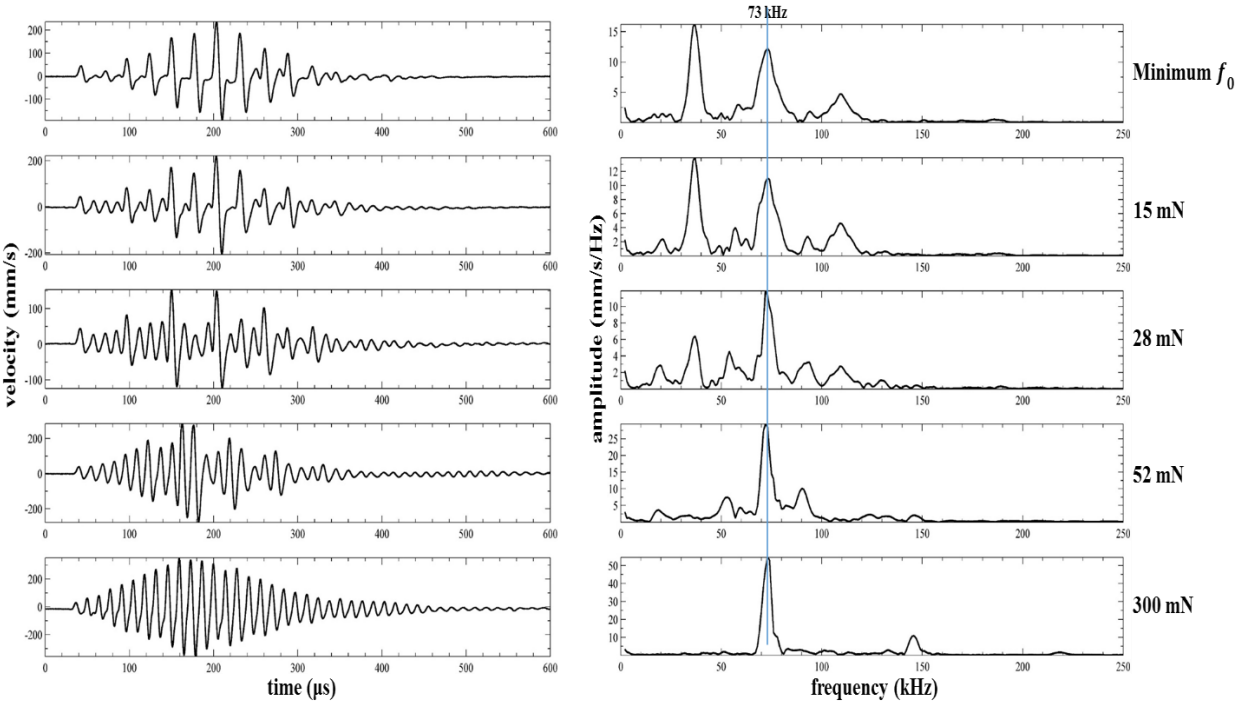

Fig. 6.24. Waveform (left) and frequency spectrum (right) of the output from a 10-sphere chain excited using a 10-cycle tone-burst from an ultrasonic horn at 73 kHz (v_m = 591 mms^{-1}) and using the modified fulcrum to vary the pre-compression.

B. Results from a 6-Sphere Chain

Here, a similar analysis to that presented earlier for the 10-sphere case is presented. The outputs from a chain of six spheres excited using a 20-cycle tone-burst signal via the horn while varying the pre-compression force is shown is Fig. 6.25. Just like in the chain comprising of three and ten spheres, at the minimum pre-compression, a set of distinct regularly spaced pulses can be observed with the frequency spectrum containing three sub-harmonics with the lowest frequency peak occurring at 17 kHz, which was approximately a quarter of the input frequency 73 kHz. At this level of pre-compression the time of flight was 18.12 μs with a propagation velocity of 331 ms^{-1}. Following the trend observed in the experiments on the chains consisting of 3 and 10 spheres using the unmodified fulcrum (acrylic and aluminium wall), the propagation velocity decreases as the output waveforms transitions from strongly to weakly

nonlinear, then it increases as the characteristics of the waveform approaches that of the input signal (Fig. 7.26). At f_0 = 28 mN, the propagation velocity had reduced to 326 ms^{-1} and there appeared to be only two sub-harmonic frequency peaks at 22 and 51 kHz. These two distinct frequency peaks were later observed at 25 and 49 kHz with an increased propagation velocity of 335 ms^{-1} when subjected to a pre-compression force of 52 mN. Finally, at f_0 = 412 mN, the propagation velocity was 375 ms^{-1}; the sub-harmonics and harmonic frequency peaks created as a result of the nonlinear contact of the spheres are non-existent and the characteristic of the waveform resembles that of the input signal. The trend with which the propagation velocity changes is shown in Fig. 6.27. Similarly, there are 3 regions highlighted in the figure: 'A' where the system appears to be unstable. At pre-compression values above 62 mN, sub-harmonics began to be suppressed, with changing amounts of harmonics of the input frequency, indicative of weakly nonlinear behaviour.

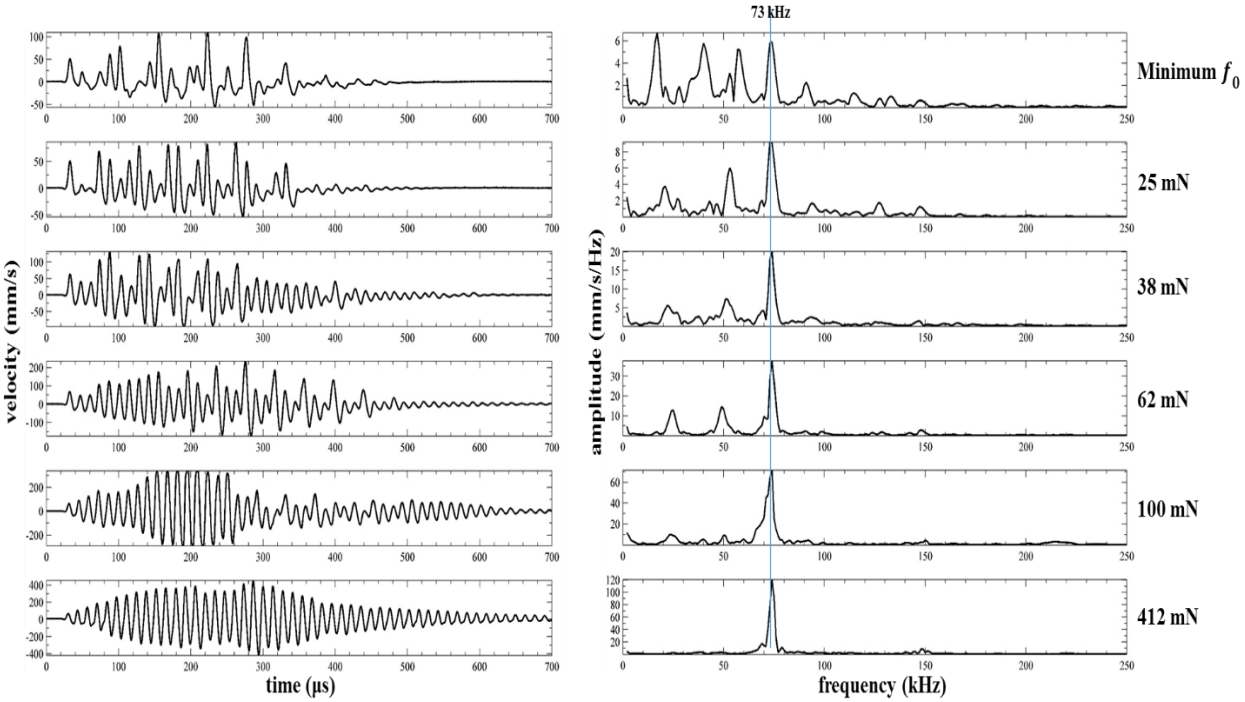

Fig. 6.25. Waveform (left) and frequency spectrum (right) of the output from a 6-sphere chain excited using a 10-cycle tone-burst from an ultrasonic horn at 73 kHz (v_m = 739 mms^{-1}) and using the modified fulcrum to vary the pre-compression.

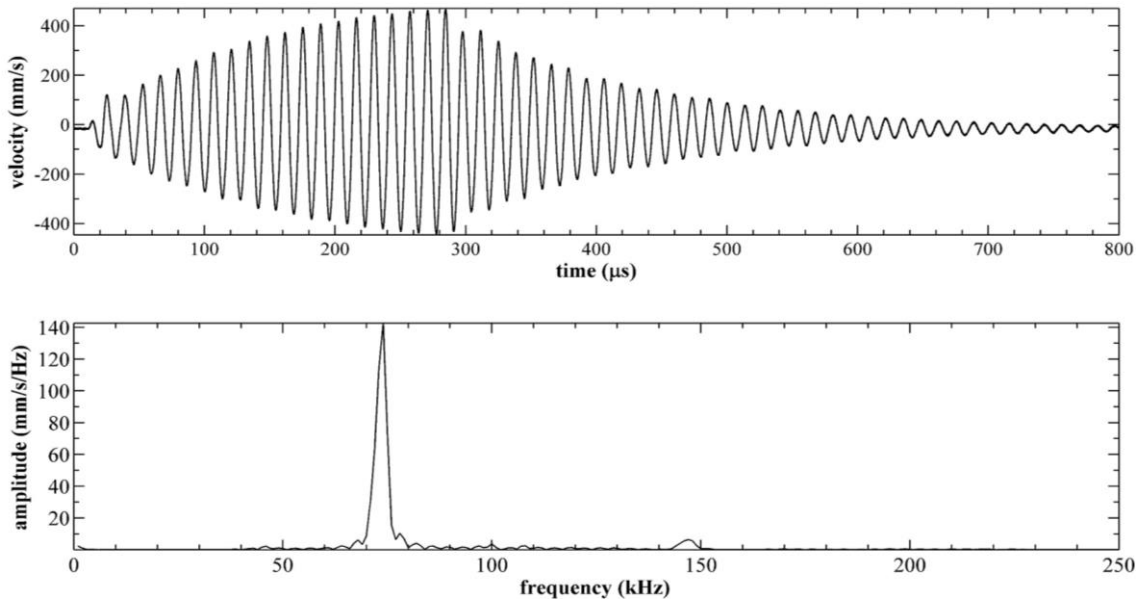

Fig. 6.26. Waveform (Top) and spectrum (Bottom) of the motion of the vibrating horn tip, as measured using a vibrometer. Excitation was a tone-burst of 20 cycles at 73 kHz (v_m = 739 mms^{-1}).

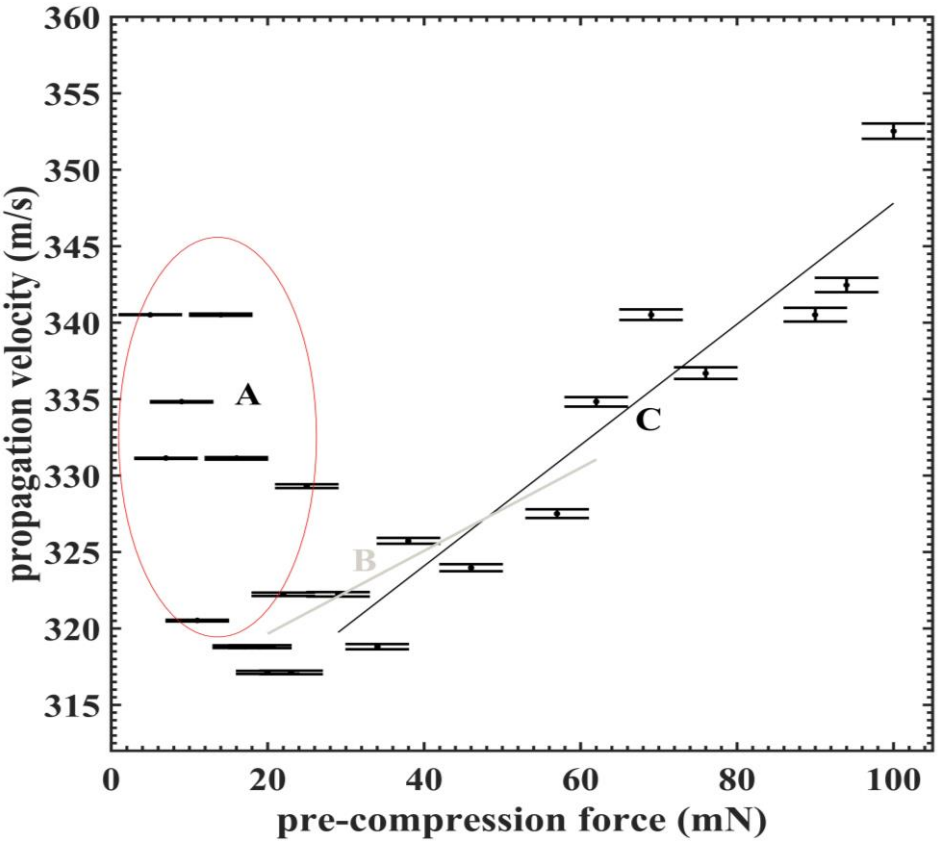

Fig. 6.27. Propagation velocity from the experiment using the unmodified fulcrum for a 6-sphere chain excited by an input of 20-cycle tone burst from an ultrasonic horn at 73 kHz at various pre-compression force.

The predicted results of the model in Fig. 6.28 described a linear increase in propagation velocity as the pre-compression force was increased. The predicted waveforms presented a similar trend to those of the experiments; at minimum pre-compression (39.975 mN) there exist a train of periodic pulses associated with three sub-harmonic frequency peaks. As the compression increases, the three sub-harmonic peaks become two sub-harmonic peaks and the accompanying pulses in the time waveform are narrower, and less regular/periodic. The propagation velocity also increased from 282 ms^{-1} to 360 ms^{-1} as f_0 increased to 130 mN.

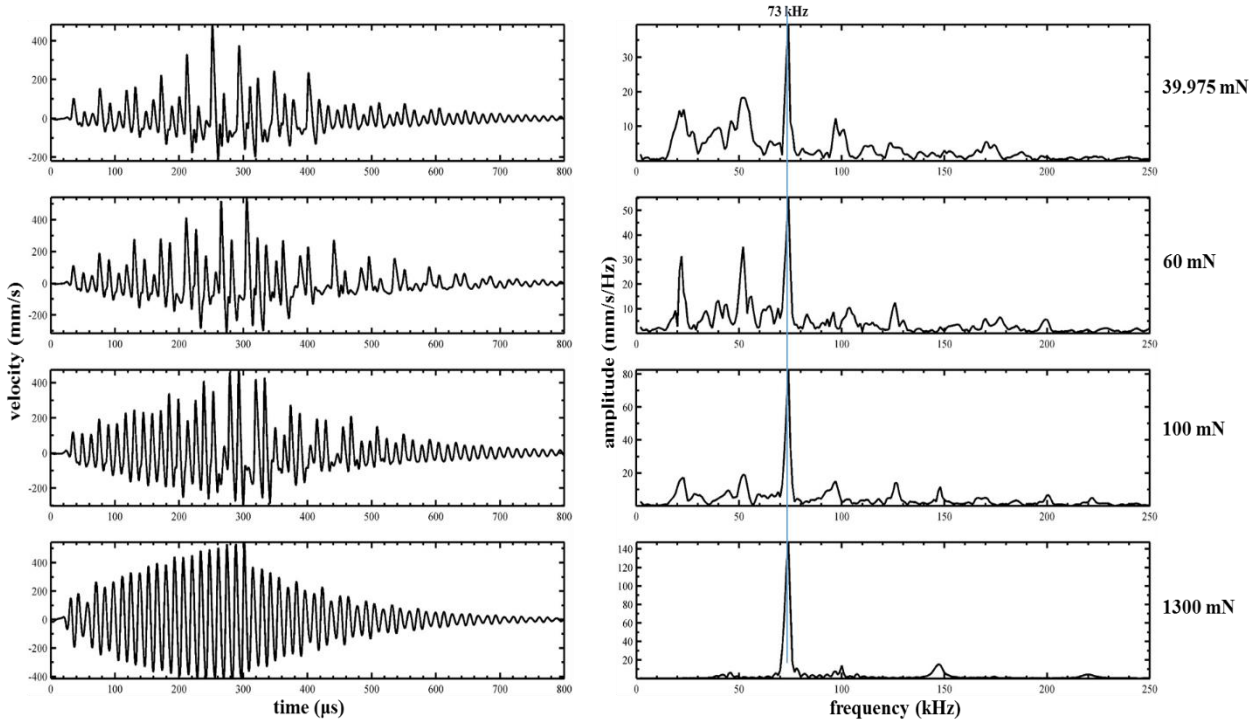

Fig. 6.28. Model prediction for a 6-sphere chain using an input of 20-cycle tone burst from an ultrasonic horn at 73 kHz (v_m = 739 mms^{-1}). Waveforms (left) and Spectra (right) at various pre-compression force.

6.5. Conclusions

This chapter demonstrated the relationship between f_0 and f_m when high amplitude input signals were used to excite resonant chain of spheres. The nonlinear nature of the Hertzian contact between the spheres was found to be dependent on the relative values of the oscillating applied force (f_m) and static pre-compression (f_0). Thus, if:

- $f_m \ll f_0$, the chain acts like a continuous medium (a normal solid) producing a linear wave.
- $f_m \approx f_0$, a weakly nonlinear wave in generated.
- $f_m \gg f_0$, propagation through the chain becomes highly nonlinear.

When f_m is considerably larger than f_0, the effect of nonlinearity is thus at its greatest.

The results from the experiments and predictive model were in agreement on the effects of pre-compression on the chain of spheres. Both cases illustrated a similar degree of sensitivity to the boundary conditions and input parameters. It was evident that applying a static pre-compression force to the spheres changes the propagation velocity along a chain. The changes can be quite large. For the chain containing three spheres, the propagation velocity was seen to more than double over the force range used in the experiments. For longer chains, the effect is still present, but with smaller increases being observed. As stated earlier, this is evidence of the applied force causing the chain to become stiffer, restricting motion and separation between individual spheres, and also reducing the amount of non-linearity present. This effectively causes solitary waves to cease to exist, and the result is only weakly nonlinear. At very high pre-compression values, the medium becomes almost linear, with the output closely resembling the input in terms of frequency content. The sound speed at high pre-compression values would be expected to tend toward that of a continuous solid of the same material, which was the trend observed experimentally. A comparison of the experiments and simulation demonstrated that a highly non-linear system would be expected

to be very sensitive to boundary conditions, and this is the case here. Thus, for example, changing the material which contacts the output sphere at the far end of the chain has an effect on the response.

6.6. References

1. A. Spadoni, C. Daraio, (2010). Generation and control of sound bullets with a nonlinear acoustic lens. Proceedings of the National Academy of Sciences, 107(16), 7230-4.
2. T. Shu-Jen Steven, (2002). Power Transformer Partial Discharge (PD) Acoustic Signal Detection using Fiber Sensors and Wavelet Analysis, Modeling, and Simulation, Master thesis, Virginia polytechnic institute and state university, pp. 35-42.
3. D.G. Chetwynd, X. Liu, and S. T. Smith, (1996). A controlled-force stylus displacement probe. Precision Engineering, 19(2), 105-111.
4. D.G. Chetwynd, X. Liu, and S. T. Smith, (1992). Signal fidelity and tracking force in stylus profilometry. International Journal of Machine Tools and Manufacture, 32(1), 239-245.
5. S. T. Smith, (2003). Foundations of ultra-precision mechanism design. Vol. 2. CRC Press.
6. V. J. S´ anchez-Morcillo, I. P´ erez-Arjona, V. Romero-Garcia, V. Tournat and V. E. Gusev, (2013). Second-harmonic generation for dispersive elastic waves in a discrete granular chain. Physical. Review. E, 88, 043203.

CHAPTER 7: Conclusions and Further Work

7.1. General conclusions

The work described in this thesis has been on the subject of the ultrasonic generation of solitary wave pulses. Much of the work was performed on developing a method which could in future be used to create a tunable acoustic lens. This was achieved experimentally using a novel technique involving spheres of millimetre diameter, and a high amplitude sinusoidal tone-burst from an ultrasonic horn. The results from the experiments were then validated using an analytical model based on Nesterenko's solution for non-linear dynamic motion of granular particles under Hertzian contact described in chapter 3.

Particular attention was paid in Chapter 1 to the fundamentals of ultrasound and how a transducer focusses ultrasound, one of the goals of this research was to produce an acoustic lens capable of generating Sound Bullets for Imaging and Therapeutic Treatment of Cancer such as HIFU. Chapter 2 contained the laws which govern granular particles under Hertzian contact and a discussion on how such granular particles react to a given stimuli and how to tune these characteristics to generate the desired effects. The process with which Hertzian contact produces the effects of non-linear behaviour between successive granular particles was described, and this in turn leads to the formation of solitary waves. The concept of cut-off frequency was introduced, indicating that the propagation effects of interest would only be expected at frequencies below a certain upper frequency limit, depending on the exact nature of the chain.

In Chapter 3, a full account of the theoretical model was given. This model was an extension of the solution provided by Nestrenko described in chapter 3. The extension involved:

1. The addition of attenuation in the form of viscous damping.

2. A more robust definition of boundary conditions for a finite chain by giving a detailed account of all the interfaces: sphere to sphere, sphere to ultrasonic horn and sphere to wall. In Nesterenko's solution (found in Chapter 3) there existed one primary form of interaction; the Hertzians contact between successive spheres.
3. The introduction of reflection which wasn't accounted for in Nesterenko's solution involving an infinite length of spheres where reflection never occurs.

The extension was necessary to model the conditions of the experimental work performed in this research. The effect of the finite boundary conditions and reflection was demonstrated using a high speed camera to capture the interaction of the spheres and their transitions between different nonlinear normal modes (NNMs) for a chain of finite length.

A detailed account was presented for the experimental work. This included the apparatus used, the modes of finely adjusting the experimental arrangement and Micro-Stereo-Lithography technique required for fabricating the cylindrical holders encasing and restricting the motion of the chain of spheres to a single plane. Preliminary results of the experiments and model were given describing how certain input parameters could alter the behaviour of the chain. The result was a comprehensive description of the model, the experiments and the expected behaviour of the highly sensitive system designed. It demonstrated a close correlation between the results of the experiment and of those from the predictive model; including how the system may be tuned from a linear to weakly and to a strongly nonlinear response. Prior to this research little work had been performed using excitations other than an impulse from strikers, and published work has shown that there are no experiments performed on spheres of this diameter (*i.e.* 1 mm).

Chapter 4 then described a series of experiments on chains of spheres of various lengths ranging from 2 to 10 spheres. Each length of chain was subjected to the smallest amount of pre-compression possible using the experimental arrangement described in Chapter 4. This amount

of pre-compression was estimated to be less than 10 mN using the theoretical model. The input parameters for each chain were varied (*e.g*. the duration and amplitude of the excitation) while the pre-compression force and excitation frequency were kept constant. This provided the means to obtain the optimal input parameters which facilitated the generation of solitary pulses associated by sub-harmonic(s) and harmonics within their spectrum. Varying these parameters also demonstrated that; for the physical properties and the dimensions of the materials used, and the initial conditions they were subjected to, there wasn't a single set of input conditions/parameters that worked for all chain lengths. It also demonstrated that although all system of chain lengths attempted to transform the sinusoidal tone-burst to a periodic pulse but only a few (2, 3, 6 and 10-sphere chains) could support the formation of the train of solitary pulses at 73 kHz. It was shown that as the length of the chain increased, so did the number of sub-harmonic and harmonics (resonant peaks) present. The spacing or periodicity of these sub-harmonics and harmonics were found to be integer fractions of the input frequency. Furthermore, the results from the theoretical model depicted a similar behaviour to those from the experiment, highlighting the sensitive nature of the system of spheres. This work was published in a journal paper and several conference papers [1 - 6].

Chapter 5 involved studying the behaviour of the chain for different excitation frequencies, radii and materials for the spheres and its cylindrical holder. The chapter described a complex interaction when each of these conditions were varied. At diameters below 4 mm, the chain supported a strongly nonlinear behaviour. Increasing the diameter above 4 mm produced undesirable effects. Depending on the features of the waveform required, the chain could be tuned by simply introducing spheres with a diameter between 1 – 3 mm which would lead to waveforms with sub-harmonics. Submillimetre diameter spheres were observed to produce narrower and sharper signals which had no sub-harmonics, only harmonic components. This suggests that diameter, and length of the chain, may be the critical parameter in dictating the

presence and number of sub-harmonics achievable by the chain. Changing the material of the spheres to Delrin, chrome-steel and tungsten-carbide produced very similar results, with each material effectively generating sub-harmonics and harmonics for the right conditions. However, in the case of Synthetic Sapphire (Ruby) which is an oxide mineral unlike the metal and polymers used, a weakly nonlinear behaviour was observed. Varying the duration and amplitude of the input signal did not alter the weakly nonlinear behaviour detected in the synthetic sapphire. The material of the cylindrical holder was also varied, steel, aluminium, Perspex and EnvisionTec^{TM} R11 were used. This was found to be a crucial component for developing a chain with the required properties of solitary wave pulse creation. Each material produced different effects. R11 was found to be the optimal, it allowed, the formation of both weakly and strongly nonlinear signals with an ability to adjust the number of sub-harmonics and harmonics. In the case of aluminium and steel, an effect which eliminated all sub-harmonics replacing them with multiple harmonic spaced at intervals of the input frequency of 73 kHz was observed, while Perspex produced a weakly nonlinear behaviour when subjected to similar conditions.

The results presented in Chapter 6 demonstrated the effect of increasing the static pre-compression f_0. It investigated the nature of the relationship between f_0 and f_m when high amplitude input signals were used to excite a resonant chain of spheres. The non-linear nature of the Hertzian contact between the spheres was found to be dependent on the relative values of the oscillating applied force (f_m) and static pre-compression (f_0). Thus, if:

- $f_m \ll f_0$, the chain acts like a continuous medium (a normal solid) producing a linear wave.
- $f_m \approx f_0$, a weakly nonlinear wave in generated.
- $f_m \gg f_0$, propagation through the chain becomes highly nonlinear.

When f_m is considerably larger than f_0, the effect of nonlinearity is thus at its greatest.

The results from the experiments and predictive model were in agreement on the effects of pre-compression on the chain of spheres. Both results illustrated a similar degree of sensitivity to the boundary conditions and input parameters. It was evident that the main area of interest does in fact occur; applying a static pre-compression force to the spheres changes the propagation velocity along a chain.

The main point to note is that the work has shown that high amplitudes from an ultrasonic horn can be used to generate a train of solitary wave impulses, with a bandwidth and pulse repetition rate that can be adjusted by changing the parameters within the chain. This is the first time that such behaviour has been observed.

7.2. Further work

It is felt that the work presented in this thesis has achieved the goal of increasing the scope of knowledge within the field of ultrasonic solitary wave generation, by using a very high input amplitude with a narrow bandwidth, and using this to create solitary wave impulses with a broader bandwidth. The hope and belief was that this research would prove useful in the development of a viable clinical device for the use in medical imaging and therapeutic treatments. In the spirit of collaboration and to further the knowledge of the works presented, the following are suggestions on how to improve and extend the research:

- Using a chain composed of ellipsoidal or oval particles to study the effects of particle geometry and orientation on the formation and propagation of highly nonlinear solitary waves. This geometry could be used to reduce the effect of friction from the holder and possibly create a smaller Hertzian point to point contact between spheres effectively increasing the energy transmitted between successive spheres depending on the orientation of the spheres as shown in Fig. 8.1.

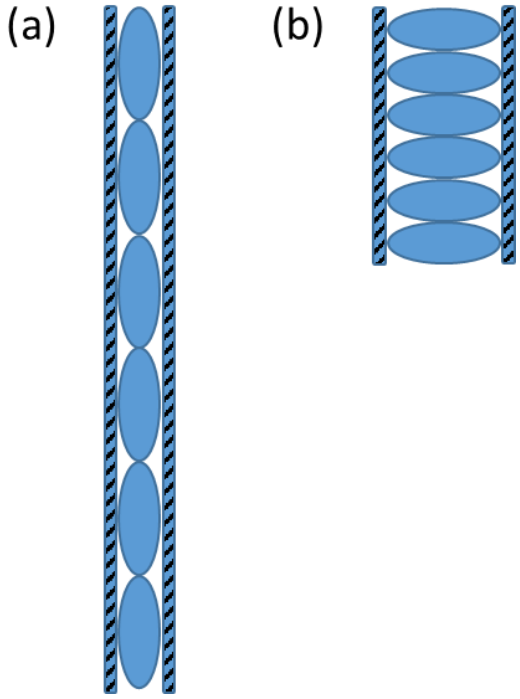

Fig. 8.1. Chain composed of ellipsoidal particles (a) Particles aligned vertically with the smallest area of contact between successive spheres (b) Particles aligned horizontally with the smallest area of contact between the spheres and the sides of the holder.

- Thus far, a chain composed of homogeneous particles were studied in this research. For each of the variations studied; materials and radii of the spheres and its holder, a heterogeneous chain could produce improved bandwidths of greater amplitudes when a combination of these is introduced. This could be in the form of a chain consisting of spheres made from different materials or diameters and even different shapes.
- The velocity and behaviour of the resultant signals where studied when the chain was subjected to various amount of pre-compression. This could be implemented in a multi-dimensional lattice or array of chains with each chain subjected to different amounts of pre-compression. This would produce a tuneable acoustic lens with an adjustable focus, similar to that shown in Fig. 8.2.

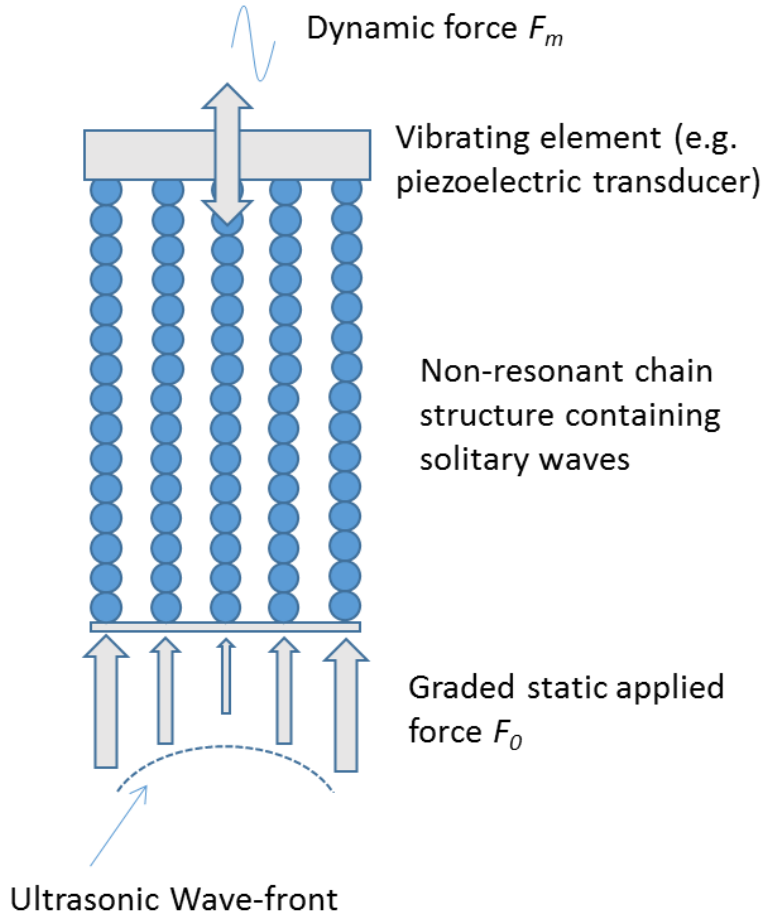

Fig. 8.2. A multi-array chain with each chain subjected to different pre-compression forces.

There are other ways in which this work could be extended. An example would be the creation of a layer beneath a single transducer, containing a layer of spheres in some form of touching geometrical arrangement. This could allow the output from a highly resonant ultrasonic transducer to be transformed into a train of impulses. This could be used for a wide range of applications, ranging from thickness gauging, to high power industrial processing.

7.3. References

1. D.A. Hutchins, J. Yang, O. Akanji, P. J. Thomas, L.A.J. Davis, S. Freear, S. Harput, N. Saffari and P. Gelat, (2014, September). The study of chain-like materials for use in biomedical ultrasound. In Ultrasonics Symposium (IUS), 2014 IEEE International (pp. 2607-2610). IEEE.
2. D.A. Hutchins, J. Yang, O. Akanji, P. J. Thomas, L.A.J. Davis, S. Freear, S. Harput, N. Saffari and P. Gelat, (2015). "Evolution of ultrasonic impulses in chains of spheres using resonant excitation), EPL, 109, 54002.
3. D.A. Hutchins, J. Yang, O. Akanji, P. J. Thomas, L.A.J. Davis, S. Freear, S. Harput, N. Saffari and P. Gelat, (2015). Evolution of ultrasonic impulses in chains of spheres using resonant excitation. EPL (Europhysics Letters), 109(5), 54002.
4. J. Yang, D. A. Hutchins, O. Akanji, P. J. Thomas, L. A. J. Davis, S. Harput, P. Gelat, S. Freear, and N. Saffari, (2015). An analysis of solitary wave impulses in granular chains using ultrasonic excitation. [Accepted August 2015 for publication in Physics Procedia].
5. D. A. Hutchins, J. Yang, O. Akanji, P. J. Thomas, L. A. J. Davis, S. Freear, S. Harput, N. Saffari and P. Gelat, Ultrasonic propagation in finite-length granular chains, submitted August 2015 to Ultrasonics journal.
6. D.A. Hutchins, J. Yang, O. Akanji, P. J. Thomas, L.A.J. Davis, S. Freear, S. Harput, N. Saffari and P. Gelat (2015). Generation of Impulses from Single Frequency Inputs Using Non-linear Propagation in Spherical Chains. Physics Procedia, 70, 131-134.

Appendix A1

Matlab Code

```
function main


   %CLEAR ALL FOR INITIALIZATION
     clear

   % ********** START OF INITIALIZATION BLOCK **********
   %DECLARE GLOBAL VARIABLES
     global N a f0 C0 C1 C2 del0 TEnd TF CF PULSE

   %DEFINE NUMBER OF SPHERES AND RADIUS
     %NOTE: Don't forget to add/delete sufficient initial conditions
     % if N is changed. 2*N values are required in ode45 at [ ... ...]
     N = 6;              % Number of spheres
     a = 0.0005;         % Radius Spheres in m

   %DEFINE PRECOMPRSESSION FORCE OF CHAIN
     F0 = 0.009;           % Precompression force in N

    %DEFINE MATERIAL PROPERTIES OF MAIN SPHERES IN CHAIN
     nu = 0.3;          % Poisson Ratio
     E  = 201*10^9;     % Modulus of Elasticity Pa
     rho = 7833;         % Density in kg/m^3



   %CALCULATE SECONDARY PARAMETERS
     Th = (3*(1-nu^2))/(4*E);                % Checked Correct
     del0 = 2*(Th*F0)^(2/3) / a^(1/3);       % Checked Correct
     m = rho*(4/3)*pi*a^3;                   % Checked Correct

   % CALCULATE NATURAL FREQUENCY FROM NON-DIMENSIONALISATION.
     Om0sq = a / (sqrt(2^3)*m*Th);
     display(['Om0sq = ' num2str(Om0sq) ' 1/s^2']);
     display(['Om = ' num2str(sqrt(Om0sq)) ' 1/s']);

   %CALCULATE CUT OFF FREQUENCY
     FC= 3/(4*pi^(1.5)) * F0^(1/6) * 1/( Th^(1/3) *  a^(4/3) *  rho^(1/2));
% CHECKED CORRECT
      display(['FC = ' num2str(FC) ' 1/s']);

   %CALCULATE COMMON FACTOR BEFORE 1st PART OF DIMENSIONAL EQS.
     C0 = (sqrt(a/2)) / (2*m*Th);
     %C0

    %DETERMINE NON-Dim. END TIME FOR CALCs
% %  tend = 0.00004; % Define end time in secs
tend = 0.0009; % Define end time in secs
        %display(['tEnd = ' num2str(tend) ' sec, End of calcs']);
         TEnd = sqrt(Om0sq)* tend; % Transform end time into non-dim
```

```
          display(['TEnd = ' num2str(TEnd) ' non-dim units, End of
calcs']);


   %DEFINE FORCING FREQUENCY AND CALC NON-DIM. END TIME FOR FORCING
    PULSE = 1;              % 1 = Pulse of n cycles; 0 = continuous forcing
     display(['PULSE = ' num2str(PULSE) '  with 1=pulse on, 0=continuous
forcing']);
      f0dim = 73000;          % Forcing frequency in Hz
       display(['f0dim = ' num2str(f0dim)]);
        t0dim = 1/f0dim;       % Dimensional time for one cycle of forcing
         T0ND = sqrt(Om0sq) * t0dim;  % Non-dimensional time one cycle of
forcing
          display(['T0ND = ' num2str(T0ND) ' non-dim units, 1 forcing
cycle']);
           f0 = 1/T0ND;         % Non-dimensional forcing frequency
            n0 = 20.0;            % Number of forcing cycles for frequency
f0
             TF = n0 * T0ND;      % Non-Dim time for n0 cycles of forcing
              display(['TF = ' num2str(TF) ' non-dim units, End of
forcing']);



    % The constatnt CF is used when forcing is done by moving the position
    % of the imaginary element y(-1) sinusoidally.
      a0D = 0.000001;   % DIM. AMPLITUDE OF FORCING IN METRES
        CF = a0D/a;
        display(['CF = ' num2str(CF)]);

    %GIVE WARNING IF TEnd SHORT COMPARED TO Tau0 - This still needs to be
    %refined to stop on condition or similar.
       if (TEnd/TF) < 2
          display('TEnd short compared to forcing time TF');
          %TEnd/TF
       end

    %CALCULATE del0/a FOR CHECKING PURPOSES ONLY.
     %del0ova = del0 / a;
     %display(del0ova)

   % ********** END OF INITIALIZATION BLOCK **********



    % ********** START COMPUTATIONAL BLOCK  **********

      options = odeset('RelTol',1e-8,'AbsTol',1e-8,'MaxStep',0.01);
                                        %[T2,Y2]=ode45(@osz3,0:.01:600,[0.0001
0 0 0 0 0 0 0 0]],options);
      [T2,Y2]=ode45(@osz3,0:.01:TEnd,[0.00000 zeros(1,2*N-1)],options);

    % ********** END COMPUTATIONAL BLOCK  **********



    % ********** START DISPLAY NON-DIMENSIONAL RESULTS BLOCK **********
      %figure(1)
```

```
      %figure
      %hold on
      %plot(T2,Y2(:,1:end/2))
      %plot(T2,Y2(:,1),'g')
      % plot(T2,Y2(:,N-5),'b')
      %plot(T2,Y2(:,N),'r')
      %plot(T2,Y2(:,N+1),'b')

      % plot(T2,Y2(:,1),'g')
      % plot(T2,Y2(:,N+1),'r')

  % ********** END DISPLAY NON-DIMENSIONAL RESULTS BLOCK **********


% **********  PLOT SEQUENCE OF CURVES SHOWING HOW WAVE TRAVELS ********
         %BUT THIS IS NOT YET QUITE RIGHT
% %       hold on
% %       for j = 1:400:15500
% %       %        %   %figure(2)
% %          figure
% %          plot(a*Y2(j,1:N),'k-');   % Amplitude displayed in metres
% %       end
figure(555)
% plot(T2,Y2(:,1:end/2));
plot(T2,Y2(:,6));
 % **********  END PLOT SEQUENCE OF CURVES SHOWING HOW WAVE TRAVELS
********


  % ********** START DISPLAY DIMENSIONAL RESULTS BLOCK **********
  time_t = (1/sqrt(Om0sq))*T2;
%   vel_v = a*Y2(:,6)*1000;
vel_v = Y2(:,6)*1000;
      %figure(1)
       figure(556)
% %        hold on
          %plot((1/sqrt(Om0sq))*T2,a*Y2(:,1:end/2))
        plot((1/sqrt(Om0sq))*T2,a*Y2(:,6), 'k')

        velo1 = [time_t vel_v];
        figure(557)
        auto_fast_vel(velo1);
filename = '6 chrome Spheres 20 cycles sine Peter (time and freq)';
% filename = '10 spheres 45 cycles no comp1';
% filename = '10 spheres theory Fig4_b';
Width = 35;
Heigth = 20;
% Width = 15;
% Heigth = 8;
FontName = 'times';
FontSize = 16;
LineWidth = 1.5;
esporta_pdf(filename,Width,Heigth,FontName, FontSize, LineWidth)
% %         plot((1/sqrt(Om0sq))*T2,a*Y2(:,1), 'k')
% %         plot((1/sqrt(Om0sq))*T2,a*Y2(:,10), 'k')
% %         plot((1/sqrt(Om0sq))*T2,a*Y2(:,15), 'k')
% %         plot((1/sqrt(Om0sq))*T2,a*Y2(:,20), 'k')
% %         plot((1/sqrt(Om0sq))*T2,a*Y2(:,25), 'k')
% %         plot((1/sqrt(Om0sq))*T2,a*Y2(:,30), 'k')
% %         plot((1/sqrt(Om0sq))*T2,a*Y2(:,35), 'k')
```

```
% %         plot((1/sqrt(Om0sq))*T2,a*Y2(:,37), 'k')
% %         plot((1/sqrt(Om0sq))*T2,a*Y2(:,40), 'k')
% %         plot((1/sqrt(Om0sq))*T2,a*Y2(:,43), 'k')
% %         plot((1/sqrt(Om0sq))*T2,a*Y2(:,45), 'k')
% %         plot((1/sqrt(Om0sq))*T2,a*Y2(:,52), 'r')
% %         plot((1/sqrt(Om0sq))*T2,a*Y2(:,54), 'g')
% %         plot((1/sqrt(Om0sq))*T2,a*Y2(:,56), 'b')
% %         plot((1/sqrt(Om0sq))*T2,a*Y2(:,58), 'y')
% %         plot((1/sqrt(Om0sq))*T2,a*Y2(:,60), 'm')

  % ********** END DISPLAY DIMENSIONAL RESULTS BLOCK **********



%keyboard

end

function dy = osz3(t,y)

   %IDENTIFY GLOBAL INPUT PARAMETERS PASSED DOWN FROM MAIN ROUTINE
    global N a f0 C0 C1 C2 del0 TEnd TF CF PULSE

%display('t=')
%display(t)

   % DEFINE dy ARRAY AND POPULATE WITH ZEROES
     dy = zeros(2*N,1);


   % ASSIGN dy(i)'s AND y(i)'s
     for i = 1:N
       dy(i) = y(N+i);
     end




     % ********** START: BLOCK OF NON-DIMENSIONAL EQUATIONS, ATTEMPTING
**********

     for i = N+1:2*N
          if i == N+1
              if PULSE == 1    % n0-Cylce Pulse Forcing
                 if t <= TF
                    y0 = CF*sin(2*pi*f0*t);
                     %y0 = CF*(2 + sin(2*pi*f0*t));
                       %ALSO CHANGE y0 below if it works
                     Term1 = (del0/a)-(y(1)-y0);
                       if Term1 >= 0
                            %display('Contact in forcing  OK OK OK OK OK
OK OK OK OK  !!!!')
                       end
                        if Term1 <0
                           Term1 = 0;
% %                            display('Lost contact in forcing   !!!!')
```

```
                            %display(['del0/a = ' num2str(del0/a) ',
y(1)=' num2str(y(1)) ',  y0=' num2str(y0)]);
                        end
                      Term2 = (del0/a)-(y(2)-y(1));
                         if Term2 <0
                            Term2 = 0;
                         end
                          %dy(i) =  (((del0/a)-(y(1)-y0))^1.5  - ((del0/a)-
(y(2)-y(1)))^1.5);
                    dy(i) =  ((Term1)^1.5  - (Term2)^1.5);
                 else
                      Term1 = (del0/a)-(y(1)- 0);
                         if Term1 <0
                            Term1 = 0;
                         end
                      Term2 = (del0/a)-(y(2)-y(1));
                         if Term2 <0
                            Term2 = 0;
                         end
                          %dy(i) =  (((del0/a)-(y(1)-0))^1.5  - ((del0/a)-
(y(2)-y(1)))^1.5);
                    dy(i) =  ((Term1)^1.5  - (Term2)^1.5);
                 end
              else          % Continuouse forcing throughout computation
time
                    y0 = CF*sin(2*pi*f0*t);
                      Term1 = (del0/a)-(y(1)-y0);
                         if Term1 <0
                             Term1 = 0;
                         end
                      Term2 = (del0/a)-(y(2)-y(1));
                         if Term2 <0
                            Term2 = 0;
                         end
                          %dy(i) =  (((del0/a)-(y(1)-y0))^1.5  - ((del0/a)-
(y(2)-y(1)))^1.5);
                    dy(i) =  ((Term1)^1.5  - (Term2)^1.5);
              end

          elseif i == 2*N
                      Term1 = (del0/a)-(y(N)-y(N-1));
                         if Term1 <0
                             Term1 = 0;
                         end
                      Term2 = (del0/a)-(0 -y(N));
                         if Term2 <0
                            Term2 = 0;
                         end
                          %dy(i) = (((del0/a)-(y(N)-y(N-1)))^1.5  -
((del0/a)-(0 -y(N)))^1.5);
                      dy(i) =  ((Term1)^1.5  - (Term2)^1.5);
                     %dy(i) =  ((Term1)^1.5);  % Refl1
                    % dy(i) =  dy(i-1);        % Refl2
          else
                      Term1 = (del0/a)-(y(i-N)-y(i-N-1));
                         if Term1 <0
                             Term1 = 0;
                         end
                      Term2 = (del0/a)-(y(i-N+1)-y(i-N));
                         if Term2 <0
                            Term2 = 0;
```

```
                        end
                         %dy(i) =  (((del0/a)-(y(i-N)-y(i-N-1)))^1.5 -
((del0/a)-(y(i-N+1)-y(i-N)))^1.5);
                    dy(i) =  ((Term1)^1.5  - (Term2)^1.5);
          end


     end
     % ********** END: BLOCK OF NON-DIMENSIONAL EQUATIONS **********




      %           COPY OF BLOCK BEFORE STARTING TO MESS AROUND ****
   % ********** START: BLOCK OF NON-DIMENSIONAL EQUATIONS, ATTEMPTING
**********
% **********     TO TAKE OUT EFECT OF CHAIN OF FORCING ELEMENT
************
     %for i = N+1:2*N
          %if i == N+1
              %dy(i) =  (((del0/a)-(y(1)-0))^1.5  - ((del0/a)-(y(2)-
y(1)))^1.5) + C1*sin(C2*t);
              %                   %disp(' i= N+1')
            %elseif i == 2*N
               %dy(i) = (((del0/a)-(y(N)-y(N-1)))^1.5  - ((del0/a)-(0 -
y(N)))^1.5);
              %                   %disp('   i = 2*N')
              %               display(  (del0/a)/ (y(2)-y(1))   )
          %else
              %dy(i) =  (((del0/a)-(y(i-N)-y(i-N-1)))^1.5 - ((del0/a)-(y(i-
N+1)-y(i-N)))^1.5);
              %                   %disp('  i is inbetween')
          %end
         %
     %end
   % ********** END: BLOCK OF NON-DIMENSIONAL EQUATIONS **********




   % ********** START: ORIGINAL BLOCK OF DIMENSIONAL EQUATIONS, ALL LINKED
**********
   %  for i = N+1:2*N
   %       if i == N+1
   %           dy(i) =  C0*((del0-(y(1)-0))^1.5  - (del0-(y(2)-y(1)))^1.5)
+ 1*sin(2*pi*f0*t);
   %                              %disp(' i= N+1')
   %         elseif i == 2*N
   %            dy(i) =  C0*((del0-(y(N)-y(N-1)))^1.5  - (del0-(0 -
y(N)))^1.5);
   %                              %disp('   i = 2*N')
   %       else
```

```
   %           dy(i) =  C0*((del0-(y(i-N)-y(i-N-1)))^1.5 - (del0-(y(i-N+1)-
y(i-N)))^1.5);
   %                              %disp('  i is inbetween')
   %       end
   %
   %  end
   % ********** END: ORIGINAL BLOCK OF DIMENSIONAL EQUATIONS **********



   % ********** START: BLOCK OF NON-DIMENSIONAL EQUATIONS **********, ALL
LINKED
   %  for i = N+1:2*N
   %       if i == N+1
   %           dy(i) =  (((del0/a)-(y(1)-0))^1.5  - ((del0/a)-(y(2)-
y(1)))^1.5) + C1*sin(C2*t);
   %                              %disp(' i= N+1')
   %         elseif i == 2*N
   %            dy(i) = (((del0/a)-(y(N)-y(N-1)))^1.5  - ((del0/a)-(0 -
y(N)))^1.5);
   %                              %disp('   i = 2*N')
   %       else
   %           dy(i) =  (((del0/a)-(y(i-N)-y(i-N-1)))^1.5 - ((del0/a)-(y(i-
N+1)-y(i-N)))^1.5);
   %                              %disp('  i is inbetween')
   %       end
   %
   %  end
   % ********** END: BLOCK OF NON-DIMENSIONAL EQUATIONS **********




  % ********** SOME OLD LINES TO KEEP FOR A WHILE **********
     %dy(1) = y(4);
     %dy(2) = y(5);
     %dy(3) = y(6);

     %coun = coun + 1;
     %disp('Back, coun =')
     %disp(coun)
     %dy(4) =  C0*((del0-(y(1)     ))^1.5 - (del0-(y(2)-y(1)))^1.5) +
1*sin(2*pi*1.0*t);
     %dy(5) =  C0*((del0-(y(2)-y(1)))^1.5 - (del0-(y(3)-y(2)))^1.5);
     %dy(6) =  C0*((del0-(y(3)-y(2)))^1.5 - (del0-(    -y(3)))^1.5);
     %dyn =  C0*((del0-(yn-yn-1))^1.5 -  (del0-(yn+1-yn))^1.5);

end
```